



A Digital Signal Processing Solution for Multichannel Base Stations

by

Scott Leyonhjelm, B.Eng (Hons.)

A thesis submitted for the degree of

Doctor of Philosophy

at

Victoria University of Technology

November, 1995.

Department of Electrical and Electronic Engineering,

PO BOX 14428, MCMC, 8001,

Australia.

FTS THESIS
621.3845 LEY
30001005034048
Leyonhjelm, Scott
A digital signal processing
solution for multichannel
base stations

Abstract

Radio communication systems of the future will require a large increase in user capacity. To achieve this, cell sizes will reduce and the number of base stations will increase. Current base station architectures use analogue combining techniques which are expensive, voluminous and inflexible. This thesis investigates a Digital Signal Processing (DSP) solution which produces a cheaper, smaller and more flexible multichannel base station transmitter design. The main design challenges of the new DSP low power combining architecture are the multichannel combining algorithm, the frequency translation of the multichannel signal to radio frequency, the Digital to Analogue Conversion (DAC) interface and the wideband ultra-linear power amplifier. This thesis considers the pre-power amplifier stages.

Combining the channels in a digital signal processing environment provides considerable flexibility, but the computational requirements are very high. The minimisation of computational load is achieved by combining the channels at baseband with efficient algorithms.

Four upconversion techniques, currently used in single channel applications, are investigated for use in a wideband multichannel environment. Comparisons reveal that analogue direct upconversion currently provides the most attractive solution because a lower performance DAC is required and less computation is needed. However, amplitude and phase mismatch between the In Phase and Quadrature circuits cause undesired sideband responses that exceed radio system specifications. A novel adaptive compensation method leads to an improved performance and a lower computational overhead compared to previous techniques.

Multichannel radio systems can only tolerate very low harmonic and intermodulation products and the DAC is a major source of these spurious responses. A new implementation of bandlimited dithering is shown to improve the performance of the DAC by 2 to 4 dB, with only a small increase in hardware.

Preface

This thesis describes the development of a low power combining digital signal processing architecture for future radio base station transmitters. The goal of the project is to produce a base station that is small, cheap and greatly more flexible than the conventional base station design.

The idea for the low power combining architecture was described in the 1980's and its advantages over the conventional design have since been well recognised. However, four technological challenges have impeded the immediate development of the digital signal processing low power combining technique:

- the large amount of computation required to combine multiple channels in a digital signal processor,
- the high degree of linearity needed to convert the multichannel signal from baseband to RF,
- the high speed and precision of the DAC required to convert the digital multichannel signal to an analogue signal, and
- the ultra-linear power amplifier needed to boost the power level of the multichannel signal for radio frequency transmission.

The ultra-linear power amplifier is seen as the most difficult design obstacle to overcome and most researchers and manufacturers of radio base stations have, and still are, focusing much research and development on this area. Through the use of advanced linearisation techniques, feedforward, feedback and predistortion, a sufficiently linear and wideband power amplifier has been developed. These developments have only occurred since the thesis began in 1991 although the power amplifier is still limited in total power output.

The objective of the thesis has been to concentrate on the design challenges of the pre-power amplifier stages. A detailed examination of the combining of multiple channels and the upconversion of the multichannel signal to RF provide clarification of the pertinent issues regarding a digital signal processing base station. These discussions lead to the choice of the analogue direct upconversion technique. A new compensation algorithm required to ensure that this upconversion technique meets the radio system specifications

is developed and has been presented in two papers:

- I Leyonhjelm, S.A., Faulkner, M. & Macleod, J., “The Effect of Reconstruction Filter Mismatch in a Digital Signal Processing Multichannel Combiner”, IEEE International Conference on Universal Wireless Access, World Congress Centre, Melbourne, Australia, April 18-19, 1994, pp 25-30.
- II Leyonhjelm, S. & Faulkner, M., “DSP Combining and Direct Conversion for Multichannel Transmitters”, 43rd IEEE/VTS Vehicular Technology Conference, Stockholm, Sweden, June 7-10, 1994, Vol. 1 of 3, pp 494-498.

The compensation technique is sensitive to frequency dependant mismatch between the In Phase and Quadrature reconstruction filters and this has been analysed in a third publication:

- III Leyonhjelm, S.A. & Faulkner, M., “The Effect of Reconstruction Filters on Direct Upconversion in a Multichannel Environment”, IEEE Transactions on Vehicular Technology, Vol. 44, No. 1, Feb. 1995, pp 95-102.

Papers I and III have an error in Eqns. (5) and (17) respectively, but it does not affect either conclusion. The error has been corrected in this thesis, Eqn. (4.17).

The digital to analogue converter quantisation nonlinearity introduces harmonic and intermodulation products, which are troublesome in a multichannel base station. Improving the DAC linearity has been approached from the point of view that it is a black box and an external algorithm has been developed to improve the performance of the DAC. Although the performance increase is small, 2 to 4 dB, it has been implemented with minimal increase in hardware. The results of this technique have been accepted for publication by the following journal:

- IV Leyonhjelm, S.A., Faulkner, M., & Nilsson, P., “An Efficient Implementation of Bandlimited Dithering”, Wireless Personal Communication, Accepted for publication on the 27th November, 1996.

It should also be mentioned that the idea of the digital signal processing base station is currently being exploited by radio communication manufacturers. However, due to reasons of commercial sensitivity, much of their work remains unpublished.

Acknowledgments

I would like to thank Dr. Mike Faulkner for providing much inspiration and guidance throughout the project. Mikes endless effort, encouragement and enthusiasm has been instrumental in me overcoming the many challenges faced during the PhD.

To Mark Briffa and Victor Taylor for their intellectually stimulating discussions and technical assistance throughout the project. My gratitude is also extended to Zosia Golbiowski and John Macleod for carefully reading the manuscript and commenting on the contents and style of this thesis. Thanks also to the technical officers, Phil & Brian, the computer doctors, Yauman & Dan, the secretaries, Rose, Shirley and Som, and the Head of the Electrical and Electronic Engineering Department, Wally, for assisting me in varied 'matters'. Thankyou also to Patto and Haze for helping me arrange the final binding and delivery of this thesis.

Many thanks must also go to my friends at the Department of Applied Electronics, Lund University for their open and warm hospitality, and providing the necessary resources needed to design and fabricate the Application Specific Integrated Circuits (ASIC's). Special thanks must go to Mats Johansson for his efforts in helping me to organise my trip to Sweden and being a generous host whilst I was at Lund University, and Peter Nilsson for teaching me the intricacies of the ASIC development tools.

To David Pope of Signal Processing Associates for his enlightening technical discussions and lending me digital to analogue converter hardware that was developed by his company.

The research described in this report obtained financial support from Victoria University of Technology in the form of a postgraduate scholarship and tutorial work that enabled me to complete the thesis without financial burden. Additional funding was also obtained from the following sources:

- The Secomb scholarship that assisted in conference expenses whilst at VTC 94 in Stockholm, Sweden.
- The DITAC Bilateral Science and Technology Co-operation Program which enabled me to travel to Lund University, Sweden to complete the eight weeks necessary to build the ASIC.
- The ATERB Research Project Grant for assisting in the purchasing of the TMS40 development system.

I am also very appreciative of the patience and support that Rachel has showed during the final stages of this work. Finally, and most importantly, I would like to thank my parents, Josi and Max, for providing immense support throughout all my lifes endeavours. They are the rock on which I stand.

Scott Leyonhjelm.
November, 1995.

List of Principal Symbols and Abbreviations

Symbol or Abbreviation	Description	First Used in Section
$a_k(t)$	Amplitude modulation of channel k	2.2.1
ACI	Adjacent Channel Interference	2.2.2
ADC	Analogue to Digital Converter	5.3.1.1
ANT-TX _{isolation}	Antenna to transmitter isolation	2.2.3
ASIC	Application Specific Integrated Circuit	6.4
BW_{cavity}	3 dB bandwidth of the cavity filter	2.2.4.1
BW_{ch}	Bandwidth of the channel	3.2
BW_{meas}	Bandwidth of the measurement bandpass filter	3.3.1.2
BW_{sys}	Switching bandwidth of the wireless system	3.2
BW_{3dB}	3dB bandwidth of a bandpass filter	3.3.2.1
%BW	Fractional 3dB bandwidth of a bandpass filter	3.3.2.1
c	Peak to peak amplitude of uniform dither	5.3.1.1
C_{FFT}	Computation power of the polyphase FFT combining algorithm.	3.2.2.1
C_{GSM}	Computation power for the GSM radio system	3.2.2.2
C_{ADU}	Computation power of Analogue Direct Upconversion	3.3.3.1
C_{IF}	Computation power of Digital IF Upconversion	3.3.1.1
C_m	Complex co-efficient	4.2
C40	Texas Instrument general purpose DSP	3.2.1
CaNAD	Carrier to Noise And Distortion ratio	6.3
CNR_{multi}	Multichannel carrier to noise power ratio	3.3.1.2
CRI	The Control and Radio Interface	1.1
dBc	Absolute power level below the reference carrier component	
dBm	Absolute power level with respect to a 1mW reference	
d(n)	Discrete dither signal	6.2.1
DAC	Digital to Analog Converter	2.4.2
DC	Direct Current	1.2
DCS	Digital Communication System	2.1
DDS	Direct Digital Synthesis	3.2.2.2
DR	Dielectric Resonator	3.3.1.2
DSP	Digital Signal Processing	1.2
$e(t)$	Error vector caused by mismatch b/n the I&Q reconstruction filters	4.3.2
f_{alias_n}	Centre frequency of the n th alias	3.3.2.1
f_c	Centre frequency	2.2.4.1
f_b	Data bit rate	3.2.2.2
f_{IF}	Intermediate frequency of a multichannel signal	3.3.1
f_k	Centre frequency of channel k	2.2.1
Δf	Frequency offset from centre frequency	2.2.4.1
Δf_{alias}	Separation between adjacent aliases	3.3.2.1
Δf_{cs}	Channel frequency spacing	2.3.1
Δf_T	Filter Transition bandwidth	3.2.2.1
f_{s-mod}	Modulation sampling frequency of a single channel	3.2.1
f_{s-comb}	Combining sampling frequency of a multichannel signal	3.2.1
f_s	Sampling frequency	3.2.2.1
f_{so}	Output sampling frequency - refers to DAC interface	3.3.3.1
FDM	Frequency Division Multiplex	2.2
FFSK	Fast Frequency Shift Keying	3.2.2.1

FFT	Fast Frequency Transform	3.2.2.1
FPGA	Field Programmable Gate Array	3.2.1
FSR	Full Scale Range of a DAC	3.3.1.2
$\overline{g(X)}$	DAC quantisation transfer function	5.2.1
$\overline{g(\overline{X})}$	DAC average quantisation function	5.4
G_{amp}	Gain of an amplifier	2.2.3
GSM	Global Speciale Mobile	2.1
$h(m), h_k$	Impulse response (tap co-efficients) of a digital FIR filter	3.2.1
$H_{cavity}(\Delta f)$	Transfer function of the cavity filter near resonance	2.2.4.1
I	In Phase component of a complex signal	2.4.2.2
$I_{isolator}$	Isolation (Reverse loss) of the ferrite isolator	2.2.3
I_{cavity}	Isolation (Reverse loss) of the cavity resonator	2.2.3
IF	Intermediate Frequency	3.3.1
IL	Insertion loss	2.3.1
IL_{cavity}	Insertion (forward) loss of the cavity resonator	2.2.3
IL_{equ}	Equivalent insertion loss of ($N_{comb}-1$) cavities	2.3.1
$IL_{isolator}$	Insertion (forward) loss of the ferrite isolator	2.2.3
IM	InterModulation	2.2.3
L	Interpolation factor	3.2.1
L_{feeder}	Forward loss of the feeder cable from the TX to the antenna	2.2.3
L_{cable}	Forward loss of the cable in the critical harness.	2.2.3
LFSR	Linear Feedback Shift Register	5.3.1.1
LSB	Least Significant Bit of a binary number	3.2.2.2
LUT	Lookup Table	3.2.2.2
m_{tap}	Number of taps in an FIR filter.	3.2.2.1
MOPS	Millions of Operations Per Second	3.2.2.1
MPT1327	Private Mobile Radio (PMR) trunking system	2.1
MOPS	Million of Operations Per Second	3.2.2.2
n_b	Number of bits or precision of a DAC	3.3.1.2
N_{comb}	Number of channels combined onto one antenna	2.2.4
N_{ch}	Total number of channels within the BW_{sys}	3.2
OS	Oversampling Ratio	3.2.1
$p_G(x), p_U(x), p_T(x)$	Gaussian, Uniform, Triangular PDFs respectively	5.3.1.1
$P_{ant-int}$	Power of interference signal received at the antenna.	2.2.3
P_{av}	Average power of a channel (carrier)	2.4.2.2
P_c	Power of a carrier signal	2.2.3
P_{IM3}	Power of the dominant 3 rd order IM product	2.2.3
P_{N-meas}	Noise power measured with a bandpass filter of bandwidth - BW_{meas}	3.3.1.2
$P_{reflect}$	Reflected power of the reverse interferer incident on the output of the amplifier.	2.2.3
P_{REV}	Power of the reverse interference signal	2.2.3
P_{tav}	Total average power of N channels	2.4.2.2
PA	Power Amplifier	2.2.2
PCS	Personal Communication System	2.1
PDF	Probability Density Function	5.1
PMR	Private Mobile Radio	2.1

$q_e(X)$	DAC quantisation error transfer function	5.2.1
$\overline{q_e(X)}$	DAC average quantisation error transfer function	5.4.2
$q_p(n)$	Polyphase filter impulse response.	3.2.2.1
Q	Quadrature component of a complex signal	2.4.2.2
Q_0	Unloaded Q factor of a cavity resonator	2.2.4.1
Q_L	Loaded Q factor of a cavity resonator	2.2.4.1
$r(t)$	Vector representation of a single channel.	4.3.2
$r_k(n)$	Complex baseband modulated single channel	3.2.1
$r_{k,IF}(m)$	Complex modulated channel, k, residing in its selected channel position	3.2.1
$R(m), R(n)$	Complex baseband multichannel signal - discrete	3.2.1
$R(t)$	Complex baseband multichannel signal - continuous	3.2.1
R_{RES}	Resistance at Resonance	2.3.1
RAM	Random Access Memory	3.2.2.1
RF	Radio Frequency	2.4.1
ROM	Read Only Memory	3.1.2.2
RX	Receiver	1.1
$s_k(t)$	Single modulated channel at an IF	2.2.1
$s(t)$	Single modulated channel at RF	4.3.2
$S(m), S(n)$	Multichannel signal at RF or an IF - discrete time	3.3.1.1
$S(t)$	Multichannel signal at RF or an IF - continuous	3.2
SAR	Sideband Amplitude Rejection Ratio	4.3.2
SAW	Surface Acoustic Wave filter	3.3.2.1
SD	Spectrum Dividing filter	2.2
SF	Shape Factor of a bandpass filter	3.3.2.1
SFDR	Spurious Free Dynamic Range	2.4.2.2
SNR	Signal to Noise Ratio	2.4.2.2
SR	Sideband Rejection ratio	3.3.3.2
t	Peak amplitude of triangular dither	5.3.1.1
TX	Transmitter	1.1
TRX1-8	GSM transmitter classes 1->8	2.2.2
TX-TX _{isolation}	Transmitter to transmitter isolation	2.2.3
$u_1(t)$	Desired signal vector	4.3.2
$u_2(t)$	Desired signal vector, phased 90° to $u_1(t)$	4.3.2
$v_1(t)$	Sideband signal vector	4.3.2
$v_2(t)$	Sideband signal vector, phased 90° to $v_1(t)$	4.3.2
V_{max}	Half the full scale range of a DAC	3.3.1.2
W_n	Total output noise of quantiser when dither is added	5.3.1.2
$x_i(t), x_q(t)$	In Phase and Quadrature components of $r(t)$	4.3.2
$x_{i,k}(n), x_{q,k}(n)$	In Phase and Quadrature components of $r_k(n)$	3.2
$x_I(t), x_Q(t)$	In Phase and Quadrature components of $R(t)$	3.2
x_k	Dither sample	5.3
Y_{ant}	Admittance of the antenna	2.3.1
Y_{equ}	Equivalent admittance of ($N_{comb} - 1$) cavities	2.3.1
Y_{cavity}	Admittance of the cavity filter	2.3.1
Y_0	Characteristic Admittance	2.3.1
Z_0	Characteristic impedance of a transmission line-nominally 50 ohm	2.3.1

$\alpha(f), \alpha$	Gain mismatch between the I & Q paths of the Quad. Upconverter	3.3.3.2
$\beta(f)$	Normalised transfer characteristic of the Quadrature Upconverter	4.3.2
δ_s	Stopband ripple	3.2.2.1
δ_p	Passband ripple	3.2.2.1
Δ	Step size or a LSB of the DAC	3.3.1.2
$\Phi_e(f), \Phi_e$	Phase error between the In Phase and Quadrature Paths (radians)	3.3.3.2
$\theta_k(t)$	Phase modulation of a single channel k at IF	2.2.1
$\theta(t)$	Phase modulation of a single channel	4.3.2
$\phi(t)$	Instantaneous phase of the multichannel signal	3.2
σ^2	Average power or variance of a random variable	5.2.1
μ	Mean value	5.3.1.1

CONTENTS

Abstract	i
Preface	ii
Acknowledgements	iv
List of Principal Symbols and Abbreviations	vi
1 Introduction	1
1.1 The Base Transceiver Station	2
1.2 Organisation of the Thesis	3
2 Base Station Transmitter Architectures	5
2.1 Introduction	5
2.2 Conventional Base Station Transmitter Architectures	6
2.2.1 Modulator	7
2.2.2 Power Amplifier	7
2.2.3 Ferrite Isolators	10
2.2.4 Multicoupling Networks	12
2.2.4.1 Cavity Resonators	14
2.2.4.2 Spectrum Dividing Filters	16
2.3 Limitations of a Conventional Base Station Transmitter	17
2.3.1 Minimum Channel Separation	18
2.3.2 Frequency Flexibility	21
2.3.2.1 Tunable Cavity Resonators	21
2.3.2.2 Dual Window Cavity Combiner	22
2.3.2.3 Hybrid Combining	23
2.3.3 Size	23
2.4 Low Power Combining Base Station Transmitter Architecture.	25
2.4.1 Hybrid Low Power Combining	25
2.4.2 Digital Signal Processing Combining	26
2.4.2.1 Advantages of DSP Combining	27
2.4.2.2 Challenges of DSP Combining	28
2.5 Conclusion	30

3	Multichannel Combining and Upconversion Techniques	32
3.1	Introduction	32
3.2	Multichannel Combining	33
3.2.1	Generation of the Digital Baseband Multichannel Signal	35
3.2.2	Multichannel Combining Applications	37
3.2.2.1	A Trunking Radio System - MPT1327	37
3.2.2.2	A Digital Cellular Radio System - GSM	42
3.2.3	Concluding Remarks on Multichannel Combining	44
3.3	Upconversion Techniques	45
3.3.1	Digital IF Upconversion	45
3.3.1.1	Computation Requirements	46
3.3.1.2	DAC Interface	50
3.3.1.3	Summary	54
3.3.2	Subsampling Upconversion	55
3.3.2.1	The Effect of Output Sampling Frequency	56
3.3.2.2	The Effect of Digital to Analogue Conversion	61
3.3.2.3	Summary	64
3.3.3	Analogue Direct Upconversion - Lowpass Reconstruction	65
3.3.3.1	Computational Requirements	66
3.3.3.2	Linear Errors	67
3.3.3.3	DAC Interface	69
3.3.4	Analogue Direct Upconversion - Bandpass Reconstruction	71
3.3.4.1	The Bandpass Reconstruction Filter	71
3.4	Conclusion	73
4	The Effect of Reconstruction Filters on Analogue Direct Upconversion	76
4.1	Introduction	76
4.2	A Novel Method for the Compensation of Gain and Phase Imbalances	77
4.3	Analysis of Frequency Dependant Imbalances	80
4.3.1	Causes of Frequency Dependant Imbalance in an Analogue Direct Upconverter	80
4.3.2	Mathematical Analysis - The Effect of Filter Mismatch on the Sideband Signal	81
4.4	Analysing the Effect of Mismatched Reconstruction Filters.	85
4.4.1	The Methodology	85
4.4.2	Numerical Computation and Analysis	89
4.4.2.1	Filter Mismatch	89
4.4.2.2	ACI Specification	90
4.4.2.3	Filter Type	91
4.4.2.4	Filter Order	92
4.4.3	Application to GSM or MPT1327 Radio Systems	92
4.5	Bandpass Reconstruction	93
4.6	Conclusion	93

5	Enhancing the Performance of Digital to Analogue Conversion	95
5.1	Introduction	95
5.2	Characteristics of an Ideal and a Practical DAC	96
5.2.1	An Ideal DAC	96
5.2.2	A Practical DAC	98
5.3	Introduction to Dither	99
5.3.1	Review of Dither Techniques	100
5.3.1.1	Probability Density Function	100
5.3.1.2	Scale	102
5.3.1.3	Spectrum	104
5.4	Average Quantisation Transfer Function	104
5.4.1	The Effect of the Scale and PDF of Digital Dither on an Ideal Quantiser.	105
5.4.2	The Effect of the Scale and PDF of Digital Dither on a Practical Quantiser.	107
5.5	Introduction of a Novel Bandlimited Dithering Technique	109
5.6	Conclusion	111
6	Implementation of the Bandlimited Dithering Technique	112
6.1	Introduction	112
6.2	Bandlimited Dithering Architecture	113
6.2.1	Design of the Interpolator	113
6.2.2	PDF Selection for the Dither Generator	116
6.3	Bandlimited Dithering Results	119
6.3.1	Wideband Dither	122
6.3.2	DC Offset Effect	122
6.3.3	An Ideal DAC	123
6.3.4	Dithering Remarks	124
6.4	The Bandlimited Dithering ASIC	124
6.4.1	Halfband Interpolator Design	126
6.4.2	Uniform Dither Generator	127
6.4.3	The Actual Bandlimited Dithering ASIC	129
6.5	Conclusion	130
7	Conclusion	132
7.1	Future Work and Critique	135
Appendices		
A	Parameters Pertaining to Cavity Resonators	137
A.1	Cavity Resonator Insertion Loss	137
A.2	Expression for the Output Admittance of a Cavity Resonator	139
A.3	Lossless Quarter Wave Transformer	140
A.4	Power Transfer at a Parallel Load.	140

B	Interpolation	142
	B.1 Polyphase Realization of an Interpolator	143
	B.2 A Halfband Interpolator	144
C	DAC Survey	146
D	The Carrier to Noise Ratio of a Quadrature Upconverter	148
E	The Schuchman ‘Sufficiency Condition’	151
F	Measurement Testbed	154
	Bibliography	156

List of Included Papers

The Effect of Reconstruction Filter Mismatch in a Digital Signal Processing Multichannel Combiner

DSP Combining and Direct Conversion for Multichannel Transmitters

The Effect of Reconstruction Filters on Direct Upconversion in a Multichannel Environment

An Efficient Implementation of Bandlimited Dithering

Chapter 1

Introduction

Radio system operators require more user capacity to meet the growth in demand for wireless communications. Reducing the coverage area and employing a more sophisticated control of the radio channel are two techniques that are currently employed to increase the capacity. This has direct implications on the design of the base transceiver station (base station), a major component of the radio communication system infrastructure.

A smaller coverage area means that more base stations must be employed. Unless the unit base station cost can be reduced this will result in a proportional increase in the capital investment. With coverage areas shrinking from 5km to 50 meters in radius, it also becomes necessary to make the physical size of the base station as small and unobtrusive as possible.

Future radio communication systems will employ advanced channel control techniques such as dynamic channel assignment, frequency hopping and power control. Base stations should also be easily reconfigured for new frequency plans or new modulation schemes. To cater for all these requirements the base station will have to be more flexible.

This thesis investigates a new base station radio architecture which is more flexible, cheaper, and physically smaller than the present conventional design.

1.1 The Base Transceiver Station

A modern radio base station can be partitioned into four functional entities [13], Fig. 1.1: the Control and Radio Interface (CRI), the modem, the support equipment and the antenna interface.

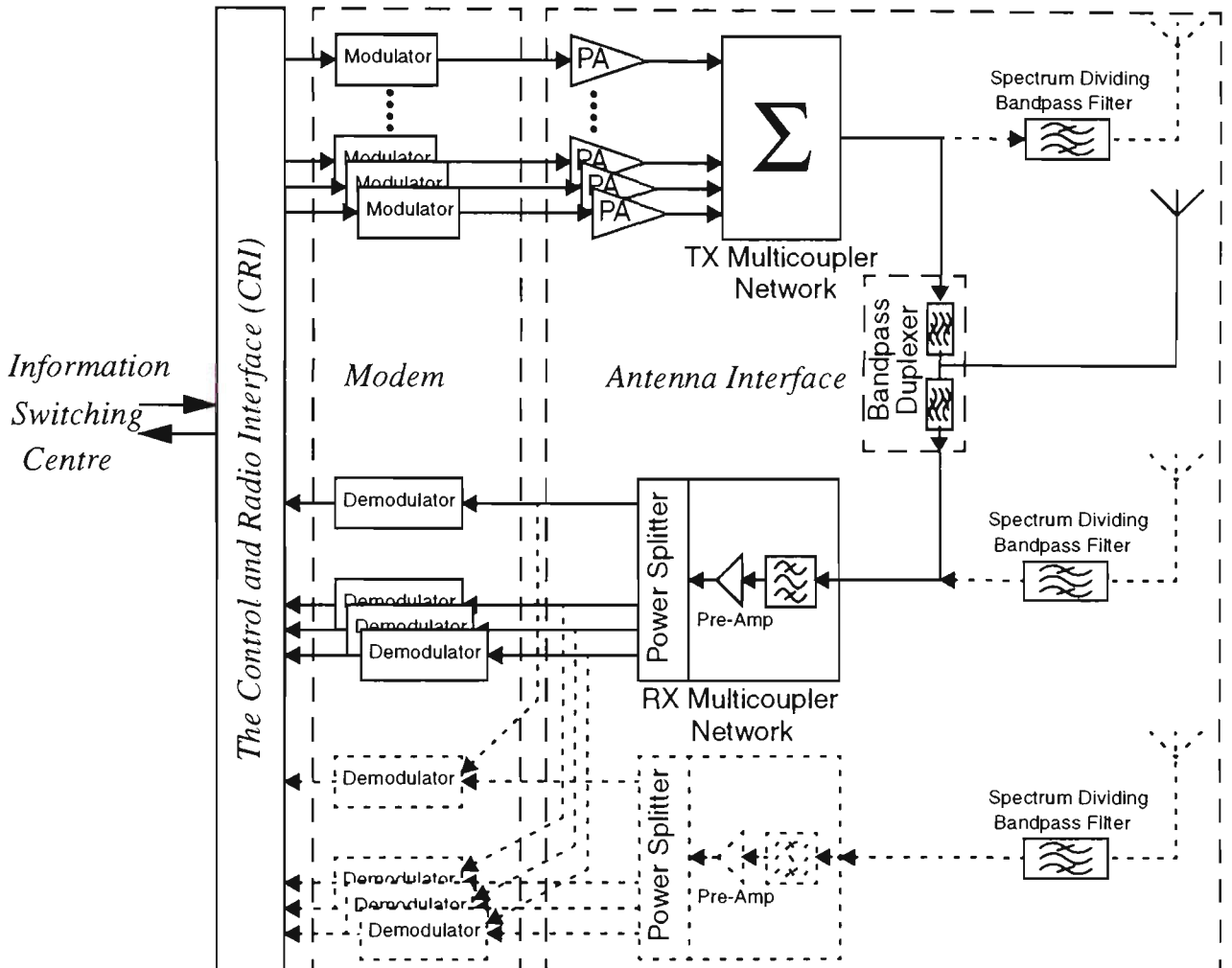


Figure 1.1: *Current Base Transceiver Station Architecture - dotted lines refer to an architecture with separate Transmit and Receive antenna's employing antenna diversity*

The CRI is essentially a software controlled microprocessor that communicates with the information switching centre. It would typically route the incoming data link to the modulators and the demodulators to the outgoing data link. It will also facilitate such functions as monitoring the alarms, interrogating the radio frequency test loop, controlling the output power and remotely configuring the base station.

The modem converts the digital data to and from a modulated radio signal. It consists of a software controlled digital signal processor which modulates a coded input data stream. Coding could include data compression, encryption, error coding and transmission coding. The coding and modulation can be modified by a change in software.

The support equipment consists of AC and DC power supplies, backup batteries and power supply monitoring equipment (not shown in Fig. 1.1).

The antenna interface includes both transmitter (TX) and receiver (RX) Radio Frequency (RF) functions. The receiver is comprised of a bandpass filter followed by a low noise pre-amplifier to make up for the losses of the power splitting network. The performance of the receiver is judged in terms of the noise figure of the RX multicoupling network which can be enhanced by employing space (antenna) diversity (shown dashed in Fig 1.1). The transmitter amplifies each modulated channel before combining these channels together into one signal which is then fed to the antenna. The base station receiver and transmitter sections can have separate antennas or be combined onto a single antenna via a bandpass duplexer.

The TX multicoupling network is responsible for combining the channels onto a single antenna after power amplification (Fig 1.1). It is the major reason for the high cost, large bulk and low flexibility of current base stations. This thesis deals with the development of a low power combining multichannel transmitter that makes the TX multicoupling network redundant.

1.2 Organisation of the Thesis

Chapter 2 reviews the conventional base station transmitter architecture and investigates how each component of the architecture contributes to satisfying the radio system specifications. The cavity resonators which are an integral part of the TX multicoupling network are found to constrain the frequency agility of the architecture and limit the number of channels that can be combined onto one antenna. Their large size and cost also make cavity based architectures unsuitable for future radio communication systems.

Digital Signal Processing (DSP) techniques can be used to combine channels without the need for cavity resonators. The new low power combining architecture offers three significant advantages: increased frequency agility, no restrictions on the number of channels that can be combined, and a dramatic reduction in size. There are a number of technical challenges that need to be met before these advantages can be realised.

Two of these technical challenges, efficiently combining the channels and upconverting the multichannel signal to RF, are explored in Chapter 3. Another major technical obstacle

is the requirement for an ultra-linear wideband amplifier. This will not be considered in the thesis.

Digital signal processing provides flexibility in the combining process, but the computational requirements are shown to be high, and thus must be minimised. This can be achieved by combining the channels at baseband with efficient algorithms which is investigated for radio base station applications using two current radio system standards.

The remainder of the Chapter deals with the upconversion of the baseband multichannel signal to RF. Four upconversion techniques, currently used in single channel applications, are investigated for use in a multichannel environment. A comparison reveals that the analogue direct upconversion technique currently provides the most attractive solution because it requires less computation and a lower performance digital to analogue converter (DAC). The disadvantage with this method is that it requires accurate phase and gain matching in the analogue quadrature circuits.

The reconstruction filters cause frequency dependence in the quadrature circuit. These frequency dependent imbalances, and the effect they have on a multichannel signal, are analysed in Chapter 4. A novel adaptive correction method for these imbalances is also presented. Its main advantages over previous adaptive compensation techniques is that implementation occurs at the lower channel sampling frequency and that frequency dependent imbalances can be corrected.

Multichannel radio systems can only tolerate very low harmonic and intermodulation (IM) products. The Digital to Analogue Converter (DAC) is a major source of these spurious responses which can be reduced by adding a dither signal to the multichannel signal prior to quantisation. This issue is discussed in Chapter 5.

Chapter 6 presents a new technique for implementing bandlimited dither. The technique improves the performance of the DAC by 2 to 4 dB, with a minimal increase in hardware. Measurements highlight the benefits of the bandlimited technique over the more traditional wideband techniques. The dithering algorithm was also implemented on an integrated circuit.

Chapter 7 concludes the thesis and suggests areas for further research.

Chapter 2

Base Station Transmitter Architectures

2.1 Introduction

Early wireless communication systems, TV and radio, used a single antenna per transmitter. The rapid growth of TV and radio through the 60's and 70's, and mobile radio in more recent times, placed enormous pressure on finding suitable transmission sites, especially in high density areas. The expansion of radio systems also saw the increase in antenna structures, which started to come under attack from the populace for aesthetic reasons.

Multiple antenna sites created technical difficulties from the point of view of spurious, intermodulation and noise emissions. This invariably resulted in the blocking or desensitising of the co-sited receivers which led to a degraded system performance. The sum of all these pressures resulted in the science of antenna combining (multicoupling), which is the transmission of a number of similar frequency channels through a single antenna.

Initially many unique solutions were implemented to match the numerous systems in existence. More recently however, systems have tended to be designed from the multicoupling perspective, and it is therefore possible to introduce a generic architecture. System parameters will still vary for different systems and across the electromagnetic spectrum.

Two different systems have been chosen as examples of typical radio communication systems.

- MPT1327 is a Private Mobile Radio (PMR) trunking system that was developed by Philips (UK), and adopted in Australia. PMR trunking systems are utilised by private users, such as taxi, train, and fleet orientated specialists, or by the public emergency service sector, such as the police, ambulance, fire, electricity and water providers.
- Global System for Mobile communication (GSM) is a digital cellular European standard that has been adopted by a large number of countries, including Australia. It is already in operation in the 900 MHz band. A system with a virtually equivalent specification has been designed for the 1800 MHz band, and more recently the 1900 MHz band in the USA. This system is called DCS or Personal Communication System (PCS).

Section 2.2 introduces the main components of the conventional base station transmitter architecture, and describes how each contributes to the architecture satisfying the radio system design specifications. The multicoupling network is shown to limit the performance of the architecture in terms of flexibility, size and minimum channel separation. These limitations will be explored further in the Section 2.3.

Section 2.4 introduces both an analogue and digital low power combining architecture which makes the high power multicoupling network redundant; the digital solution is shown to be more flexible than the analogue solution. The remaining Section of this Chapter discusses the advantages and technical challenges of the low power combining digital signal processing architecture. The technical challenges provide the basis for the thesis.

2.2 Conventional Base Station Transmitter Architectures

A typical base station transmitter has a channelised architecture that complements a Frequency Division Multiplex (FDM) communication system. That is, each channel undergoes separate modulation and amplification before being combined onto a single antenna.

The basic elements that make up the architecture are a modulator, amplifier, ferrite isolator, cavity resonator and the spectrum dividing (SD) filter. Figure 2.1 illustrates how these basic building blocks are combined to make up the transmit path of a base station.

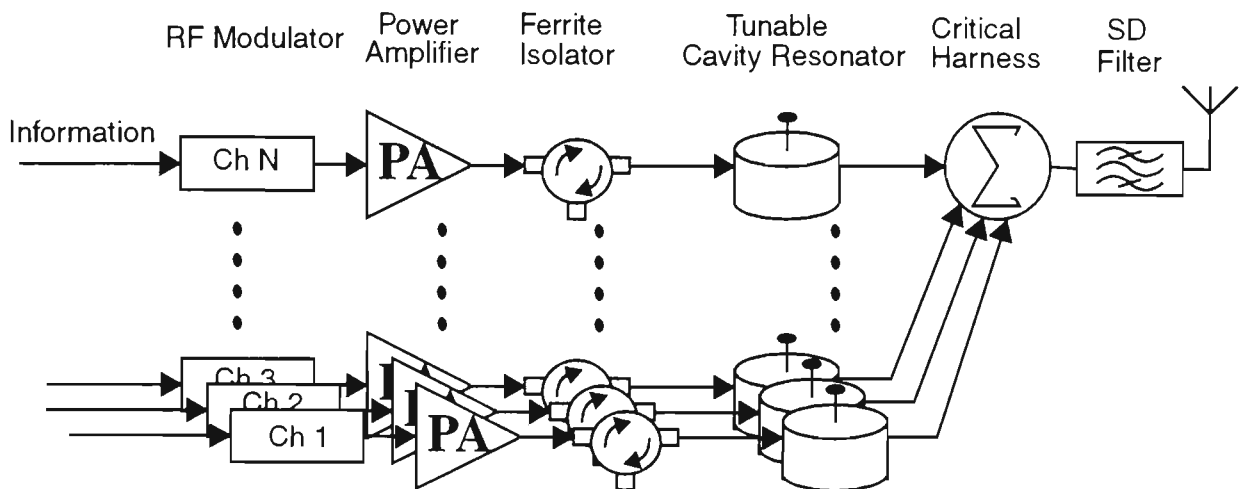


Figure 2.1: *Conventional multicoupling base station transmitter architecture.*

2.2.1 Modulator

The modulator encodes the source information onto a bandpass signal with a centre frequency of f_k . The generic single modulated channel can be written as:

$$s_k(t) = a_k(t) \cos(2\pi f_k t + \theta_k(t)) \quad (2.1)$$

where $a_k(t)$ is the amplitude modulation, f_k represents the centre frequency of the channel, and $\theta_k(t)$ the phase modulation.

2.2.2 Power Amplifier

The Power Amplifier (PA) increases the level of the modulated signal whilst limiting the amount of distortion generated. The distortion allowed is set by the specifications of the radio system. This specification covers the region of the spectrum within the channel being amplified, 'in channel', and also the region adjacent to the channel in question, 'out of channel'.

The effect of 'in channel' distortion will be to degrade the noise margin of the link. This is very important in low noise margin systems with dense signal constellations, such as satellite and fixed microwave links, but has little effect on the performance of mobile systems that require higher noise margins to overcome fading and interference effects.

Very stringent requirements apply to 'out of channel' distortion in all wireless systems. If a given channel is unoccupied, a receiver listening to that channel should not detect a

signal. ‘Out of channels’ signals must therefore be tightly controlled. The specification of the spectrum resulting from the modulation and amplification is usually given in the form of a modulation mask. Examples of modulation masks for a trunking radio system, MPT1327, and a cellular radio system, GSM, are shown in Fig. 2.2(a) and Fig. 2.2(b).

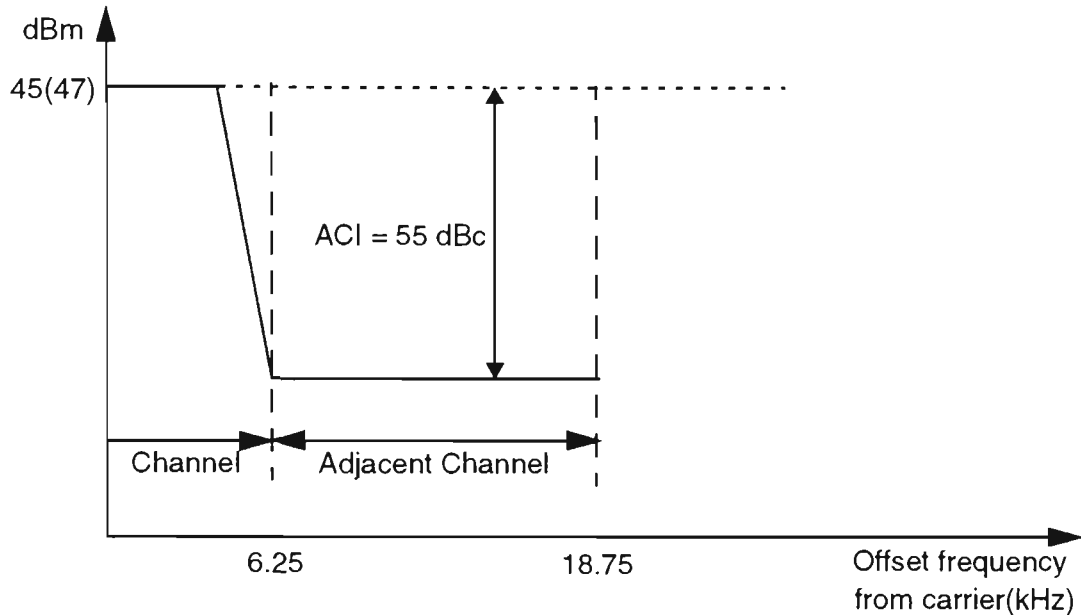


Figure 2.2(a) : *MPT1327 modulation mask for 12.5 kHz channel spacing and 50 W (47 dBm) average output power. The measurement bandwidth is 8.5 kHz (45 dBm) [11].*

Note that the modulation mask is most important in the region of the carrier. The multicoupling network will have little or no control in this region. The primary role of the mask is then to specify the allowable Adjacent Channel Interference¹ (ACI). The vertical axis on Fig. 2.2(a) shows the total power level of the channel written in the parenthesis, whilst the other value is derived from the fact that the measurement filter is specified as having 8.5 kHz bandwidth. Consequently, if we assume that the whole channel is equally activated, only a proportion (8.5/12.5) of the actual power will be measured using this filter.

The ACI specification for the trunked radio system is very stringent, 55 dBc from Fig. 2.2(a). This is due to the near-far² problem where the physical location of each base station is uncontrolled and where higher power levels are used to broadcast signals across large areas (compared to cellular systems).

1. The adjacent channel interference refers to “that part of the total power output of a transmitter under defined conditions of modulation, which falls within the specified passband centred on the nominal frequency of that of the adjacent channels. This power is the sum of the mean power produced by the modulation, hum and noise of the transmitter” [11]

2. The near far problem is simply due to geographical location of the mobile user. If a user is close to the base station and the base station is transmitting a signal to another mobile some distance away (i.e. high power levels) then the situation could arise whereby the spurious signals generated would be of a sufficient level to open the mute of another mobile listening at a completely different frequency (or system).

Cellular systems, Fig. 2.2(b), allow for a weaker ACI specification of 30 dBc, primarily due to the controlled nature of their operation. That is, blocks of frequency are allocated to a specific system, and the use of frequency planning means that adjacent channels are not transmitted concurrently in the same basestation (cell). Neighbouring channels (2 or more channels from the carrier centre frequency) are well protected. For these channels the specification becomes between -60 dBc and -70 dBc.

Different power classes of transmitters are also highlighted in Fig. 2.2(b). GSM specifies 8 classes ranging from TRX 1 (55 dBm) through to TRX8 (34 dBm). This accounts for different cell sizes, ranging from large cells (TRX 1) to small cells (TRX 5) and down to micro cells (TRX 8). The base station can also utilise downlink RF power control. This consists of 15 power steps in 2 dB increments (30 dB), and has the effect of incrementally moving the mask through the shaded area as shown in Fig. 2.2(b). The measurement bandwidth for GSM is specified as 30 kHz and power levels using this bandwidth are shown prior to the parenthesis.

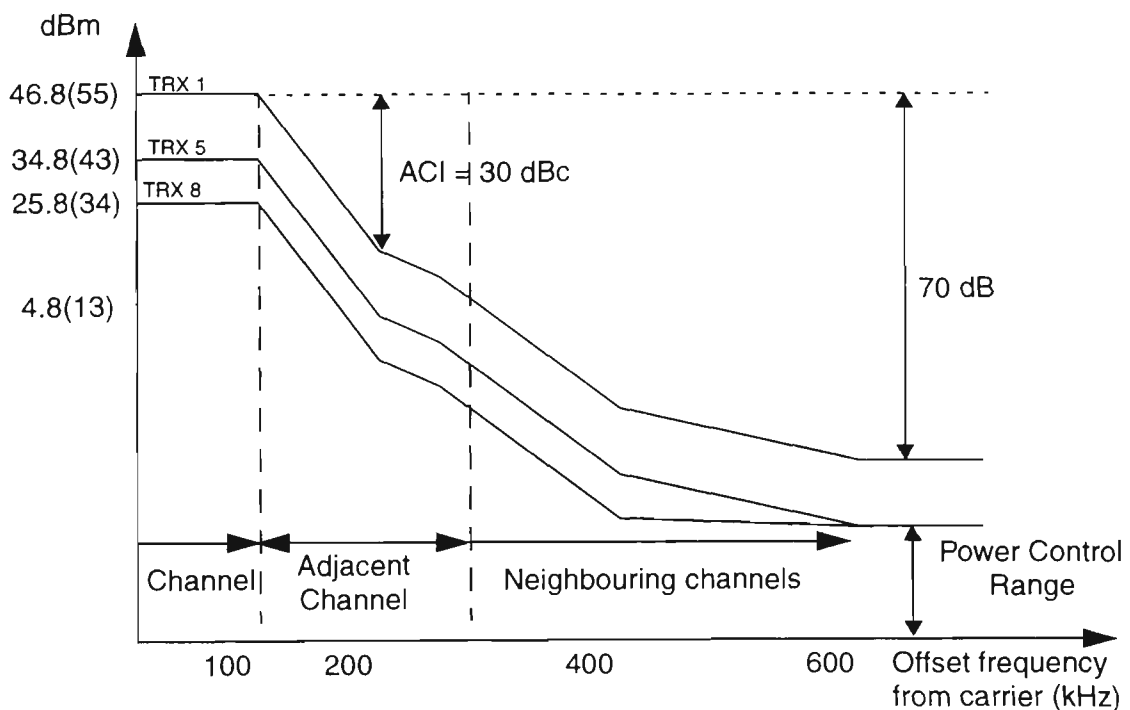


Figure 2.2(b): GSM modulation masks for three transmitter power output classes; TRX 1 - 320W (55 dBm), TRX 5 - 20 W (43 dBm), TRX 8 - 2.5 W (34 dBm). The measurement bandwidth is 30 kHz [9].

2.2.3 Ferrite Isolators

Reverse leakage can allow signal power from transmitters on the same combining network, or signal power directly received from the transmitting antenna, to enter the output of another channel's power amplifier. The mixing of the wanted and reverse interference signals in the power amplifier will generate unwanted InterModulation (IM) products. A vital component in the protection of the power amplifier from the reverse interferer is the unidirectional characteristic of the ferrite isolator.

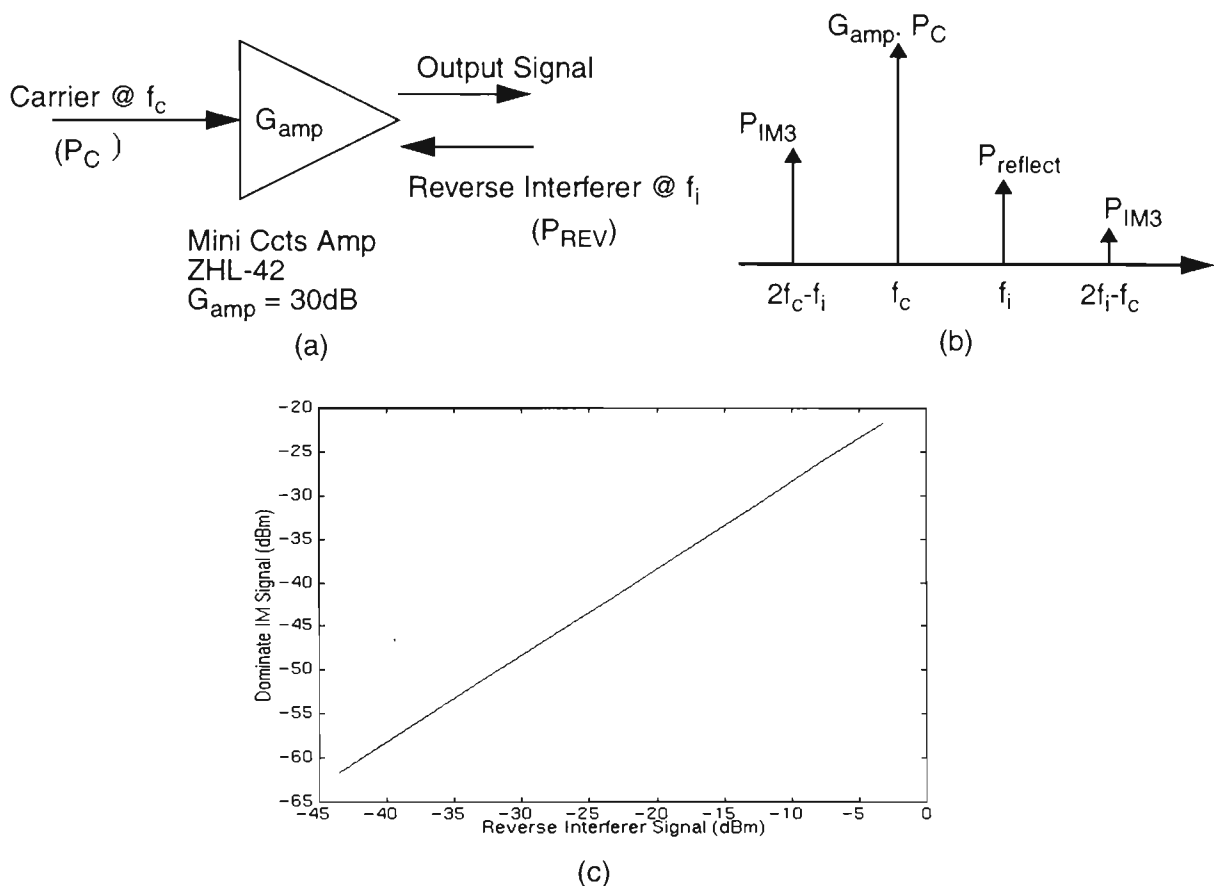


Figure 2.3: (a) Reverse interferer arriving at the output of the amplifier and mixing with the carrier to create an output spectrum consisting of IM products. (b) Spectrum of the amplifiers output signal (c) Reverse interferer (P_{REV}) plotted against the dominant third order intermodulation product (P_{IM3}). Class A amplifier operated at its 1 dB compression point, $G_{amp} \cdot P_C = 30\text{ dBm}$.

The ferrite isolator attenuates the amplified signal, travelling in the forward direction, by a nominal amount ($\sim 0.5\text{ dB}$), whilst the interfering signal, travelling in the reverse direction, is significantly attenuated ($\sim 25\text{-}50\text{ dB}$ [14]). The amount isolation is related directly to the intermodulation attenuation³ specification, which is specified as 70 dBc for both the GSM and MPT1327 radio systems.

3. Intermodulation Attenuation "is a measure of the capability of the transmitter to inhibit the generation of signals in its non-linear elements, caused by the presence of the carrier and an interfering signal reaching the transmitter...." [11].

Calculation of the exact amount of isolation requires knowledge of the relationship between the return interfering signal level and the resulting intermodulation product level at the output of the amplifier. Fig. 2.3(a) illustrates the situation more precisely assuming that the amplifier has a dominant third order characteristic. The amplifier's output signal, Fig. 2.3(b), consists of a wanted carrier P_C , amplified by the gain factor G_{amp} , an interferer $P_{reflect}$, which is directly related to the output reflection coefficient of the amplifier, and the third order products P_{IM3} , caused through the mixing of these two signals.

The relationship between the reverse interferer, P_{REV} , and the dominant third order intermodulation product, P_{IM3} , was measured for a 'Mini Circuits' class A amplifier with a rated output power of 30 dBm. This is plotted in Fig. 2.3(c) and it shows that the relationship can be accurately written as:

$$P_{IM3} = P_{REV} - 18 \text{ dB} \quad (2.2)$$

Thus to achieve an intermodulation specification of 70 dBc (-40 dBm), the reverse travelling signal incident on the amplifier must be no larger than -22 dBm.

There are two possible sources of interfering signals: those that come from transmitters on the same combining network, and those directly received from the transmitting antenna. For the transmitters on the same combining network, the amount of reverse power arriving at the transmitter in question is:

$$P_{REV} = P_C + G_{amp} - TX-TX_{isolation} \text{ dBm} \quad (2.3)$$

where the transmitter to transmitter isolation, $TX-TX_{isolation}$, is given by the following formula [14]:

$$TX-TX_{isolation} = IL_{isolator} + IL_{cavity} + I_{cavity} + I_{isolator} + L_{cable} + 6 \text{ dB} \quad (2.4)$$

where $IL_{isolator}$, IL_{cavity} = the insertion loss of the isolator and cavity, L_{cable} = cable losses and $I_{isolator}$, I_{cavity} = isolation of the ferrite isolator and cavity filter. Given that the carrier input power is 0 dBm and the gain is 30 dB, then from Eqn. (2.3) the amount of $TX-TX_{isolation}$ required is 52 dB.

Similarly, for signals arriving from the antenna, the amount of reverse power arriving at the transmitter is:

$$P_{REV} = P_{ant-int} - ANT-TX_{isolation} \quad (2.5)$$

where $P_{ant-int}$ is the interference power received at the antenna and the amount of antenna to transmitter isolation is given by:

$$ANT-TX_{isolation} = I_{cavity} + I_{isolator} + L_{feeder} + L_{cable} \text{ dB} \quad (2.6)$$

where L_{feeder} = the loss of the feeder. Given that the typical test interferer power received at the antenna [11], $P_{ant-int}$, is -30 dBc (0 dBm), the amount of $ANT-TX_{isolation}$ calculated from Eqn. (2.5) is 22 dB, significantly lower than the required $TX-TX_{isolation}$.

The amount of $TX-TX_{isolation}$ required for the GSM or MPT1327 (same intermodulation attenuation specification) multichannel systems is therefore determined from a neighbouring transmitter on the same combining network. The value, 52 dB, calculated is somewhat small compared to the 70-80 dB of $TX-TX_{isolation}$ quoted as a typical requirement [14]. The difference can be attributed to the use of higher power amplifiers with class C output stages and a more stringent intermodulation specification.

For the class C amplifier the dominant intermodulation product is typically only 6 dB smaller than the reverse interference signal. Eqn. (2.2) is subsequently modified for a class C amplifier such that the amount of $TX-TX$ isolation required is 64 dB. This value will be further increased for a more stringent intermodulation specification such as that defined for the maximum spurious level (this is discussed Section 2.2.4.2).

The ferrite isolator is a very important device in the conventional base station architecture because it is used to provide a significant proportion of the required 70-80 dB of $TX-TX$ isolation. Only small quantities of isolation are contributed by the other components of the $TX-TX$ isolation equation, Eqn. (2.4).

2.2.4 Multicoupling Networks

The multicoupling network combines the individual transmitters onto a single antenna. It consists of high Q cavity resonators coupled together with a critical harness, Fig. 2.4(b). The cavity resonators are typically two pole bandpass filters which perform the role of reducing intermodulation products, out of band transmitter noise and spurious products from the transmitter section. They also provide some isolation between adjacent channels, Fig. 2.4(a), but this is less than the contribution from the ferrite isolators.

The number of channels combined onto one antenna (N_{comb}) is dependent on the system. For the GSM cellular system, with a cell reuse factor of 3 and cells that are split into 3 sectors, then each sector antenna will only be assigned 1/9 of the total channels available in the system. For a system bandwidth of 5 MHz and a 200 kHz channel separation, this directly computes to 3 combined channels per sector. Currently, a fully configured GSM cell site has 4 channels combined onto one antenna. However, in the future, the introduction of frequency hopping will decrease the cell reuse factor, subsequently increasing the number of channels combined on to the antenna. On the other hand, the combining requirements for the MPT1327 system are inherently limited by the minimum transmitter spacing of the cavity combining networks; for a 12.5 kHz trunking system the minimum transmitter separation is approximately 200 kHz. Thus it is possible that up to 25 channels could be activated across a 5 MHz bandwidth, although current systems typically combine between 5 and 10 channels.

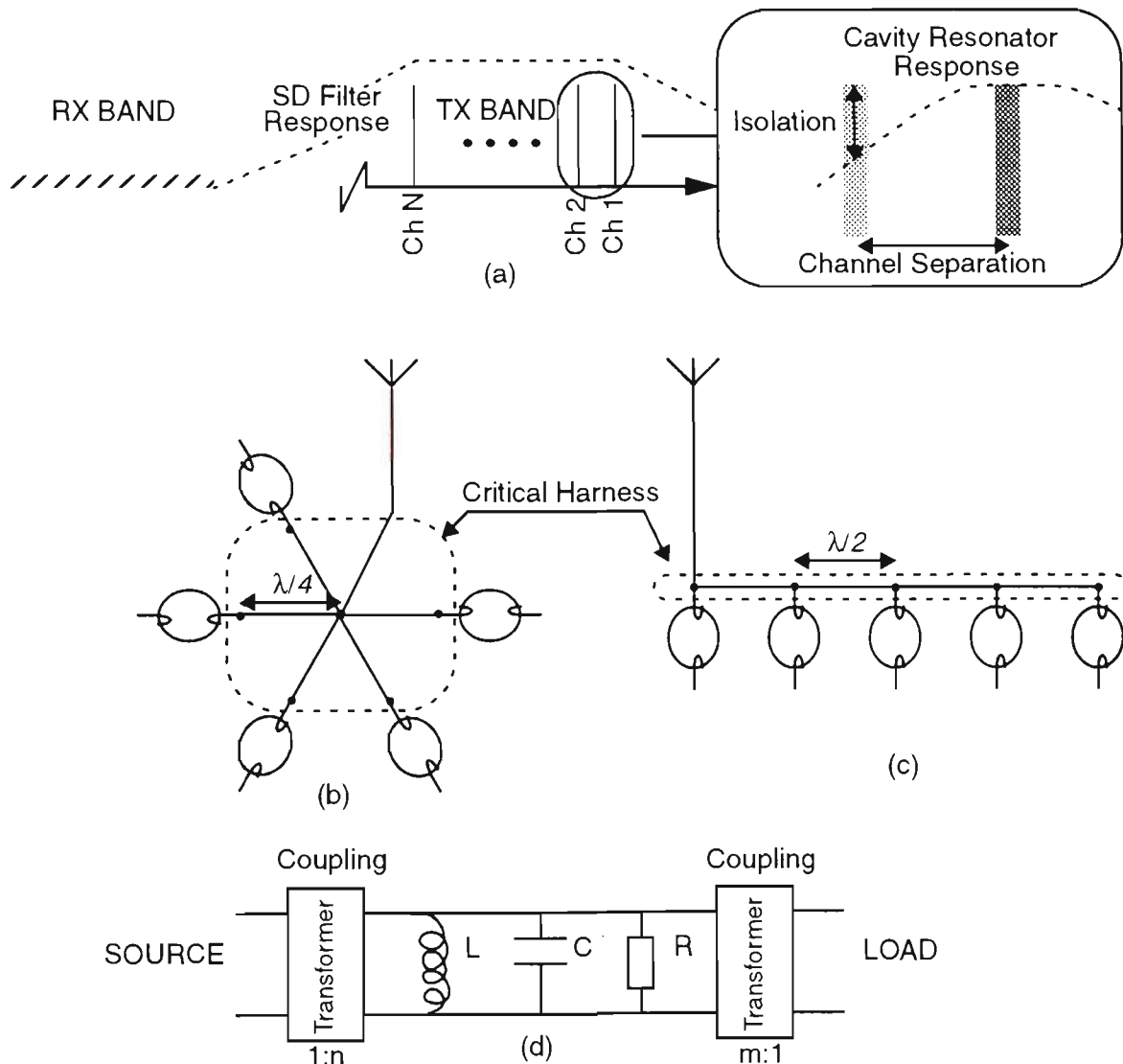


Figure 2.4: (a) The response of the Cavity Resonators and Spectrum Dividing (SD) filters. (b) & (c) illustrate two common critical harness configurations. (d) Model of a cavity resonator near resonance.

Once combined, and as a final measure to ensure that no interference problems will exist, the signal passes through another cavity resonator covering the total transmitter bandwidth. This resonator is used to reduce the transmitter's noise floor (consisting of broadband noise and spurious products [2]) so that there will be no interaction with other systems or nearby receivers, which may or may not be connected to the same antenna. They are commonly referred to as Spectrum Dividing (SD) filters since they isolate different segments of the spectrum (as shown in Fig. 2.4(a)).

2.2.4.1 Cavity Resonators

As depicted in Fig. 2.1, each amplified channel is fed into a cavity resonator which is manually tuned through the means of a tuning stub or screw. The output of each cavity filter is then coupled into a single output through a critical harness. The critical harness acts as an impedance transformer, so that the cavity only loads the antenna when resonant.

The behaviour of a cavity resonator is analogous to that of a parallel resonant circuit, Fig. 2.4(d), in the vicinity of resonance, with very high Q values (high selectivity) and low insertion loss. Coupling into and out of the cavity is modelled as an ideal transformer. At resonance both the source and load see an impedance that is dependent on the coupling coefficient into and out of the cavity. It will not be necessarily matched to the source or load impedances.

The transfer function, $H_{\text{cavity}}(\Delta f)$, of the resonator can be approximately modelled near resonance as:

$$|H_{\text{cavity}}(\Delta f)| = 10 \log (1 + (2\Delta f / BW_{\text{cavity}})^2) \text{ dB} \quad (2.7)$$

where Δf is the offset from the centre frequency, f_c , and BW_{cavity} is the 3 dB bandwidth of the cavity. The bandpass response will suppress the IM products, broadband noise and spurious products, but it is not selective enough to affect the responses in the adjacent channel or neighbouring channels (as mentioned in Section 2.2.2).

The selectivity of the resonator is directly related to the loaded Q, Q_L , of the cavity:

$$Q_L = f_c / BW_{\text{cavity}} \quad (2.8)$$

Q_L must be a large value to obtain sufficient selectivity at UHF frequencies, i.e. for

$BW_{\text{cavity}} = 600 \text{ kHz @ } 900 \text{ MHz}$ for GSM, $Q_L = 1500$. Given that the insertion loss of the cavity is approximately (see Appendix A.1):

$$IL_{\text{cavity}} = -20 \log (1 - Q_L / Q_0) \text{ dB} \quad (2.9)$$

The unloaded Q (Q_0) must be significantly greater than Q_L . To keep the insertion loss lower than 1 dB, Q_0 must be at least a factor of 8.2 greater than Q_L . The design of cavities is therefore based around attaining large values of Q_0 . Q_0 is fundamentally defined as:

$$Q_0 = 2\pi f \cdot \text{energy stored} / \text{power dissipated} \quad (2.10)$$

The volume and the surface area are the mechanisms that store and dissipate energy respectively. Therefore, the dimensions of the cavity, the use of high quality materials (such as silver or copper) and the use of advanced fabrication techniques [15] are important parameters to achieve large Q_0 values. As a result, high quality cavities are expensive, voluminous and heavy.

In the UHF band, the most common kind of cavity is the quarter wavelength coaxial cavity, operating in TEM mode [3]. These cavities achieve good temperature stability, high unloaded Q (Q_0) values of between 5000 - 10,000 and are relatively compact.

At lower radio frequencies i.e. the VHF band, where the physical size of a quarter wavelength cavity becomes large, electrically short coaxial cavities, helical resonators and lumped LC circuits (although these are only practical at the lower end of the VHF spectrum) become favourable. Helical resonators usually provide Q_0 factors of up to 1000. They can also be used at higher frequencies where they usually perform as wideband spectrum dividing filters.

More recently, high temperature (70K-100K) superconductor technology has been developed for cavity filter applications. The surface resistance of such a resonator is a factor of a thousand times smaller than copper. This translates into Q_0 values of 40,000 or more (low insertion loss). The Q_L value is correspondingly higher (high selectivity) and the physical size is about one-sixth of copper cavity filters[12]. However, the cost and the need for a complex cooling system are sufficient obstacles to its universal use in the short term at least.

2.2.4.2 Spectrum Dividing Filters

The spectrum dividing filter follows the physical channel combination stage. It serves to attenuate broadband noise and spurious emissions generated by all the prior processes. Spurious emissions are “emissions at frequencies other than those of the carrier and sidebands associated with normal modulation” [11]. They are usually specified as an absolute power level (nominally 0.25uW) measured in a certain measurement bandwidth, and are a more stringent requirement than either the spectrum mask or intermodulation attenuation specifications. Additionally, spurious levels are specified at large frequency offsets from the carrier, as depicted in Fig. 2.5(a).

Both Figs. 2.5(a) and (b) are normalised to a measurement bandwidth, 30 kHz and 8.5 kHz for GSM and MPT1327 systems respectively. The power is written with respect to the measurement bandwidth, whilst the power figure given in the parenthesis indicates the total output power of the channel. Note that the spurious emission level specification takes precedence over the other specifications. For example, if power control was implemented for GSM, the lowest level for which the 8th class transmitter (TRX 8) could take would be 4.8(13) dBm. Interference into neighbouring channels should be below -55.2(-47) dBm as defined by the modulation mask, Fig. 2.5(a), a level substantially below that of the specified spurious emission level, -41.2 dBm. It is in this situation that the less stringent spurious emission specification would apply.

The spurious emission level specification sets the transmitter’s out of band noise floor which permits the operation of co-sited receivers without degradation when the transmitters are turned on. This is particularly important when the transmitter and receiver are duplexed to the same antenna, as shown in Fig. 2.5(c). The bandpass duplexer achieves isolation between the receive and transmit paths through the use of bandpass (SD) filters so that the transmit energy will not desensitise the receiver. A typical requirement in the transmit path would be for 1 dB insertion loss and 60 dB of isolation [3]. Both coaxial cavity or helical resonators are used as SD filters.

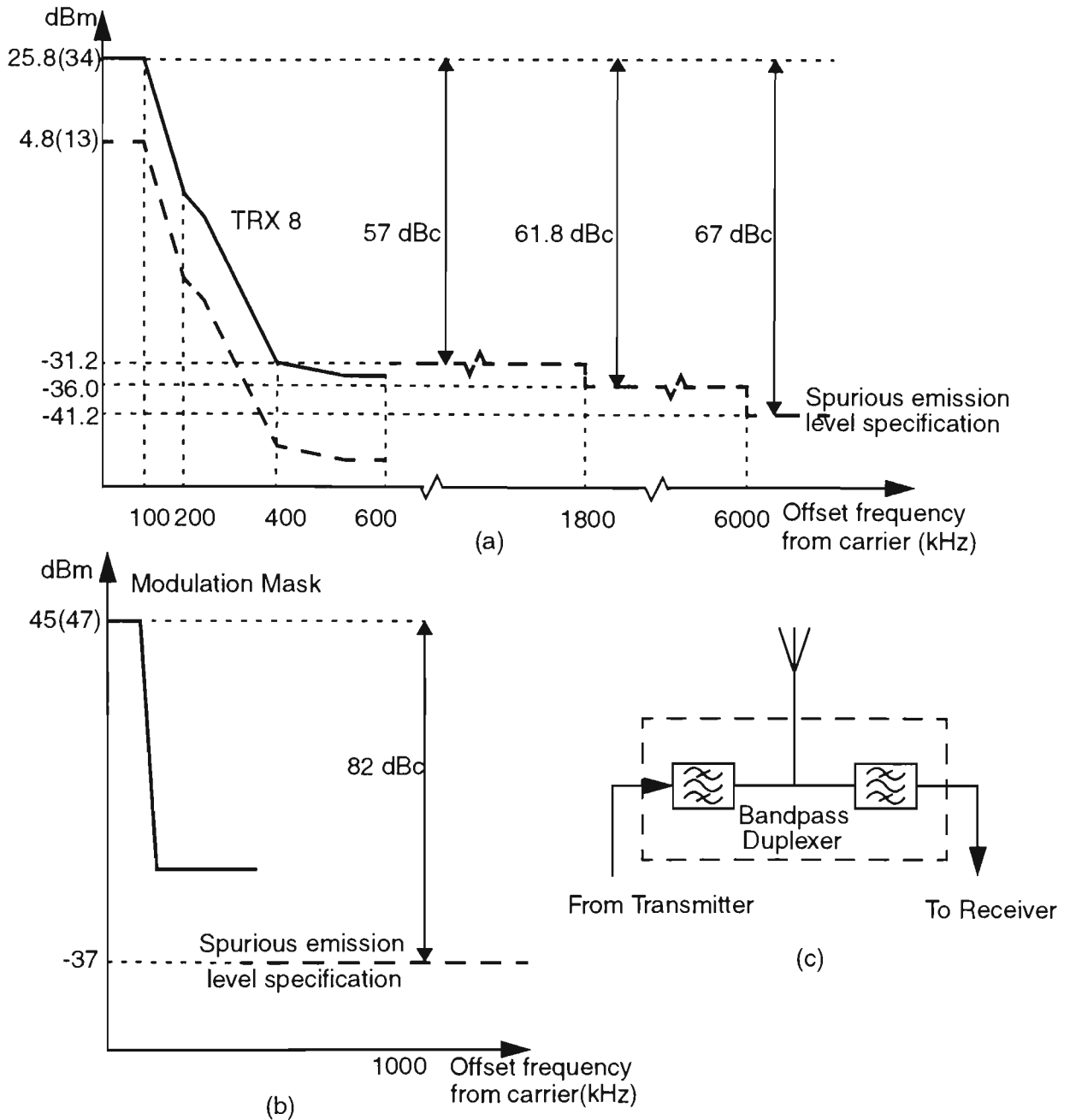


Figure 2.5: (a) GSM modulation mask and spurious emission level normalised to a measurement bandwidth of 30 kHz [9]. (b) MPT1327 modulation mask and spurious emission level normalised to a measurement bandwidth of 8.5 kHz [11]. (c) Spectrum dividing (SD) filters used in a bandpass duplexer.

2.3 Limitations of a Conventional Base Station Transmitter

The high power cavity filter is central to the success of the base station design, however, the cavity filter also introduces the following limitations, the minimum channel separation, the limited frequency flexibility and the large size. These will now be discussed with reference to both current and future wireless systems.

2.3.1 Minimum Channel Separation

Future wireless systems have requirements that are based around frequency agility, frequency hopping and dynamic channel allocation. Many more channels will therefore have to be available for transmission, although not necessarily all at the same time. The nature of cavity resonators place fundamental restrictions on the minimum channel separation, which limits the number of channels that can be combined onto a single antenna. As the channel spacing between the cavities is reduced the insertion (power) loss increases and the isolation between adjacent transmitters ($TX-TX_{isolation}$) decreases.

As the channel spacing is reduced, the isolation between transmitters will decrease assuming that the cavity is operating at a fixed Q_L . Ferrite isolators can be used to compensate for the lost isolation however, it is the problem of increasing insertion loss due to cavity loading of closely spaced transmitters that is more serious.

It is assumed that N_{comb} channels are to be combined onto a single antenna. As illustrated in Fig. 2.6(a), each transmitted channel gets fed through an isolator, cavity resonator and quarter wavelength line, before being combined at a common point. The quarter wavelength line acts as an impedance transformer (see Appendix A.3).

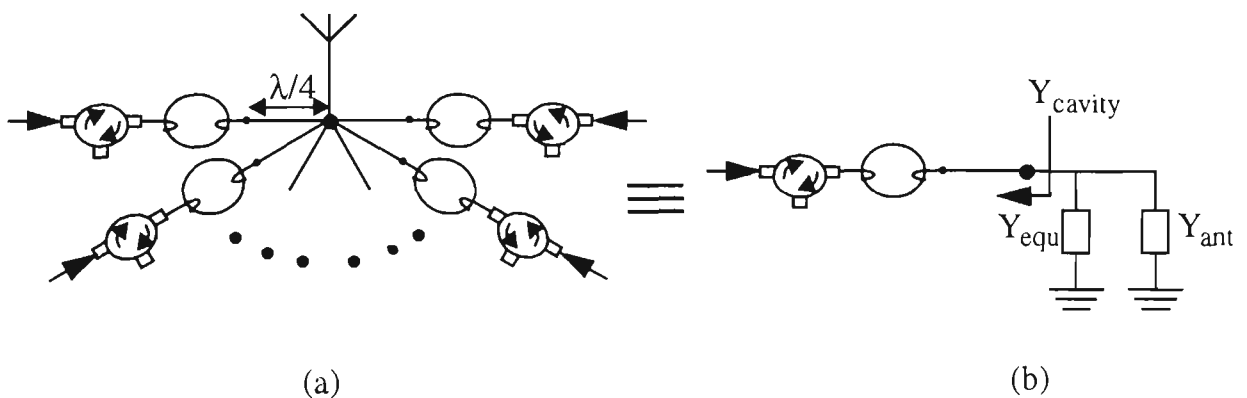


Figure 2.6: (a) Multicoupling N channels onto a single antenna (b) equivalent circuit

The coupling of the cavity is assumed to be arranged so that the output admittance of the cavity is matched at resonance (special case of Appendix A.2 where $R_{RES} = Z_0$). The admittance, as a function of Δf , of a single cavity looking from the junction point (i.e. after the quarter wave transformation) is given by:

$$\begin{aligned}
 Y_{cavity} &= Y_o^2 / Y_{out} = (1/Z_o)^2 / ((1 + 2\Delta f / BW_{cavity}) / Z_o) & (2.11) \\
 &= (1 - j 2\Delta f / BW_{cavity}) / Z_o(1+(2\Delta f / BW_{cavity})^2)
 \end{aligned}$$

The equivalent circuit has been drawn such that the network is under consideration at the resonant frequency of one of the cavity resonators. Therefore, the admittance of the resonant cavity, Y_{cavity} , is equal to $1/Z_0$ (from Eqn. (2.11) when $\Delta f=0$). The antenna is also assumed to be matched to the characteristic impedance, Z_0 , whilst Y_{equ} refers to the equivalent admittance of the remaining $(N_{comb}-1)$ cavities (Fig. 2.6(b)).

The amount of insertion loss that the channel under consideration undergoes is equal to the insertion loss of the cavity itself ($\mathbb{I}L_{cavity}$ as defined in Eqn. (2.8)) and the insertion loss caused by the power absorbed in Y_{equ} (see Eqn. (A.22) in Appendix A.4). Total insertion loss is therefore defined as:

$$\mathbb{I}L = 20 \log(1 - Q_L / Q_0) + 10 \log((1+\Gamma)(1+\Gamma)^*) \text{ dB} \quad (2.12)$$

where the reflection coefficient is given by (see Eqn. (A.17) in Appendix A.4):

$$\Gamma = -Y_{equ} / (2Y_0 + Y_{equ}) \quad (2.13)$$

When only one resonant cavity is connected to the antenna, $Y_{equ} = 0$ and the total insertion loss is given by that of the cavity itself. The effect of adding more and more cavities to the antenna results in Y_{equ} being non zero as described below:

$$Y_{equ} = \sum_{n=1}^{(N_{comb}-2)/2} Y_{cavity}(n \cdot \Delta f_{CS}) + Y_{cavity}(-n \cdot \Delta f_{CS}) + Y_{cavity}\left(\frac{N_{comb}}{2} \cdot \Delta f_{CS}\right) \quad N_{comb} \text{ even} \quad (2.14a)$$

$$Y_{equ} = \sum_{n=1}^{(N_{comb}-1)/2} Y_{cavity}(n \cdot \Delta f_{CS}) + Y_{cavity}(-n \cdot \Delta f_{CS}) \quad N_{comb} \text{ odd} \quad (2.14b)$$

where Δf_{CS} is the channel spacing. Thus, the effect of combining more and more channels to one antenna has a significant effect, especially when the channel spacing is reduced. This is depicted in Fig. 2.7(a).

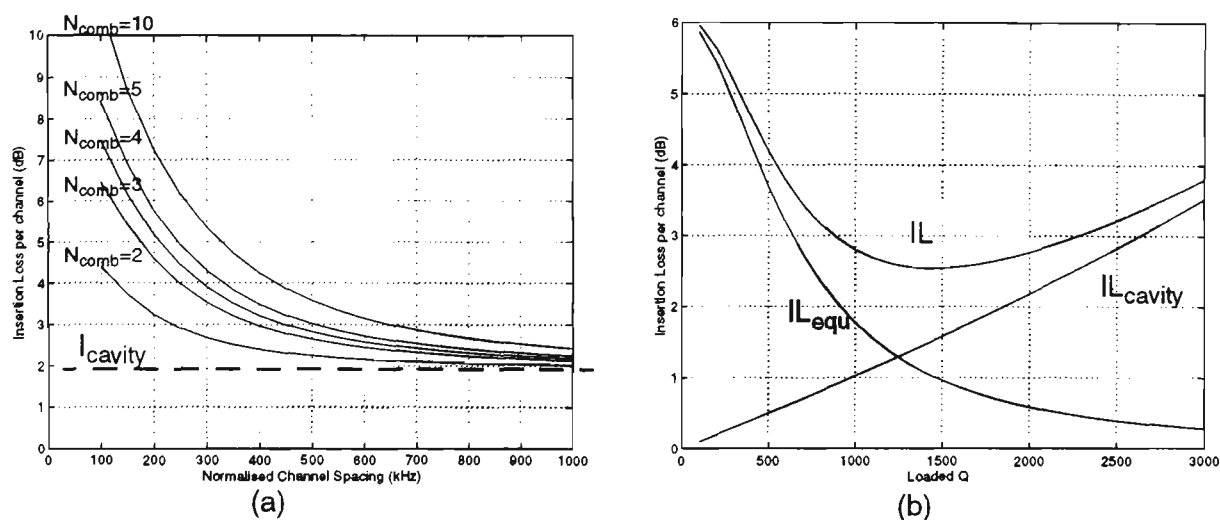


Figure 2.7: (a) Total insertion loss (IL) for N_{comb} combined channels. System parameters $Q_0 = 9000$, $f_0 = 450$ MHz & $Q_L = 1800$ (b) Total insertion loss (IL) = $IL_{cavity} + IL_{equ}$ as a function of the Loaded Q . $N=3$ and channel spacing = 500 kHz.

In the case when the channels are spaced by large frequencies, Y_{equ} will be negligible (i.e. open circuit for all resonators at the frequency of consideration) and the additional insertion loss will also be small. As the channel spacing is reduced, the adjacent cavity circuits will take on finite values of impedance rather than look like open circuits. This creates a mismatch at the junction causing both reflection of power and power being absorbed by the loading of the other cavity circuits. The overall effect is that less power will arrive at the antenna.

As the channel spacing is further reduced the effect is amplified. Immediately adjacent channels have a more significant effect on Y_{equ} , and the other neighbouring cavity circuits also begin to make contributions. Fig. 2.7(a) shows that the insertion loss rises rapidly as the channel spacing is reduced. The effect is further pronounced as more channels are combined onto a single antenna.

The coupling into the cavity was assumed for all previous calculations to be fixed for all cavities i.e. $Q_L = 1800$. In fact, the coupling into and out of the cavity (directly proportional to the Q_L) can be changed to minimise the insertion loss at a given channel spacing. As the coupling into the cavity is reduced, the loaded Q increases and so does the cavity insertion loss. However, the high loaded Q shrinks the cavity bandwidth and reduces the loading effect of the other cavities in the combiner. The insertion loss to other parallel connected cavities is reduced. Fig. 2.7(b) illustrates the trade-off between IL_{cavity}

and IL_{equ} . The total insertion loss curve results in an optimum setting of coupling ($Q_L = 1500$), to achieve a minimum amount of insertion loss.

Although measures can be taken to minimise the insertion loss, the amount of insertion loss that can be tolerated within a given system will still restrict the minimum channel spacing. This is a limitation of the conventional transmitter architecture.

2.3.2 Frequency Flexibility

Frequency agility is the ability of a system to rapidly and easily change the channel frequency, it is seen as an integral component in enhancing the capacity of future radio systems. For example, the technique of frequency hopping requires the transmitter to change from one carrier frequency to another in some pre-determined hopping pattern. The GSM radio system specifies 216.68 hops per second [11]. Frequency agility is also required to cope with the dynamic load changes within a system. Examples of areas which may experience large load changes are the main arterials during rush hour, and the CBD during working hours. Future systems will incorporate flexible frequency plans that require the dynamic allocation (daily, hourly or even instantaneous changes) of channel frequencies on a continual process.

The conventional base station architecture as discussed in Section 2.2 has very limited frequency agility due to the manual tuning mechanism. The architecture can be extended to achieve limited frequency agility, however, through the use of electro-mechanical tuning resonators and the dual windows approach. This is at the expense of increased complexity and cost. Replacing the cavity resonators with a hybrid combiner can achieve unbridled frequency agility but this technique is very expensive in terms of lost signal power.

2.3.2.1 Tunable Cavity Resonators

Electro-mechanical tuning resonators are used in the case of a system requiring regular re-calibration or remote re-tuning of the cavity to a new transmit frequency.

The electro-mechanical solution tunes remotely through the use of stepper motors, RF sensors, feedback loops and microprocessors. This additional complexity increases the cost and affects the reliability (mainly due to the introduction of mechanical parts). There

are various techniques for the rapid re-tuning of resonators [17]. The tuning range varies between 0.05% - 1% of the centre frequency with a degradation in unloaded Q value of around 50%. Although tuning times in the order of microseconds are achievable, electro-mechanical resonators usually take between 0.1 - 10 seconds to tune [4].

2.3.2.2 Dual Window Cavity Combiner

Another technique for making the cavity resonator solution somewhat more frequency agile is the dual window combiner, Fig. 2.8(a). This combiner utilises fixed tuned window filters arranged so that by interleaving two electrically de-coupled sets, continuous coverage of a dedicated portion of the spectrum can be obtained [4], Fig. 2.8(b).

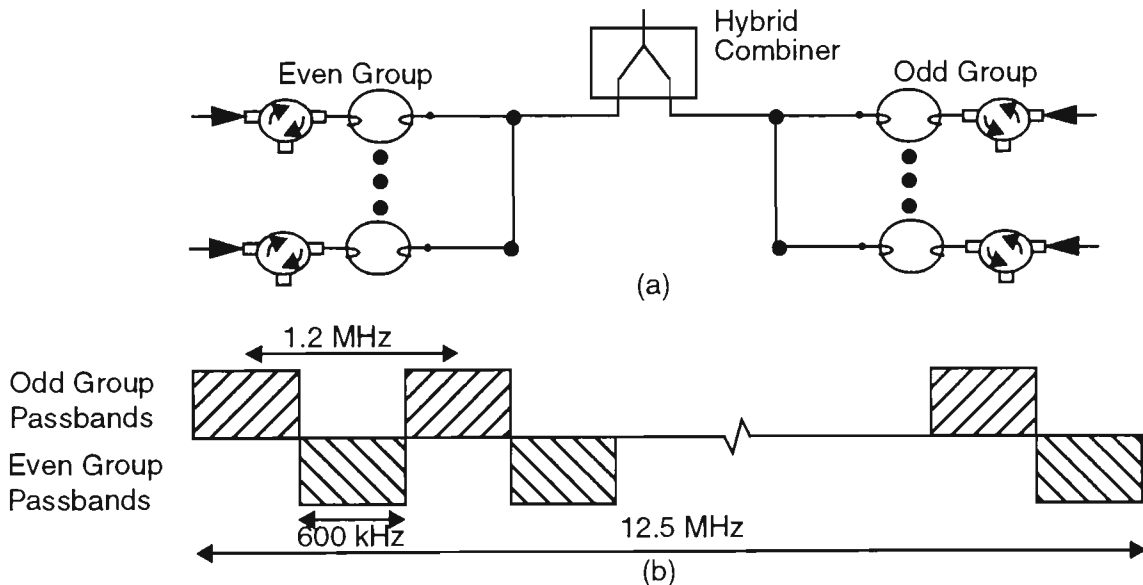


Figure 2.8: (a) Dual window cavity combiner architecture (b) Diagram displaying nominal frequency values for the dual window cavity combiner.

Each window utilises two $\lambda/4$ cavity resonators to give an overall four pole (bandpass) filter response to maintain sufficient isolation between the adjacent channels in each window. The bandwidth of each window is approximately 600 kHz, 3 channels (@ 200 kHz) for GSM or 48 channels (@ 12.5 kHz) for MPT1327. Two groups, an even and an odd, are made up of 19 of these windows coupled together. The two groups of filters are coupled to a single antenna by means of a 3 dB coupler. The overall transmitter to antenna loss is 5.2 dB, about 1.4 dB greater than the conventional architecture [4].

Each window can only accommodate one transmitted channel so that there is no increase in the number of channels combined but there is added flexibility as the channels may move dynamically within a 600 kHz wide window. Additionally, the spectrum must be

continuous, making it more suitable for cellular systems than for other radio systems where the spectrum is not allocated in a dedicated block.

2.3.2.3 Hybrid Combining

A technique of combining very closely spaced transmitters (i.e. less than 100 kHz), is performed through the use of a high power hybrid combiner, Fig. 2.9. There are many different hybrid topologies [8] that can adequately perform the combining process. However, they will all exhibit an insertion loss that varies depending upon the phase and amplitude of the input signals [8]. If the signals are uncorrelated, then the theoretical average insertion loss that each input undergoes is $10\log_{10}N_{\text{comb}}$, where N_{comb} is the number of signals being combined. Obviously this is very expensive in terms of lost power, and this constitutes the major disadvantage of hybrid combining.

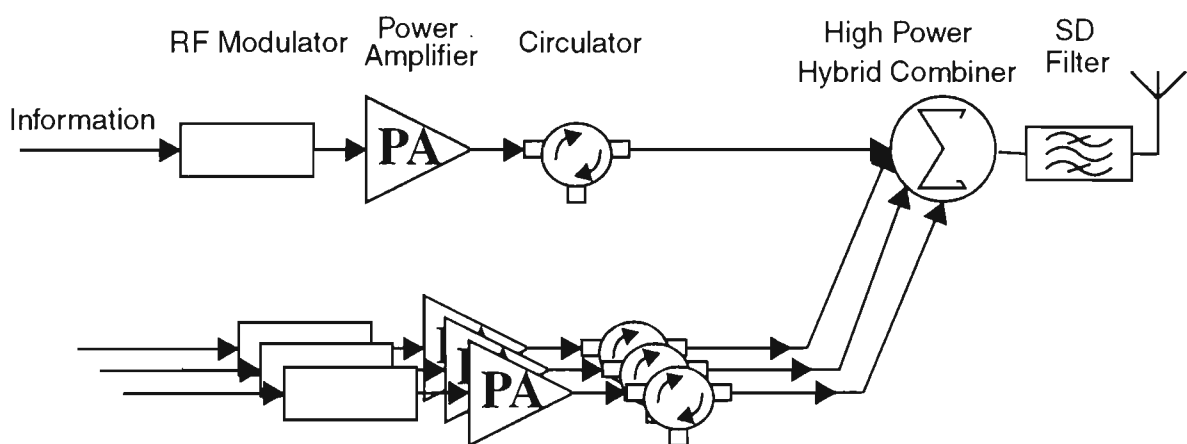


Figure 2.9: *Hybrid Combining Base Station Transmitter Architecture*

A significant advantage of hybrid combining over conventional combining is the ability to combine channels with no restrictions on channel spacing. However, to maintain high isolation between ports, it is very important to have a well matched output port. With accurate manufacturing of the hybrid, only 35 dB of isolation is achievable [2] and so ferrite isolators will still be needed to achieve the required $\text{TX-TX}_{\text{isolation}}$.

2.3.3 Size

The need to cope with the increase in equipment because of the huge demand for wireless systems in the future makes size a primary goal for all system components, including the base stations [13]. Given that base station sites are both a limited and expensive resource, the efficient use of space is also essential. Over the last decade this has resulted in the shrinking in size of base stations. For example, in the NMT (Nordic Mobile Telephone)

system, the volume per channel of a base station was reduced by a factor of around 4 between 1985 and 1990 [13]. If forecasts hold true, the volume of base stations must continue to be considerably reduced so that the number and area of basestation sites do not expand at the same rate.

The open market approach to wireless communications, adopted worldwide, allows for new private operators to compete against the established telecommunication operators. These operators will also require premises for their infrastructure. This will place enormous pressure on sites in urban environments. Small base stations will be highly desired to keep site costs minimal.

Future wireless systems, especially cellular, also make provisions for hierarchical cell structures that consist of very small cell sizes, micro and pico. An unobtrusive base station might be located on a lamp post, in a mall, or in the corner of an office. It will have a major aesthetic requirement, which will again most easily be met by small size.

Cavity resonators account for the considerable volume in the conventional base station transmitter. Typically they take up around 30% of the rack space. As highlighted in Table 2.1, the volume and weight of a cavity resonators is very significant. The removal of cavity filters from the architecture will result is considerable size and weight reductions.

Table 2.1: *Nominal Cavity Resonator Data [19]*

Frequency Band (MHz)	Resonator Type	Volume (m ³) / Channel	Weight / channel
420-512	$\lambda/4$ coaxial	0.05	6 Kg
900 MHz	$\lambda/4$ coaxial	0.01	4 Kg

2.4 Low Power Combining Base Station Transmitter Architecture.

By using a low power combining scheme, followed by a high power, linear and wideband amplifier a significant improvement can be achieved in terms of flexibility and performance. The concept essentially involves the removal of the voluminous and inflexible cavity resonators, and a subsequent rearrangement in the amplification and combining processes. The low power combining can occur in either an analogue or digital environment, giving rise to two architectures, hybrid combining or digital signal processing combining.

2.4.1 Hybrid Low Power Combining

The low power hybrid combiner architecture [5,6a,6b,20], as opposed to the high power hybrid combiner (Section 2.3.2.3), combines the analogue radio frequency outputs of the individual channel modulators. The modulators are the same devices as those used in the conventional combining architecture. A well designed hybrid combiner provides 35 dB of isolation. If this isolation is not sufficient to limit intermodulation then additional isolation can be easily provided by circulators and low power amplifiers with good reverse isolation.

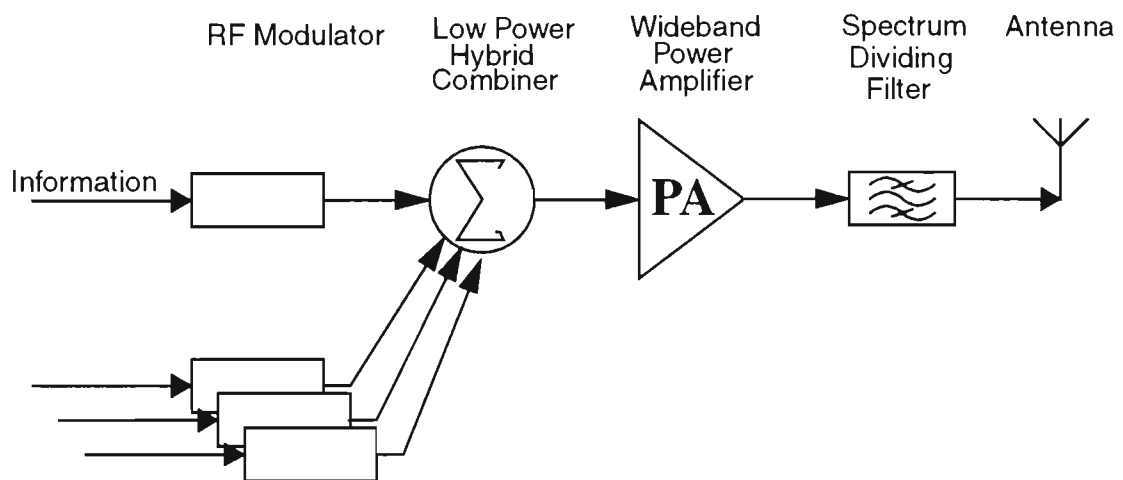


Figure 2.10: *Hybrid low power combining in the analogue environment.*

The actual combining circuitry is frequency insensitive. The circuitry places no restriction on the channel separation and it can combine channels with different bandwidths and/or modulation schemes. The inherent flexibility of the low power combining architecture lends itself perfectly to implementing future frequency agile systems. However, the theoretical loss of $10\log N_{\text{comb}}$ will still occur, but it can be cheaply and easily accounted for at low power levels, by simply amplifying the outputs from the prior modulator blocks.

The wideband amplifier has been the major technological obstacle. It has low DC-RF efficiency, high cost and limited total output power. The most important problem, however, is that the necessary linearity specifications are hard to meet. To achieve sufficient linearity from the amplifier, the technique of 'back-off' has traditionally been used [5,6a,6b]. However, in a multichannel situation, the DC-RF efficiency is consequently very low, and a large back-off will mean that the amplifier becomes expensive mainly due to the large amount of over-rating required. Linearisation techniques are seen as a means of improving the DC-RF efficiency and lowering the device power rating. Extensive research has been carried out into the linearisation of wideband amplifiers, utilising techniques such as predistortion and feedforward. Commercial solutions are now becoming available for small cell sizes.

2.4.2 Digital Signal Processing Combining

The combining can also be implemented in a digital signal processor. This further increases the overall flexibility of the design by incorporating the modulating and combining tasks together in a common processor under complete software control. Ultimately the DSP solution would mean a single hardware platform for the implementation of a generic base station architecture.

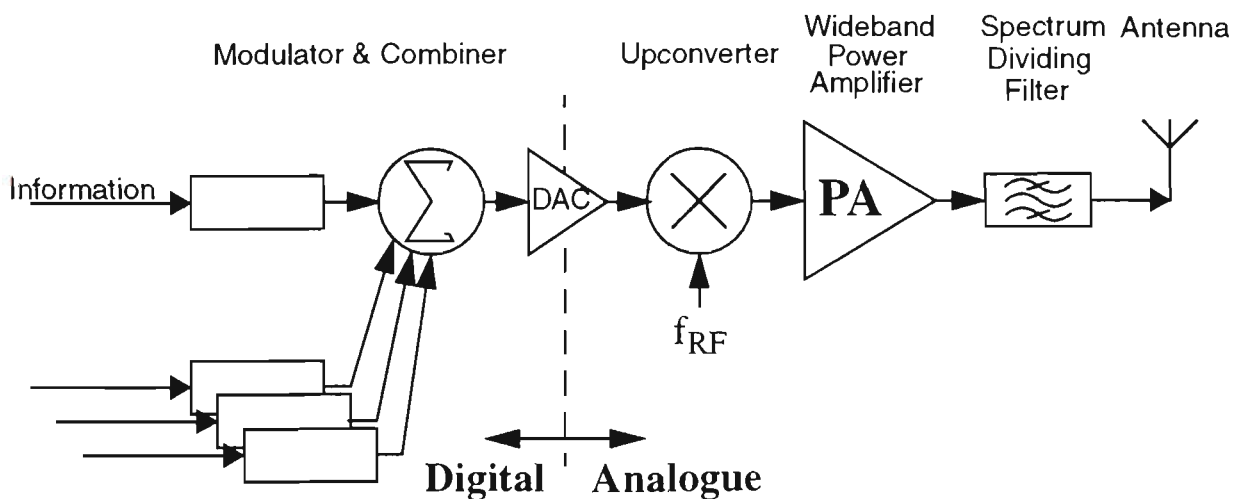


Figure 2.11: DSP low power combining in the digital environment.

There is also a considerable saving in hardware. The hybrid combiner requires a separate synthesiser, local oscillator and upconverter on a per channel basis, whilst the DSP solution requires this hardware only on a per system basis. The architecture highlights the modulation and combination occurring in a DSP environment, Fig. 2.11. Both the advantages and challenges relating to the DSP low power combining architecture will now be discussed.

2.4.2.1 Advantages of DSP Combining

Software Flexibility

The digital signal processor is inherently flexible because the functionality is programmable. That is, the modulation format or channel frequency can be dynamically changed by selecting a different subroutine or variable. It is technologically feasible to produce a generic base station for many different radio system standards.

High TX-TX Isolation

The transmitter to transmitter isolation is set by the precision of the DAC and DSP, because the modulated channels are combined in a DSP environment. It can be easily controlled by ensuring sufficient precision in both components.

Low Power Loss

Any power loss that occurs after amplification is critical as it increases the effective power rating of the amplifier. In the conventional architecture, a significant amount of power loss occurs due to the cavity resonators, isolators, SD filters and cable loss. Combining at low power levels means that the power loss after amplification is somewhat smaller, equal to that of the SD filter and the cable only.

No Restrictions on the Minimum Channel Separation

The cavity resonators restrict the minimum separation between channels in the conventional base station transmitter architecture. In the DSP low power combining architecture no restriction exists and all channels within a given bandwidth can be combined and transmitted simultaneously. Channels with different bandwidths and/or modulation schemes can also be combined. The inherent flexibility of the DSP combining architecture therefore lends itself perfectly to implementing future frequency agile systems.

Silicon Integration

Most components leading up to the wideband amplifier, including the DSP, DAC, mixers and hybrid combiners, can currently be implemented in silicon. As with all types of electronic equipment, significant reductions in size can be made through silicon integration. Considering that the cavity resonators have also been removed, a major size reduction in the base station transmitter will result.

Cost of Equipment and Maintenance

Removal of the expensive precision made cavity resonators from the base station architecture will contribute to a reduction in the cost of equipment. In addition, maintenance (calibration) and re-tuning of the cavities requires a technician to make a site visit to mechanically tune the cavities. This process is both time consuming and expensive, especially if frequency re-planning of the radio system occurs regularly.

2.4.2.2 Challenges of DSP Combining

Multichannel Combining

A number of channels will require both modulation and combination, and this could occur across a bandwidth of up to 50 MHz. Consequently the computation load will be large. Efficient algorithms for the combining and modulating process are an essential element for practical implementation in a DSP environment. The output sampling rate of the digitally produced multichannel signal will also place large demands on the digital signal processor. Chapter 3 will investigate efficient DSP combining algorithms.

DAC Interface

The high precision and speed requirements of the DAC interface have always been considered a limitation of the DSP architecture. This is primarily because the high speed requirements correspond to lower precision commercially available devices.

The performance of the DAC is measured by the Signal to Noise Ratio (SNR) and the Spurious Free Dynamic Range (SFDR), both of which are degraded by static and dynamic errors of the device. These errors will generate harmonic and IM products that will fall into neighbouring channels, and can exceed the stringent spurious emission specification, Fig. 2.5(a) & (b). A technique for improving the SFDR will be introduced in Chapters 5 and 6.

Frequency Conversion to RF

Upconversion to RF will incorporate either quadrature or heterodyne techniques, or a combination of both.

Quadrature upconverters have a well known source of error, namely amplitude and phase imbalance between the In Phase (I) and Quadrature (Q) paths [1]. The imbalances result in

undesired sideband signals that will fall into a neighbouring channel. In addition, both quadrature and heterodyne upconversion stages incorporate mixers, which are nonlinear devices. Subsequently, the multichannel signal will generate intermodulation components, or more unwanted spurious responses. The different spurious signals will invariably fall into neighbouring channels, and therefore must not exceed the spurious emission specification of the particular system.

Intermodulation caused by mixer nonlinearity can be controlled by incorporating high intercept point mixers and lowering the input signal level into the mixer. This does not present any serious technical problems [6b], however the amplitude and phase errors of analogue quadrature upconverters require correction. A novel compensation circuit will be introduced in Chapter 4.

Wideband Ultra-Linear Power Amplifier

The wideband power amplifier is a major technical challenge because of the problems of non-linearity and power output. The nonlinearity of the amplifier will produce intermodulation components which must not exceed the system specification. From Fig. 2.5(a) (GSM, power class TRX8) the spurious emission level must be at least -61.8 dBc within 6 MHz of the carrier, and from Fig. 2.5(c) the MPT1327 requirement is in the order of -82 dBc spurious rejection. The spurious rejection must be consistent across a wide bandwidth; therefore, ultra-linear amplifier behaviour is required. This is technologically feasible as an amplifier in the 900 MHz cellular band has been reported to suppress third order products to 70 dBc over a 5 MHz bandwidth [7].

The maximum power output level achieved by wideband, ultra-linear amplifiers also presents a major technical obstacle. This is aggravated by the fact that the peak power level of multichannel signals significantly increases the total power rating of the amplifier. For example, if N_{comb} channels are simultaneously activated at an average power of P_{av} , the total average power of the N_{comb} channels is:

$$P_{\text{tav}} = N_{\text{comb}} \cdot P_{\text{av}} \quad (2.15)$$

The actual peak power is significantly larger than this value. In fact, assuming a worst case scenario, where all channels peak powers are coherent, the Peak Envelope Power (PEP) is N_{comb} times the total average power (P_{tav}). For example, with 4 channels activated, each

having an average channel output of 20 watts (GSM power class TRX5), the PEP is equivalent to 320 Watts. A good linear amplifier has intermodulation products 30 dB down at rated power [5] given that the third order distortion is dominant. Therefore to achieve -72 dBc of spurious rejection, the amplifier must be operated at a backoff of 21 dB. The rated power of the amplifier required for combining 4 channels would therefore be 40,000 Watts! For the PMR trunking system with more combined channels the situation is even worse.

A way of decreasing the effective rating of the amplifier is to linearise the amplifier. Currently commercially available feedforward linearised amplifiers obtain in the order of 60-65 dBc suppression of intermodulation products at up to 25 Watts of total average power [Microwave Power Devices feedforward amplifier]. For a 4 channel system this amounts to 6 Watts of average power per channel, matching only the 7th (TRX7) and 8th (TRX8) power class specifications in the GSM base station transmitter.

It is obvious that high power transmission, using a low power combining architecture is restricted by the practical size of the ultra-linear amplifier. Current amplifier technology is capable of meeting only low power outputs, synonymous with small or micro cells. Therefore, this thesis will consider the GSM TRX8 transmitter specification as an example of smaller sized cells and the MPT1327 radio system as an example of a larger sized cells. The wideband amplifier will not be considered any further.

2.5 Conclusion

This chapter has discussed the conventional base station transmitter architecture, central to which is the cavity resonator. It has been shown that the cavity resonators limit the flexibility and minimum channel separation of the transmitter and they are also very large and heavy. A low power combining architecture has been introduced to overcome these limitations. It rearranges the amplification and combining processes in order to eliminate the requirement for a voluminous and inflexible cavity filter.

Low power combining can occur in the analogue environment through the use of a hybrid combiner. However, by combining in a digital signal processing environment, a more flexible solution is possible. The advantages of a DSP combining architecture over the

conventional architecture is the large and easily controlled TX-TX_{isolation}, low power loss, no restriction on the minimum channel separation and the possibility of silicon integration. All these factors will result in a smaller, less costly and more flexible base station transmitter.

However, there are also a number of challenges presented by the DSP low power combining architecture. The thesis will concentrate on these design challenges leading up to but not including the ultra-linear wideband amplifier.

The next chapter will consider both the DSP combining of the channels and the upconversion of the multichannel signal to RF.

Chapter 3

Multichannel Combining and Upconversion Techniques

3.1 Introduction

This chapter explores the two central issues of the digital signal processing base station transmitter: the combining of multiple channels and the upconversion of the multichannel signal to RF.

Section 3.2 defines the relevant parameters of the multichannel RF signal and introduces a generic architecture for generating the baseband multichannel signal. The architecture is implemented in a DSP environment and is extremely flexible in terms of channel shaping, modulation format, power control and frequency allocation. The combining process must also be computationally efficient. It is shown that the amount of computation is dominated by the sample rate interpolators and for this reason three efficient interpolation techniques are investigated.

The remaining sections of the chapter concentrate upon the upconversion of multichannel signal to RF. This involves digital to analogue conversion and the translation of the baseband multichannel signal to RF. Section 3.3 investigates the main design issues of four upconversion techniques:

- digital IF upconversion
- subsampling upconversion
- analogue direct upconversion - lowpass filter reconstruction
- analogue direct upconversion - bandpass filter reconstruction

The Chapter concludes that the two analogue direct upconversion techniques offer a less complex and a more practical solution than the digital IF techniques.

3.2 Multichannel Combining

Multichannel combining involves stacking N modulated channels together into a Frequency Division Multiplex (FDM) format. An example of a symmetrical stacking arrangement is shown in Fig. 3.1. The system (or switching) bandwidth, BW_{sys} , is related to the channel bandwidth, BW_{ch} , and the number of channels, N_{ch} , by:

$$BW_{sys} = N_{ch} \times BW_{ch} \quad (3.1)$$

The actual system bandwidth, BW_{sys} , over which any channel may exist, could be up to 50 MHz. However, this thesis will consider 5 MHz as the system bandwidth, BW_{sys} , since this is more representative of the bandwidth allocated to a single operator in Australia (e.g. Optus, Telecom, Vodafone).

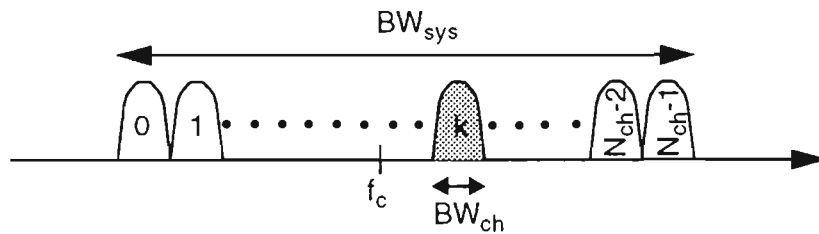


Figure 3.1: A multichannel signal centred at a frequency f_c .

Figure 3.1 suggests that every channel across the system bandwidth is being combined and transmitted simultaneously. This is definitely not the case, GSM and MPT1327 radio systems typically only combine up to 4 and 10 channels respectively. However, the need for more capacity in the future will see radio systems simultaneously transmitting (combining) more channels.

The multichannel signal as illustrated in Fig. 3.1 can be written as:

$$\begin{aligned} S(t) &= \sum_{k=0}^{N_{comb}-1} a_k(t) \cos(w_k t + \theta_k(t)) \\ &= \text{Re} \left[\sum_{k=0}^{N_{comb}-1} a_k(t) e^{j(w_k t + \theta_k(t))} \right] \end{aligned} \quad (3.2)$$

where the number of combined (or simultaneously activated) channels is denoted by N_{comb} . The multichannel expression can also be rewritten in a number of different ways.

For example, the complex baseband signal can be derived by substituting $w_k = (w_k - w_c + w_c)$ into Eqn. (3.2):

$$S(t) = \left(\sum_{k=0}^{N_{comb}-1} a_k(t) \cos((w_k - w_c)t + \theta_k(t)) \right) \cos w_c t - \left(\sum_{k=0}^{N_{comb}-1} a_k(t) \sin((w_k - w_c)t + \theta_k(t)) \right) \sin w_c t \quad (3.3)$$

The bracketed terms can be replaced by:

$$x_I(t) = \sum_{k=0}^{N-1} a_k(t) \cos((w_k - w_c)t + \theta_k(t)) \quad (3.4)$$

$$x_Q(t) = \sum_{k=0}^{N-1} a_k(t) \sin((w_k - w_c)t + \theta_k(t)) \quad (3.5)$$

so that Eqn. (3.3) can be simply re-written as:

$$S(t) = x_I(t) \cos w_c t - x_Q(t) \sin w_c t \quad (3.6)$$

Equations (3.2), (3.3) and (3.6) describe the same multichannel signal transmitted about a carrier frequency f_c . This can be termed a narrowband complex bandpass system if the bandwidth of the multichannel signal is smaller than the carrier frequency. With no loss of generality, the multichannel signal can be represented as an equivalent low pass signal or a complex baseband signal:

$$R(t) = x_I(t) + j x_Q(t) \quad (3.7)$$

The multichannel signal at RF can now be written in the following two forms:

$$S(t) = |R(t)| \cos(w_c t + \phi(t)) \quad (3.8)$$

$$= \text{Re} \{ R(t) e^{j w_c t} \} \quad (3.9)$$

where the instantaneous amplitude and phase is given by $|R(t)| = \sqrt{x_I(t)^2 + x_Q(t)^2}$, and $\phi(t) = -\tan^{-1} (x_Q(t) / x_I(t))$ respectively.

It is difficult to generate the RF multichannel signal, $S(t)$, due to the high sample rate requirements. The sample rate requirement can be substantially reduced if the multichannel complex baseband signal, $R(t)$, is generated in the DSP. Analogue techniques are then used to translate the signal to RF.

3.2.1 Generation of the Digital Baseband Multichannel Signal

The synthesis of the complex baseband multichannel signal using DSP is shown in Fig. 3.2. The input data for each channel is modulated and frequency translated to the desired channel location, before being combined with the other channels. The output from the modulator is in the form of a complex baseband signal, $r_k(n)$, sampled at a much lower sampling frequency of f_{s-mod} .

$$\begin{aligned} r_k(n) &= x_{i,k}(n) + jx_{q,k}(n) \\ &= a_k(m)e^{j\theta_k(m)} \end{aligned} \quad (3.10)$$

This signal requires interpolation to the output sampling rate of f_{s-comb} (see appendix B), before being frequency converted, via digital multiplication, to the desired channel location (intermediate frequency of f_k). The resultant signal is given by $r_{k,IF}(m)$:

$$r_{k,IF}(m) = a_k(m) \cos\left(\frac{2\pi f_k}{f_{s-comb}}m + \theta_k(m)\right) + ja_k(m) \sin\left(\frac{2\pi f_k}{f_{s-comb}}m + \theta_k(m)\right) \quad (3.11)$$

The discrete complex baseband multichannel signal can be written as:

$$R(m) = \sum_{k=0}^{N_{comb}-1} r_{k,IF}(m) \quad (3.12)$$

The output sampling frequency, f_{s-comb} , is selected such that the system bandwidth meets the Nyquist criteria. Some oversampling is required to reduce the complexity of the subsequent filtering operations, and it is defined as:

$$OS = f_{s-comb} / BW_{sys} \quad (3.13)$$

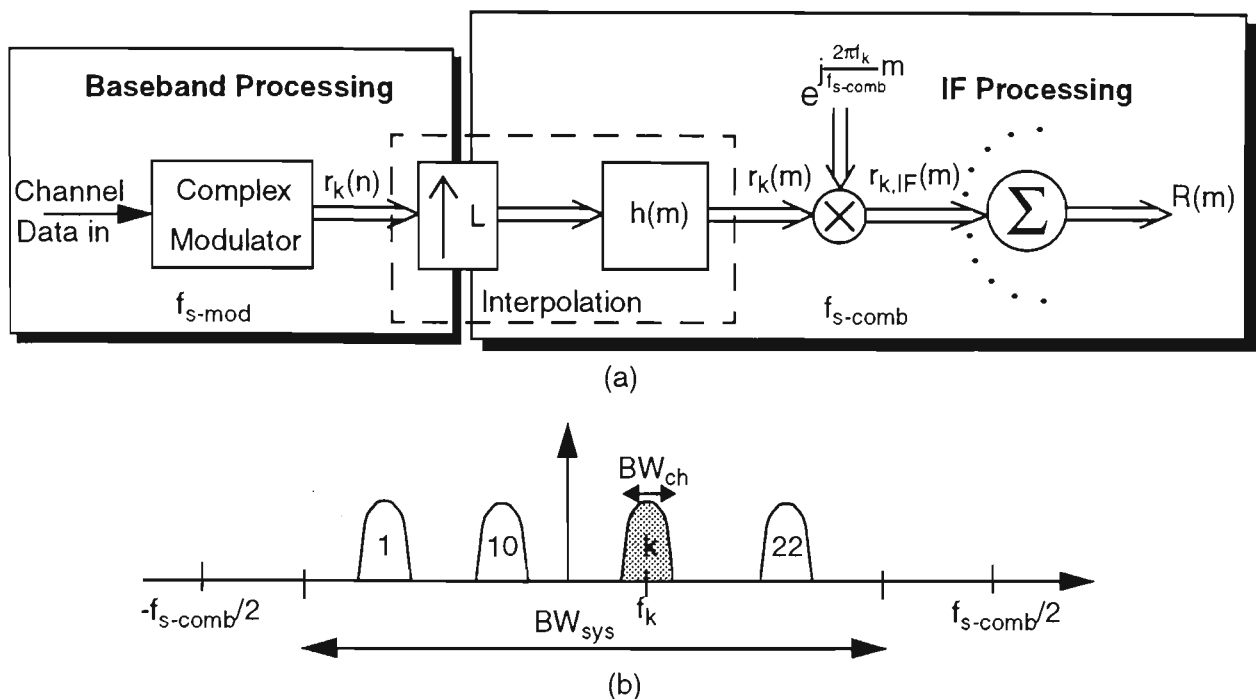


Figure 3.2: (a) Generic architecture (only one channel shown) for generating a complex baseband multichannel signal, $R(m)$. (b) Multichannel complex baseband signal represented in the frequency domain

The multichannel combining technique described and illustrated in Fig 3.2(a) is extremely flexible. Frequency and power control can be instantaneously applied at the multiplier and the channel spectral shaping can be controlled by the interpolating low pass filter, $h(m)$. However the computational requirements, determined by the complexity of the interpolation, frequency conversion and summation stages, are very large and optimisation of these stages is therefore necessary.

The hardware platform places constraints on the optimisation of the computational requirements. There are two types of hardware platforms: general purpose¹ or special purpose² digital signal processors. Crochiere and Rabiner [28] present optimal techniques for general purpose digital signal processors based on minimising the number of operations per second and the amount of storage (memory) required. Their approach centres around multistage interpolation, where each stage employs an efficient filter design, such as a polyphase (Appendix B.1) or a halfband (Appendix B.2) filter. These two filter designs will be used as a means of approximating the number of operations³ per second required by a general purpose signal processor.

1. General Purpose - The implementation of algorithms is completed in software, e.g. C40. The main advantage is flexibility.

2. Special Purpose - The implementation of algorithms is completed in hardware i.e. ASIC's, FPGA's. The main advantage is the higher computation capabilities.

Special purpose digital signal processors (hardware) can use many other optimisation techniques. For example, the careful choice of filter coefficients [40] or the use of multiplier-less filters [39] will lower the hardware requirements. The benefits of these techniques do not necessarily apply to a general purpose digital signal processor, and they will not be considered in this thesis.

3.2.2 Multichannel Combining Applications

3.2.2.1 A Trunking Radio System - MPT1327

A Private Mobile Radio (PMR) trunking system, such as MPT1327, is an example of an analogue narrowband wireless system. MPT1327 specifies a channel bandwidth of 12.5 kHz, for frequency modulated speech or data input signals (typically 2.55 kHz deviation). The modulator is illustrated in Fig. 3.3, and produces a complex baseband signal, $r_k(n)$, which has a constant amplitude rotating phasor.

A sampling frequency of 12.5 kHz (equal to the channel bandwidth) is sufficient to represent the FM signal, because the main body of the FM spectrum is contained within 10 kHz⁴. Cellular systems on the other hand intentionally allow the spectrum to spread into adjacent channels. This enables a higher data transmission rate, but forces the complex baseband modulator to operate at a faster sampling rate ($f_{s-mod} \gg BW_{ch}$).

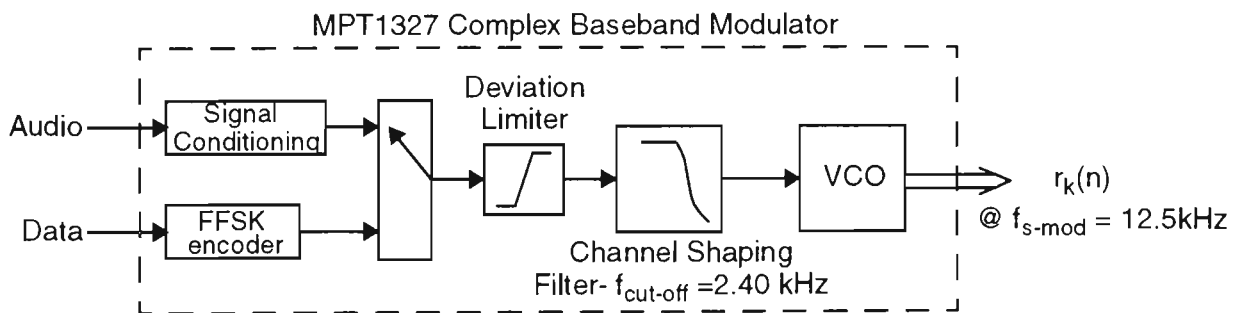


Figure 3.3: *MPT1327 Complex Baseband Modulator*

PMR wireless systems are also considered to have non-overlapping channels i.e. the spectrum does not spread across into adjacent channels. The channels are therefore considered to be well defined segments which are stacked together to form the

3. An operation is classed in terms of a general purpose signal processor as "the amount of work that can be accomplished by a given resource (i.e. a CPU which may include a multiplier, ALU, address multiplexer and internal registers) in a single clock cycle"[35]. For example the add and multiply instructions will take one cycle or operation on most processors. But for a FIR filter implemented using a repeat loop will take $\{7+(m_{tap}-1)\}$ cycles or operations to complete (on a C40 [37]). This value will be different for other processors. A C40 operation will be assumed in this thesis.

4. Carlson's rule $BW_{fm} = 2*(f_{deviation} + f_{input}) = 2*(2.55+2.4) \text{ kHz} = 9.9 \text{ kHz}$.

multichannel signal. From the modulation mask and maximum spurious level specifications, Fig. 2.5, the adjacent channel power must be 82 dB below the maximum carrier level (82 dBc).

Before combining the channels, the complex baseband modulated signal must be first interpolated and frequency translated, Fig. 3.4(a). The amount of computation required to complete the interpolation, using a single stage polyphase filter, and multiplication of one channel is:

$$C_{poly}(\text{per channel}) = \{ \text{One stage Polyphase Interpolation} \} + \{ \text{Multiplication} \} \quad (3.14)$$

$$= (2 \times m_{tap} \times f_{s-mod} + 2 \times f_{s-comb}) \times 10^{-6} \text{ MOPS}^5$$

where m_{tap} is the number of filter taps. The C40⁶ processor will be used to calculate the number of operations.

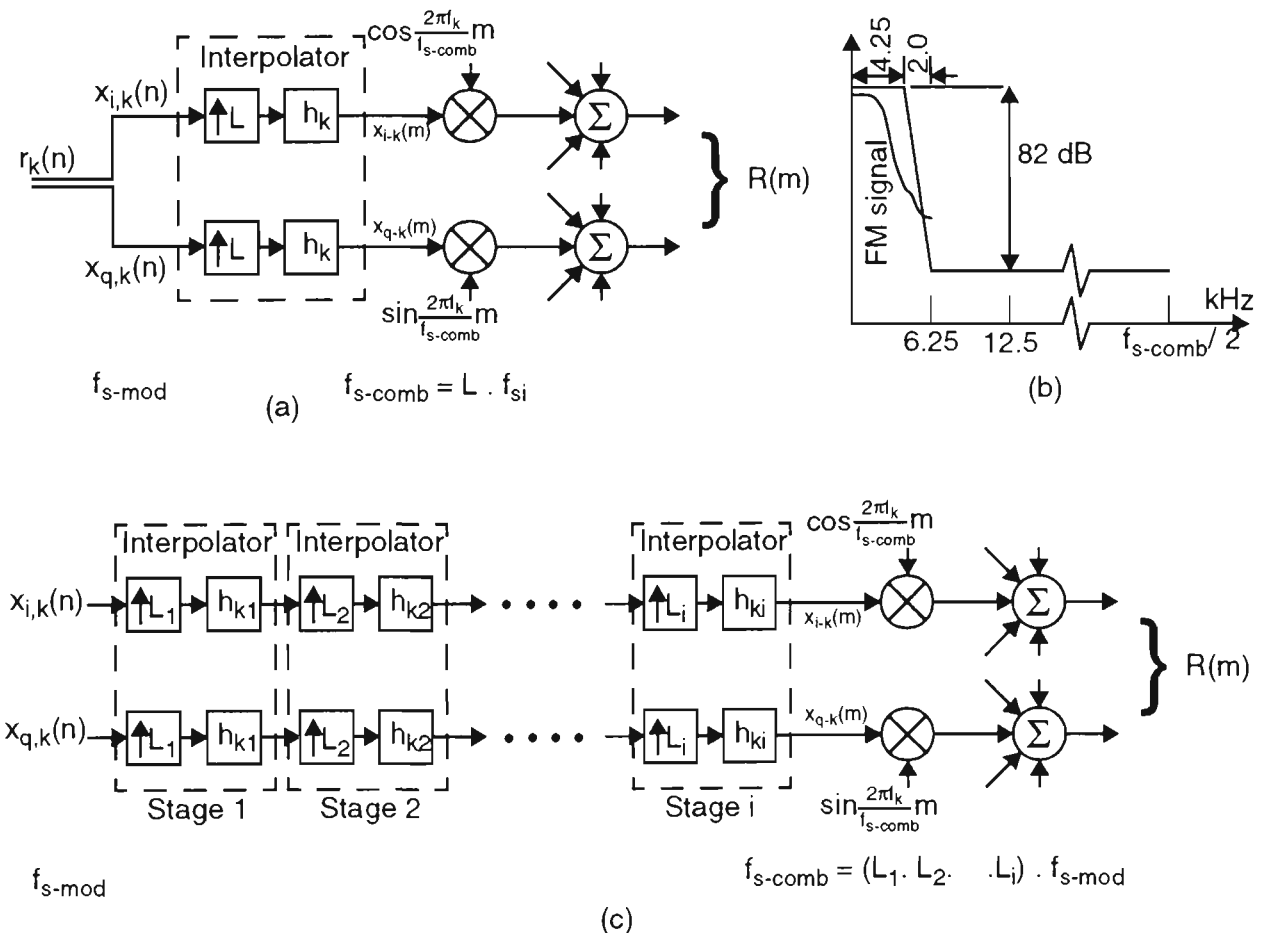


Figure 3.4: (a) Brute force multichannel combining - One stage interpolation and then frequency conversion before the final summation. (b) Specification for the first stage interpolation filter. (c) A more efficient multichannel combining technique - Multistage interpolation and then frequency conversion before the final summation.

5. MOPS - Millions of Operations per Second

6. C40 refers to the TMS 320C40 processor, which is capable of 25 MOPS when the processor clock is 50 MHz.

The number of taps for the single stage interpolator will be large because the transition width of the filter is small (2 kHz) compared to the output sampling frequency, as illustrated in Fig. 3.4(b). A useful approximation for computing the number of taps, m_{tap} , given a set of specifications [23] (Parks McClellan Technique) is:

$$m_{tap} = \frac{(-20 \log \delta - 13) \cdot f_s}{14.6 \cdot \Delta f_T} \quad (3.15)$$

where δ is equal to the passband and stopband ripple, Δf_T is the transition region and f_s is the output sampling frequency of the filter. For the MPT1327 radio system, Fig. 3.4(b), the stopband ripple is equal to 82 dB and the transition bandwidth is 2 kHz. The system bandwidth, or minimum sampling rate (f_{s-comb}) is assumed to be 5 MHz, resulting in at least 11,815 taps! The interpolation process can be made more efficient if a multistage design is employed, Fig. 3.4(c).

It will be assumed that each stage will have an interpolation factor of 2, although other interpolation factors are possible. Therefore, assuming a system bandwidth of 5 MHz, the minimum total interpolation factor is 512 i.e. $f_{s-comb} = 12.5 \text{ kHz} \times 512 = 6.4 \text{ MHz}$. This can be achieved by 9 'interpolate by 2' stages, Table 3.1. The efficiency is brought about by making use of the fact that the transition width increases for each subsequent stage causing the number of taps per stage to converge to an asymptotic limit. The limit occurs as the transition width approaches half the sampling frequency; $m_{tap} = 10$ (Eqn. (3.15)).

Table 3.1: *Multistage interpolation using a cascade of interpolate by 2 stages.*

Stage	1	2	3	4	5	6	7	8	9
L	2	2	2	2	2	2	2	2	2
$\Delta f_T/f_s$	0.08	0.25	0.375	0.438	0.47	0.485	0.493	0.497	0.498
m_{tap}	60	19	15	11	11	11	11	11	11
Type	Poly ^a	Half ^b	Half	Half	Half	Half	Half	Half	Half

a. Poly - Polyphase interpolator

b. Half - Halfband interpolator

The first stage uses a polyphase interpolation filter because the passband and stopband frequencies are not symmetrical about a quarter of the output sampling frequency (see Appendix B.2). However, the remaining stages can use the more efficient half-band filter. The halfband interpolator is shown to have approximately half the number of operations, $(m_{\text{tap}}+1)/2$, of the polyphase interpolator for a given number of taps (Appendix B). Additionally, the halfband filter has a lower hardware complexity, making it ideal for implementation as a special purpose digital signal processor.

Further efficiencies in the multichannel combining algorithm can be gained through the use of a transmultiplexer algorithm. A transmultiplexer efficiently converts time division multiplex signals to frequency division multiplex signals. Digital implementation of transmultiplexers has been subject to a large amount of research and development, commencing in the 1960's and continuing into the 1980's. A comprehensive survey by Scheuermann and Gockler [27] presented every type of transmultiplexer proposed as of June 1981. In this thesis only one transmultiplexer technique, arguably the most computationally efficient, has been isolated as an example for use as a multichannel combiner. This technique is called the polyphase Fast Frequency Transform (FFT) filter bank, illustrated in Fig. 3.5. The efficiency of the algorithm is intuitive if compared to Fig. 3.2(b). The polyphase FFT technique computes the interpolation multiplication and summation of the channels at the lower sampling rate, $f_{s\text{-mod}}$.

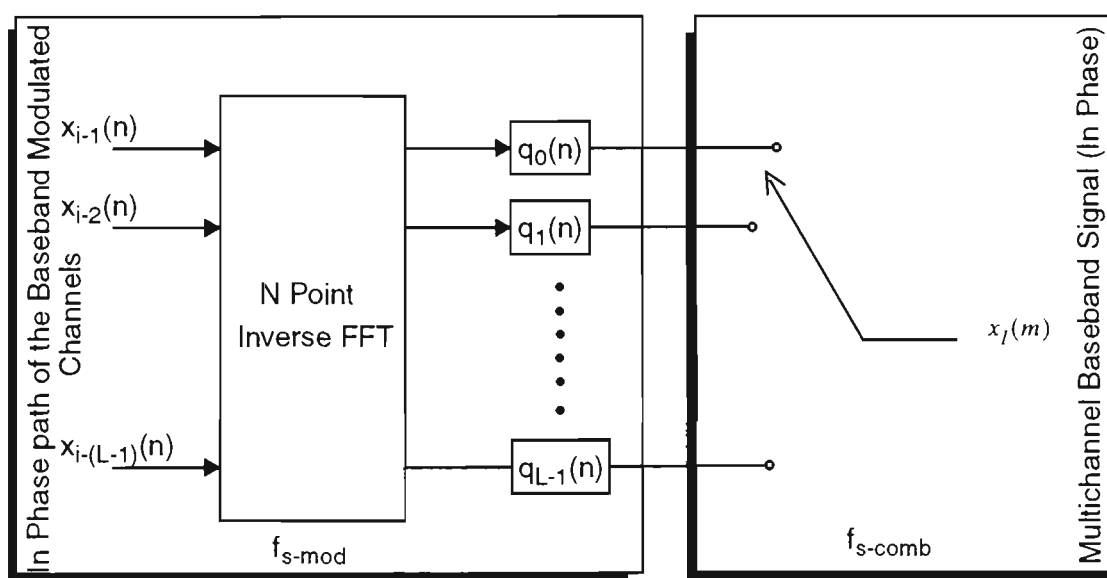


Figure 3.5: Polyphase FFT filter Bank. Only showing the In Phase processing path, the Quadrature Phase path is identical.

The polyphase FFT filter bank can actually be derived directly from the single channel structure described in Fig. 3.2(b). This derivation is completed in detail in reference [28] and will not be considered here. A few of the important details are:

- The number of channels is made to equal the interpolation rate, L .
- The input sampling frequency, $f_{s\text{-mod}}$, sets the channel bandwidth, BW_{ch} .
- The original low pass interpolation filter, h_k , is decomposed down into L polyphase filters:

$$q_{\rho}(n) = h(nL + \rho) \quad \rho = 0, 1, \dots, L - 1$$

- The number of channels is made to equal a number that is a power of 2. Therefore, the more efficient FFT as opposed to the discrete fourier transform, can be used.

From previous discussions, an interpolation factor of 512 meets all the above requirements and the combining sampling frequency of the polyphase FFT algorithm is $(512 \cdot 12.5 \text{ kHz}) = 6.4 \text{ MHz}$. Given that only 5 MHz of system bandwidth is required, the outer 112 (1.4 MHz) channels will not be used. Using only 400 of the 512 available channels has the benefit of oversampling the system bandwidth.

The amount of computation power required for the polyphase FFT technique, using the C40 processor, can be determined using reference [37]. It states that a 512 point inverse FFT will take 16,067 operations. The number of operations can then be written as:

$$C_{\text{FFT}} = \{\text{FFT}\} + \{\text{Polyphase Filter}\} \quad (3.16)$$

$$= 2 \times (16,067 \cdot f_{s\text{-mod}} + m_{\text{tap}} \cdot f_{s\text{-mod}}) \times 10^{-6} \text{ MOPS}$$

The factor of two in Eqn. (3.16) takes into account both the In Phase and Quadrature paths.

For each of the techniques discussed, the computation power has been plotted against the number of combined channels in Fig. 3.6. The following parameters have been used for the calculations: $f_{s\text{-mod}} = 12.5 \text{ kHz}$, $BW_{\text{sys}} = 5 \text{ MHz}$ and $f_{s\text{-comb}} = 6.4 \text{ MHz}$.

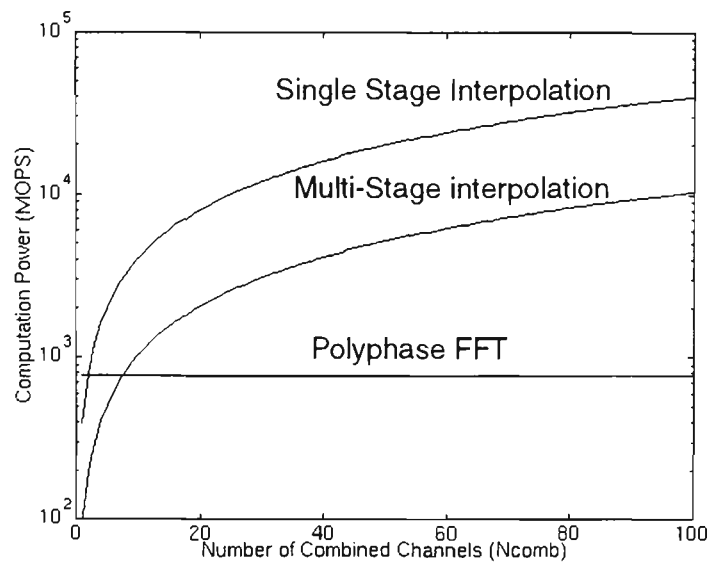


Figure 3.6: The number of computations versus the number of channels combined for the MPT1327 trunking radio system with the following parameters; $f_{s-mod} = 12.5 \text{ kHz}$, $BW_{sys} = 5 \text{ MHz}$, $f_{s-comb} = 6.4 \text{ MHz}$

The Polyphase FFT technique has a constant computation load, regardless of the number of channels combined, whilst for the other two techniques, the computation load increases linearly with the number of combined channels. The polyphase FFT technique requires a total of 780 MOPS (32 general purpose C40's) of computation whereas the cascaded halfband interpolator requires 90 MOPS (4 general purpose C40's) per channel.

Figure 3.6 also reveals that the halfband technique is about 4 times more efficient than single stage interpolation, and is more efficient than the polyphase FFT technique when the number of channels being combined is less than 8. For the MPT1327 radio system, it is typical for between 5 and 10 channels to be combined. Either multi-stage interpolation or the polyphase FFT technique could therefore be used. The polyphase FFT technique becomes a lot more attractive if we take into consideration future systems, where a larger number of channels will be combined.

3.2.2.2 A Digital Cellular Radio System - GSM

The GSM radio system specification states that the information bit rate, f_b , is 270.833 kbps. To minimise the complexity of the interpolation stage, the output sampling frequency, f_{s-comb} , is best set to an integer multiple of the input data rate. An overall interpolation factor of 24 ($f_{s-comb} = 24 \times f_b = 6.5 \text{ MHz}$) will satisfy the above requirement. The sampling rate is similar to the previous MPT1327 example, and this will provide a basis for a fair comparison of computation load between the two systems..

Figure 3.7(a) illustrates the more traditional filtering approach for implementing the interpolation process. There are two filtering stages, the first is the channel shaping filter with a Gaussian impulse response. The interpolation ratio, say $L_1 = 8$, is chosen so as to limit the aliasing error. The second interpolation stage will simply complete the overall required interpolation factor, i.e. $L_2 = 3$.

A significant reduction in computation power can be achieved by using a memory Look Up Table (LUT) to implement the Gaussian shaping filter [36] and the first interpolation stage [38], Fig. 3.7(b). The LUT is addressed by the past data samples and a state machine [22], which adjust the 7 MSB's, and the counter that implements the overall interpolation ratio of 24, the 5 LSB's. The LUT will require a memory size of 8192 ($2 \times 2^{(7+5)}$) 8 bit bytes, and an access speed of 150ns. These specifications can be easily achieved by inexpensive ROM or static RAM.

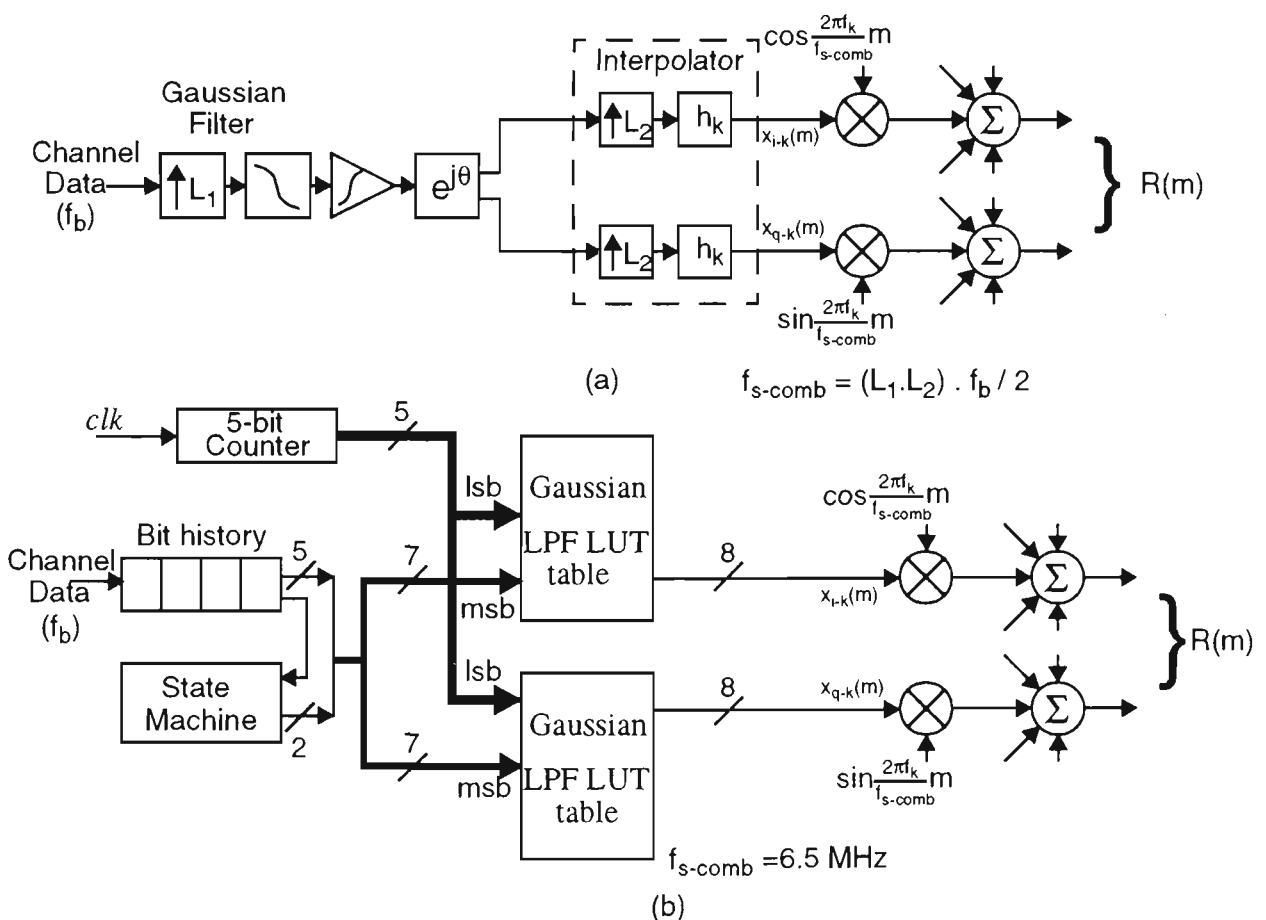


Figure 3.7: (a) Traditional filtering technique of implementing GMSK (b) A more efficient memory LUT implementation of (a).

Both the interpolation process and frequency translation multiplier are one operation tasks. This also assumes that the sine and cosine waveforms are generated via the memory LUT approach (synonymous with DDS). It should be noted that for accurate synthesis a large amount of memory will be required.

The overall computation (C_{GSM}) required to combine N_{comb} channels is then:

$$C_{\text{GSM}} = N_{\text{comb}} \cdot (\{ \text{LUT Interpolator} \} + \{ \text{Multiplier} \}) + \{ \text{Summer} \} \quad (3.17)$$

$$= (N_{\text{comb}} \cdot (2 \cdot f_{\text{s-comb}} + 2 \cdot f_{\text{s-comb}}) + (N_{\text{comb}} - 1) \cdot f_{\text{s-comb}}) \times 10^{-6} \text{ MOPS}$$

where the number of addition operations required is equal to $(N_{\text{comb}} - 1)$. Using Eqn. (3.17), the amount of computation needed to combine 4 GSM channels is 123.5 MOPS. This would be equivalent to five C40 digital signal processor devices.

3.2.3 Concluding Remarks on Multichannel Combining

The combining of multiple channels consists of a sample rate interpolator, a multiplier, and a summer. To minimise the computational load, three interpolator techniques were investigated: memory LUT approach, cascaded half-band filters and the polyphase FFT technique.

The most efficient combining scheme incorporated the memory LUT interpolator approach. This technique required 31 MOPS per channel but can only be applied to digital modulation schemes where there is a small number of output states (trajectories). Analogue modulation schemes are impractical because the large number of output states would require an enormous amount of memory for implementation.

The other two combining techniques incorporated interpolators that could be used for both digital and analogue modulation schemes. Approximately 90 MOPS per channel are required for a combining architecture using cascaded half-band filters. For less than 8 channels this technique is more efficient than the polyphase FFT combining algorithm, which needs 780 MOPS of computation regardless of the number of channels combined (less than 512).

The techniques of multichannel combining will not be considered any further in this thesis. This thesis will now concentrate on issues relevant to the DAC and the upconversion of the complex baseband multichannel signal to RF.

3.3 Upconversion Techniques

The process of upconverting the combined digital multichannel signal to the desired RF band involves both quadrature and heterodyne frequency conversion stages, which can be implemented in either the digital or the analogue domains. Digital to analogue conversion is also critical to the process.

3.3.1 Digital IF Upconversion

Digital Intermediate Frequency (IF) upconversion consists of frequency translating the baseband multichannel signal, $R(m)$, via a digital quadrature upconverter, Fig. 3.8(a). The In Phase $x_I(t)$ and Quadrature phase $x_Q(t)$ multichannel signals are mixed with their respective quadrature phased oscillator signals (f_{IF}) and combined. The digital multichannel signal is now centred at a digital intermediate frequency of f_{IF} , Fig. 3.8(b) and undergoes digital to analogue conversion, followed by low pass (or even bandpass) reconstruction. The resulting analogue intermediate frequency⁷ of the multichannel signal is still f_{IF} .

An analogue heterodyne upconversion stage translates the multichannel signal to the required RF band, Fig. 3.8(c). The attenuator is used to control the mixer intermodulation products, and the image filter removes the image signal also generated by the heterodyne mixer stage. The image filter also suppresses out of band spurious signals, intermodulation products and wideband noise prior to amplification.

Implementation of the quadrature upconverter in a DSP environment (as opposed to the analogue environment) has significant advantages in that phase and amplitude imbalances do not exist and perfect mixing of the signals (no intermodulation products) will occur. However, the technique requires extra computation and a high performance DAC. These will now be investigated.

7. The analogue intermediate frequency refers to the reconstructed IF after the DAC, whilst the digital intermediate frequency refers to the IF before the DAC.

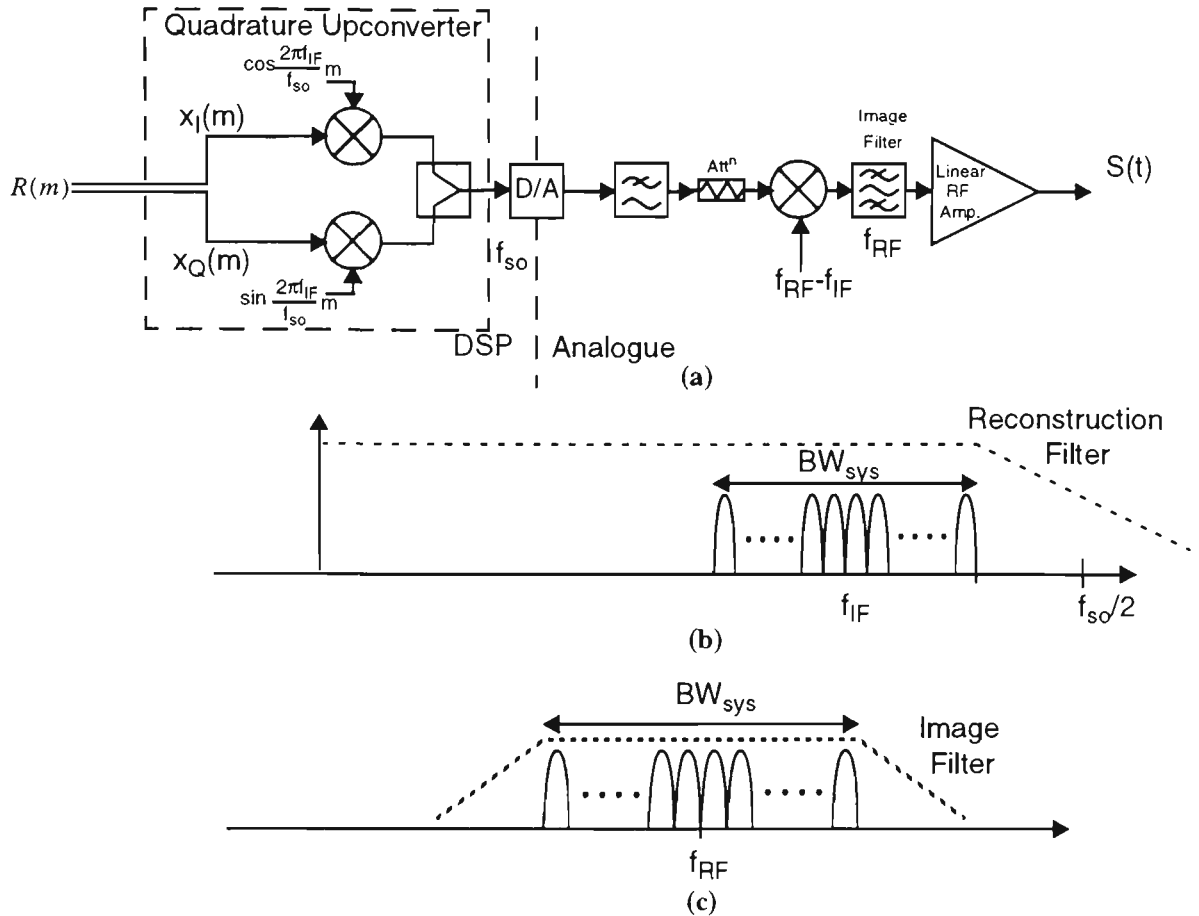


Figure 3.8: (a) Digital IF upconversion architecture (b) Multichannel signal after DAC (c) Multichannel signal after RF upconversion.

3.3.1.1 Computation Requirements

The frequency of the IF output signal determines the trade-off between analogue complexity and the computational load. A higher IF requires more computation but reduces the number of analogue upconversion stages needed to reach the desired RF band. The additional computation load of digital quadrature upconversion requires careful consideration.

The baseband multichannel signal, $R(m)$, must be interpolated to the higher output sampling frequency (f_{so}) before quadrature mixing and summation, as shown in Figs. 3.9(a) and (b). It is a very similar problem to that discussed in Section 3.2.2. The calculation of computation will assume a multistage interpolation technique, using halfband interpolators:

$$C_{IF} = 2 \cdot \{ \text{stage 1} \} \cdot f_{s\text{-comb}} + 2 \cdot \{ \text{stage 2} \} \cdot 2 \cdot f_{s\text{-comb}} + \dots + 2 \cdot \{ \text{stage } j \} \cdot f_{so} + 2 \cdot \{ \text{multiplier} \} \cdot f_{so} + \{ \text{summer} \} \cdot f_{so} \quad (3.18)$$

The factor of 2 takes into account both I & Q paths. The multiplier and summer are 1 operation calculations, where each half-band filter stage takes $(m_{\text{tap}}+1)/2$ operations. The number of taps is calculated from Eqn. (3.15). Overhead processing, such as trigonometric generation (via lookup tables) and general program code, is neglected for simplicity.

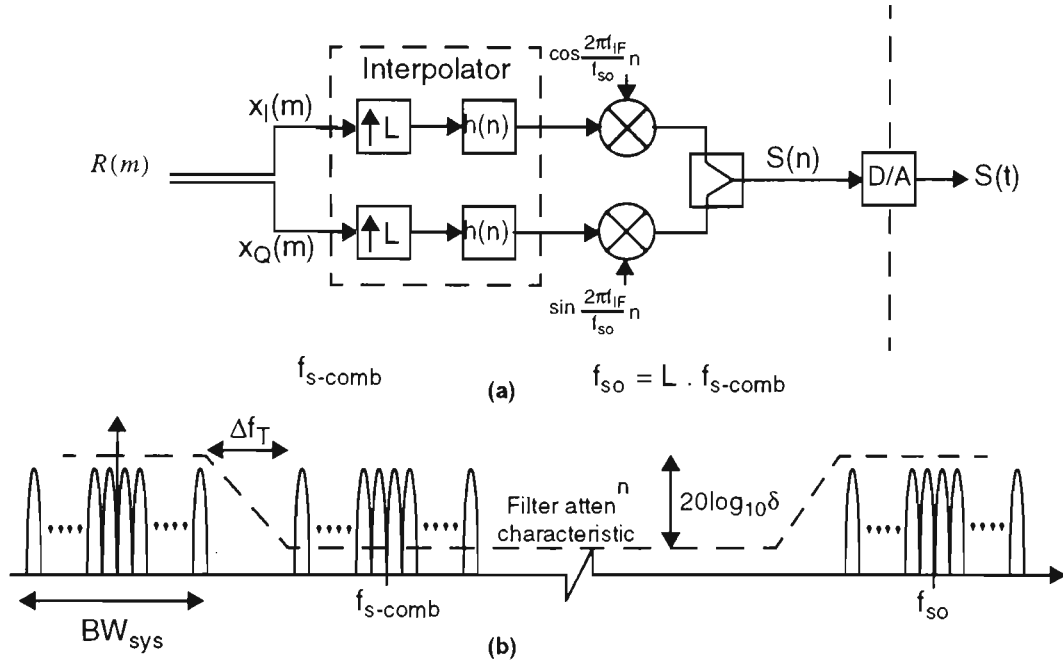


Figure 3.9: (a) Digital signal processing architecture for interpolation and quadrature upconversion. (b) Periodic spectral components of the multichannel signal after interpolation overlaid with the filter attenuation characteristics of the interpolation filter.

Additional computational savings can be made by incorporating the multiplier and summer into the last interpolation stage, Fig. 3.10(a). The savings centre around the selection of the intermediate frequency to equal a quarter of the output sampling frequency. The cosine and sine carriers then reduce to:

$$\cos(2\pi f_{IF} n / f_{so}) = 1, 0, -1, 0, 1, 0, -1, \dots \quad \& \quad \sin(2\pi f_{IF} n / f_{so}) = 0, 1, 0, -1, 0, 1, 0, \dots \quad (3.19)$$

$$\text{where } f_{IF} = f_{so}/4$$

This eliminates the need for generation of the trigonometric functions (although they may only be in the form of a look-up table). The multiply and addition operations are now replaced by the multiplexer and negation operations, offering substantial speed and hardware savings. The whole quadrature upconverter (multiplication and summer) can be incorporated into the last interpolation operation as shown in Fig 3.10(b) so that the total amount of computation can be written as:

$$C_{IF} = 2 \cdot \{\text{stage 1}\} \cdot f_{s\text{-comb}} + 2 \cdot \{\text{stage 2}\} \cdot 2 \cdot f_{s\text{-comb}} + \dots + 2 \cdot \{\text{stage } i-1\} \cdot f_{so}/2 + \{2 + (\text{stage } j)\} \cdot f_s \quad (3.20)$$

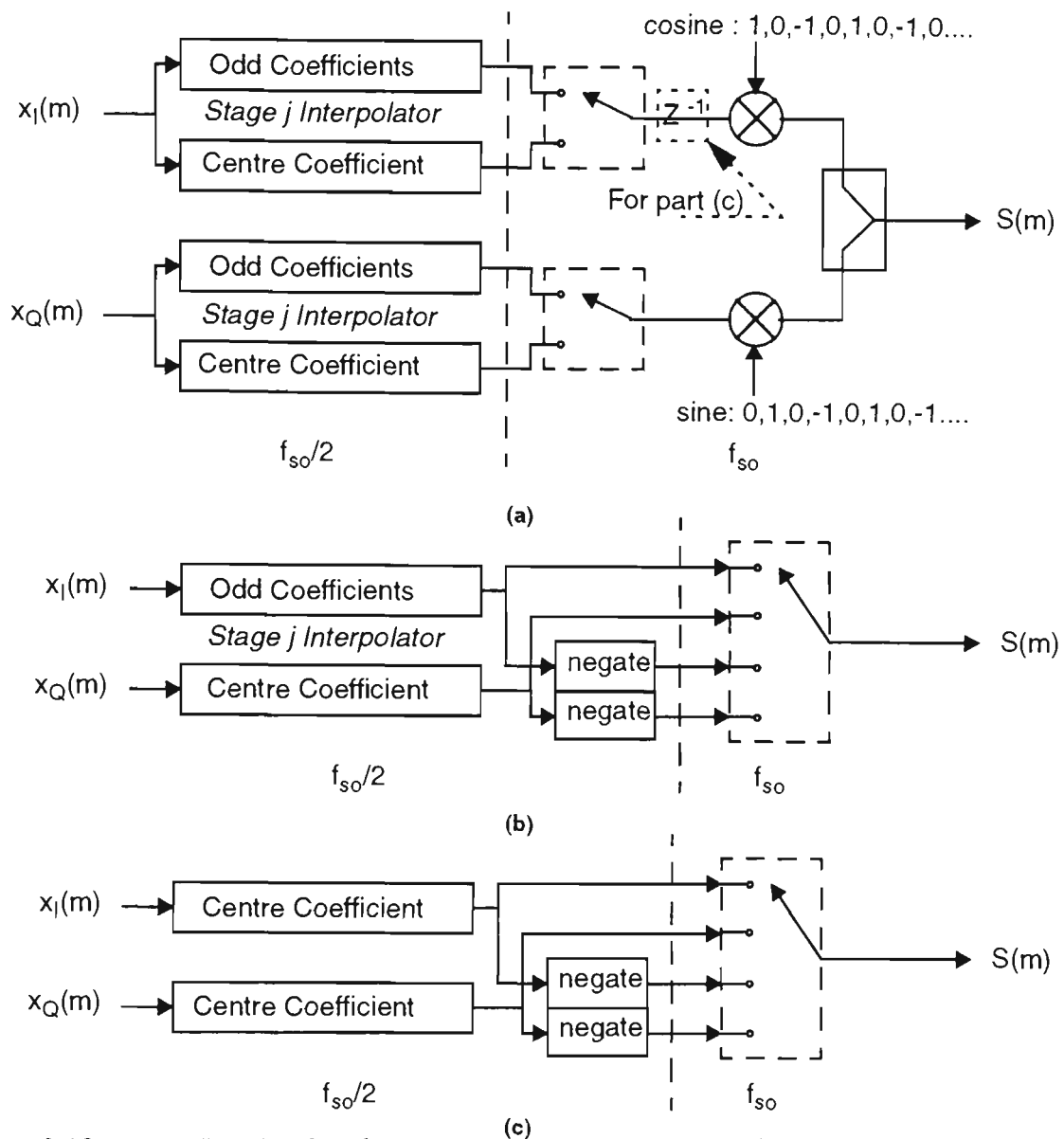


Figure 3.10: (a) Last halfband interpolator followed by a quadrature upconverter with an intermediate frequency of $f_{so}/4$. (b) Efficient implementation of (a). (c) An even more efficient implementation of (a).

A further simplification can be made by delaying the In Phase path by one sample, as shown dotted in Fig. 3.10(a). The equivalent circuit is illustrated in Fig. 3.10(c). The interpolator, multiplier and summer reduce to two negation operations because the centre coefficient for a halfband design is equal to 1 (Appendix B.2). The drawback is that the delay introduces a linear phase shift to the In Phase channel, but not the Quadrature channel. This establishes a phase imbalance in the quadrature upconverter, which will generate an unwanted sideband response (Chapter 4 will explore this in detail). The unwanted sideband can be cancelled by generating the equal and opposite sideband using the original signal, the same technique that is discussed in Chapter 4. This correction

scheme will require additional processing. Given that the multichannel wireless specifications are very stringent, the correction may actually introduce more processing than what has been saved by introducing the single delay.

The computation power (in MOPS) expressed in Eqn. (3.20) has been plotted for both the GSM and MPT1327 systems, Fig. 3.11. The system bandwidth for both systems is set to 5 MHz, and the sampling frequency of the combining stage, $f_{s\text{-comb}}$, is taken as 6.5 MHz. The reason that the GSM system is more efficient than MPT1327 for any given sampling frequency is related to the differing maximum spurious level specifications. GSM requires only -61.8 dBc alias attenuation, whilst MPT1327 requires -82 dBc.

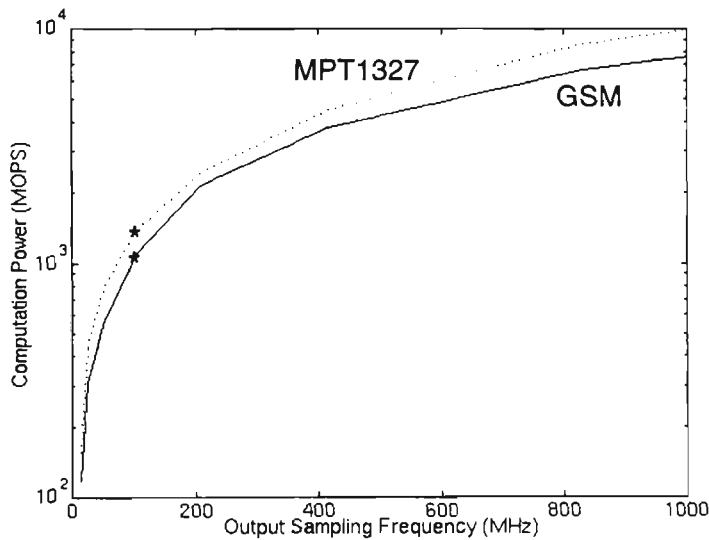


Figure 3.11: *Computation power required to interpolate and quadrature upconvert a multichannel signal to an intermediate frequency. Parameters are $BW_{sys} = 5$ MHz, $f_{s\text{-comb}} = 6.5$ MHz: MPT1327 - alias attenuation = 82 dBc; GSM - alias attenuation = 61.8 dBc.*

From Fig. 3.11, the amount of computation required to upconvert the complex baseband signal to an intermediate frequency is very large. For example, to achieve an intermediate frequency of 26 MHz approximately 1100 & 1400 MOPS are required for GSM and MPT1327 respectively (marked with a ‘ * ’ on Fig. 3.11). This is equivalent to 44 or 56 general purpose digital signal processors which is prohibitive in terms of size, complexity of hardware, cost, and power consumption.

Some additional reductions could be made by optimising the interpolators or by lowering the intermediate frequency. Regardless of these savings, implementation using currently available general purpose digital signal processors is impractical. Special purpose digital signal processors might be able to handle the processing requirements, by utilizing optimised filter designs [38-40] and introducing many arithmetic operations in parallel

simply by increasing the number of multipliers and adders on the special purpose chip. Such special purpose chips have recently become available. One example is the Harris HSP50016 Digital Down Converter, which performs the opposite task to that described here. It achieves an overall decimation factor ranging from 64 to 131072 at a maximum sampling rate of 75 MSPS. The Harris HSP43216 halfband decimation filter is another example which downconverts the IF signal to DC (using $f_{so}/4$ multiplication) but at a maximum sampling rate of 90 MSPS.

3.3.1.2 DAC Interface

The high intermediate frequency will place stringent demands on the speed and accuracy of the DAC interface, both of which affect the output carrier to noise ratio (CNR). This means that the DAC will limit the maximum channel power, and it will be the dominant source of noise, i.e. quantisation noise is greater than any contribution from thermal, shot or other noise sources.

The following analysis assumes that each transmitted channel is unmodulated with a peak amplitude of a_k , see Eqn. (3.2). The DAC is also assumed to have a Full Scale Range (FSR) of $2V_{max}$. If N_{comb} channels are to be combined, then the peak amplitude of each channel is limited to:

$$a_k = V_{max} / N_{comb} \quad (3.21)$$

This assumes the worst case scenario when all the channels are coherent, and the peak channel voltages add. Allowing for this scenario ensures that the multichannel signal can not clip. The resulting maximum average power (into one ohm) of each channel is then defined in terms of the V_{max} :

$$P_{av} = \frac{a_k^2}{2} = \frac{V_{max}^2}{2 \cdot N_{comb}^2} \quad (3.22)$$

Quantisation error will generate noise, which is assumed to be spread evenly across the Nyquist bandwidth ($f_{so}/2$) with a total power into one ohm equal to $\Delta^2/12$ [29], where Δ is defined as the step size of the DAC:

$$\Delta = \frac{2 \cdot V_{max}}{2^{n_b}} \quad (3.23)$$

and n_b is the number of bits or precision of the DAC.

Radio system specifications define the maximum out of band noise and spurious limits using a certain measurement bandwidth, BW_{meas} . Thus the quantisation noise power contained within this bandwidth is:

$$P_{N-meas} = \frac{\left(\frac{2 \cdot V_{max}}{2^{n_b}}\right)^2}{12} \cdot \frac{BW_{meas}}{f_{so}/2} = \frac{2 \cdot V_{max}^2 \cdot BW_{meas}}{3 \cdot 2^{2n_b} \cdot f_{so}} \quad (3.24)$$

The multichannel carrier to noise power ratio (CNR_{multi}) provided by an ideal DAC is then found by combining Eqns. (3.22) & (3.24):

$$CNR_{multi} = \frac{P_{av}}{P_{N-meas}} = \frac{3 \cdot 2^{2n_b} \cdot f_{so}}{4 \cdot BW_{meas} \cdot N_{comb}^2} \quad (3.25)$$

It can be shown that that Eqn. (3.25) reduces to the commonly used SNR parameter of a DAC, $(6.02n_b + 1.76)$ dB, if N_{comb} and BW_{meas} are set to 1 and $f_{so}/2$ respectively. That is, the input is a single sinusoid with a peak-peak amplitude equal to the full scale range of the DAC, and the noise power is measured across the entire Nyquist bandwidth.

The required multichannel CNR_{multi} ⁸ can now be derived directly from the system specifications. For example, a GSM transmitter, power class TRX8, specifies an average channel power of 34 dBm (P_{av}) whilst the amount of noise allowed in a 30 kHz bandwidth is -36 dBm (P_{N-meas}), a CNR_{multi} of 70 dB. In contrast, MPT1327 specifies a 47 dBm signal level and -36 dBm of noise within a 8.5 kHz bandwidth, a CNR_{multi} of 83 dB. Figure 3.12 plots the relationship between the output sampling frequency and the required precision of the DAC using these values of CNR_{multi} .

8. The CNR_{multi} value for the different systems, 70 dB (GSM) and 83dB (MPT1327), relates directly to the DAC. These values are different to that prescribed by the maximum spurious emission levels in Fig. 2.5(a) & (b), 61.8 dBc (GSM) and 82 dBc (MPT1327).

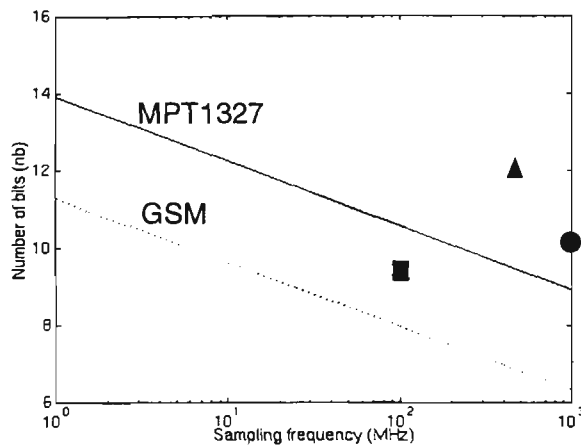


Figure 3.12: The output sampling frequency, f_{so} , versus the number of bits, n_b , for GSM and MPT1327 systems employing the digital IF upconversion technique. GSM (dotted) $N_{comb} = 4$, $BW_{meas} = 30$ kHz and $CNR_{multi} = 70$ dB. MPT1327 (solid) $N_{comb} = 10$, $BW_{meas} = 8.5$ kHz and $CNR_{multi} = 83$ dB.

The different CNR_{multi} system specification explains the variation between the two curves (accounting for about 1.5 bits in DAC precision). Additionally, the MPT1327 system combines more channels and this will account for an additional bit in DAC precision, Eqn. (3.25). Figure 3.12 also highlights the fact that as the sampling frequency increases the required precision of the DAC becomes less. On face value this is a very favourable situation, since commercial high speed DAC's have lower precision. However, can commercially available DAC's cope with the precision and speed requirements of the digital IF upconversion technique?

From the survey of DAC's (see Appendix C), the current state of the art is best represented by the Burr Brown 650, 12 bit @ 500 MHz. This point has been highlighted as a triangle on Fig 3.12. However, static and dynamic errors cause the real operation of the BB 650 to exhibit only 9.5 bit precision at 100 MHz sampling frequency (shown as a square on Fig. 3.12). Hence only the GSM system can be converted within the specifications. The intermediate frequency is also limited to a quarter of the DAC maximum sampling rate which would be approximately 25 MHz.

It should be highlighted that in the near future the speed and accuracy of commercially available DAC's should advance considerably. Recently published material suggests that state of the art DAC techniques are achieving sampling rates in the order of 1 GSample/s at over 10 bits in precision (see Appendix C). From Fig 3.12, highlighted as a circle, this would represent enough DAC precision for IF's in the order of 250MHz (assuming $f_{IF} =$

$f_{s0}/4$) to become possible. Regardless of these advances, static and dynamic errors will still compromise DAC performance and need serious consideration.

Static errors

The three static errors which are used to describe the accuracy of the DAC are gain error, offset error, and step (non)linearity. Step linearity errors are the most important of the static errors because they cannot be easily cancelled. The other two can be simply compensated for through calibration.

All calculations thus far have assumed that the step sizes of the DAC are uniform, resulting in the quantisation noise being white and uniformly distributed across the Nyquist Bandwidth [29]. However, non-uniform step size is a characteristic of a practical DAC, and this nonlinearity will cause some of the quantisation noise to be concentrated into harmonic and intermodulation products. These spurious responses are produced above the theoretical quantisation noise floor and are measured using the Spurious Free Dynamic Range (SFDR) parameter. The SFDR defines the ratio in power between the signal of interest (channel power) and the largest spurious or harmonic signal. Spurious and harmonic levels are of particular importance in a multichannel system because they can fall into unoccupied channels. Directly relating this to a radio system specification, the SFDR of the DAC must be greater than or equal to the CNR_{multi} .

The SFDR depends on the input signal and the specific quantiser transfer function [31-34]. It can be maximised by making the step sizes as accurate as possible in the fabrication process or by using a pre-processing algorithm to compensate for the static nonlinearity. The later technique will be investigated in Chapter 5 and the implementation is discussed in Chapter 6.

Dynamic Errors

There are many forms of dynamic errors including settling time, slew rate, glitches, ringing and sampling jitter. These dynamic errors are time domain effects, that are related to code dependent transitions and it is therefore difficult to predict the equivalent frequency-domain effects. Additionally, for high speed DAC's, circuit layout problems can introduce unwanted effects, such as the feedthrough of clock or data transitions to the DAC output.

As reference [30] explains, “Theoretically relating a DAC’s AC time domain characteristics to its frequency domain performance is neither feasible nor recommended.” “One simple observation about the AC non-linearities is possible: ..., the DAC spurious content can be expected to degrade at higher frequencies”. Therefore measurement is required to accurately characterise the dynamic performance of a specific DAC.

3.3.1.3 Summary

Digital IF upconversion requires the multichannel signal to be upconverted to a suitably high IF in the digital signal processing environment. The main considerations are the large amount of computation and the need for a high performance DAC.

Table 3.2: *Summary of IF upconversion using halfband filters*

IF (MHz)	System	C_{IF} (MOPS)	DAC precision (n_b)
26	MPT1327	1400	10.5
	GSM	1100	8
208	MPT1327	8700	8.5
	GSM	6700	6

Currently, the maximum sampling frequency and effective precision of the commercially available DAC limits the maximum intermediate frequency to around 25 MHz. A significant amount of computation is also needed to achieve this intermediate frequency. The combination of highly efficient upconversion algorithms and special purpose digital signal processing devices is essential for implementation.

Higher intermediate frequencies will require a faster DAC but with lower precisions, Table 3.2. Published results suggest that IF’s in the order of 100 MHz’s will soon be possible (see Appendix C). The amount of computation is therefore the major obstacle. This may be considered impractical today, but with costs dropping by a “factor of two every few years”, and “absolute capacities continuing to climb... per chip” [35], this technique will definitely become possible in the near future.

3.3.2 Subsampling Upconversion

Subsampling upconversion, Fig 3.13(a), is similar to the process of digital IF upconversion, except that the bandpass filter selects an alias of the output signal. The digital intermediate frequency generated in the DSP environment is lower than the analogue intermediate frequency after digital to analogue conversion. The main advantage of the technique is that it minimises the amount of digital signal processing for a given analogue IF. However, the output signal levels are lower and there is a greater amplitude variation across the transmitted band. A high performance DAC is still required.

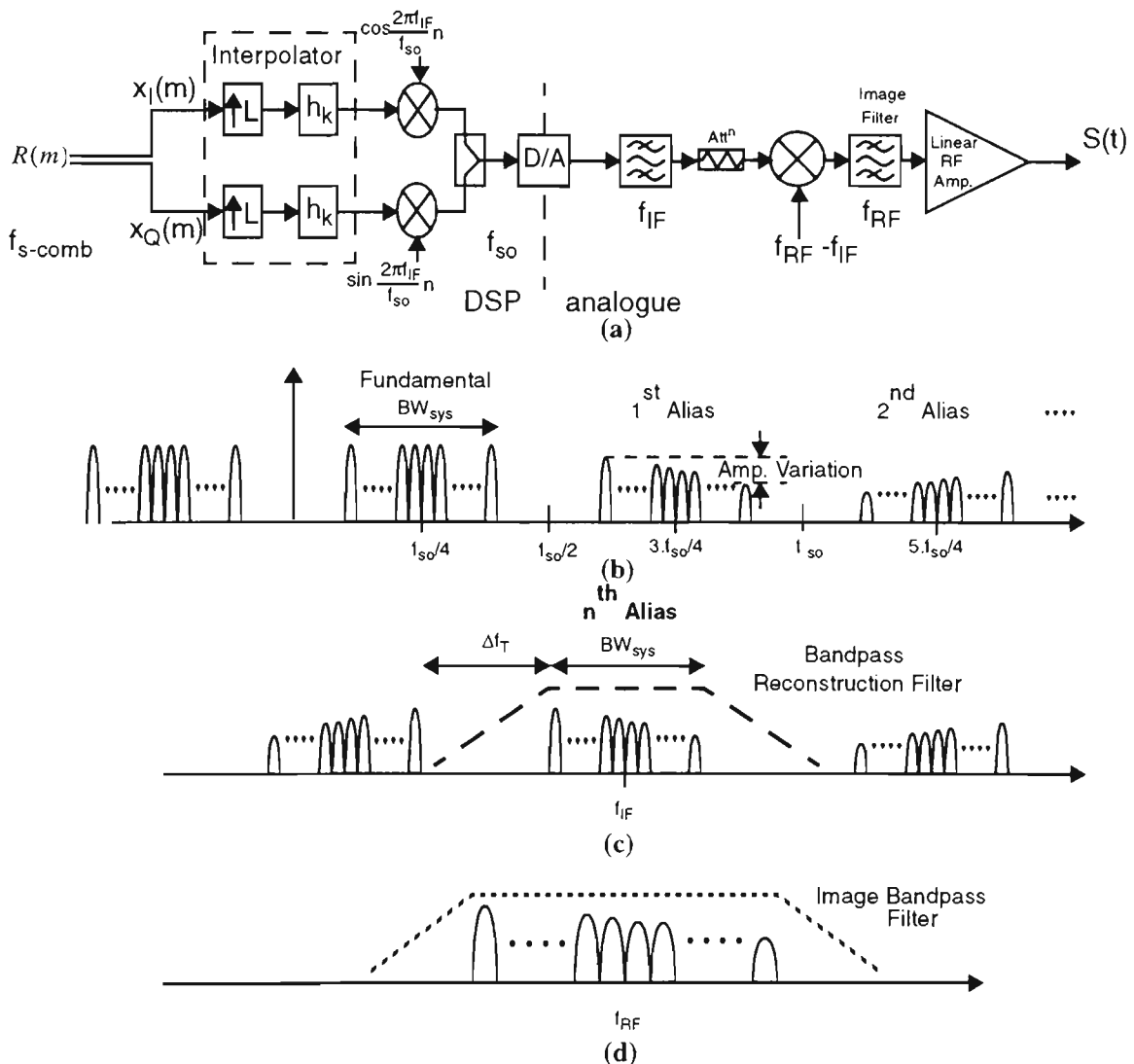


Figure 3.13: (a) Subsampling upconversion architecture. (b) Multichannel signal after DAC (c) Multichannel signal after bandpass reconstruction of the n^{th} alias. (d) Multichannel signal after RF upconversion.

The output from the DAC consists of the multichannel signal centred at $f_{so}/4$, and images (aliases) of the signal centred at frequencies of $(2n+1) \times f_{so}/4$, where n refers to the order (or number) of the alias. Subsampling upconversion makes use of the fact that the alias spectral components are replicas of the original signal.

Instead of reconstructing the signal by low pass filtering, one of the alias components is selected with a bandpass filter, Fig. 3.13(c). The odd aliases are simply frequency inverted versions of the even aliases. The higher analogue intermediate frequency can lead to the elimination of an analogue heterodyne upconversion stage without the large computational expense of the previous digital IF upconversion technique.

Subsampling is a technique that is being actively used in receiver structures. Although equally applicable, the use of subsampling in the transmitter has not been as widely reported. On the basis of the literature search, it seems that the only practical application of transmitter subsampling used the second alias to produce an analogue IF of 10 MHz, followed by two heterodyne stages to reach the final RF band of 1.9 GHz [24]. There has been no published implementations or analysis for multichannel transmitters. Published analysis for single channel transmitters has also been superficial. The next sections will present such an analysis for multichannel transmitters which is also applicable for the less stringent requirements of single channel systems. The analysis will include:

- the effect of output sampling frequency (f_{so}) and
- the effect of digital to analogue conversion.

3.3.2.1 The Effect of Output Sampling Frequency

The output sampling frequency affects four important design parameters; the alias frequency, the separation between adjacent aliases, the computation load and the required precision of the DAC.

The centre frequency of a given alias will vary with the sampling frequency. Given that the multichannel signal is centred at a quarter of the output sampling frequency, $f_{so}/4$, then the centre frequency of the alias can be written as:

$$f_{\text{alias}_n} = f_{so} / 4 + n \times f_{so} / 2 \quad (3.26)$$

As the sampling frequency increases, the aliases will move further apart. Given that the system bandwidth of the multichannel signal is constant, then the separation between the edges of each alias, Δf_T , will increase. The separation between adjacent alias components is given by:

$$\Delta f_{\text{alias}} = f_{so} / 2 - BW_{\text{sys}} \quad (3.27)$$

The amount of computation required for the subsampling technique is the same for digital IF upconversion, Eqn. (3.20) or Fig. 3.11. Therefore, the least amount of computation will result when the output sampling frequency is minimised. The lowest possible sampling frequency is 10 MHz (as predicted by Nyquist), given that the 5 MHz multichannel signal is centred at a quarter of the output sampling frequency, $f_{so}/4$. However, some oversampling is necessary for the subsequent bandpass filters (see the next section on 'Bandpass Reconstruction Filter').

The precision of the DAC is related to the output sampling frequency by Eqn. (3.25), plotted in Fig. 3.12. Increasing the sampling frequency will lower the required precision of the DAC.

The above discussions have highlighted that separation between adjacent alias components, the computational load and the required precision of the DAC are not dependent on the actual alias selected. They are only dependent on the sampling frequency.

Two output sampling frequencies, $f_{so} = 13$ MHz and 26 MHz, will now be used to explore the subsampling upconversion technique, Table 3.3. The corresponding n^{th} alias and Δf_T have been calculated from Eqns. (3.26) & (3.27) respectively. The computation load and required precision have been calculated for the two radio systems, GSM and MPT1327.

Table 3.3: Comparison of subsampling upconversion for two output sampling frequencies, $f_{so} = 13$ MHz and 26 MHz. $BW_{sys} = 5$ MHz and $f_{s-comb} = 6.5$ MHz.

f_{so}	Digital IF (MHz)	n^{th} Alias analogue IF (MHz)	Δf_T (MHz)	System	C_{IF} (MOPS) ^a	DAC precision - n_b ^b
13MHz (L=2)	3.25	3.25+(6.5 × n)	1.5	GSM	117	9.5
				MPT1327	156	12
26MHz (L=4)	6.5	6.5+(13 × n)	8	GSM	312	9
				MPT1327	442	11.5

a. Values taken from Fig. 3.11

b. Values taken from Fig. 3.12

The lower output sampling frequency minimises the amount of computation. However, a higher precision DAC is required and the separation between the aliases is smaller.

Doubling the sampling frequency reduces the required DAC precision by half a bit. Eqn. (3.25), but increases the computational load by more than a factor of two. The separation between the aliases, Δf_{alias} , is also increased by a factor of 5.3, regardless of the alias selected. This will significantly decrease the complexity and the bandpass filter and make its design easier.

Bandpass Reconstruction Filter

The bandpass filter is best discussed with reference to its parameters as illustrated in Fig. 3.14.

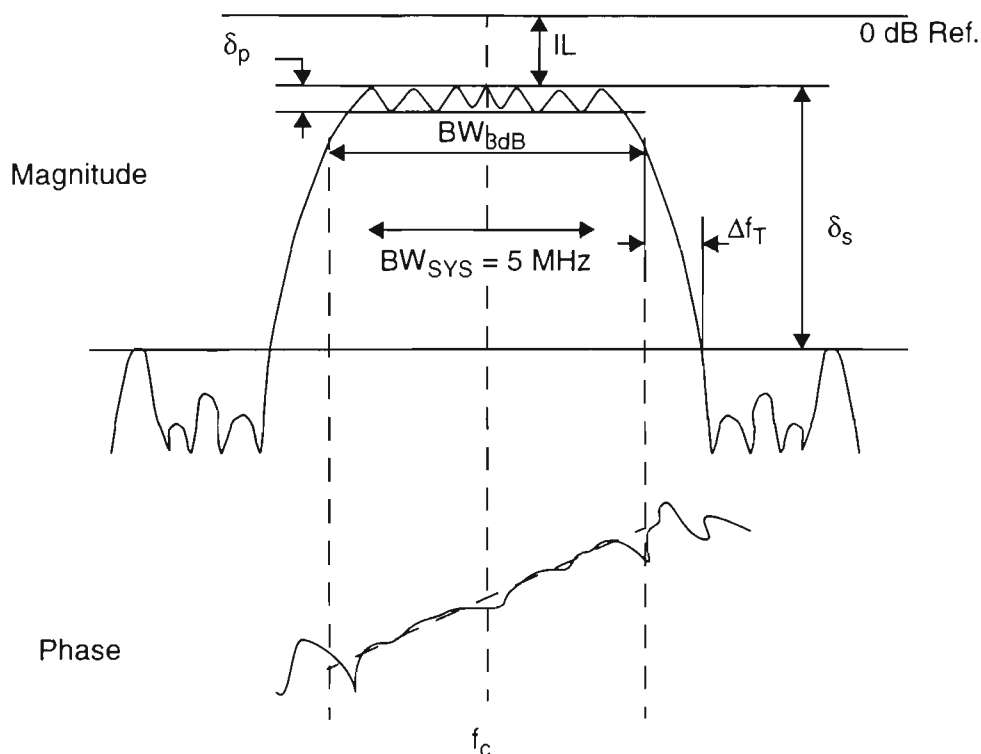


Figure 3.14: *Bandpass Filter Parameters.* δ_s = stopband ripple, δ_p = passband ripple, Δf_T = transition width, BW_{3dB} = 3dB bandwidth, IL = Insertion Loss, f_c = centre frequency.

An excellent review of bandpass filter technologies is given in reference [41]. The fractional 3 dB bandwidth (or %BW for brevity) is used to determine the filter technology for a specified centre frequency. It is defined as:

$$\%BW = \frac{BW_{3dB}}{f_c} \times 100 \% \quad (3.28)$$

Fractional bandwidths greater than 0.1% are seen as being practical for centre frequencies ranging between 25 MHz and 2 GHz [41].

The Shape Factor (SF), defines the attenuation characteristics of the filter, so that a certain amount of attenuation, δ_s , is achieved in a given transition width, Δf_T :

$$SF = \frac{BW_{3dB}/2 + \Delta f_T}{BW_{3dB}/2} \quad (3.29)$$

The relationship between the shape factor and the order of a Chebychev filter with a 0.1 dB ripple is shown in Fig. 3.15. Filter realisation is made increasingly difficult for shape factors less than about 2.5 because the filter order⁹ is large. For example, a filter order that is greater than 6 will occur for 61.8 dB of stopband attenuation.

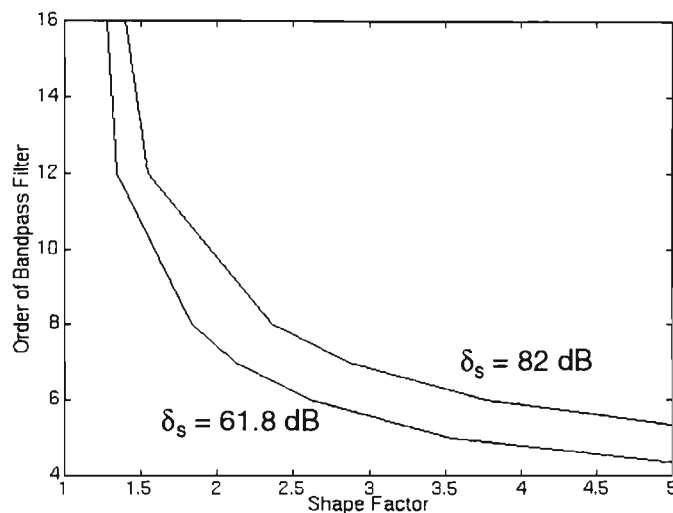


Figure 3.15: *Shape factor vs. the order of a Chebychev bandpass filter with a 0.1 dB ripple for two attenuation specifications of 61.8 dBc and 82 dBc.*

A trade-off exists between the computational load and the complexity of the bandpass filter. A higher sampling frequency, or larger amount of computation, is required to increase the shape factor and consequently lower the filter order. A lower order filter will have a lower insertion loss, a more linear phase response, a reduced size and cost. For example, an analogue IF of 29.25 MHz can be achieved from a sampling frequency of 13MHz and selecting the 4th alias, or an analogue IF of 32.5 MHz can be achieved from a sampling frequency of 26 MHz and selecting the 2nd alias (Table 3.4).

The most appropriate filter technology for both cases is the lumped element filter [41]. This has been selected using the %BW, which was calculated using a 3 dB filter bandwidth which is 10% larger than the system bandwidth. A larger bandwidth is a means of improving the phase response across the signal spectrum.

9. The number of poles for a bandpass filter is 2 times the filter order. This definition is in common use by filter manufacturers.

Table 3.4: Example to achieve an analogue IF of approximately 30 MHz.

f_{so} MHz	Analogue IF MHz (Alias)	BW_{3dB} (MHz)	%BW	Tech ^a	Δf_T (MHz)	SF	δ_s (dB)	Order ^b
13	29.25 (4 th)	5.5	18%	LC ^c	1	1.4	61.8	11
							82	15
26	32.5 (2 nd)	5.5	17%	LC	7.5	3.7	61.8	5
							82	6

a. Tech - Technology chosen using Reference [41]

b. Order - From Fig. 3.15

c. LC - Lumped element filter

The required filter order is calculated using the transition width, Δf_T , and the stopband attenuation, δ_s (Table 3.4). The lower sampling frequency generates such a small shape factor that the required order of the filter (> 11) is impractical for a single filter implementation. The higher sampling frequency significantly lowers the order which results in a less complex filter.

The subsampling IF upconversion technique can also generate a higher analogue intermediate frequency by reconstructing a higher order alias, Table 3.5. Generation of a 250 MHz analogue IF, as opposed to 30 MHz, requires no increase in the output sampling frequency (computation load), transition width, shape factor and filter order. However, a number of filter technologies are now possible because of the lower %BW. These include LC filters, SAW transversal filters, cavity resonators and Dielectric Resonators (DR) [41].

Table 3.5: Example to achieve an analogue IF of approximately 250 MHz.

f_{so} MHz	Analogue IF (alias) MHz	BW_{3dB} MHz	%BW	Tech ^a	Δf_T MHz	SF	δ_s dB	Order ^b
26	253.5MHz (19 th)	5.5	2.2%	LC SAW Helical DR	7.5	3.7	61.8	5
							82	6

a. Tech - Technology chosen using Reference [41]

b. Order - From Fig. 3.15

The choice of the best filter technology requires the consideration of many design issues. The LC filter is sensitive to temperature and vibration [41], whilst at least two cascaded SAW transversal filters will be required to achieve the desired attenuation characteristics. Given that the insertion loss of each SAW filter will be greater than 15 dB, this represents at least 30 dB of insertion loss! Dielectric resonators have spurious responses which can be removed by a low Q filtering stage. The helical resonator has the lowest amount of insertion loss, but is larger in size than the other technologies. Selection of the best bandpass technology will also need the consideration of manufacturer dependent parameters such as phase response, temperature stability and cost.

In conclusion, the analogue intermediate frequency is NOT limited by the bandpass filter. A number of filter technologies are possible, although there is a complicated choice of design trade-offs.

3.3.2.2 The Effect of Digital to Analogue Conversion

The digital to analogue conversion process will introduce $\sin(x)/x$ and nonlinear distortion. The effect of these distortions on the multichannel signal at the analogue IF will now be analysed.

Sin(x)/x Distortion

The DAC completes the digital to analogue conversion by holding each sample constant for the duration of a sample period. The holding action of the DAC distorts the signal with a roll-off characteristic that can be accurately described by the $\sin(x)/x$ function, where $x = \pi \times f / f_s$. The effect causes significant amplitude variation and attenuation of the aliased multichannel signal.

Amplitude variation across the multichannel signal can be illustrated by considering a multichannel signal centred at $f_{s0}/4$ with a system bandwidth of 5 MHz. The output sampling frequency, f_{s0} , is then varied (Fig. 3.16(a)). At $f_{s0}=13$ MHz the first and second alias experience huge amplitude variation of 17 dB and 11 dB across the system bandwidth. This drops to 8 dB and 4 dB at $f_{s0}=26$ MHz. Any other alias will experience an amplitude variation bounded by the first and second alias values.

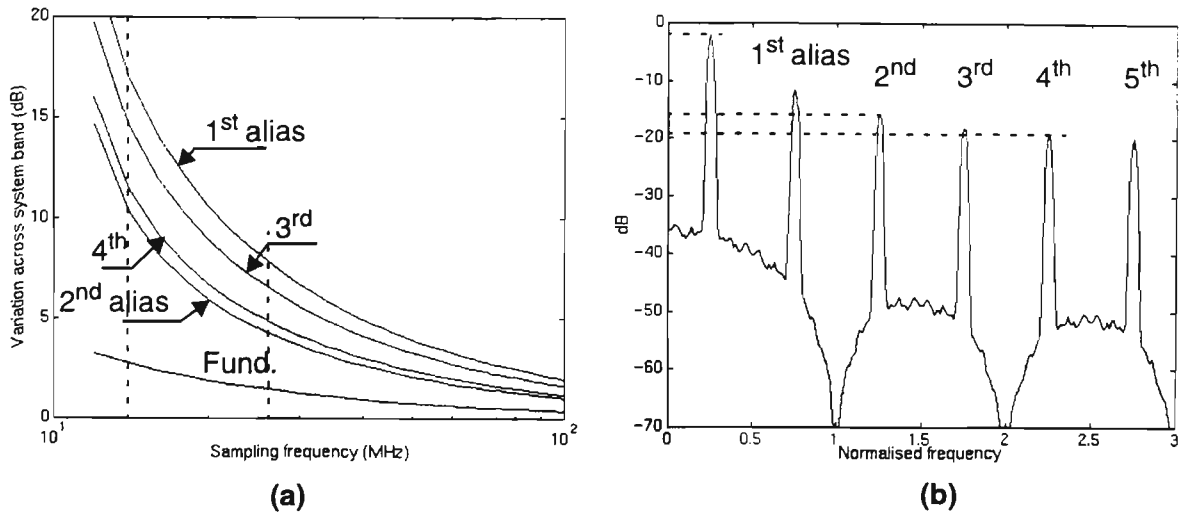


Figure 3.16: (a) Amplitude variation (dB) across system bandwidth of 5 MHz vs sampling frequencies for different aliases. (b) Simulated output from an ideal DAC showing the attenuation of the different aliases. The sampling frequency is normalised to 1.

Compensation is necessary for lower sampling frequencies regardless of the actual alias used. This is not a problem when narrowband channels are being transmitted, i.e. MPT1327, since it is possible to amplitude correct each channel. Correction for systems with a large channel bandwidth, i.e. GSM, is more difficult since the amplitude change across the channel will be significant, requiring equalisation across the channel band rather than a simple amplitude adjustment. Digital IF upconversion utilises the fundamental signal and the required $\sin(x)/x$ compensation is much less. For example 3 dB of amplitude variation occurs at $f_{s0} = 13$ MHz, and this drops to a negligible 0.3 dB at $f_{s0} = 100$ MHz.

The $\sin(x)/x$ roll-off also affects both the aliasing components and the quantisation noise as illustrated in Fig. 3.16(b). The CNR_{multi} for any alias at the output of the DAC will be unaffected and can therefore be predicted by Eqn. (3.25), provided external sources (thermal, pickup and shot noise) are less than the quantisation noise. This situation becomes less likely when selecting a higher order alias. For example, Fig. 3.16(b) shows that the 2nd and 4th aliases undergo 13 dB and 18 dB attenuation respectively. This amount of attenuation could lower the quantisation level below the external noise levels, subsequently reducing the CNR_{multi} predicted by Eqn. (3.25).

Therefore, as long as the quantisation noise continues to dominate the external sources of noise, the CNR_{multi} for all aliases will be unaffected. However, nonlinear distortion of a practical DAC does reduce the SFDR performance with increasing frequency and this will subsequently limit the selection of the alias.

Nonlinear DAC Distortion

The performance of a practical DAC is compromised by the static and dynamic non-linear (see Section 3.3.1.2), as illustrated in Fig. 3.17 (taken from Ref. [42]). The signal spectrum, which consists of the fundamental and alias components, has the characteristic $\sin(x)/x$ roll-off characteristic, whilst the magnitude of the spurious and harmonic distortion remains approximately constant. The result is a dramatic reduction in the DAC performance for each successive alias, as measured by the SFDR. An 11dB reduction in the SFDR is experienced in the second alias, whilst an 18dB reduction in SFDR has occurred by the 4th aliasing component. The level of the sampling clock harmonics also increases with frequency..

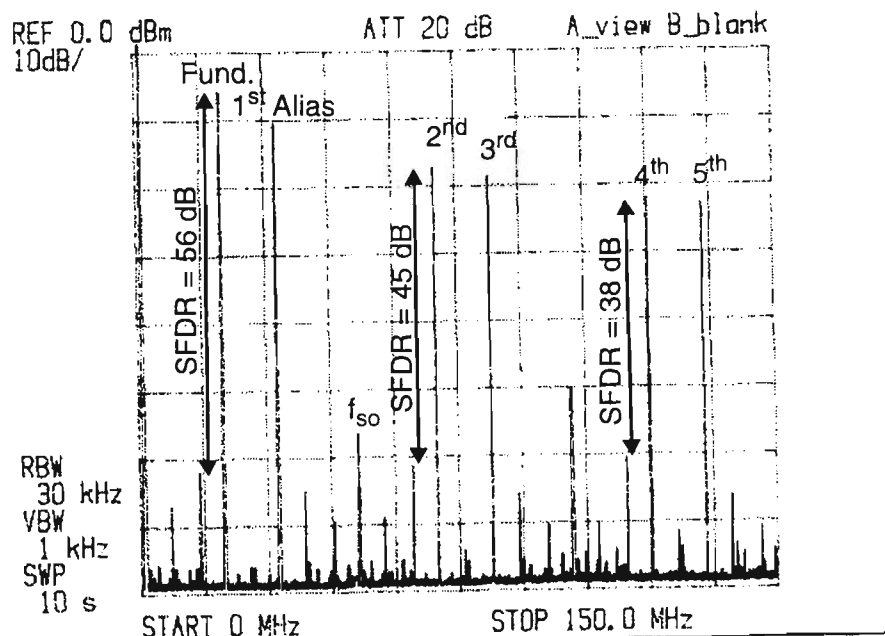


Figure 3.17: The wideband spectral plot from DC to 150 MHz (taken from Reference [26]). Fundamental signal frequency = 20 MHz; Output sampling frequency (f_{so}) = 50 MHz; 10 bit DAC (AD9721BBN)

The DAC performance therefore degrades with each subsequent alias. This restricts subsampling upconversion to lower order aliases. Also, the DAC precision would have to be larger than that determined from Eqn. (3.25) to compensate for the degradation experienced with increasing frequency. This would make the design substantially more expensive, if not impractical.

3.3.2.3 Summary

Compared to digital IF upconversion, subsampling upconversion minimises the amount of computation, producing a circuit that is smaller, with lower power consumption and cost. However, the selection of the analogue IF is limited to lower order aliases by the decreasing SFDR of a practical DAC when the frequency increases. Therefore, the analogue IF may still not be enough to reduce the number of analogue heterodyne upconversion stages.

The $\sin(x)/x$ roll-off characteristic of the DAC causes amplitude variation across the band which requires compensation. For a narrowband system, MPT1327, this compensation could be a simple amplitude correction, however, for systems with wider channel bandwidth, GSM, a more complicated equaliser will be required.

The bandpass filter is not seen as a limitation in subsampling upconversion.

3.3.3 Analogue Direct Upconversion - Lowpass Reconstruction

Analogue direct upconversion, Fig. 3.18(a), is a technique that has received a lot of attention recently due to its suitability as a universal single channel modulator (and demodulator); it is simple, small, has low (DC) power consumption, and can be applied to any modulation scheme. The analogue direct conversion transmitter translates the baseband multichannel signal directly to the desired frequency band using analogue components.

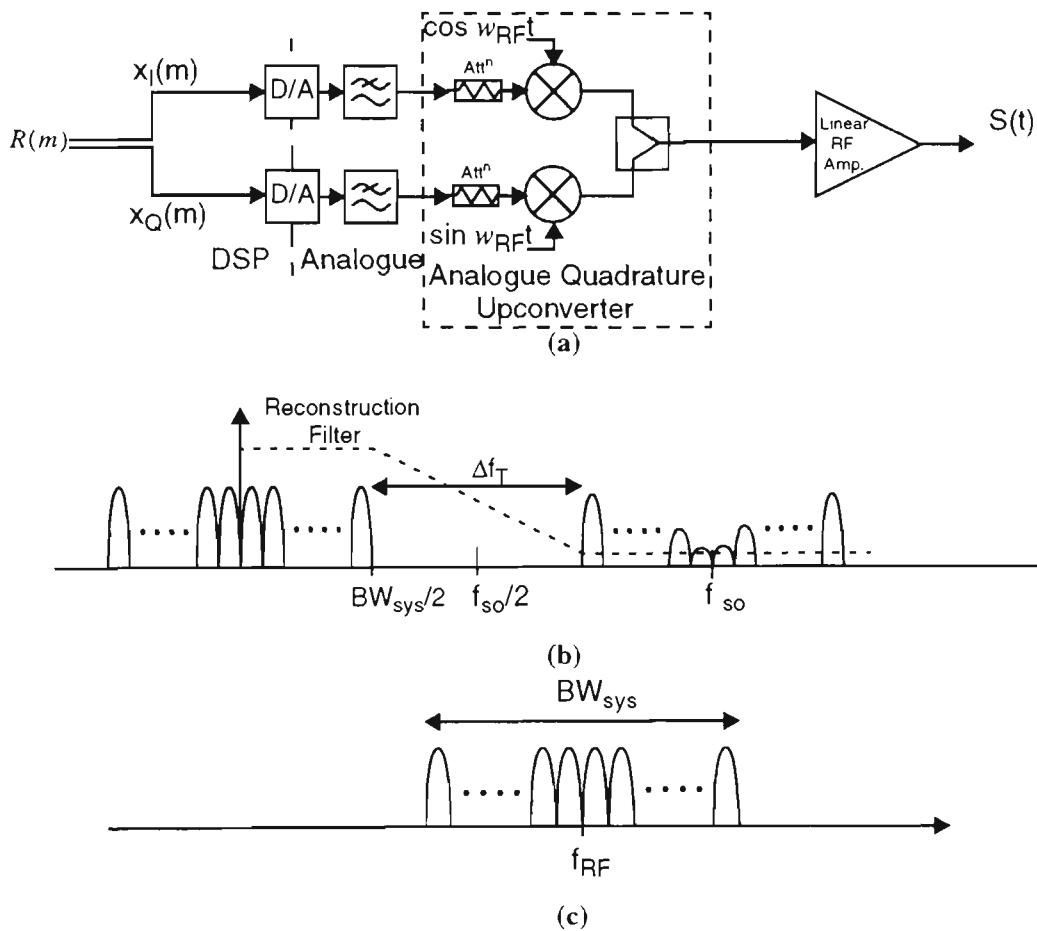


Figure 3.18: (a) Analogue direct conversion with low pass reconstruction (b) Multichannel signal after DAC showing the aliases and the $\sin(x)/x$ response. The lowpass reconstruction filter response is also shown. (c) Multichannel signal after analogue upconversion.

The baseband multichannel In Phase, $x_I(t)$, and Quadrature, $x_Q(t)$, signals generated in a DSP environment, are first converted to an analogue signal (DAC) and reconstructed by a low pass filter. They are then mixed with quadrature phased carrier signals (w_{RF}) and combined to form the multichannel RF signal, Fig. 3.18(c). The digital signal processing computation load is potentially less than that for the previously discussed digital IF upconversion techniques.

3.3.3.1 Computational Requirements

Calculation of the analog direct upconversion computational requirements will assume a multistage interpolation technique using halfband interpolators:

$$C_{ADU} = 2 \cdot \{\text{stage 1}\} \cdot f_{s\text{-comb}} + 2 \cdot \{\text{stage 2}\} \cdot 2 \cdot f_{s\text{-comb}} + \dots + 2 \cdot \{\text{stage } j\} \cdot f_{s0} \quad (3.30)$$

The computational power (in MOPS) versus the output sampling frequency has then been plotted for both the GSM and MPT1327 systems, Fig. 3.19.

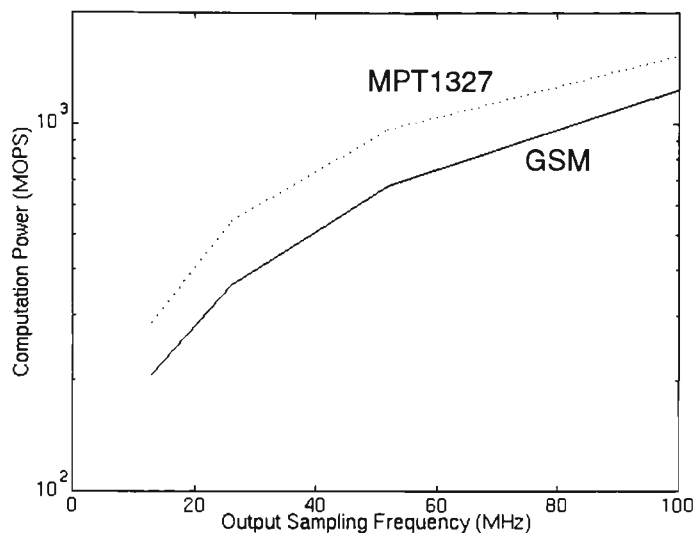


Figure 3.19: Computation power required to interpolate and quadrature upconvert a multichannel signal for analogue direct conversion. Parameters are $BW_{sys} = 5 \text{ MHz}$, $f_{s\text{-comb}} = 6.5 \text{ MHz}$; MPT1327 - alias attenuation = 82 dBc; GSM - alias attenuation = 61.8 dBc

The computational load for the analog direct upconversion is greater than that for the two digital upconversion techniques, Eqn (3.20) and Fig. 3.11, for a given output sampling frequency. However, the output sampling frequency (computation load) is potentially a lot lower for analog direct upconversion. Digital IF upconversion requires a sampling frequency of 104 MHz to achieve an intermediate frequency of 26 MHz, whereas to achieve approximately the same intermediate frequency, subsampling upconversion will require a sampling frequency of 26 MHz. The resulting 8 MHz of transition width allows for the practical implementation of the bandpass reconstruction filter. Analogue direct upconversion requires only a sampling frequency of only 13 MHz to achieve the same 8 MHz of transition width.

A sampling frequency of 13 MHz translates to 208 & 286 MOPs of computation for GSM and MPT1327 systems respectively. The computation load for analog direct upconversion is therefore significantly lower than digital IF upconversion and marginally lower than subsampling upconversion. Unfortunately, analogue quadrature upconverters have a well known source of linear error, namely the amplitude and phase imbalance (mismatch) between the I and Q paths [43], and this is a significant problem.

3.3.3.2 Linear Errors

Different phase and amplitude responses introduce most of the imbalance between the I and Q paths. Additionally, some phase imbalance can be attributed to the local oscillator signals not being in exact quadrature; due to the non-ideal characteristics of the mixers and phase splitter.

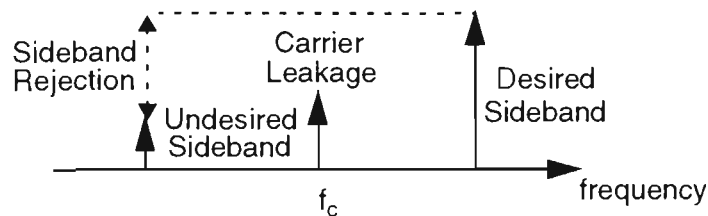


Figure 3.20: Error signals in an quadrature upconverter.

The imbalances result in an undesired (image) sideband. For example, if a single sideband (SSB) tone is output through the quadrature upconverter, then the resulting signal will consist of the desired sideband, an undesired sideband and some carrier leakage, as shown in Fig. 3.20. If the imbalances are small then it can be shown that the power ratio of the undesired to desired sideband (referred to as the sideband rejection) is [21]:

$$\text{Sideband Rejection (SR)} = 10\log\left(\frac{\text{undesired sideband}}{\text{desired sideband}}\right) = 10\log\left(\frac{1}{4}\left(\alpha^2 + \Phi_e^2\right)\right) \text{ dBc} \quad (3.31)$$

where α and Φ_e are the relative gain and phase mismatch between the I and Q paths respectively. It is reasonable to talk of component imbalances (neglecting the reconstruction filters) of 0.3 dB and 3° in a well designed analogue quadrature upconverter. Imbalances of this magnitude would result in -30 dBc of sideband rejection, sufficient for some single channel applications.

The multichannel application highlights a unique problem due to the need for tighter

control of the amplitude and phase imbalance compared to the single channel case. When a multichannel signal, Fig. 3.21(a), is passed through an unbalanced quadrature upconverter, the resulting sideband signals, Fig. 3.21(b), will either fall into an occupied channel or an unoccupied channel. Analysis of these two cases gives insight into the amount sideband rejection, or imbalance, that can be tolerated.

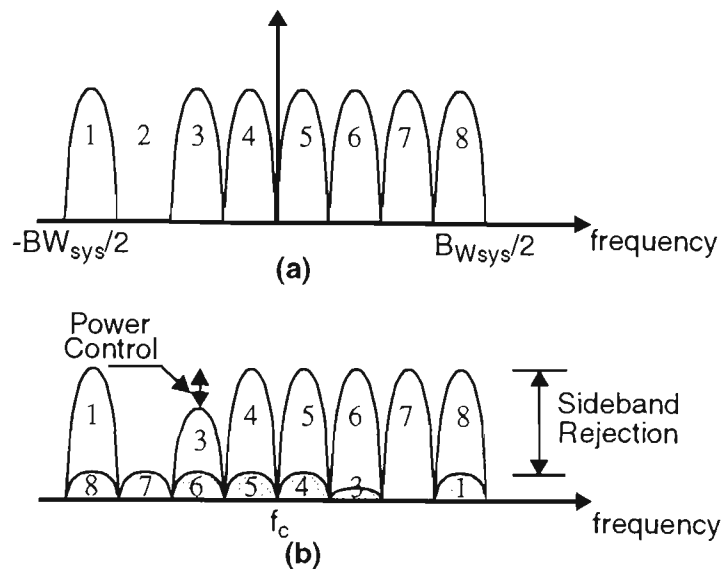


Figure 3.21: (a) Ideal multichannel signal before upconversion displayed in complex baseband format. (b) Desired and undesired (image) signals after imbalanced quadrature upconversion. Note that channel 2 is not activated and channel 3 is subject to power control. In both these situations, the image signal of channel 7 and 6 are more of a problem.

If the sideband signal falls into a channel that is currently being transmitted, it will cause distortion (shown shaded in Fig. 3.21(b)). This is similar to the self distortion that occurs for a single channel quadrature modulator. The required sideband rejection is related to the carrier to noise performance of the modulation (for a given bit error rate). The GSM system will operate at a 9dB carrier to noise ratio at the receiver. The distortion introduced by the imbalances of the transmitter would need a margin of around 6 dB below this level so that there is no noticeable effect. Additionally if power control is employed (30 dB from GSM specifications, channel 3 in Fig. 3.21(b)) then sideband rejection at the transmitter should be greater than -45 dBc so not to affect the error rate performance of the system.

The sideband signal could equally fall into a vacant channel position (the image of channel 7 falling into the vacant channel 2, Fig. 3.21(b)). In this situation the system must meet the spurious emission level specification. For the GSM system with an 8th power class transmitter, Fig. 2.5(a), the SR specification would be -61.8 dBc, whereas for the MPT1327 system, Fig. 2.5(b), the SR specification is more stringent at -82 dBc. The

tolerance of phase and amplitude imbalance is illustrated in Fig. 3.22. Obviously the analogue quadrature upconverter is not practically usable in a multichannel environment without some form of refinement that corrects the amplitude and phase imbalance. A novel technique for correcting these imbalances will be introduced in Chapter 4.

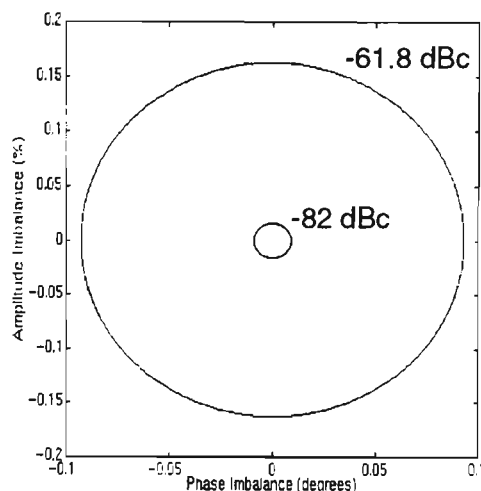


Figure 3.22: *To meet a given amount of sideband rejection, the corresponding phase and amplitude imbalance must fall within the boundary indicated.*

Carrier leakage, Fig 3.20, is another source of error. It is caused by the lack of local oscillator isolation in the mixer, and by any DC offsets in the I and Q paths. DC compensation techniques used in single channel applications [25-26] can be utilised to suppress the carrier leakage component.

3.3.3.3 DAC Interface

The lower output sampling frequency of analogue quadrature upconversion will lessen the speed requirements of the DAC interface. The minimum output sampling rate of the DAC is 6.5 MHz for a system bandwidth of 5 MHz. This is lower than that of the previous two upconversion techniques. The value of sampling frequency would be higher if oversampling is incorporated to reduce the reconstruction filter complexity. For a combining sampling frequency of 6.5 MHz, the filters transition bandwidth (Δf_T) is 1.4 MHz. Interpolating the complex baseband multichannel signal by a factor of 2 ($f_{so} = 13$ MHz) will increase the transition bandwidth to 8 MHz, a factor of 6 times larger than the previous value. Therefore the reconstruction filter will be much simpler.

Two consequences of increasing the oversampling ratio are the additional computation and the increased speed of the DAC. The latter is less of a problem compared to the previous digital IF techniques because the multichannel signal is contained at baseband,

where the DAC nonlinearity generates lower spurious levels.

Appendix D shows that the carrier to noise ratio at the output of the analogue direct upconverter is twice that of the carrier to noise ratio at the output of each DAC. Therefore the required precision of the two DAC's used in direct upconversion is 3dB less than that required by the single DAC used in the two previous upconversion techniques (at the same sample rate). Equation (3.25) can therefore be appropriately modified:

$$CNR_{multi} = \left(\frac{3 \cdot 2^{2n_b} \cdot f_{so}}{4 \cdot BW_{meas} \cdot N_{comb}^2} \right) \times 2 \tag{3.32}$$

Figure 3.23 plots the relationship between the output sampling frequency and the required precision of each DAC interface. Note that the curves on Fig. 3.23 are half a bit lower than that on Fig 3.12 for the same sampling frequency. This fact highlights a small advantage of analogue direct upconversion over the two previous upconversion techniques.

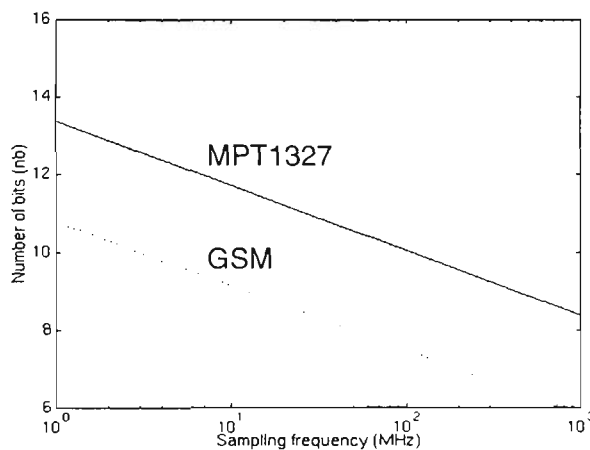


Figure 3.23: The output sampling frequency, f_{so} , versus the number of bits, n_b , for GSM and MPT1327 systems employing the analogue, quadrature upconversion technique. GSM (dotted) $N_{comb} = 4$, $BW_{meas} = 30$ kHz and $CNR_{multi} = 70$ dBc; MPT1327 (solid) $N_{comb} = 10$, $BW_{meas} = 8.5$ kHz and $CNR_{multi} = 83$ dBc

For an output sampling frequency of 6.5 MHz, 9.5 and 12 bits of precision are required for GSM and MPT1327 systems respectively. This reduces by half a bit at 13 MHz sampling frequency. The differing amount of precision can be attributed mainly to the number of combined channels (N_{comb}) and the system specification (CNR_{multi}).

3.3.4 Analogue Direct Upconversion - Bandpass Reconstruction

This technique of upconversion utilises the quadrature upconverter structure but rather than reconstructing the signal using lowpass filters immediately after the DAC's, the signal reconstruction occurs in a bandpass filter after the quadrature upconverter, Fig 3.24(a). This removes one source of amplitude and phase imbalance, which is significant in a multichannel situation as will be seen in the chapter 4.

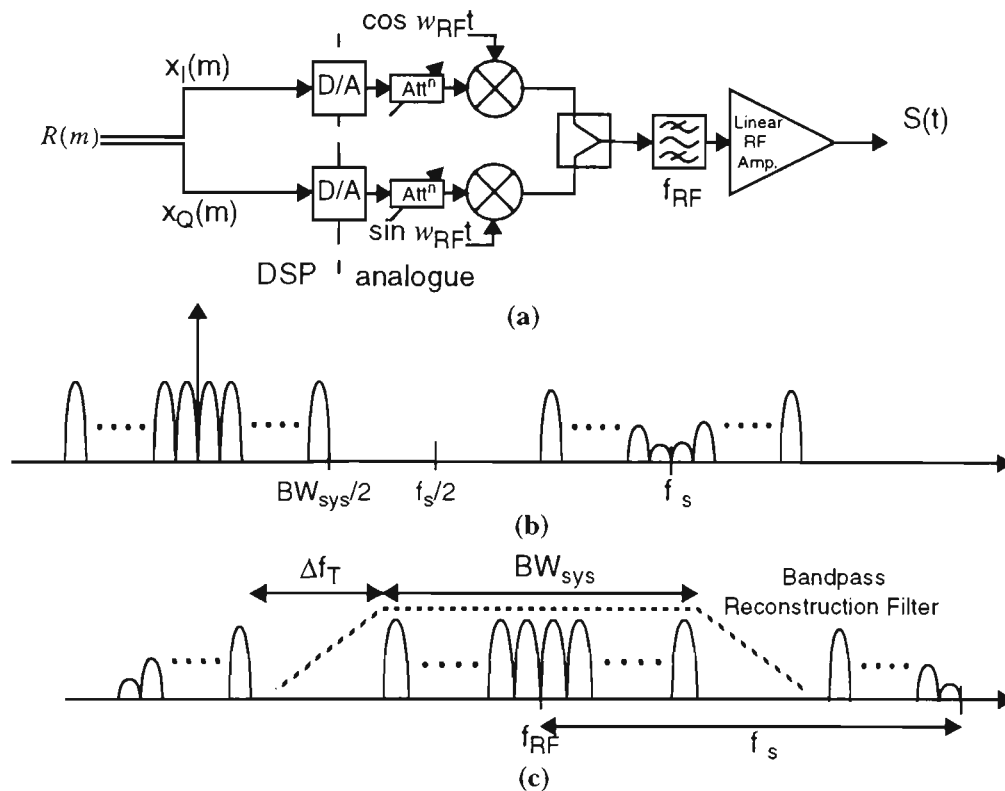


Figure 3.24: (a) Analogue direct upconversion- bandpass reconstruction architecture (b) Ideal multichannel signal after DAC showing the aliasing components and the sinc/x response (c) Multichannel signal after RF upconversion showing the bandpass reconstruction filter characteristic.

The bandpass reconstruction filter must attenuate the digital aliasing signals that are still present from the sampling process, Fig. 3.24(c), and it will have a similar performance requirement to the previously described sub-sampling upconverter, although the centre frequency is now the final RF transmitting frequency.

3.3.4.1 The Bandpass Reconstruction Filter

The RF transmitting frequency will depend on the radio system. Currently cellular and trunking radio systems are operated at around 900MHz, whilst future PCS systems will operate in the 1.8 GHz frequency band. These two frequencies will now be used to

illustrate the bandpass filter design requirements.

This example will again assume that the baseband multichannel signal has been interpolated by 2 ($f_{s0} = 13$ MHz) to widen the filter transition bandwidth. The amount of computation power is the same at 208 MOPS for GSM and 286 MOPS for MPT1327.

The filter %BW is quite small because of the high final centre frequency, Table 3.6. The best choice of technology for both the 900 MHz and the 1.8 GHz band is therefore the cavity (coaxial) or dielectric resonators, although SAW (transversal or coupled-resonator) filters could be applied at the 900MHz band. SAW filters are not practical at 1.8GHz [41].

Table 3.6: Example to achieve a final RF transmission frequency of 900MHz and 1.8GHz.

L	Centre frequency	BW _{3dB} (MHz)	%BW	Tech ^a	Δf_T (MHz)	SF	δ_s (dB)	Order ^b
2	900 MHz	5.5	0.6 %	SAW Cavity DR	7.5	3.7	61.8	5
	1.8 GHz		0.3 %	Cavity DR			82	6

a. Tech - Technology chosen using Reference [41]

b. Order - From Fig. 3.15.

The bandpass filter requires a filter order of 5 or 6 which is practical in at least two technologies, Table 3.6.

3.4 Conclusion

This chapter focused on the use of DSP combining for multiple channels in a frequency division multiplex format and the frequency translation of the multichannel signal to RF.

The combining of multiple channels consists of a sample rate interpolator, a multiplier and a summer. To minimise the computational load three interpolator techniques were investigated. Cascaded halfband interpolator stages were shown to be more efficient than the polyphase FFT technique for less than 8 channels. The polyphase FFT technique incorporates the interpolator, multiplier and summer into one efficient algorithm and the computation load is constant regardless of the number channels combined. The memory LUT approach is usable for digital modulation schemes, where the number of output states (trajectories) is small enough not to require an excessive amount of memory. The modulated signal is generated at the higher sampling frequency directly from the LUT, eliminating the need for an interpolation (filtering) stage. This technique has the lowest computation load with only modest memory size and access speed requirements.

The computation load of multichannel combining is dependent on the radio system and the number of channels to be combined, N_{comb} . The GSM cellular radio system needs 124 MOPS (the equivalent of 5 general purpose C40s) to combine 4 channels using the memory LUT approach, whereas the trunking radio system, MPT1327, requires 780 MOPS (the equivalent of 32 general purpose C40s) to combine more than 8 channels.

The final sections of the chapter discuss the upconversion of the multichannel signal to RF. Four different techniques are summarised in the first column of Table 3.7. All techniques required further sample rate interpolation before upconversion to RF.

Digital IF upconversion translates the baseband multichannel signal to an intermediate frequency at a quarter of the output sampling frequency. There is a need for a very high performance DAC, which presently limits the intermediate frequency to approximately 25 MHz (a sampling frequency of 100 MHz). However, published results (Appendix C) suggest that DAC's capable of 1 GHz sample rates and of sufficient performance will soon be available.

Table 3.7: Summary of the four different upconversion techniques.

Upconversion Technique	Computation Power (MOPS)		DAC Precision (n_b)		Upconverter Stages		Main design issues (in order of importance)
	GSM	MPT1327	GSM	MPT1327	Quadrature	Heterodyne	
Digital IF	1100	1400	8	10.5	1-digital	2	(i) Computation Power. (ii) DAC Performance
Subsampling	312	442	9	11.5	1-digital	1->2	(i) Analogue IF limited by DAC (ii) $\text{Sin}(x)/x$ compensation. (iii) Bandpass Filter
Analogue Direct - LPF	208	286	9	11.5	1-analogue	0	(i) Linear Errors - esp. LPF (ii) DAC Performance
Analogue Direct - BPF	208	286	9	11.5	1-analogue	0	(i) Linear errors (ii) DAC performance (iii) Bandpass Filter

The main disadvantage of the digital IF upconversion technique is the computational requirements of the interpolation process. Between 1100 and 1400 MOPS are required to achieve an IF of 26 MHz using halfband filters. The implementation of more efficient interpolation architectures [38-40] could lower the amount of computation required. In addition improvements in technology will make this technique more viable in the future.

Subsampling upconversion, substantially lowers the computational requirements of the previous technique. This technique uses a bandpass filter to select an alias of the DAC output signal rather than the fundamental. A higher analogue intermediate frequency can be obtained and thus the potential exists for eliminating one of the following heterodyne stages.

A disadvantage of subsampling with wide channel bandwidths is the amplitude variation (up to 20 dB) caused by the $\text{sin}(x)/x$ roll-off. Correction for amplitude variation is necessary and will require additional computation. The ultimate analogue IF is also limited by the performance of the DAC, which degrades as the frequency increases. Therefore at the frequency of the selected alias, the DAC must exhibit performance consistent with the precision stated in Table 3.6. The bandpass filter is not seen as a limiting factor here.

The last two techniques consist of translating the baseband multichannel signal directly to RF using an analogue quadrature upconverter. Both schemes are very similar in design,

one reconstructs the signal with a LPF whilst the other uses a BPF. Compared to the digital IF techniques, analogue direct upconversion has the advantages of low computation power and a lower performance DAC. Therefore, analogue direct upconversion justifies further study.

Unfortunately, amplitude and phase imbalances, inherent in the analogue quadrature upconverter, require compensation. A new technique of compensation to overcome the phase and amplitude imbalances will be investigated in the next Chapter.

The performance, in terms of SFDR, of the DAC is degraded by the step nonlinearity. A pre-processing algorithm used to overcome the step nonlinearity and improve the SFDR will be investigated in Chapter 5 and the implementation discussed in Chapter 6.

Chapter 4

The Effect of Reconstruction Filters on Analogue Direct Upconversion

4.1 Introduction

The previous chapter highlighted the issue of phase and amplitude imbalance in an analogue quadrature upconverter and the need for circuitry to correct the frequency dependent phase and amplitude imbalances.

In Section 4.2, an adaptive compensation technique is introduced as a means of overcoming frequency dependent imbalances. Whereas previous compensation techniques have only compensated for a single gain and phase imbalance, this novel compensation method cancels the undesired sideband at a number of frequencies across the system bandwidth.

Section 4.3 shows that the reconstruction filters are a major contributor to frequency dependent imbalances across a wide band. Previous analysis [3,44,45,25,26] has generally neglected the significance of the effect of a mismatch in the reconstruction filters. Although it has been reported [47] that “in a predistortion linearising system the reconstruction filters are a major source of error”, the analysis was restricted to a single channel (narrowband) system with predistortion.

Section 4.3 also models the effect of frequency dependent imbalances on the sideband signal. This model is then used to show that the error vector between the reconstruction filters in the In Phase and Quadrature paths is related directly to the amount of sideband rejection.

Section 4.4 uses the relationship found in Section 4.3 to develop a methodology for analysing the effect of mismatched filters driving an analogue quadrature upconverter. Two parameters, oversampling ratio and the 'channel to system bandwidth' ratio, are introduced to objectively judge the performance of the multichannel adaptive compensation technique.

The analysis of the classical all-pole filter equations reveals the sensitivity of filter order, filter type, percentage mismatch and a differing sideband rejection specification in the novel compensation technique. The results of this analysis for different radio systems relate the amount of oversampling required for the compensation technique to achieve the required sideband rejection.

Finally, Section 4.5 proposes the use of bandpass reconstruction to avoid the frequency dependent mismatch problems of the lowpass reconstruction filters.

4.2 A Novel Method for the Compensation of Gain and Phase Imbalances

A number single channel correction techniques for amplitude and phase imbalances of quadrature upconverters currently exist [44,45,25,26]. Implementation of one correction technique which utilised the CRISIS network [26], adjusted the gain and phase imbalances to 0.02 dB and 0.4° respectively. This is equivalent to -49 dBc of sideband rejection, Eqn. (3.31), which constitutes a definite improvement, but is unacceptable in multichannel applications. Additionally, the effectiveness of current compensation techniques decreases dramatically in the presence of frequency dependent imbalances.

The novelty of the compensation technique presented revolves around the multichannel combining algorithm, which could take any of the forms discussed in Section 3.2. Figure 4.1 illustrates the proposed technique. Channels 1, 5, 8 and N_{ch} are combined, $N_{comb} = 4$, through a multichannel combining algorithm to form the complex baseband signal. The resultant signal is then interpolated by a nominal factor of L , before being output through the digital to analogue converter. The oversampled multichannel signal lessens the complexity of the reconstruction filters as will be shown later in the chapter. The oversampled complex baseband signal is finally upconverted to RF via an analogue quadrature upconverter.

The inherent gain and phase imbalances of the upconversion scheme will cause undesired sideband signals. The compensation method deliberately introduces a signal component into the image (where the undesired sideband exists) channel. From Fig. 4.1, channel 5 is transmitted and requires correction. The conjugated signal component is then introduced into the image channel, $N_{ch}-4$, and the complex coefficient (C_m) is adaptively adjusted until the undesired sideband is cancelled.

The adaption technique measures the sideband power in a vacant channel using a tuned receiver (error sensing circuitry in Fig. 4.1) and adjusts the complex coefficient (C_m) to minimise the power of the undesired signal.

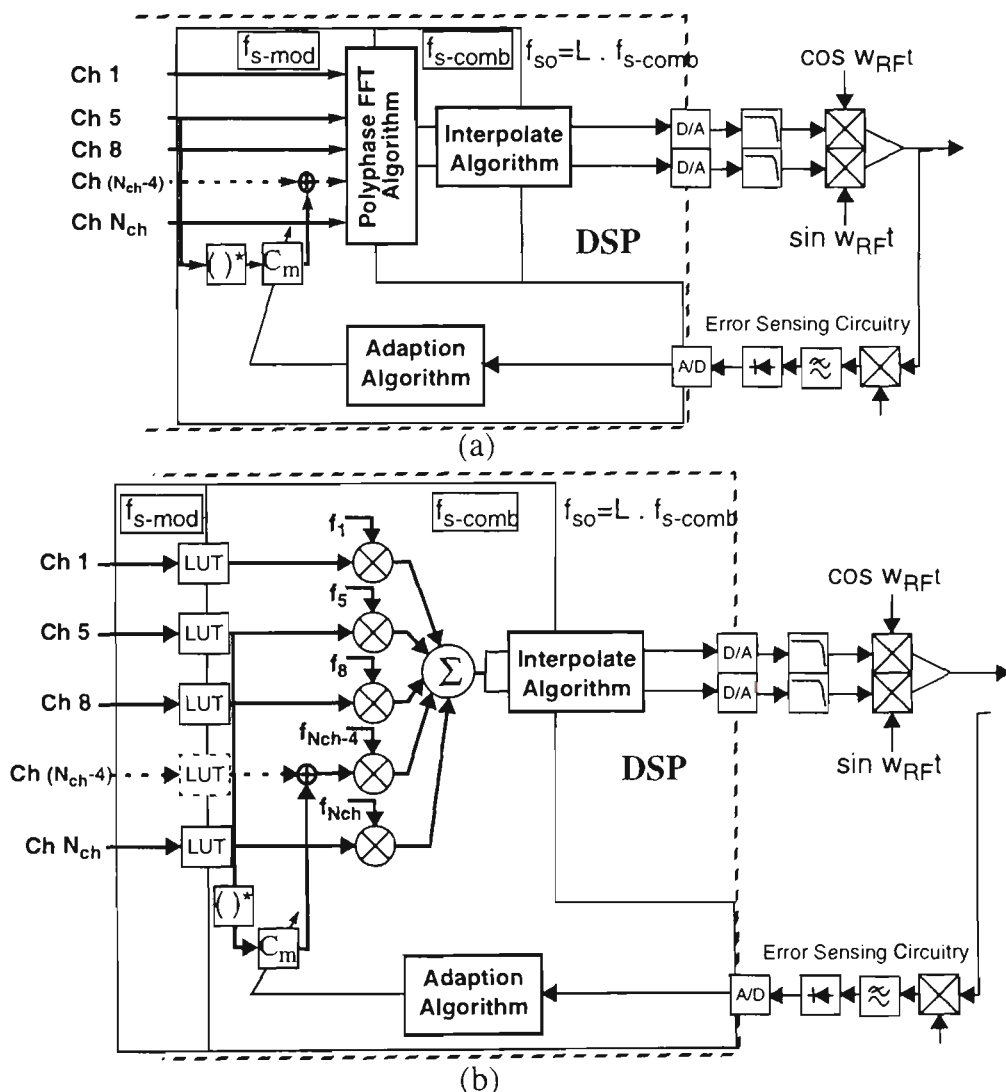


Figure 4.1: Multichannel adaptive compensation technique for correcting gain and phase imbalances using the (a) polyphase FFT combining algorithm or the (b) LUT algorithm. Channel N_{ch-4} is the image of Channel 5.

The process described above is repeated for every channel in the system but only whilst the channel is vacant. The update rate is slow, but this is not considered a problem as the

gain and phase imbalances drift slowly with time. The polyphase FFT combining technique, Fig. 4.1(a), gives access to all channels and the correction algorithm will only require one additional complex multiply operation per active channel at the low $f_{s\text{-mod}}$ sample rate. Other schemes, Fig. 4.1(b), will need the correction algorithm to operate at the higher $f_{s\text{-comb}}$ sample rate.

The compensation technique described has a number of advantages over previous adaptive correction techniques:

- *Reduced Computational Load* - The adaption algorithm and the scaling coefficient operate at the channel or combining sampling rate, as opposed to the output sampling rate [25,26,44-46].
- *Ability to Correct for Frequency Dependent Imbalances across the System Bandwidth* - Previous techniques only compensate for a single bulk gain and phase imbalance across the system band.
- *Increased Sensitivity of Feedback Signal* - This technique detects only the undesired signal, as opposed to both the desired and undesired signal [26], thus increasing the dynamic range of the correction network.

For an uncorrected analogue quadrature upconverter the power of the sideband will invariably exceed the spurious emission specification (Fig. 2.5), and it is therefore necessary to reduce the power in the sideband to comply with this spurious specification. The amount of sideband rejection required to meet the spurious specification was calculated in Section 3.3.3.2, for GSM and MPT1327 radio systems; it is -61.8 dBc and -82 dBc respectively.

The multichannel compensation technique also exploits the fact that there is room for non-ideal cancellation by cancelling the phase and gain imbalance at a single frequency (bulk imbalance). The sideband will be completely removed at this frequency. However, the frequency dependent imbalances mean that a differential phase and gain imbalance will remain across the remainder of the channel (differential imbalance), causing a residual sideband response, Fig. 4.2(b). The residual sideband response must be kept below the sideband rejection specified for the radio system.

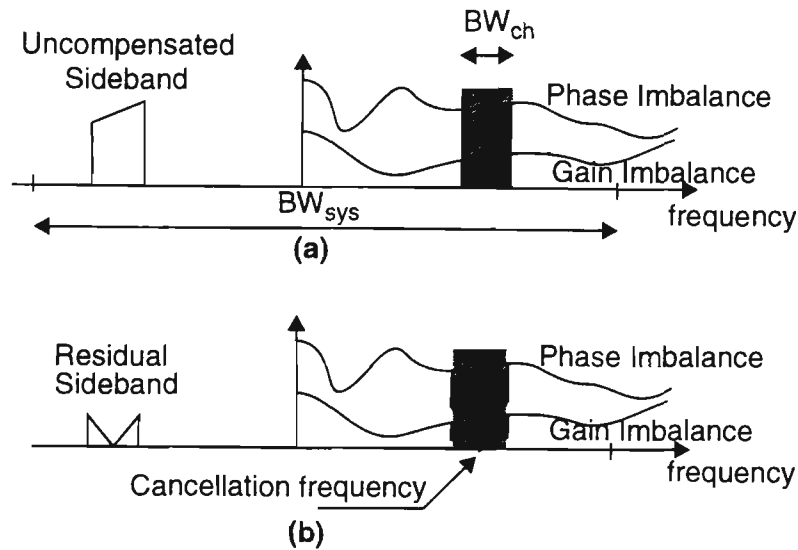


Figure 4.2: (a) Sideband response due to frequency dependent imbalances (b) Sideband response after cancellation of the channels bulk imbalance.

To comply with the amount of the sideband rejection required, the following condition must hold:

$$SR > 10 \log \frac{\text{Power in Sideband}}{\text{Power in Signal}} \text{ dBc} \quad (4.1)$$

The ability to quantify the frequency dependent imbalances is the next step in analysing the performance of the multichannel adaptive compensation technique.

4.3 Analysis of Frequency Dependent Imbalances

4.3.1 Causes of Frequency Dependent Imbalance in an Analogue Direct Upconverter

Frequency dependent gain and phase imbalances arise from both the quadrature upconverter and the mismatch in the reconstruction filters.

The quadrature upconverter consists of the mixer, phase splitter and summer components. The gain and phase through each of these components is to some extent dependent on frequency, although the amount of dependence will depend on the complex design strategies employed. However, these issues lie beyond the scope of the thesis.

A typical Mini Circuits IQ modulator was chosen as an example (Table 4.1 generated from

the Mini Circuits data sheet). It can be seen that over a channel bandwidth of 5 MHz, around -54 dBc of sideband rejection exists if the bulk imbalance is removed (leaving the differential imbalance). Over -70 dBc could be achieved if the bandwidth was reduced below 100 kHz.

Table 4.1: *Absolute variation of gain and phase imbalance across a specified bandwidth for a Mini Circuits IQ Modulator (MIQD 895).*

Bandwidth	Differential gain Variation (dB)	Differential Phase Variation (degree)	Sideband Rejection
100 kHz	0.01	0.05	70 dBc
500 kHz	0.02	0.10	64 dBc
5 MHz	0.05	0.30	54 dBc

In most communication systems utilizing the FDM format the channel bandwidth is less than 200 kHz. Therefore, the quadrature upconverter, with a single point of cancellation, will achieve significant suppression of the undesired sideband to around 70 dBc. A larger amount of sideband rejection will occur when more compensation points are used. Thus, frequency dependence will be apportioned entirely to the reconstruction filters, which will now be analysed with respect to the compensation technique.

4.3.2 Mathematical Analysis - The Effect of Filter Mismatch on the Sideband Signal

To analyse the effects of filter mismatch, the reconstruction filters are modelled with relative gain mismatch, $\alpha(f)$, and phase error from quadrature, $\Phi_c(f)$ (radians). The variable $\beta(f)$ is used to account for the absolute attenuation characteristic (or gain transfer function) of the filter and serves to normalise the magnitude at any frequency.

The gain of the I path will be given by the transfer function, $\beta(f)$, of the ideal filter in question:

$$\beta(f) = \beta(f)(1 + (\alpha(f)/2)) - \beta(f) \cdot \alpha(f)/2 \quad (4.2)$$

and the gain of the Q path will be given by a percentage change, $\beta(f) \cdot \alpha(f)$, in the transfer function of the ideal filter:

$$\beta(f)(1 + \alpha(f)) = \beta(f)(1 + (\alpha(f)/2)) + \beta(f) \cdot \alpha(f)/2 \quad (4.3)$$

Similarly, the phase mismatch between the filters is split equally between the two paths. $\Phi_e(f)/2$. The quadrature upconverter and DAC's are assumed to be ideal. These assumptions isolate the reconstruction filters as the source of error. Fig. 4.3 presents the summary of the model:

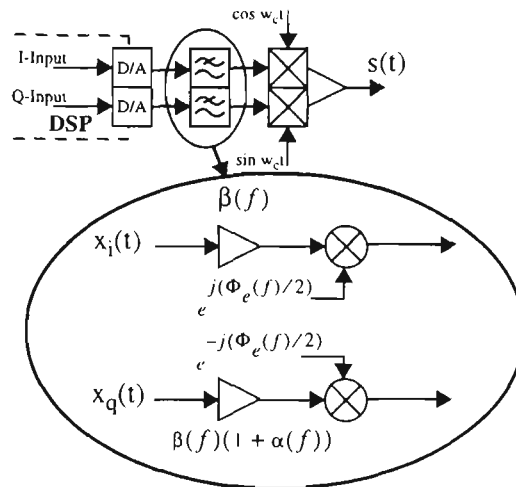


Figure 4.3: Modelling the mismatch between reconstruction filters

The quadrature signal that is driven from the DSP, can be represented as a complex signal with a real (I channel) and an imaginary (Q channel) component. The same signal can be represented as a vector with an instantaneous magnitude and phase:

$$\begin{aligned}
 r(t) &= x_i(t) + jx_q(t) \\
 &= |r(t)|e^{j\theta(t)}
 \end{aligned}
 \tag{4.4}$$

If there is no mismatch between the filters then the upconverted signal is given by:

$$s(t) = \text{Re} \left\{ r(t) \cdot e^{j\omega_c t} \right\}
 \tag{4.5}$$

The mismatch in the reconstruction filter design causes the original signal to be distorted (undesired sideband) when it is translated to the carrier frequency. The output, $s(t)$, from the quadrature upconverter shown in Fig. 4.3 is given by the following equation:

$$s(t) = \text{Re} \left\{ \begin{aligned} &\beta(f) \left(1 + \frac{\alpha(f)}{2} \right) \cdot \left[\begin{aligned} &|r(t)|e^{j\theta(t)} \cos\left(\frac{\Phi_e(f)}{2}\right) + \\ &j|r(t)|e^{-j\theta(t)} \sin\left(\frac{\Phi_e(f)}{2}\right) \end{aligned} \right] e^{j\omega_c t} \\ &+ \beta(f) \left(\frac{\alpha(f)}{2} \right) \cdot \left[\begin{aligned} &|r(t)|e^{j\theta(t)} \cos\left(\frac{\Phi_e(f)}{2}\right) + \\ &j|r(t)|e^{-j\theta(t)} \sin\left(\frac{\Phi_e(f)}{2}\right) \end{aligned} \right] e^{-j\omega_c t} \end{aligned} \right\}
 \tag{4.6}$$

After mathematical analysis Eqn. (4.6) can be shown to be equivalent to:

$$\begin{aligned}
 s(t) = & \beta(f) \left(1 + \frac{\alpha(f)}{2} \right) \cos \left(\frac{\Phi_e(f)}{2} \right) |r(t)| \cos(\omega_c t + \theta(t)) - \\
 & \beta(f) \left(1 + \frac{\alpha(f)}{2} \right) \sin \left(\frac{\Phi_e(f)}{2} \right) |r(t)| \sin(\omega_c t - \theta(t)) + \\
 & \beta(f) \left(\frac{\alpha(f)}{2} \right) \cos \left(\frac{\Phi_e(f)}{2} \right) |r(t)| \cos(\omega_c t - \theta(t)) + \\
 & \beta(f) \left(\frac{\alpha(f)}{2} \right) \sin \left(\frac{\Phi_e(f)}{2} \right) |r(t)| \sin(\omega_c t + \theta(t))
 \end{aligned} \tag{4.7}$$

Equation (4.7) mathematically describes four signals generated by the mismatch between the reconstruction filters. By selecting a complex plane referenced to the carrier frequency of the quadrature upconverter, the four signals can be represented as baseband complex vectors:

$$u_1(t) = \beta(f) \left(1 + \frac{\alpha(f)}{2} \right) \cos \left(\frac{\Phi_e(f)}{2} \right) \cdot r(t) \tag{4.8}$$

$$u_2(t) = \beta(f) \left(\frac{\alpha(f)}{2} \right) \sin \left(\frac{\Phi_e(f)}{2} \right) e^{j\frac{\pi}{2}} \cdot r(t) \tag{4.9}$$

$$v_1(t) = \beta(f) \left(\frac{\alpha(f)}{2} \right) \cos \left(\frac{\Phi_e(f)}{2} \right) \cdot r^*(t) \tag{4.10}$$

$$v_2(t) = \beta(f) \left(1 + \frac{\alpha(f)}{2} \right) \sin \left(\frac{\Phi_e(f)}{2} \right) e^{j\frac{\pi}{2}} \cdot r^*(t) \tag{4.11}$$

The vectors have been classified as a desired ($u(t)$) signal or a sideband ($v(t)$) signal. The desired signals are determined from the fact that they rotate in the same direction as the original signal, $r(t)$, whereas the sideband signals rotate in the reverse direction, thus appearing in the image channel position illustrated in Fig. 4.2(b).

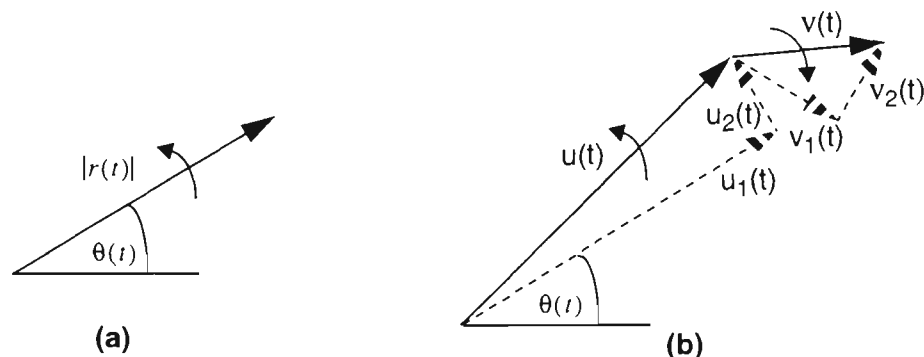


Figure 4.4: Vector representation of (a) Undistorted signal - $r(t)$ (b) Distorted signals due to direct conversion imbalances.

Fig. 4.4(a) represents the original signal upconverted to the carrier frequency by an ideal quadrature upconverter. If the quadrature upconverter is non-ideal, as modelled in Fig. 4.3, the original signal will be distorted to form four vectors as shown in Fig. 4.4(b), and described by Eqn. (4.8) to (4.11). The sideband signal is therefore the vector sum of Eqn. (4.10) and (4.11):

$$v(t) = r^*(t) \cdot \beta(f) \left(\left(\frac{\alpha(f)}{2} \right) \cos\left(\frac{\Phi_e(f)}{2} \right) + j \left(1 + \frac{\alpha(f)}{2} \right) \sin\left(\frac{\Phi_e(f)}{2} \right) \right) \quad (4.12a)$$

$$v(t) \approx r^*(t) \cdot \beta(f) \left(\frac{\alpha(f)}{2} + j \left(1 + \frac{\alpha(f)}{2} \right) \frac{\Phi_e(f)}{2} \right) \quad (4.12b)$$

Eqn. (4.12a) shows that the sideband signal can be represented as the complex conjugate of the original signal multiplied by a complex coefficient, which is a function of both gain and phase imbalance. For small phase error the sideband signal can be approximated by Eqn. (4.12b) and therefore expressed as an absolute magnitude:

$$|v(t)| = \frac{|r(t)| \cdot \beta(f) \sqrt{\alpha(f)^2 + \Phi_e(f)^2}}{2} \quad (4.13)$$

From the vector addition of Eqn. (4.8) and (4.9), the approximate magnitude of the wanted signal can be shown to be approximately $|r(t)| \cdot \beta(f)$. Therefore, the amount of Sideband Amplitude Rejection ratio (SAR) is given as the absolute magnitude of the image vector, divided by the absolute magnitude of the wanted signal, the form of which is the same as in the static case analysed in [3]:

$$\begin{aligned} \text{SAR} &= \frac{|v(t)|}{|u(t)|} \quad (4.14) \\ &\approx \frac{\sqrt{\alpha(f)^2 + \Phi_e(f)^2}}{2} \end{aligned}$$

Note that the sideband rejection (SR) ratio is equal to the SAR ratio squared.

An alternative way of visualising the previous analysis is to consider the I and Q path filters as vectors. When they are matched, they are both equal in magnitude and phase (Fig. 4.5(a)), subsequently causing no distortion or sideband response. When the filters are mismatched, there exists a phase and gain difference (frequency dependence). This is illustrated in Fig. 4.5(b).

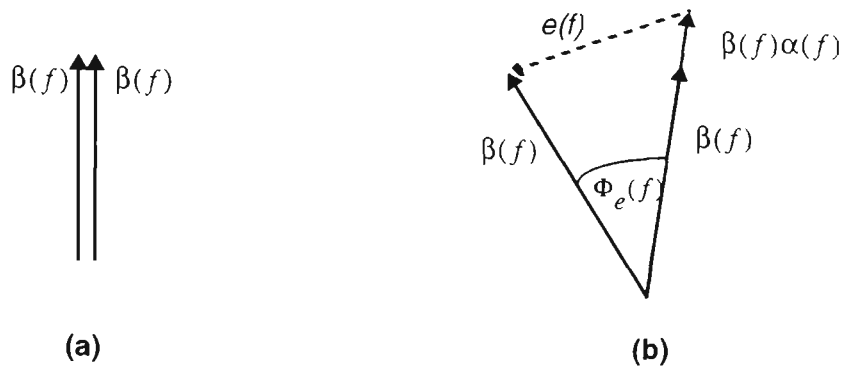


Figure 4.5: (a) *I and Q path filters matched* (b) *I and Q path filters mismatched*

It can be shown that the error vector is related to the SAR ratio by:

$$\text{SAR} = |e(f)| / 2 \times \beta(f) \quad (4.15)$$

This can be verified by calculating the magnitude of the error vector in Fig. 4.5(b) for small gain and phase imbalances and comparing it to the approximate SAR calculated in Eqn. (4.14). For typical values of sideband rejection in multichannel radio systems, the sideband has to be of a magnitude that implies very small gain and phase mismatch. The magnitude of sideband rejection can now be accurately predicted from Eqn. (4.15) and used as a means of objectively judging the performance of the multichannel compensation technique.

4.4 Analysing the Effect of Mismatched Reconstruction Filters.

4.4.1 The Methodology

The methodology calls for a relative comparison of performance when adjusting parameters relevant to filters. It is based on modelling the mismatch between the filters as a percentage increase in the cut-off frequency of one filter. This has limitations, especially when considering the real implementation issues of filters, but for practical analysis purposes it is seen as a realistic yardstick. The relative performance of a particular filter will then be judged by two parameters, the oversampling ratio and 'channel to system bandwidth' ratio.

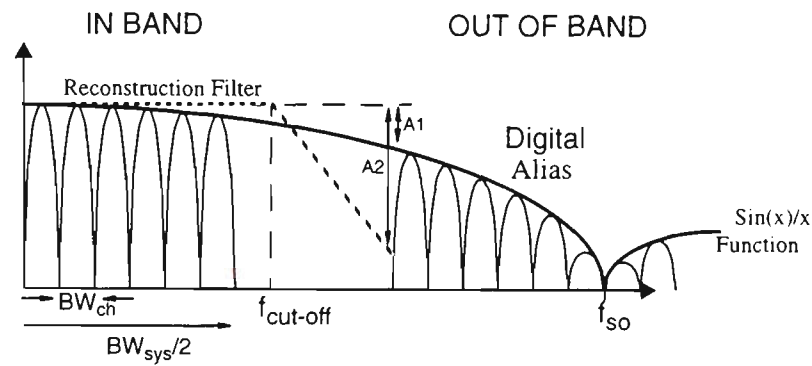


Figure 4.6: Overview of Communication System Parameters relevant to Direct Upconversion and a Multichannel Environment.

For the purpose of analysis, the communication system will be described by:

- channel bandwidth - BW_{ch}
- system bandwidth - BW_{sys}
- and the amount of sideband rejection - SR.

The channel and system bandwidth parameters can be combined to give the total number of channels across the system bandwidth (not the same as the number of combined channels [N_{comb}]):

$$N_{ch} = \frac{BW_{sys}}{BW_{ch}} \quad (4.16)$$

The number of channels indicate the total number of cancellation frequencies available across the system bandwidth, using the novel cancellation technique.

Adherence of the sideband rejection specification implies the following two objectives:

- In System Band: Given a percentage mismatch between the two quadrature filters, the amount of sideband rejection in the image channel must comply with Eqn. (4.1).
- Out of System Band: The digital alias must be attenuated below that indicated by the same sideband rejection specification. This is achieved by the reconstruction filter (A2) and the $\sin(x)/x$ response of the digital to analogue converters (A1).

The number of cancellation frequencies, i.e. the number of channels across the system bandwidth, is derived solely from the 'In System Band' objective. The mismatch between the filters creates frequency dependent imbalances that require periodic cancellation

across the system band to meet a given sideband rejection. The worse the mismatch between the filters, the smaller the channel bandwidth must be so that after cancellation, the power of the residual sideband complies with the spurious specification. For a fixed system bandwidth, this can be equally expressed as more channels. The number of channels, or compensation frequencies, is essentially a measure of the frequency dependent mismatch in the system.

To illustrate how the number of channels is calculated, a fifth order Butterworth filter is used as a case study. The error vector between the two filters is used to calculate the sideband rejection Eqn. (4.15). Fig. 4.7(a) illustrates the amount of sideband amplitude rejection ratio for a 5% mismatch in the reconstruction filters cut-off frequency. Note that the filters cut-off frequency has been normalised to 1 radians/second. Here the filters are perfectly matched at DC (no sideband), whilst a sideband magnitude exists throughout the passband, due to the frequency dependent imbalance.

To calculate the number of channels needed for effective cancellation of the sidebands, it is more instructive to view the gradient of the SAR across the passband of the filter, as illustrated in Fig. 4.7(b), i.e. the larger the gradient, the more frequent cancellation should occur.

The multichannel adaptive compensation technique will cancel a single frequency in every channel. Total cancellation across the entire channel band, however, does not occur. Imperfect cancellation will result in a residual sideband, as shown in Fig. 4.2(b).

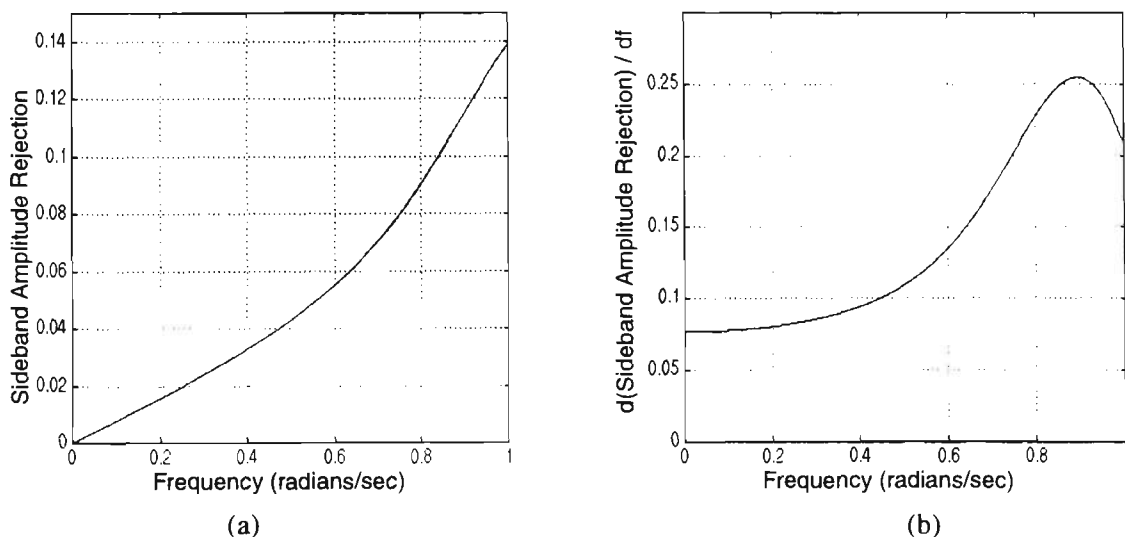


Figure 4.7: *Fifth order Butterworth filter with 5% mismatch in the cut-off frequency (a) Sideband amplitude rejection ratio (b) Gradient of sideband amplitude rejection ratio.*

If the gradient is assumed constant across the channel band, a first order approximation can be assumed for calculating the power in the sideband. That means that the sideband amplitude resembles a triangular function and therefore the sideband power approximates a square law function. This assumes a uniform distribution of signal power across the channel bandwidth, Fig. 4.2(b).

It is assumed that in a worst case scenario, the largest gradient to occur across the system bandwidth (which is a fraction of the cut-off frequency) is taken as the absolute constant gradient across any channel.

Given the above and using Eqns. (4.1) & (4.16), the minimum number of channels is related to the systems sideband rejection specification (SR):

$$N_{ch} = \frac{BW_{sys} \times \left. \frac{d(SAR)}{df} \right|_{max}}{10^{SR/20} \times \sqrt{12}} \quad (4.17)$$

By varying the system bandwidth, the minimum number of channels needed to comply with the systems SR specification can be plotted as shown in Fig. 4.8(a). As expected, more channels are needed as the system bandwidth approaches the cut-off frequency of the filter.

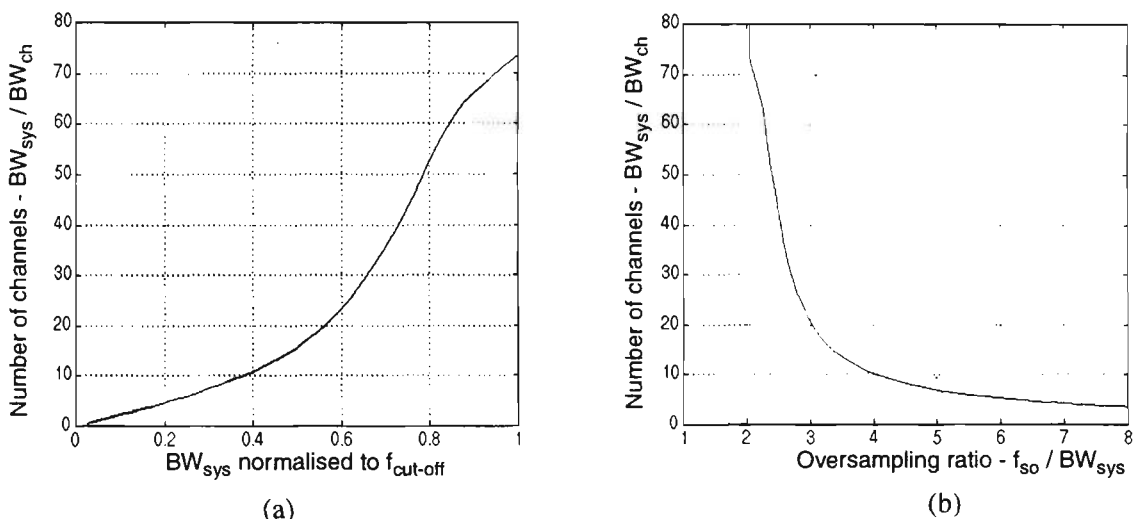


Figure 4.8: *Fifth order Butterworth filter with 5% mismatch in the cut-off frequency complying with a -60 dBc SR specification (a) In System Band objective (b) Combination of In and Out Of System Band Objectives.*

The second objective, Out of System Band, is achieved by attenuating the sampling aliases by an amount equal to the sideband rejection. The filter attenuation characteristic will

determine the output sampling rate, f_{so} , required to achieve this condition. The sampling frequency has been normalised to the Nyquist sampling rate of the system, BW_{sys} . This is expressed as the oversampling ratio:

$$OS = \frac{f_{so}}{BW_{sys}} \quad (4.18)$$

By combining the In and Out of System Band objectives, the minimum number of channels (or cancellation frequencies) can be related to the oversampling ratio for a given mismatch and system sideband rejection specification, Fig. 4.8(b). This methodology is now used to comparatively analyse the performance of the filters by modifying different parameters.

4.4.2 Numerical Computation and Analysis

The effect of mismatched reconstruction filters driving an analogue quadrature upconverter has been shown to introduce frequency dependent imbalances. These imbalances can be corrected by the adaptive compensation technique introduced in Section 4.2. However, the amount of mismatch in the reconstruction filters will put certain restrictions on the design, that is, the number of channels and the oversampling ratio needed to comply with the systems sideband rejection specification.

By varying different filter parameters, the methodology relating the number of channels in a communication system to the oversampling ratio can be used to analyse the effect of the reconstruction filters on the analogue direct upconverter.

Four parameters have been considered:

4.4.2.1 Filter Mismatch

Increasing the mismatch between the filters is the same as increasing the tolerance of the components used in implementing the filter. This effect has been modelled as a percentage shift in the cut-off frequency.

For a small number of channels, the oversampling ratio increases with an increase in percentage mismatch, Fig. 4.9(a). However, in a system with a large number of channels, 100 and upwards, the amount of mismatch, as long as it is less than 5%, becomes

irrelevant as the oversampling limit (vertical asymptote in Fig. 4.9(a)) for the 5th order Butterworth filter is reached.

The oversampling limit occurs when the system bandwidth equals the cut-off frequency. It is possible to go beyond this point by pre-emphasising the outer channels but this alternative will not be considered here. The In System Band condition therefore determines the minimum number of channels. Any further increase in the number of channels will improve the undesired sideband to further below the sideband rejection specification (In System Band condition) but will have no effect on the oversampling ratio. This phenomenon occurs because the system bandwidth cannot be extended further and therefore the Out of System Band objective, or the roll-off of the filter which is not dependent on percentage mismatch, will govern the lowest oversampling ratio.

It can be concluded that the filters must be able to be designed to meet tight specifications and also be reliably reproduced in the manufacturing process.

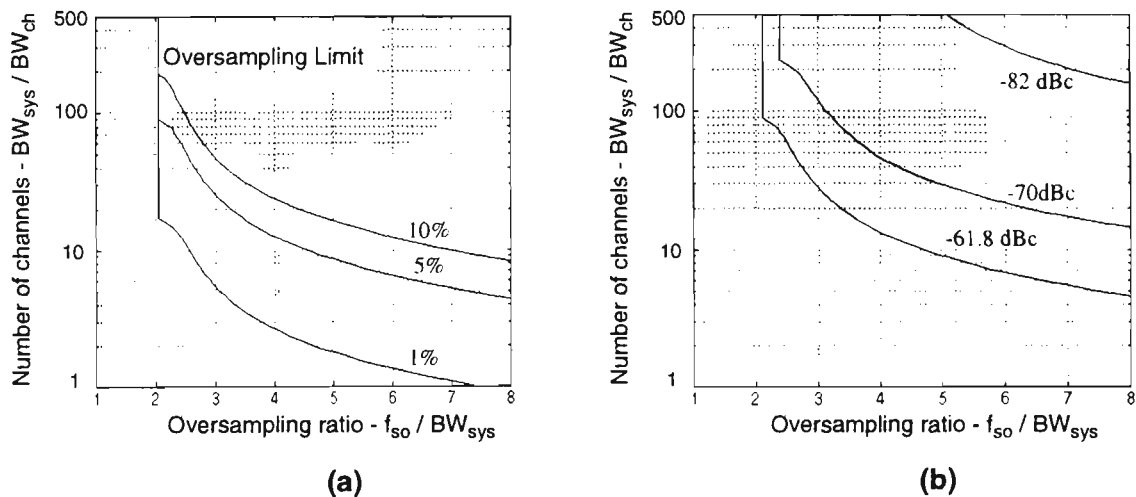


Figure 4.9: *Fifth order Butterworth filter with a 5% mismatch in the cut-off frequency, and a sideband rejection of -61.8 dBc is assumed unless otherwise stated (a) Percentage mismatch of the filter cut-off frequency varied (b) Sideband rejection specification varied.*

4.4.2.2 ACI Specification

Increasing the sideband rejection specification has a similar effect to increasing the percentage mismatch. Fig. 4.9(b) illustrates that the larger the sideband rejection, the higher the oversampling ratio required for a fixed number of channels. This is especially important for a small number of channels, say around 10, which for a SR specification of -70 dBc would require an oversampling ratio greater than 8. Depending on the bandwidth

of the channel, such a large oversampling ratio will place severe limitations on the bandwidth of the system, primarily due to the large output sampling frequency that would be required for the digital processing.

The oversampling limit also decreases with a lowering of the systems sideband rejection specification. To further lower this limit, the filter order would have to be increased.

4.4.2.3 Filter Type

The filters chosen contribute one desirable characteristic each: maximum flat amplitude response, maximal flat group delay and the steepest roll-off obtained by the Butterworth, Bessel and Chebychev filters respectively. The cut-off frequency is defined as the frequency for which the filter attenuation has reached 3 dB.

The Chebychev filter is shown in Fig. 4.9(c) to have the best overall performance. The lowest oversampling limit is achieved by a higher ripple in the Chebychev filter, this is due to the inherently steeper roll-off. It is difficult to discern from Fig. 4.9(c) whether varying the ripple of the Chebychev filter increases performance below the oversampling limit. However, as the ripple approaches zero the Chebychev response will approach the Butterworth response. The Butterworth filter is comparable to the Chebychev filter, although it consistently has slightly worse performance.

The Bessel filter has difficulties achieving a low oversampling ratio which is mainly due to its relatively slow roll-off and this could be lowered by using a higher order filter.

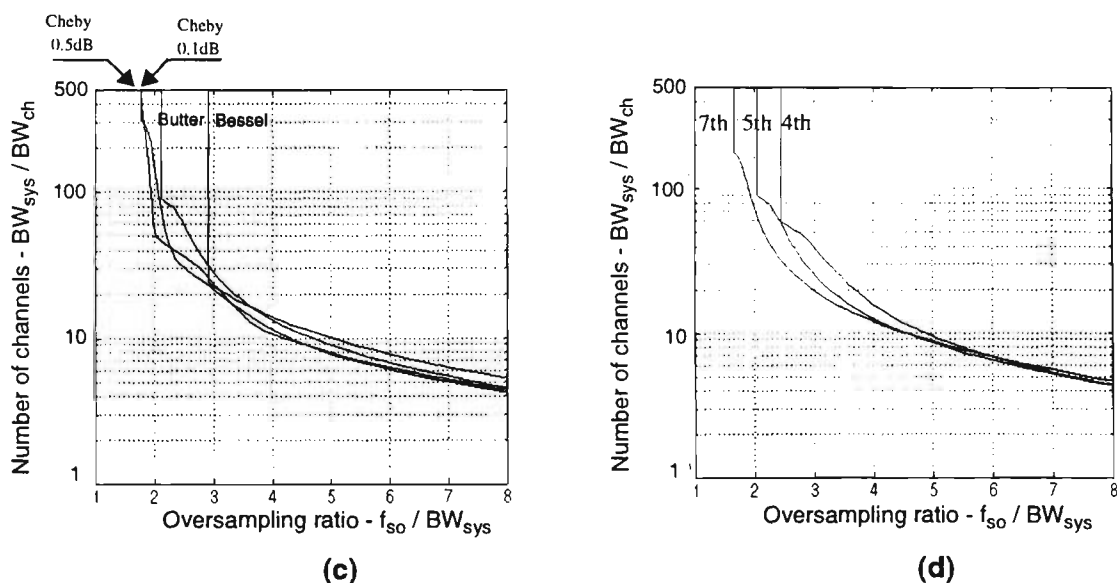


Figure 4.9: Fifth order Butterworth filter with a 5% mismatch in the cut-off frequency and a sideband rejection of -61.8 dBc is assumed unless otherwise stated (c) Fifth order Chebychev (0.1 dB & 0.5 dB ripple), Bessel & Butterworth Filter types (d) Butterworth 4th, 5th & 7th order filters

4.4.2.4 Filter Order

Increasing the filter order lowers the oversampling limit because of the steeper roll-off. Fig. 4.9(d). However, for an increase in the order of the filter there is not an equivalent improvement in performance, because a steeper roll-off is accompanied by a larger In System Band gradient. For example, a system with 10 channels requires an oversampling ratio of 5 and 4.5 for a fourth and fifth order filter respectively. Whereas increasing the order of the filter to 7 only achieves a small gain in performance; the oversampling ratio is still 4.5.

In a system that has many channels it would be better to use a higher order filter as long as the percentage mismatch could be guaranteed. The higher the filter order, the more sensitive it is to component tolerances and its overall percentage mismatch will rise. However, for a system with a small number of channels a lower order filter should be employed because of its reduced complexity and comparative performance to higher order filters.

4.4.3 Application to GSM or MPT1327 Radio Systems

The GSM radio system (class TRX 8) has twenty five 200kHz channels within a system bandwidth of 5 MHz. This equates to 25 cancellation frequencies, using the multichannel compensation technique. Assuming that the two reconstruction filters can be designed to an accuracy of 5%, an oversampling ratio of 3.2 will ensure that -61.8 dBc of sideband rejection can be achieved, Fig. 4.9(b).

The MPT1327 specification requires a sideband rejection of -82 dBc. However, the channel bandwidth is only 12.5 kHz, and therefore 400 channels, or cancellation frequencies, exist across a system bandwidth of 5 MHz. Again assuming that the two reconstruction filters can be designed to an accuracy of 5%, an oversampling ratio of 5.4 will be sufficient to ensure -82 dBc of sideband rejection, Fig. 4.9(b).

In both systems, a lower oversampling ratio could be achieved by using a similar order (5th) Chebychev filter or by increasing the order of the filter. The 5% tolerance of the filter must be assured.

4.5 Bandpass Reconstruction

This chapter has highlighted that most of the frequency dependent imbalance in the analogue direct upconverter is caused by the mismatch between the I and Q lowpass reconstruction filters. The proposed design requires a 5% tolerance between the filters so that the compensation technique can adequately correct the undesired sideband signals. Although resistors can achieve better than 5% tolerance, capacitors will require manual tuning to achieve this degree of accuracy. In addition, variations due to temperature will compromise the match between the two filters. A possible solution is to employ bandpass reconstruction.

Bandpass reconstruction operates on the RF signal and therefore does not affect the amplitude and phase mismatch between the In Phase and Quadrature paths. The main source of frequency dependent mismatch is therefore removed and the oversampling ratio is also reduced to 2 (Section 3.3.4.1). In theory a single channel correction technique (i.e. CRISIS circuit [26]) could be used to correct for the bulk amplitude and phase mismatch. The correction circuit would have to operate at the higher output sampling frequency, requiring a large amount of computation. The scheme described in this chapter is still the preferred choice since it will correct for any residual frequency dependence in the imbalances and in most cases it will normally have a lower computational load.

4.6 Conclusion

The mismatch between the reconstruction filters produces frequency dependent imbalances which cause undesired sideband responses in an analogue direct upconverter. A novel adaptive compensation technique has been introduced to reduce these sideband signals to comply with radio communication system specifications. The ability to correct frequency dependent imbalances and the fact that the correction occurs at the lower channel sampling frequency (polyphase FFT combining) are the two distinct advantages this technique possesses over previous adaptive compensation techniques.

The analysis of the frequency dependent imbalances yielded a relationship between the error vector of two mismatched filters and the amount of sideband rejection. This relationship was used to develop a methodology that related the number of channels to the oversampling ratio, required for the new adaptive compensation technique to achieve the

sideband rejection specification. The methodology compared the performance of the system when four parameters were varied. The main objective was to keep the oversampling ratio as low as possible, both for technology and power consumption reasons.

It was found that the Chebychev filter offered the best overall performance irrespective to the number of channels in the system. However, the order of the filter should be chosen on the size of the system. For small systems (less than 10 channels), a low order filter offers lower complexity with comparable performance to higher order filters. Larger systems benefit from higher order filter, although the implementation of a higher order filter presents an anomaly. Due to their higher complexity, they will be more sensitive to component tolerances, and therefore their ultimate performance will be degraded. Ultimately, the achievable tolerance of the filter is the highest priority design issue.

Through the examination of both the GSM and MPT1327 systems, an oversampling ratio of approximately 3.2 and 5.4, respectively, was found to be acceptable to meet the sideband rejection specification whilst assuming that the tolerance of the reconstruction filters could be kept to around 5%. For a system bandwidth of 5 MHz, this translates to an output sampling frequency of 16 MHz and 27 MHz, or interpolation by a factor of 2.5 and 4.2, assuming that the original combined baseband multichannel signal is sampled at 6.5 MHz (f_{s-comb} - Chapter 3).

The design requirement of 5% tolerance between the two lowpass reconstruction filters is difficult to meet in an analogue environment. A way of improving the solution is to use analogue direct upconversion with bandpass reconstruction which has a lower oversampling requirement. Compensation for the imbalances using the technique introduced in this chapter is also suited to this application and often requires less computation load than previous adaptive compensation techniques.

The next chapter introduces an algorithm that enhances the performance of a DAC when interpolation of the output sampling frequency is necessary. The algorithm can be used for analogue direct upconversion with either lowpass or bandpass reconstruction. It is based on the fact that a 5% mismatch in the lowpass reconstruction filters of an analogue direct upconverter requires the baseband multichannel signal to be interpolated by a factor of 4. This interpolation can be achieved by using two halfband stages.

Chapter 5

Enhancing the Performance of Digital to Analogue Conversion

5.1 Introduction

The digital signal processing base station employs digital to analogue conversion to convert the multichannel signal to an analogue waveform. Chapter 3 calculated the required DAC precision for the analogue direct upconversion technique to be equal to 9 and 12 bits, for the GSM and MPT1327 radio systems respectively. This calculation used a system bandwidth of 5 MHz sampled at 26 MHz.

The additive white noise model for the quantisation error of a DAC was assumed in the above calculations. Section 5.2 reviews the model and its underlying assumptions, one of which is that the quantisation levels must be evenly spaced. A practical DAC has non-evenly spaced quantisation levels which will generate harmonic and intermodulation products. Dynamic errors will also contribute similar spurious responses, but these will not be considered in the thesis.

Spurious responses are very important in a multichannel system, because they will fall into neighbouring channels, above the theoretical quantisation noise floor. The spurious free dynamic range of a DAC is therefore a very important specification for the multichannel application. A means of improving the SFDR performance of a DAC is through the addition of a random signal prior to quantisation.

The technique of adding a random signal before quantisation is known as dithering.

Section 5.3 reviews current dithering techniques which are described by three distinct qualities; Probability Density Function (PDF), scale and spectrum shape.

Calculation of the average quantisation transfer function in Section 5.4 yields insight into how dither will perform in the presence of an ideal or non-ideal quantiser. The average transfer function is used to explore the necessary scale of the digital dither required to overcome the non-linearity of a quantiser.

Section 5.5 draws upon the previous discussions to introduce the technique of bandlimited dithering, which is most suitable for application to multichannel base stations.

5.2 Characteristics of an Ideal and a Practical DAC

5.2.1 An Ideal DAC

The use of floating point digital signal processors allows for the very precise generation of digital signals. In fact, the precision of such DSP's is much greater than that of any currently available DAC. This is illustrated in Fig. 5.1(a), where n refers to the number of information or integer bits, and m is equal to the number of fractional bits. To interface the DSP to the DAC, the m fractional bits are truncated.

The process of digital to analogue conversion is described by the quantisation transfer function, $g(X)$, where the infinite precision input signal X is truncated to a multiple of a step size, Δ (Fig. 5.1(b)). The m least significant bits are simply ignored, whilst the n most significant bits produce a set of discrete analogue levels. The quantisation error transfer function, $q_e(X)$, is defined as the error between the quantiser and linear transfer function, shown in Fig. 5.1(c), as:

$$g(X) = X + q_e(X) \quad (5.1)$$

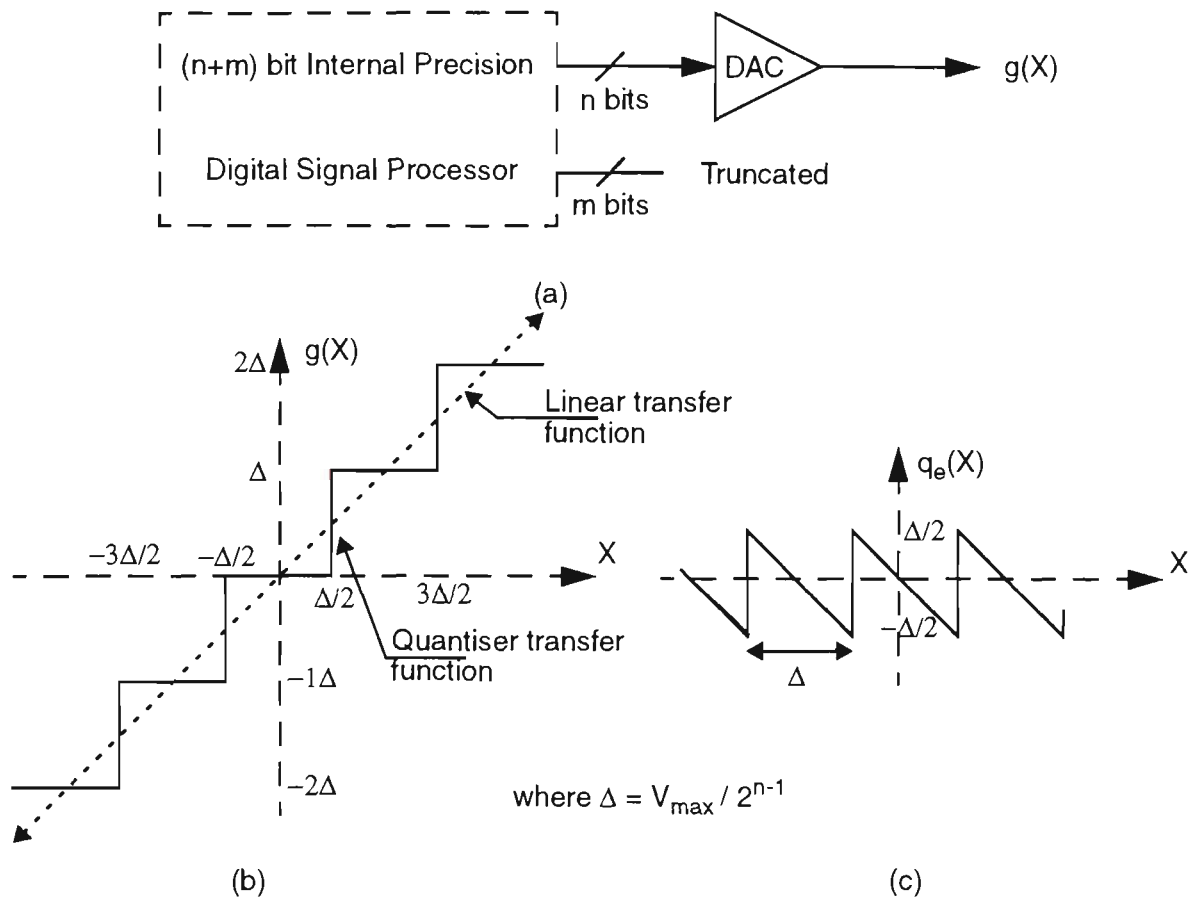


Figure 5.1: (a) The internal precision of the DSP will invariably have higher precision than that of the DAC. Truncating the m LSB's is the simplest way of interfacing the DSP to the DAC. (b) Ideal n bit DAC transfer function, $g(X)$, given truncation of the m LSBs as shown in (a). The ideal linear transfer function is also shown. (c) Quantisation error, $q_e(X)$, of an ideal DAC.

The quantisation error is strongly dependent on the characteristics of the input signal, X , and is quite complex to analyse. However, Bennett [56] showed that the sequence of error samples that make up the error waveform, $q_e(X)$, are uncorrelated with each other and the input signal. Further, the quantisation error can be modelled as a random variable that is uniformly distributed over a step interval. Using this model, the quantiser can be replaced by the simple additive white noise model, Fig. 5.2, where the average power, or variance, of the quantisation error is given by $\Delta^2/12$. More importantly, this model will only apply when the following conditions hold:

- the quantisation levels are evenly spaced and small,
- there is a large number of quantisation levels (this implies that a large number of levels are exercised), and
- the input probability density function of the signal is smooth.

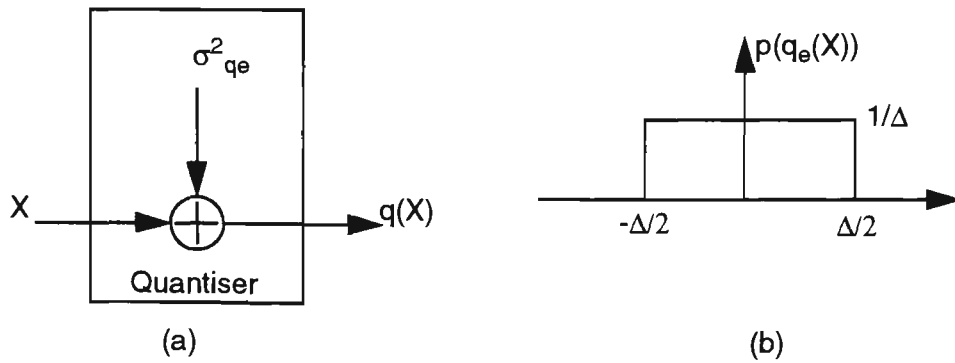


Figure 5.2: (a) Additive noise model of a quantiser (DAC) (b) Probability density function of the additive noise i.e. Uniform.

These conditions limit the use of the model in certain situations. For example, in the case of a periodic sinusoid that is a sub-harmonic of the sampling frequency, only a few quantisation levels are used, and the quantisation noise is not evenly spread, but is concentrated into a finite number of frequencies. The additive noise model also does not apply to Sigma-Delta ADC's because they have relatively few levels and a relatively large step spacing. Strictly speaking, the additive white noise model does not apply to practical DAC's because the quantisation levels are not evenly spaced.

5.2.2 A Practical DAC

A non-uniform step size (quantisation levels that are not evenly spaced) is an intrinsic quality of a practical DAC, Fig. 5.3. This means that the transfer function passing through the centre of each step tread is not linear. Abuelma'atti [33-34] examined the effect of non-ideal quantisation and came up with expressions for the amplitudes of the output fundamental and the harmonics when the input consists of a single sinusoid [33] or multiple sinusoids [34]. Both papers showed that the additional non-linearity may reduce the amplitude of some harmonics, but the total distortion power in all harmonics and IM products will inevitably be increased.

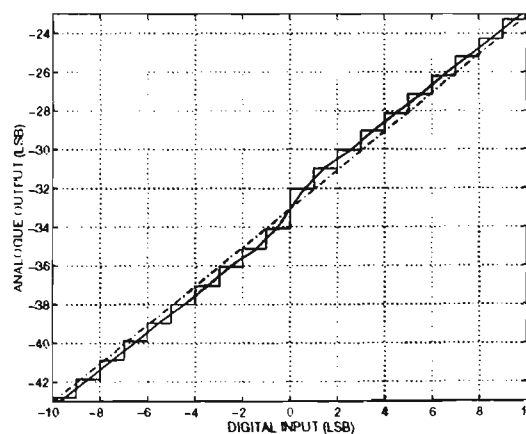


Figure 5.3: A practical DAC quantisation transfer characteristic, showing a strong odd order characteristic. Both axis are calibrated to a LSB - the average step size.

The harmonics and intermodulation products of a multichannel signal will invariably fall into neighbouring channels and must be kept within the radio system specifications (Fig. 2.5). The levels of these spurious responses will be very dependent on the non-ideal quantiser transfer function which can only be controlled by the manufacturer of the DAC. Therefore, to ensure that the spuri meet the required specifications, the DAC must be over-designed.

Another solution is to linearise the DAC through some pre-processing algorithm. Linearising the DAC will mean that the quantisation error will become less dependent on the input signal, and the spurious levels will reduce. Dithering is one such technique of increasing the SFDR of a DAC.

5.3 Introduction to Dither

Dither refers to the addition of a random signal before quantisation, and it can also imply the subtractive process of the same random signal after the quantisation process, as illustrated in Fig 5.4.

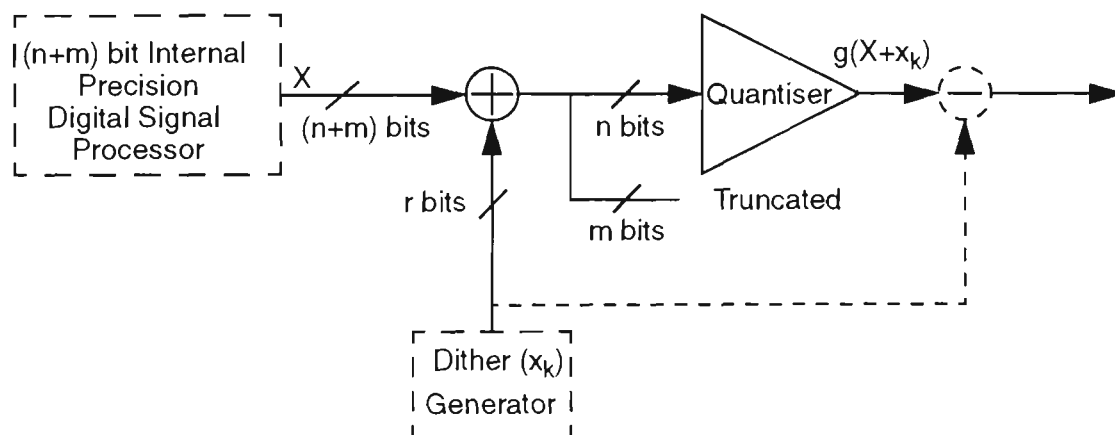


Figure 5.4: *Generic Dither Architecture, where the quantiser is a DAC.*

The effect of dither is to improve the quantisation process by forcing the quantisation error to become a random signal [53]:

Dithering is based on the concept of forcing the quantisation error, q_e , conditional to a given input X , to be a zero mean random variable, rather than a deterministic function of X . The randomisation of the conditional error $q_e(X)$ is accomplished by the addition of a random dither noise sample, x_k , to the input, and quantising $(X+x_k)$ instead of X .

More specifically, the signal X is correlated to the quantisation error $q_e(X)$. Adding dither to the signal ($X+x_k$) will force the quantisation error $q_e(X+x_k)$, to become a random signal that is obviously uncorrelated with (or independent) of the signal.

The technique was first used to remove the contour effects created by the quantisation (5 bit - 32 levels) of intensity levels in pulse code modulated video systems. It has since been used in audio and video encoding, DDS applications, sigma-delta ADC converters, extracting signals below 1 LSB and in high resolution spectrum analysers. A review of existing dither techniques is now presented.

5.3.1 Review of Dither Techniques

Each unique dither technique can be described by three dither qualities: the dither PDF, the scale of the added dither, and the spectrum over which the dither exists. As each of the qualities has a number of variations (Fig. 5.5), a large number of possible dither techniques exist. In reviewing dither, each of the qualities will be looked at individually.

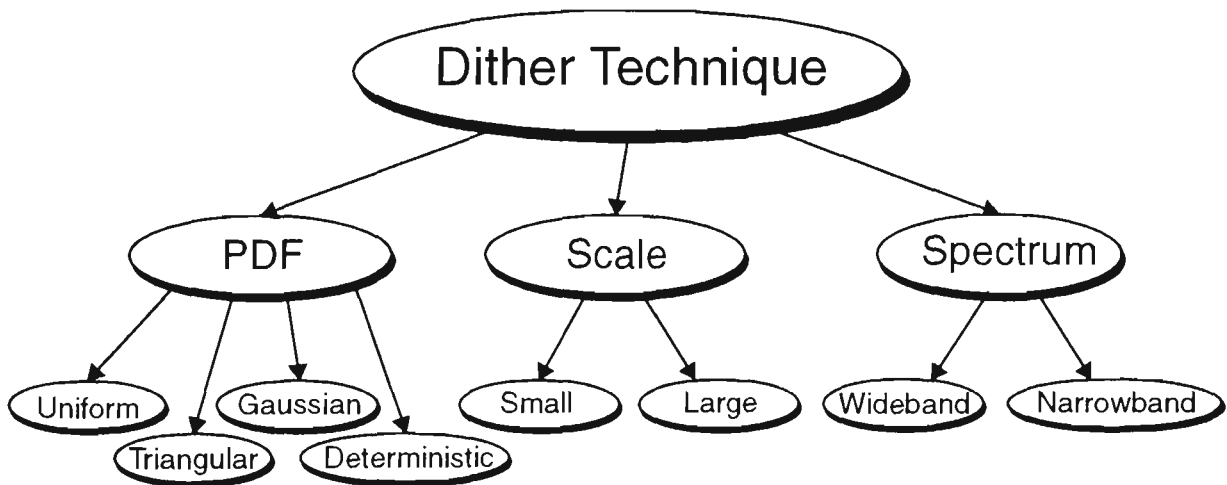


Figure 5.5: An overview of the three qualities that make up a dither technique and the different variations in each of these qualities.

5.3.1.1 Probability Density Function

The amplitude probability distribution function is the most important defining characteristic of the dither signal. The three PDF's shown in Fig. 5.6 are part of a class of PDF's that force the quantisation error to be a random signal (see Appendix E for proof of this fact by applying the Schuchman 'sufficiency condition'). They also seem to encompass all the published implementations of dither to date.

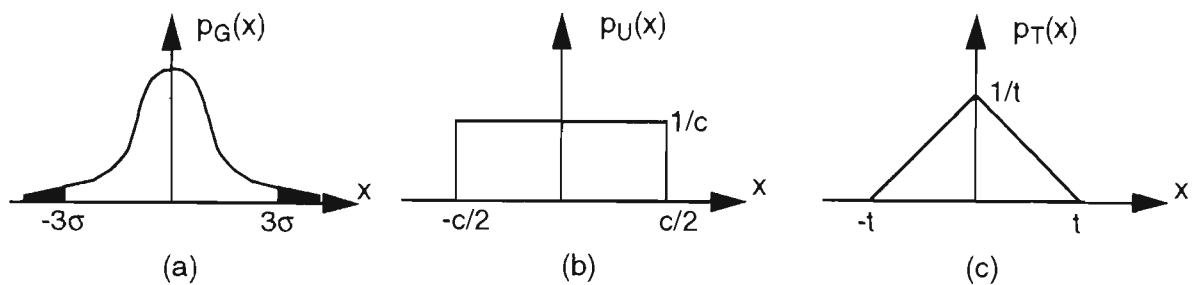


Figure 5.6: Dither probability density functions (a) Gaussian (b) Uniform (c) Triangular

The Gaussian PDF is drawn in Fig. 5.6(a), and can be described by the following equation:

$$p_G(x) = \frac{1}{\sqrt{2\pi}\sigma} e^{-\frac{(x-\mu)^2}{2\sigma^2}} \quad (5.2)$$

The power of the distribution is given by the variance σ^2 . The mean μ is set to zero when the DC power is zero (which is usually the case).

The Gaussian distribution was widely used in the early development of dither techniques and is the favoured dither PDF in analogue implementations i.e. ADC dithering. This is primarily due to the ease of generating an analogue Gaussian waveform. In a digital implementation a large number of bits is required to accurately model the Gaussian PDF, especially the tail region. In the simulations carried out later in this chapter, the Gaussian PDF is truncated to $\pm 3\sigma$. This models 97.4% of the function and is considered to be a reasonable trade-off with the number of bits needed for accurate representation.

Dither with a uniform PDF, Fig. 5.7(b), was found to be an optimal form when the peak to peak amplitude excursion, c , is equal to 1 LSB [55]. This only applies to quantisers with uniform step sizes, of 1 LSB. Generation of a digital uniform PDF can be accomplished by the simple Linear Feedback Shift Register (LFSR) technique. However, in an analogue dithering application there are additional complications, in converting this sequence from digital to analogue and adjusting the magnitude to exactly 1 LSB (in the optimal case). For digital implementations, uniform dither is a lot less complex to implement than Gaussian dither.

The Triangular PDF, Fig. 5.7(c), is generated by adding together two independent random

signals with a uniformly distributed PDF. Recently this has been considered to be the optimal form of dithering [51] for audio applications, and is also well suited to digital implementation.

Deterministic signals, such as a sinusoid with a frequency of half the sampling rate, have also been investigated as a possible dither source. They are not as effective as random noise, but the combination of both random and deterministic signals can produce similar benefits to optimal random noise [50].

5.3.1.2 Scale

Adding dither to the signal before quantisation is shown in Fig. 5.7(a). The output of the quantiser, $g(X+x_k)$, is written as:

$$g(X + x_k) = (X + x_k) + q_e(X + x_k) \quad (5.3)$$

Assuming that dither forces the quantisation error to be a random variable, the total noise power is given by the sum of two independent random processes, dither, x_k , and quantisation error, $q_e(X+x_k)$. Thus, the dithering system, Fig. 5.7(a), can be equivalently modelled in Fig. 5.7(b). The overall error statistics of the total output noise, $Wn = x_k + q_e(X+x_k)$, signal are given by [52]:

$$\mu_{Wn} = \mu_{x_k} + \mu_{q_e} \quad (5.4)$$

$$\sigma_{Wn}^2 = \sigma_{x_k}^2 + \sigma_{q_e}^2 \quad (5.5)$$

$$Wn^2 = \sigma_{x_k}^2 + \sigma_{q_e}^2 + (\mu_{x_k} + \mu_{q_e})^2 \quad (5.6)$$

where μ and σ^2 are the mean and variance, or power, of the random signal respectively. The subscript x_k refers to the original dither signal, q_e refers to the quantisation error, and Wn refers to the total output noise signal. Wn^2 is the total average power of the output noise signal.

From Eqn. (5.6), the total noise power is equal to a DC term (the sum of the means squared) and a wideband noise contribution. It is really only the wideband contribution, Eqn. (5.6), that is important. Adding a dither signal, x_k , increases the total wideband noise power and reduces the signal to noise ratio. The SNR can be improved by subtracting the

added dither after quantisation (see Fig. 5.4). In fact, during the early investigations into dithering techniques, the term ‘dither’ actually implied both the additive and subtractive processes.

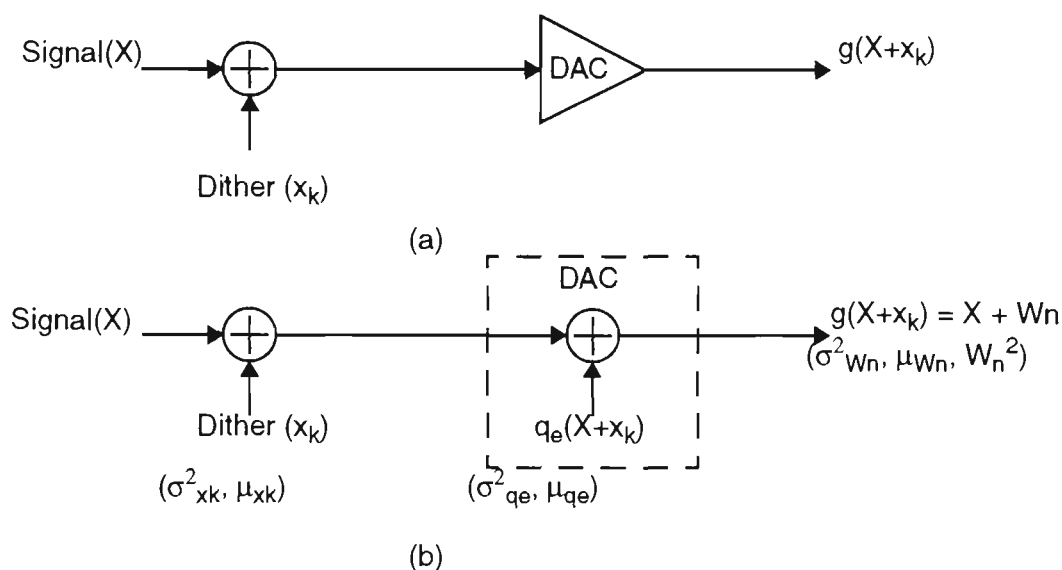


Figure 5.7: (a) Model of the quantisation process when dither is added. (b) Model of quantisation process assuming that the Schuchman ‘sufficiency condition’ is adhered to. That is both quantisation error and the dither signal are independent random processes. The statistics are shown in the parenthesis.

The additive-subtractive technique is generally accepted to be both complex and expensive to implement. By not incorporating the subtractive stage, the technique becomes very simple, but a noise penalty must be suffered. This is not always a disadvantage, for example in the first use of non-subtractive dither, random noise that was 40 dB below the signal level was added. Although this increased the noise power, an acceptable result was achieved because it enhanced the subjective appearance of the picture.

Larger scale dither is advantageous when the quantisation levels are not uniform. It overcomes the non-linearities in the step size better than smaller scale dither ([50] & [54]). Larger scale dither has the effect of smoothing both the quantisation error and the larger scale non-linearities caused by non-uniform step sizes. However larger scale dither means that the signal level must be reduced to avoid clipping. Both of these effects can seriously impact on the SNR.

Therefore, choosing between a small or a large scale dithering architecture requires considering a number of trade-offs, such as assessing the amount of dither overhead to avoid clipping, the linearity achieved versus the amount of additional dither added, and the level of hardware complexity that can be tolerated.

5.3.1.3 Spectrum

Virtually all implementations of dither simply consider adding wideband dither, using the three random PDF's discussed in Section 5.3.1.1. However, Blesser and Locanthi [48] investigated using a narrowband dither noise signal, Gaussian PDF, centred at the Nyquist frequency in an ADC application. The bandwidth of the dither signal was 1 kHz in a 22 kHz Nyquist frequency interval. In terms of spectrum, narrowband dither centred around the Nyquist frequency and the wanted signal occupied mutually exclusive parts of the spectrum.

Narrowband techniques have the disadvantage of requiring a larger amplitude dither signal [48] to achieve the same performance. Consequently the amplitude of the signal must be made smaller to avoid clipping. This allowance for the dither signal, called dither overhead, reduces the SNR. A design trade-off therefore exists between the spectral width and the required dither amplitude.

5.4 Average Quantisation Transfer Function

The average quantisation transfer function is an objective measure that will be used to examine the effect of different dither signal properties, PDF and scale, on an arbitrary DAC transfer function.

To calculate the average quantisation transfer function requires knowledge of only the original quantisation transfer function, $g(X)$, and the statistical properties, in the form of a PDF of the dither signal. The average transfer function (averaged over all values of x_k) can be defined as:

$$\overline{g(X)} = \sum_k g(X + x_k) p(x_k) \quad (5.7)$$

where $p(x_k)$ is the PDF of the dither signal, and $g(X+x_k)$ is the instantaneous transfer function of the quantiser.

Equation (5.7) is equivalent to the digital convolution of the PDF and the quantiser transfer function¹. The result will be a smoothed quantiser transfer function that approaches the ideal linear response. Equation (5.7) can now be used as a quantitative

1. Note that the general form of convolution is $\sum_k g(X - x_k) p(x_k)$, but this becomes equivalent to Eqn. (5.7) when the PDF is symmetrical about the origin.

means of comparing the effect of different types of dither PDF's on arbitrary quantisation transfer functions. This objective measure consists of comparing the average quantisation transfer function to an ideal straight line. The closer the match, the better the performance.

5.4.1 The Effect of the Scale and PDF of Digital Dither on an Ideal Quantiser.

Initially, an ideal quantiser will be used to investigate the scale of digital dither on the average transfer function, Eqn. (5.7). Uniform, triangular and Gaussian dither PDF's will be used in the comparisons.

For dither with either a uniform or a triangular PDF, the calculation of the average transfer function, plotted in Fig. 5.8 (a) & (b), shows that a linear transfer function results when c and t are equal to $n\Delta$ (Fig. 5.6). This is exactly what the Schuchman 'sufficiency condition' predicts (Appendix E). At any other peak to peak amplitude excursion of the dither signal some deviation from linearity will occur. For Gaussian dither, Fig. 5.8(c), an increasingly linear average transfer function will be achieved when the scale increases. This is also predicted by the Schuchman 'sufficiency condition'.

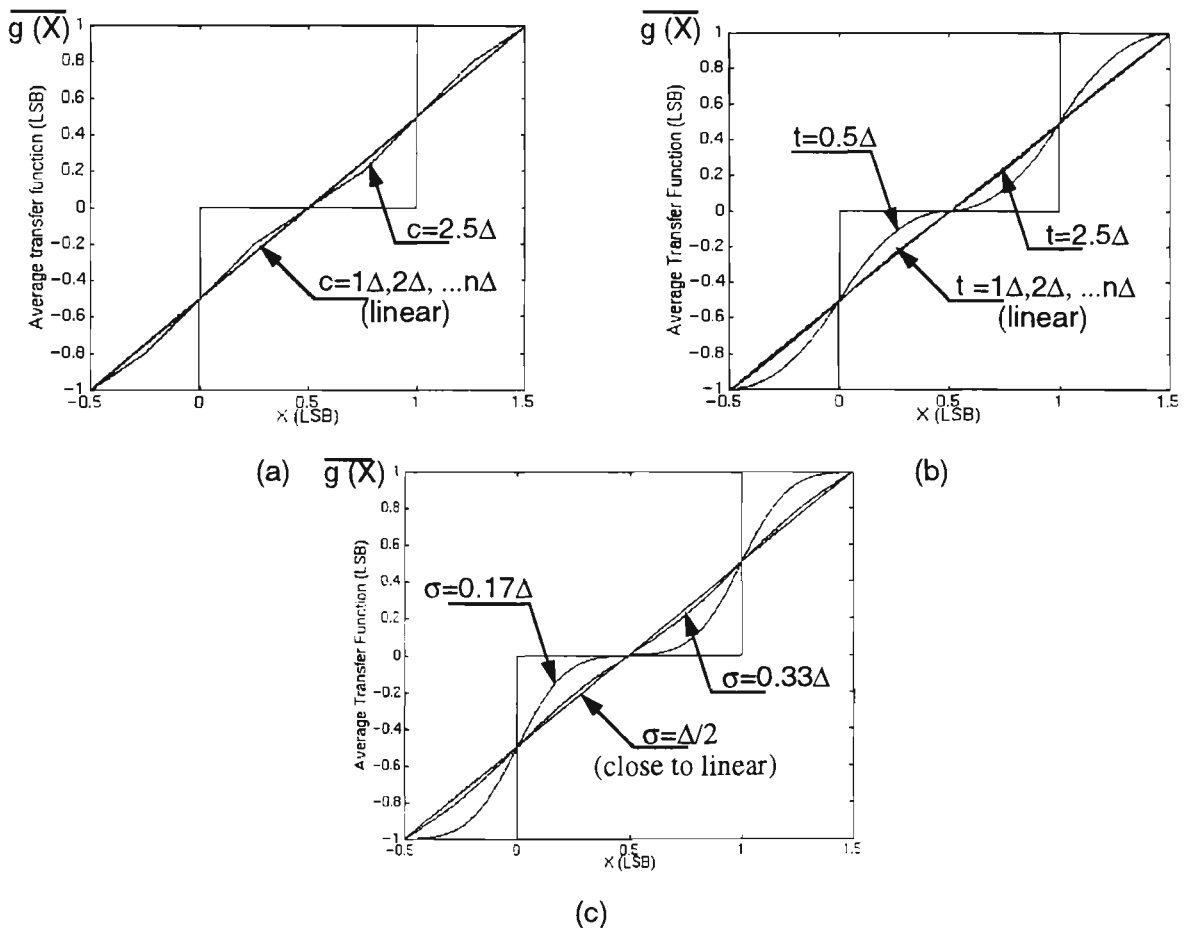


Figure 5.8: Effect of scale on the different probability distribution functions (a) Uniform (b) Triangular (c) Gaussian

The lowest scale at which linearity is achieved for uniform and triangular dither is when c and t are equal to Δ . This corresponds to an increase in the wideband noise quantity of 3 dB (uniform) and 4.77 dB (triangular). For Gaussian dither, the linearity is perceptively quite good at $\sigma = \Delta/2$, or a 5 dB increase in noise power, although the 'sufficiency condition' predicts that σ should be greater than Δ (Appendix E). It can be concluded that a uniform PDF forces a linear average quantisation transfer function for the lowest amount of added dither power.

In the case of an ideal quantiser, there is no benefit in using larger scaled uniform or triangular dither. Larger scales, which are multiples of Δ , increase the output noise power but achieve no additional linearity. This is not the case when practical quantisers are considered.

Incorrect conclusions can be drawn if Eqn. (5.7) is used alone as a quantitative measure. For example, a uniform, $c = \Delta$, and a triangular, $t = \Delta$, PDF have been shown to generate a perfectly linear average transfer function for an ideal quantiser. However, in audio applications, an improvement in the perceptible performance of sound occurs when there is no noise modulation [50]. In other words, the noise modulation, or second central moment [57], must be constant across the quantisation interval:

$$\begin{aligned} E\left\{(g(X + x_k) - \overline{g(X)})^2\right\} &= \sum_{k=2^r} (g(X + x_k) - \overline{g(X)})^2 p(x_k) \\ &= \overline{g^2(X)} - \{\overline{g(X)}\}^2 \end{aligned} \quad (5.8)$$

It can be shown that only triangular dither satisfies this latter condition [50], and for audio applications it is considered a better choice than uniform dither.

The audio application suggests that all n^{th} order central moments, $E\left\{(g(X + x_k) - \overline{g(X)})^n\right\}$, are potentially important and should be considered with the given application in mind. However, in the context of the simple quantitative analysis that is to follow, the first order moment is considered sufficient.

5.4.2 The Effect of the Scale and PDF of Digital Dither on a Practical Quantiser.

A measured quantisation (DAC) error transfer function, $q_e(X)$, is shown in Fig 5.9. The characteristic triangular quantisation error waveform, step sizes of approximately 1 LSB, is a dominant feature, but there is also a major discontinuity which occurs at the point where the DAC digital input goes from negative to positive. The step size here is 2 LSB's, constituting quite a significant non-linearity.

The average quantisation error transfer function (averaged over all values of x_k) can be written as:

$$\overline{q_e(X)} = X - \sum g(X + x_k)p(x_k) \quad (5.9)$$

and it will replace the average quantisation transfer function, Eqn. (5.7), in this section as the quantitative measure.

The average quantisation error transfer function, $\overline{q_e(X)}$, has been calculated for uniform, triangular and Gaussian dither, with $c=\Delta$, $t=\Delta$ and $\sigma=\Delta/2$ respectively. These are the same conditions as those found in the last section which make $\overline{g(X)}$ linear (or approximately linear in the case of Gaussian); Fig 5.9(a). All the dither signals achieve a smoothing or averaging effect on the original quantisation error transfer function.

By magnifying a small section of Fig. 5.9(a), the effects of the different dither signals can be more closely observed, Fig. 5.9(c). Uniform dither generates a more angular curve, due to the abrupt nature of the PDF, whereas both triangular and Gaussian dither generate somewhat smoother curves.

The use of a larger scale dither can also remove the larger scale non-linearities, i.e. at the point where the digital input goes from negative to positive. Figures 5.9(b) and (d) illustrate the effect of increasing the amplitude of the dither further. In fact, the power for each of the different dither signals has been made to equal $4\Delta^2/3$ so that a fairer comparison of the dither signals could be made. By comparing Fig. 5.9(a) and Fig. 5.9(b), it can be seen that an increase in scale causes further smoothing of $\overline{q_e(X)}$, especially at the point of the larger scale non-linearity.

Close examination of Fig. 5.9(b) and (d) shows that the Gaussian PDF produces a smoother, more linear average quantisation transfer function than the other two PDF's. This would suggest that the spurious levels would be lower in the case of Gaussian dither.

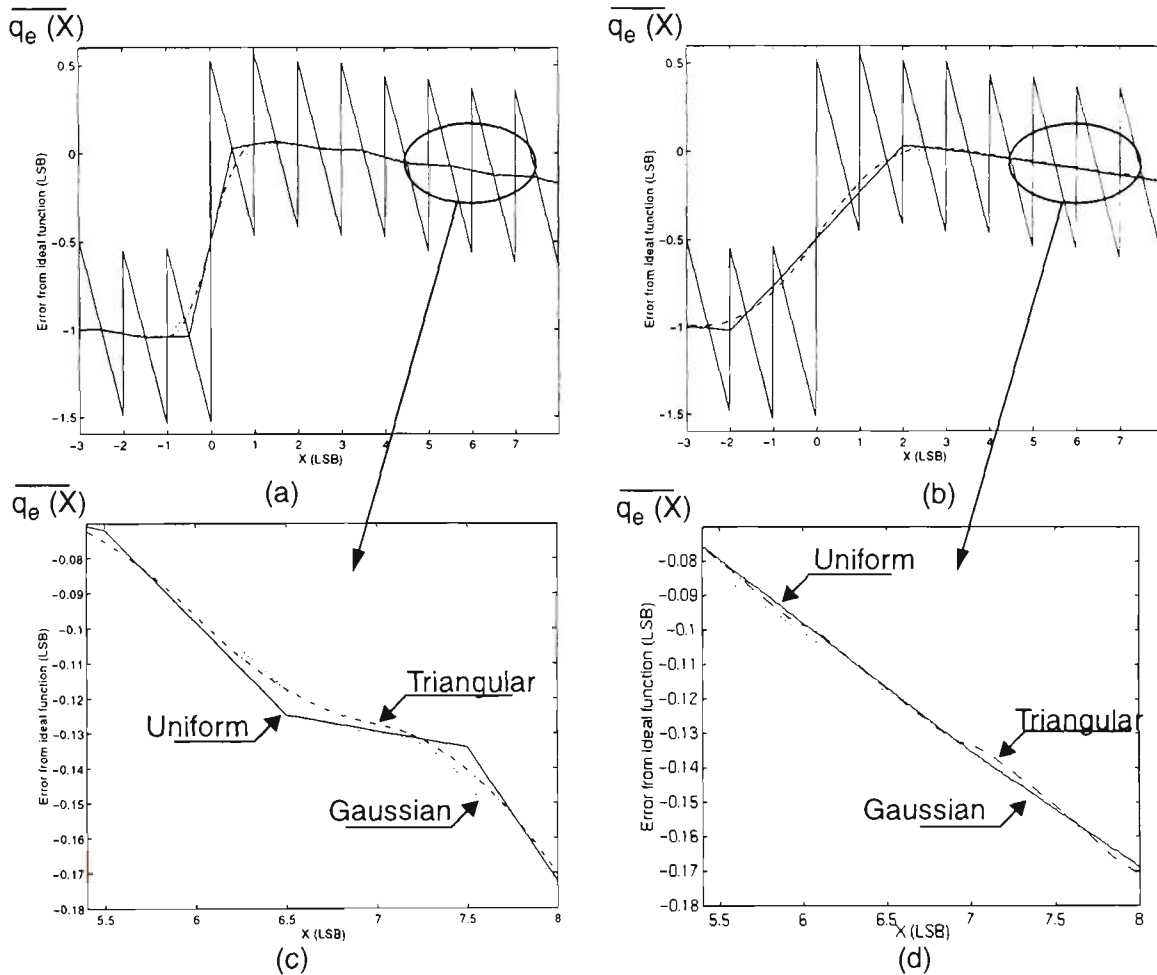


Figure 5.9: Effect of scale on the non-uniform step size quantisation transfer function (a) Average error transfer function, $\overline{q_e(X)}$ shown. Also shown is uniform ($c=\Delta$), triangular ($t=\Delta$) and Gaussian ($\sigma=\Delta/2$) dither signals added. (b) Average error transfer function, $\overline{q_e(X)}$ shown. Also shown is uniform ($c=4\Delta$), triangular ($t=2.82\Delta$) and Gaussian ($\sigma=1.155\Delta$) dither signals added (Note equal power). (c) Expanded portion of (a). (d) Expanded portion of (b). Uniform dither = solid line, Triangular Dither = dash-dot line, Gaussian dither = dotted line.

In conclusion, a larger scale dither does help to overcome both the local and larger scale non-linearities in non-uniform step size quantisers, and a Gaussian PDF also provides a more linear average transfer function than either uniform or triangular dither. However, the optimal dither amplitude and the corresponding amount of spurious level reduction can only be examined accurately through measurement.

5.5 Introduction of a Novel Bandlimited Dithering Technique

Wideband dithering could be used to reduce the level of harmonic and IM products introduced by a practical DAC. Large scale dithering will also be necessary (Section 5.4.2). However, a degradation in the signal to noise ratio must be endured by adding a large scale wideband dither signal. Obviously there is a point when the increasing noise power starts to dominate the spurious levels and at which point no further performance gain can be made. To rectify this problem, dither could be subtracted after the DAC, Fig. 5.4, but at the expense of dramatically increasing the complexity. Instead, a novel implementation of bandlimited dithering has been chosen for the multichannel application. The bandlimited dithering technique will minimise the increase of 'in-band' noise power when the dither signal is added, whilst at the same time reducing the spurious level.

Implementation of bandlimited dithering also takes advantage of the multichannel signals oversampling ratio which is required to reduce the design requirements on the reconstruction filters following the DAC (Chapter 5). The oversampling ratio means that there exists some frequency spectrum not being utilised by the signal. This unused spectrum can therefore be used by the dither signal.

The novel implementation of bandlimited dithering is shown in Fig 5.10(a). The interpolation factor chosen is dependent on oversampling ratio required to meet the specification of a given radio system. From the conclusions of the previous chapter the GSM and MPT1327 radio systems require an oversampling ratio of 3.2 and 5.4 respectively, which best translates to an interpolation factor of 4 for both systems.

The multichannel signal and dither spectrums are shown to be mutually exclusive in Fig. 5.10(b). A transition band is required for the digital interpolation filters and the analogue reconstruction filters. The reconstruction filters must remove the added dither signal so that it does not cause interference in neighbouring bands. In Chapter 4, these filters were designed for the suppression of images and not the dither power. Given that the dither power is closer to the desired signal than are the images, then a higher order reconstruction filter with better matching will be required.

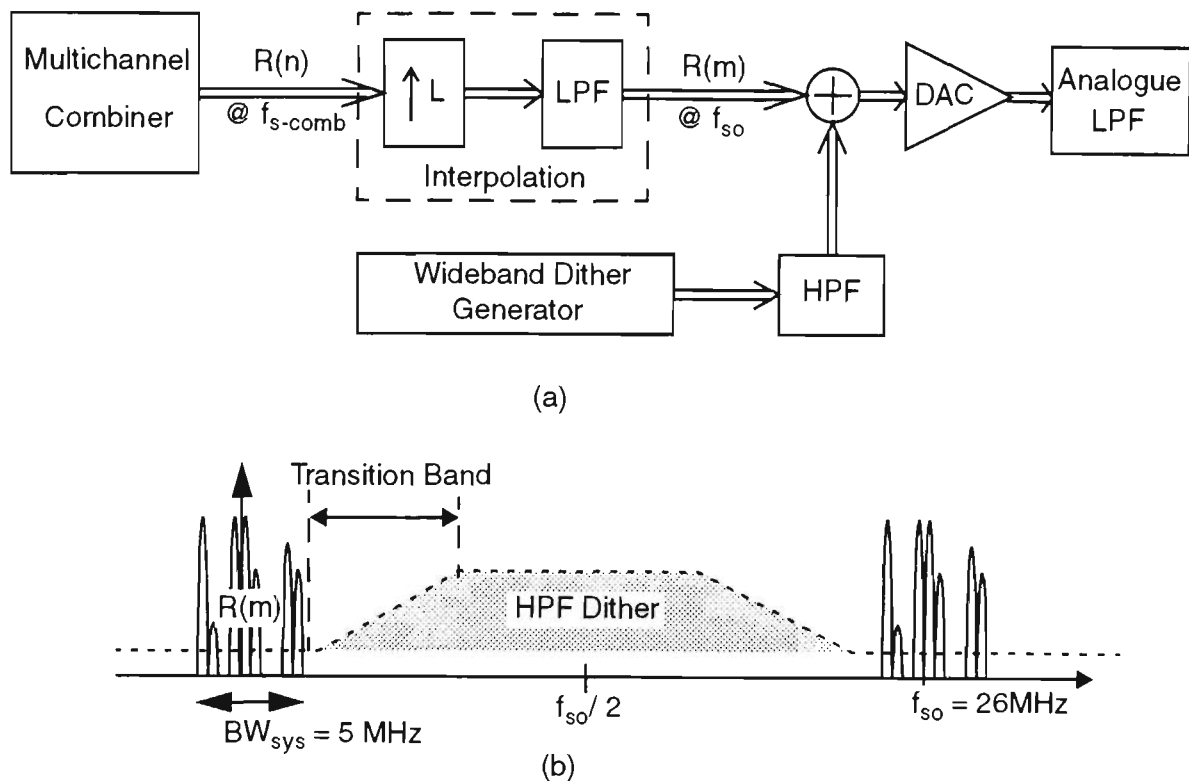


Figure 5.10: (a) Novel Implementation of a bandlimited dither architecture (b) Spectrum description of (a).

Significant efficiencies can be made in the implementation of the bandlimited dither architecture. This is brought about because the interpolation factor is a power of two, and efficient halfband filters can be used to interpolate the signal. In addition, the halfband filter design can incorporate the high pass shaping of the dither and the subsequent addition to the interpolated multichannel signal with very little increase in hardware (Chapter 6 will explore this in more detail). The cost of dither implementation is therefore insignificant as there is virtually no increase in hardware.

The novel implementation of bandlimited dithering presented in this Chapter essentially builds upon that described in [48], where the wanted signal and dither signal are added with mutually exclusive spectrums. However, in this application of bandlimited dither, the dither signal occupies a significant part of the spectrum. Therefore, the amplitude of the bandlimited dither signal, required to overcome local or larger scale non-linearities in the quantisation function, can be significantly smaller than that expressed in [48].

5.6 Conclusion

The non-ideal transfer characteristic of the DAC interface will introduce signal dependent harmonic and IM products which cannot be accurately modelled by additive white noise. The spurious responses are important for the application of a multichannel transmitter because they can fall into neighbouring channels, and directly affect the overall performance. The use of dithering, addition of a random signal before quantisation, can be used to minimise the spurious level.

Calculation of the average quantisation transfer function highlighted the favourable properties of the dither PDF for an arbitrary quantiser transfer function. If the quantiser is ideal, uniform dither was shown to produce a linear result for the least increase in noise power. For a practical DAC, the average quantisation error transfer function was used to show that the Gaussian PDF produced a smoother and more linear result than dither with a uniform or triangular PDF, indicating lower spurious levels. Large scale dithering was also shown to be advantageous in overcoming the local and larger scale non-linearities of a non-ideal quantiser. This will be experimentally verified in Chapter 6.

Many different dithering techniques have been implemented with the aim of reducing the spurious levels. The dither PDF and scale are unique in most implementations, whereas the dither spectrum is wideband in all known implementations, except for one [48]. Bandlimited dithering has been selected for the multichannel application primarily to add large scale dither whilst minimising the increase of 'in-band' noise power. The 'out-of-band' dither noise power must be removed by higher order and better matched reconstruction filters than that described in Chapter 4. However, the bandlimited dither can be added with a small increase in hardware, since the filtering functions required to spectrally shape the dither signal are already in existence.

The next Chapter will introduce the hardware implementation of bandlimited dithering, and measurements will be used to quantify the improvement of the spurious free dynamic range for larger scale dither with either a Gaussian or uniform PDF .

Chapter 6

Implementation of the Bandlimited Dithering Technique

6.1 Introduction

The analysis work in the previous chapter helped to devise a new technique, bandlimited dithering, that can be used to lower the level of the spurious responses introduced by a digital to analogue converter. This chapter describes the implementation of the bandlimited dithering algorithm on both general and special purpose digital signal processors and discusses some measured results.

The design of the halfband interpolators and the dither generator used in the bandlimited algorithm are described in Section 6.2. These designs were then implemented in hardware using a general purpose DSP, which was subsequently used to obtain measured results in a multichannel system. The results in Section 6.3 show that bandlimited dithering reduces the spurious levels generated by the DAC, producing between 2 and 4 dB improvement in performance. It is shown that large scale dither is necessary to produce these positive results and for this reason, the use of wideband dithering techniques is impractical because of the large increase in the in-band noise floor.

The low sampling frequency achieved using a general purpose DSP was a major limitation. Section 6.4 describes a special purpose DSP (ASIC) that was designed to obtain sampling frequencies which are a factor of 100 times faster than the general purpose DSP.

6.2 Bandlimited Dithering Architecture

The bandlimited dithering architecture adds the dither signal to the multichannel signal during the interpolation process, Fig. 6.1. The architecture consists of two halfband filter stages which achieve an overall interpolation factor of 4. This was found to be an adequate value for overcoming a 5% mismatch in the reconstruction filters used in analogue direct upconversion (Chapter 4). Note that dither is only added in the second stage of interpolation to ease the analogue reconstruction filter requirements.

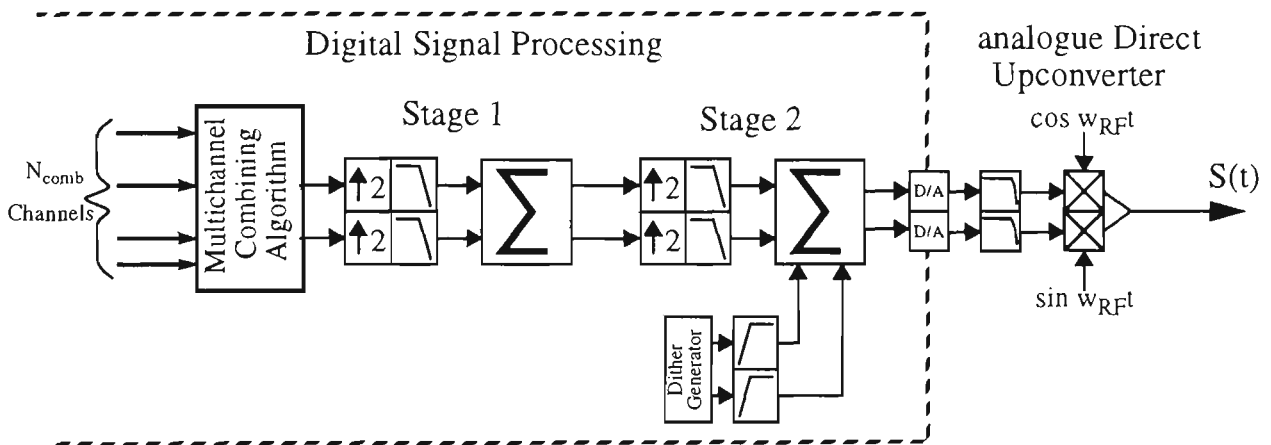


Figure 6.1: The bandlimited dithering architecture.

The next two sections will examine the design of the halfband interpolators and the dither generator.

6.2.1 Design of the Interpolator

The multichannel signal is interpolated by a halfband filter (Appendix B.2) with a lowpass spectral shape of $H_{LPF}(f)$, whilst the added wideband dither signal is required to be spectrally shaped by a filter with the opposite frequency specifications. The dither filter (highpass) parameters are derived from the lowpass parameters as follows:

$$f_{\text{stop-HPF}} = f_{\text{pass-LPF}} \quad (6.1)$$

$$f_{\text{pass-HPF}} = f_{\text{stop-LPF}}$$

Note that the stopband, δ_s , and passband, δ_p , ripple specifications for both filters are equal. The resulting frequency response for the HPF has the same shape as that of the lowpass filter but it is frequency translated by half the sampling frequency:

$$H_{HPF}(f) = H_{LPF}(f_s/2 - f) \quad (6.2)$$

The coefficients of the HPF required to shape the dither signal can now be directly obtained from the LPF by changing the sign of every second coefficient:

$$h_{\text{HPF}}(n) = (-1)^{n+1} \cdot h_{\text{LPF}}(n) \quad (6.3)$$

For a halfband filter the transformation is trivial because the even coefficients are all zero, except for the centre tap which is simply negated. Each halfband interpolator stage can then be drawn as shown in Fig. 6.2(a), where the multichannel signal is interpolated, $R(m)$, by a standard halfband architecture (Appendix B.2) before being added to the spectrally shaped dither signal, $d(m)$.

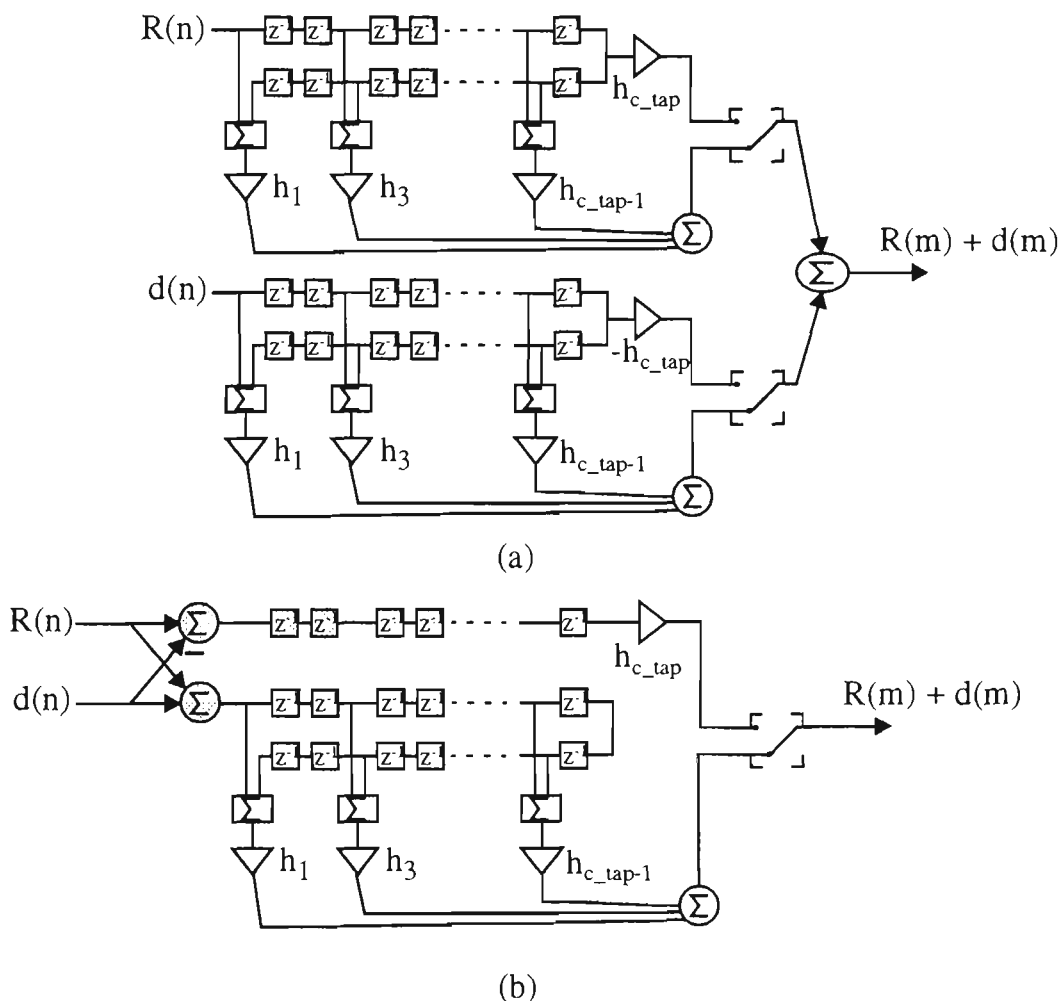


Figure 6.2: (a) Interpolation half-band stage. Addition of the interpolated multichannel signal and the highpass filtered dither signal (b) Optimised architecture of (a)

The filter required to spectrally shape the dither signal is identical to the interpolator, except that the centre tap, h_{c_tap} , is negated. The two filters in Fig. 6.2(a) can therefore be easily merged to form a highly efficient architecture as shown in Fig. 6.2(b). Note that each delay shown, z^{-1} , is simply implemented as a register clocked at the output sampling

frequency. Two registers of this type can be combined together into a single register which is clocked at the lower input sampling frequency. Compared to the original interpolator, only two more adders and a delay line (shown shaded in Fig. 6.2(b)) are needed to carry out the additional dithering tasks. Thus the benefits of bandlimited dithering can be obtained for very little increase in circuitry.

The spectral interpretation of the interpolation process is illustrated in Fig. 6.3. The original baseband multichannel signal has a system bandwidth of 5 MHz (BW_{sys}) and is sampled at 6.5 MHz (f_{s-comb}), Fig. 6.3(a). After the first interpolation stage, the output consists of the multichannel signal interpolated by a factor of 2, Fig. 6.3(b). The second stage interpolates this entire signal and adds an amount of bandlimited dither, as shown in Fig. 6.3(c). The difference between the two interpolator stages is that the filtering requirements are less stringent for the second stage.

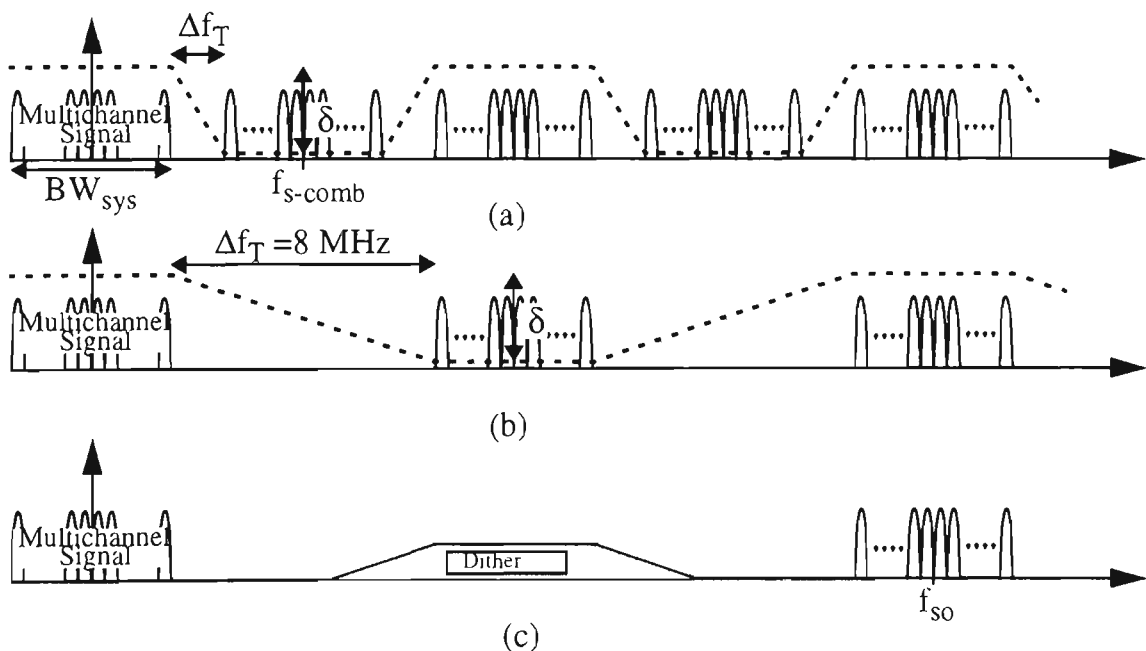


Figure 6.3: (a) Multichannel signal, $BW_{sys} = 5\text{MHz}$, sampled at $f_{s-comb} = 6.5\text{MHz}$. The first stage interpolation filter spectral shape is shown dotted. (b) Spectral interpretation at the output of the first stage interpolation filter. The second stage interpolation filter spectral shape is shown dotted. (c) Spectral interpretation at the output of the second stage interpolation filter.

Overall the architecture adds 2.5 MHz of dither with a transition width of approximately 8 MHz. This added dither signal has to be removed by the reconstruction filters.

6.2.2 PDF Selection for the Dither Generator

The dither source is a random number generator with a given PDF. Selection of the PDF used in the dither generator is based on two criteria, ease of implementation and performance.

The dither PDF must be simple to implement in a digital environment. The uniform PDF is better suited and less complex in a digital implementation than the Gaussian PDF, given that only a Gaussian and a uniform PDF are considered.

Selection of the PDF based on performance is not as simple. The previous chapter used the average quantisation transfer function, Eqn. (5.7), to compare the effect of different dither PDF's on a practical DAC transfer characteristic. The analysis indicated that a Gaussian PDF would perform slightly better than the uniform PDF. The remainder of this section uses measurement to quantify the performance of different PDF's in the bandlimited architecture.

Three dither sources, one with Gaussian and two with uniform PDF's, Table 6.1, are tested using the hardware described in Appendix F. The difference between the two uniform sources is the DC bias of the dither generator. In all cases the dither is wideband before it is shaped and added to the interpolated signal.

Table 6.1: Definition of the bandlimited dithering sources

PDF of the dither source	DC bias of the dither source ^a	Terminology used in text
Gaussian	NO	Gaussian Bandlimited dithering
Uniform	NO	Uniform bandlimited dithering
Uniform	YES ^b	Uniform bandlimited dithering with bias

a. Refers to the input dither source having a finite statistical mean.

b. The input dither source has a statistical mean is equal to $c/2$.

The measurements are based around the operation of a 9 bit DAC, primarily due to the dynamic range limitations of the spectrum analyser used. A higher precision DAC could be measured if notch filters are used to eliminate the main signals and low noise amplifiers are used to enhance the intermodulation products. However, both of these techniques would increase the complexity of the measurements and have the potential to further

distort the output. The measurements will highlight the benefits and disadvantages of the different dithering techniques that would be equally applicable to a higher precision DAC.

The 9 bit DAC¹ used is quite nonlinear, as illustrated via the DAC quantisation error transfer function, $q_e(X)$ in Fig. 6.4(a). The peak to peak error is almost 3Δ , in contrast to an ideal DAC where $q_e(X)$ would be uniformly distributed between $-\Delta/2$ and $\Delta/2$ (peak to peak error of Δ), Fig. 5.1(c).

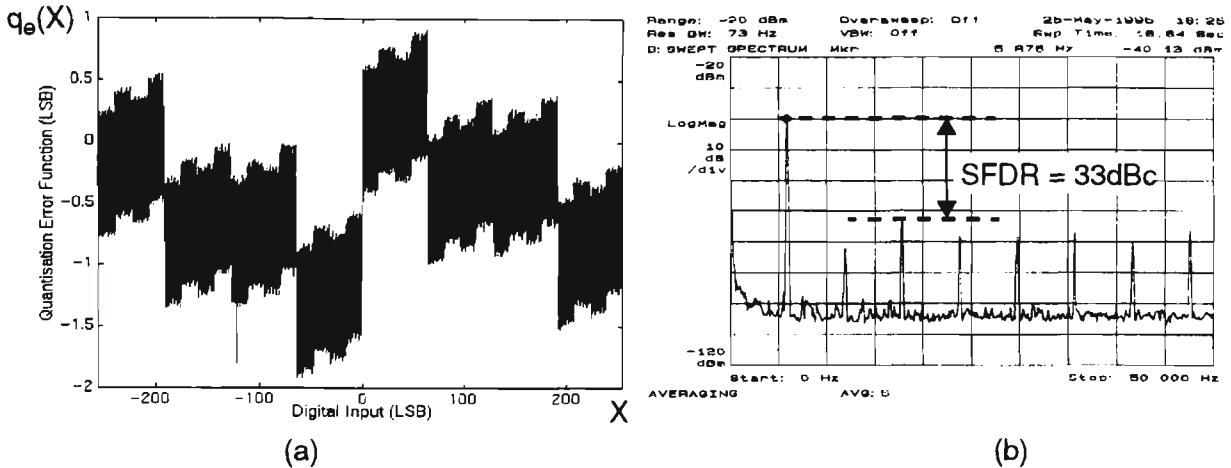


Figure 6.4: (a) 9 bit DAC quantisation error transfer function, $q_e(X)$. (b) The DAC output spectrum of a sinusoid with no dither added.

The different dither sources will be compared using a single tone generated in a lookup table, with the signal frequency set to an integer multiple of the sampling frequency. Although the signal is not what would be typically encountered, it does highlight the beneficial effects of dithering. The DAC output spectrum of the interpolated tone with no dither added is shown in Fig. 6.4(b), where the quantisation noise is concentrated into harmonics of the original signal, resulting in an SFDR of 33 dBc.

The effect of increasing the power of the different dither sources is shown in Fig. 6.5(a). The signal amplitude has a constant 7 bit full scale amplitude whilst the dither amplitude is increased. For all dither signals, the worst spurious level is shown to decrease when the dither power is increased i.e. the SFDR increases. The measurements show that uniform and Gaussian bandlimited dithering, i.e. sources with no DC bias, perform very similarly. However, a performance increase of 1->2dB is observed for the uniform bandlimited dithering with bias technique, Fig. 6.5(a). The difference in performance can be attributed to PDF of the bandlimited dither added and the DC offset of the dither source.

1. All measurements were performed on the 9 least significant bits of a 16 bit DAC device..

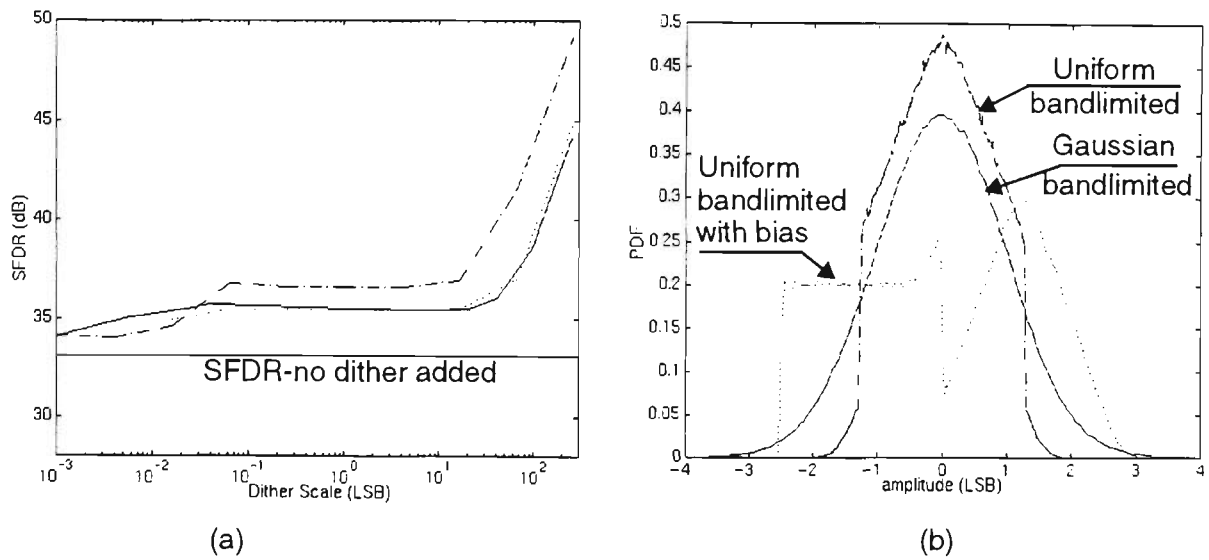


Figure 6.5: Plot of SFDR versus power of the added dither signal. (a) Uniform bandlimited dithering '...', Uniform bandlimited dithering with bias '-.-.', Gaussian bandlimited dithering- solid (b) PDF's of the bandlimited dither added before quantisation. Power is normalised to Δ^2 .

If the dither source into the halfband shaping filter is Gaussian then the PDF of the bandlimited dither added to the upconverted signal will also be Gaussian, Fig. 6.5(b). Further, when the dither source is uniformly distributed, with no DC bias, then the resulting PDF also has a shape similar to Gaussian, Fig. 6.5(b). Both of these dither sources have a similar level of measured performance, as would be predicted through the calculation of the average quantisation transfer function. However, if the source is uniformly distributed, with a DC bias, then the PDF is a combination of a uniform distribution, in the negative region, and a Gaussian PDF, in the positive region, Fig. 6.5(b). This PDF gives a greater probability of large dither amplitudes than the other two schemes.

The DC offset of the dither PDF source also generates a sinusoid at half the sampling rate (see Fig. 6.7(b)). The combination of a random dither signal with a sinusoid at half the sampling frequency has been reported to result in an improved performance [50]. This situation has also been observed here.

Based upon the ease of implementation and measured performance, the dither source has been selected to be uniformly distributed with a DC bias of $c/2$.

6.3 Bandlimited Dithering Results

This section presents the measured results of bandlimited dithering in a multichannel system. A scaled version of the GSM radio system has been implemented due to the sampling rate limitations of the development system. Figure 6.6 shows the full GSM system frequencies and the corresponding scaled system frequencies.

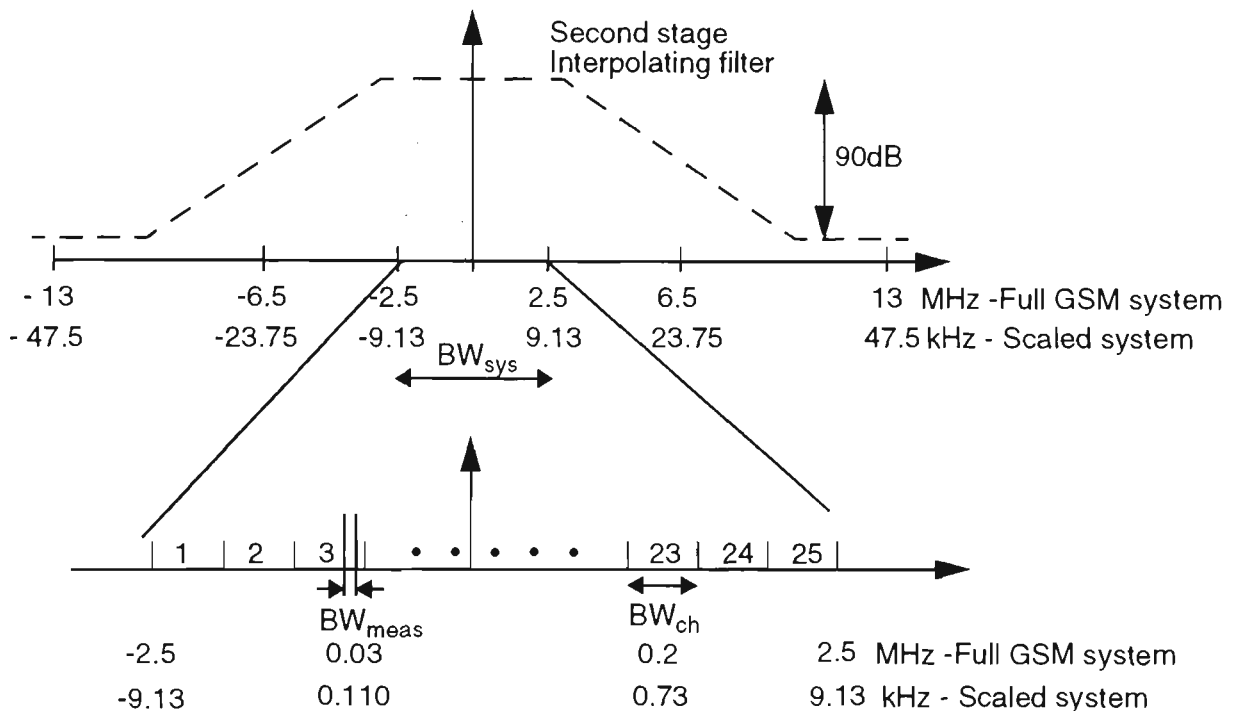


Figure 6.6: Graphical illustration of the frequencies required for a full GSM system with a system bandwidth of 5MHz and the corresponding scaled GSM system used in measurements.

Equation (3.32) predicts that the $\text{CNR}_{\text{multi}}$ at the output of the quadrature upconverter will be 73.26 dBc, assuming that 4 channels are combined and that both 9 bit DAC's are ideal. This is more than sufficient for a GSM transmitter with a power class of 8 (TRX8), which requires a $\text{CNR}_{\text{multi}}$ of 70dBc. However, the DAC is not ideal, as shown in Fig. 6.4(a), and the performance will be lower than predicted.

The effect of the non-ideal DAC is demonstrated in Fig. 6.7(a), where four channels are activated within the system bandwidth. The output spectrum from the DAC shows many spurious responses occurring across the Nyquist bandwidth. Only the spurious responses that fall in-band or close to the edges of the system bandwidth are considered in the calculation of the SFDR. The other spuri will be eliminated by the subsequent filters. The calculated SFDR is therefore 47dBc, a massive 23dB less than the 70dBc system specification.

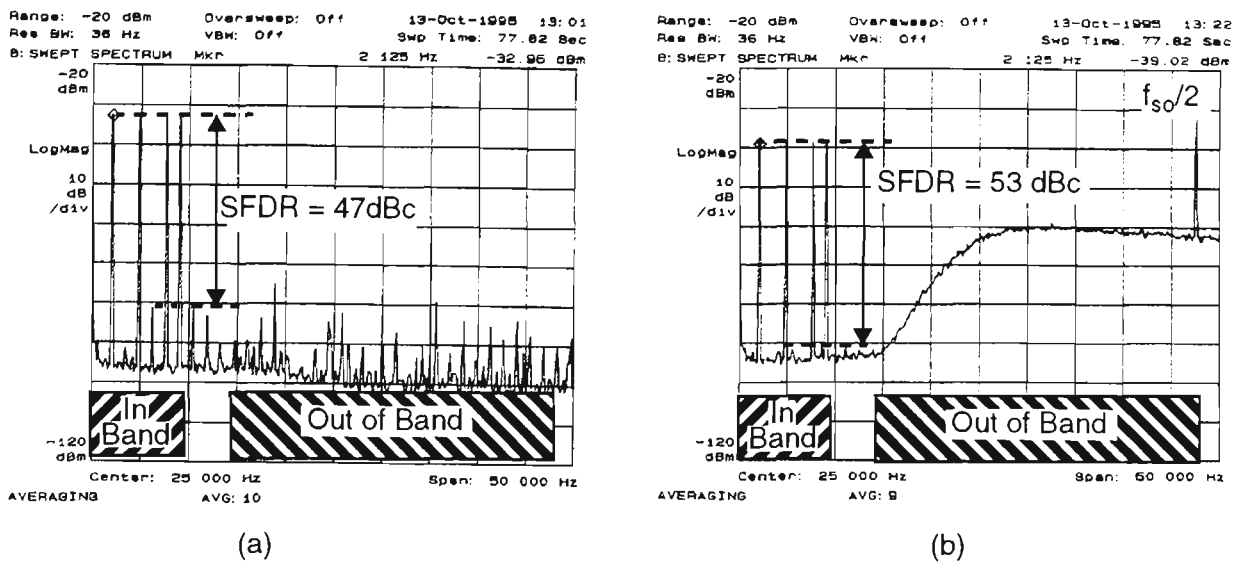


Figure 6.7: (a) Scaled GSM system with no dither added. $f_{so} = 95\text{kHz}$ (b) Scaled GSM system with bandlimited dither added.

The level of the spurious responses can be reduced through the addition of bandlimited dithering, as is illustrated in Fig. 6.7(b), where the SFDR has been increased to 53 dBc. The dither is also shown to be added ‘out of band’, and so it will not affect the in-band noise floor. The DC offset of the dither PDF source has also generated a sinusoid at half the sampling rate, Fig 6.7(b).

The effect of dither power (amplitude) on the SFDR is shown in Fig. 6.8(a). The SFDR only improves when there is at least $100\Delta^2$ of dither power, highlighting the benefit of larger scale dither on the spurious levels. Note, that as the dither level was increased, the carrier level was reduced so that the sum of the two signals did not exceed the 9 bit full scale range of the DAC. In other words, no clipping was allowed to occur.

The carrier to noise ratio uses a noise measurement bandwidth of BW_{meas} . As the dither level increases, the carrier power decreases, whilst the in-band noise floor remains approximately constant. The carrier to noise ratio will therefore decrease as shown in Fig 6.8(b). The reduction is substantial at high dither levels.

An ideal DAC has a CNR of 73.3 dBc (dash-dot line on Fig. 6.8(b)) which is substantially better than the measured DAC, even with no dither added. This is due to the poor quantisation error of the measured DAC (peak to peak error is 2.6Δ in Fig 6.4(a), and this explains the 7 dB of additional quantisation noise.

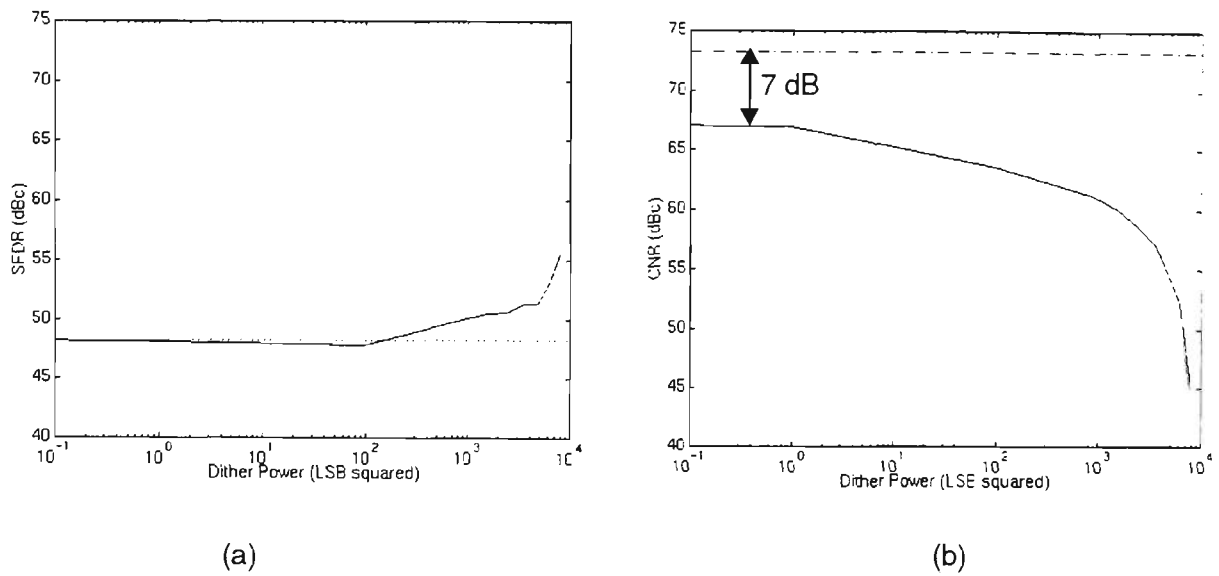


Figure 6.8: (a) Plot of the SFDR vs. the Dither power. The SFDR when no dither is added is shown '....'. (b) Plot of CNR versus Dither Power. The ideal CNR_{multi} for a 9 bit DAC when 4 channels are activated is shown '-.-.-'.

The CNR and the SFDR can now be combined into a quantity called the Carrier to Noise and Distortion ratio (CaNAD), where the distortion power is the sum of the noise (CNR) and spurious power (SFDR) measured within a bandwidth of BW_{meas} . The carrier to noise and distortion ratio of the worst channel is defined as:

$$CaNAD = (SFDR^{-1} + CNR^{-1})^{-1} \quad (6.4)$$

where the SFDR and CNR are expressed as linear power ratios, not in decibels.

The CaNAD has been plotted in Fig. 6.9(a), shown with a dashed line. The SFDR dominates the CNR for small values of dither power, whilst the reverse is true for larger values of dither power. The resulting CaNAD therefore arrives at an optimum value of 50 dBc when the SFDR and CNR are approximately equal. Although the addition of bandlimited dither resulted in a 2 dB improvement, the level of improvement is still not enough to meet the GSM CNR_{multi} system specification of 70 dBc.

Dither power equal to $2000\Delta^2$ or a dither amplitude equal to half of the 9 bit full scale range of the DAC is required to achieve this 2 dB of improvement. Therefore, large scale dither is necessary to overcome nonlinearity in a practical DAC. Small scale dither (amplitude variation is the order of 1 LSB) has no effect on performance.

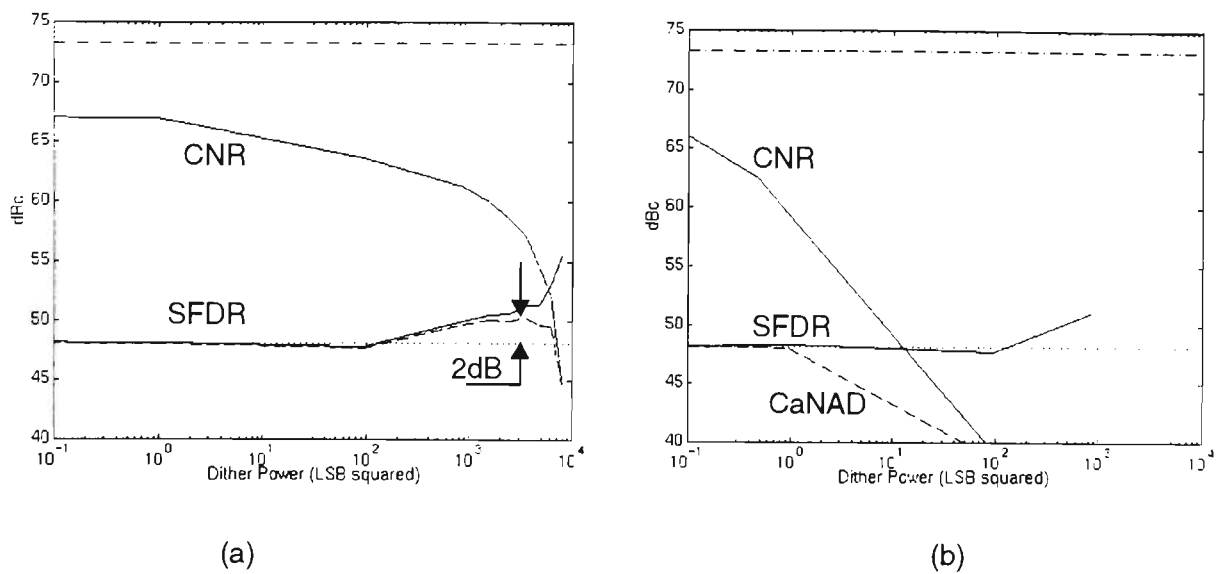


Figure 6.9: (a) The effect of adding bandlimited dither. The CaNAD is shown dotted. (b) The effect of adding wideband dither. The CaNAD is shown '---'. The SFDR when no dither is added is shown '...' and the ideal CNR_{multi} for a 9 bit DAC when 4 channels are activated is shown '-.-.-'.

6.3.1 Wideband Dither

One of the main advantages of bandlimited dither over wideband dither is that the dither power is added out of band. The addition of wideband dither increases the in-band noise power and causes the CNR curve to decrease at a much faster rate. This is illustrated in Fig. 6.9(b), where the CNR curve dominates the SFDR curve before any enhancements in the level of the spurious can be made. Adding wideband dither for this application therefore provides no benefits unless the added dither can be successfully subtracted after the DAC.

6.3.2 DC Offset Effect

The performance of bandlimited dithering was found to be enhanced by removing the DC offset from the DAC transfer characteristic.

It was noticed that the odd harmonics or intermodulation products dominated for small amounts of dither. This can be attributed to the odd order transfer characteristic of the DAC, Fig. 6.10(a). However, the even harmonics became more significant as the dither power increased and dominated at the point of optimal performance. It is well known that even harmonics and intermodulation products can be generated from a third order transfer characteristic if a DC offset exists. The DAC transfer characteristic has a DC offset of 34 LSBs, Fig. 6.10(a).

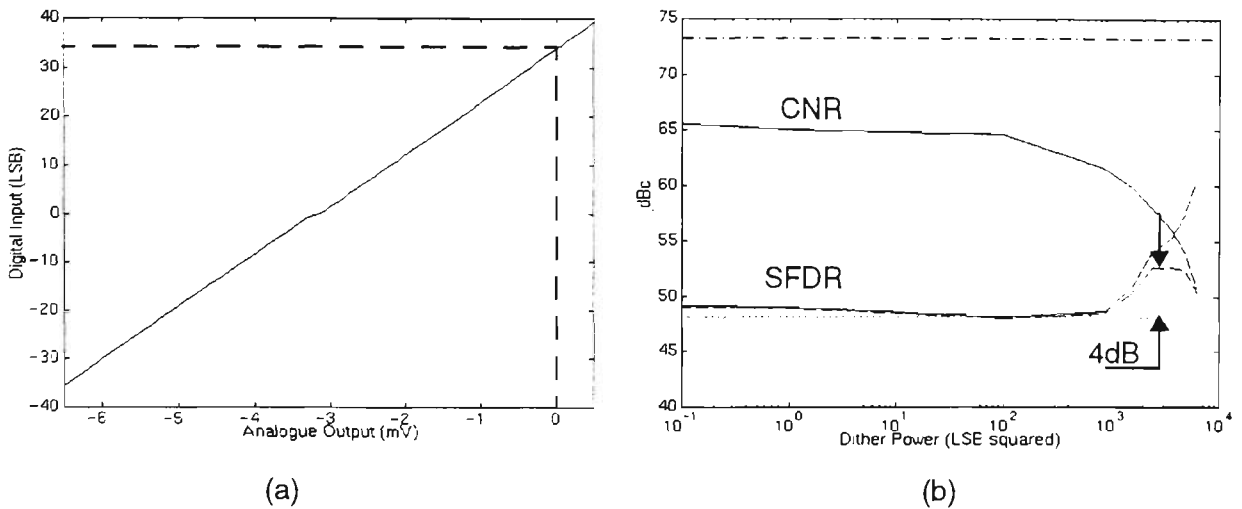


Figure 6.10: (a) DAC transfer function (b) The effect of adding bandlimited dither with DC offset removed. The CaNAD is shown '---'. The SFDR when no dither is added is shown '...' and the ideal CNR_{multi} for a 9 bit DAC when 4 channels are activated is shown '----'.

When the DC offset was removed the even harmonics were no longer dominant at the point of optimal performance and the SFDR was subsequently enhanced. The optimal point of the CaNAD curve has now increased to 4 dB, Fig. 6.10(b).

6.3.3 An Ideal DAC

The effect of bandlimited dither on a close-to-ideal DAC was also measured by using the 9 MSBs of a 16 bit DAC, as opposed to the 9 LSBs. As expected, the measured quantisation noise, CNR, was within 1 dB of the ideal value, Fig. 6.11.

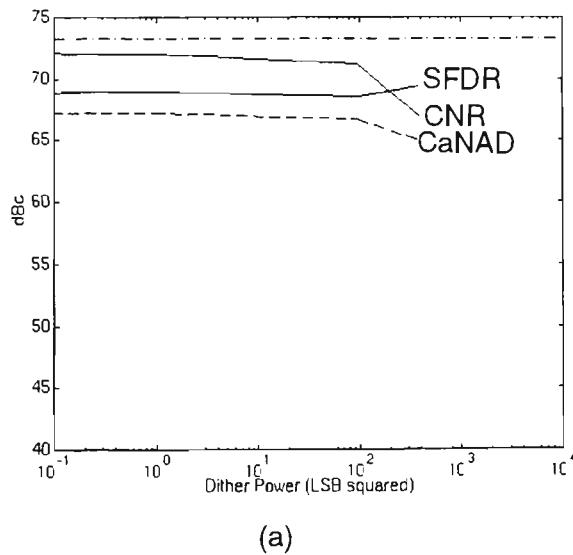


Figure 6.11: The effect of adding bandlimited dither for a close-to-ideal DAC. The CaNAD is shown '---'. The ideal CNR_{multi} for a 9 bit DAC when 4 channels are activated is shown '----'.

The worst spurious response for the close-to-ideal 9 bit DAC was 20 dB better than for the practical 9 bit DAC measured previously, and when dither was added the spurious responses decreased. However, the SFDR remained constant because the signal level also decreased. Additionally, the CNR decreases and dominates the CaNAD equation almost immediately. The result is that no gain in performance is observed by adding bandlimited dithering for a DAC with a close-to-ideal transfer function.

6.3.4 Dithering Remarks

The measurements have shown that adding large scale bandlimited dither to the multichannel signal improves the performance of the DAC, whilst small scale dither has no affect on performance of the practical DAC. The larger scale bandlimited dither will place a more stringent requirement on the reconstruction filters discussed in Chapter 4, because the dither signal is closer to the desired signal than are the images. Higher order filters with better matching will be required.

Conventional wideband dithering provides no benefit for the multichannel base station application. This is because the large scale dither, that is required to overcome the non-linearity of the DAC, causes the in-band noise floor to dominate the CaNAD before any improvement in the spurious level can be made. Similarly, dithering of any form will not enhance the performance of the DAC, for a close-to-ideal DAC.

6.4 The Bandlimited Dithering ASIC

One of the major limitations of the C40 digital signal processing development system was the maximum sampling rate. The large number of instructions required to implement the second stage interpolator and dither generator meant that the output sampling frequency was limited to 95 kHz, a lot lower than the output sampling frequency of 26 MHz required for a GSM system with a 5 MHz system bandwidth. This section describes an Application Specific Integrated Circuit (ASIC), whose main purpose is the increase of the output sampling speed, Fig 6.12.

Two separate ASIC's were designed for the In Phase and Quadrature channels. Both have the same architecture, except for the uniform random number generators, which must be independent. The output sampling frequency is set by an external clock which also drives the DAC's.

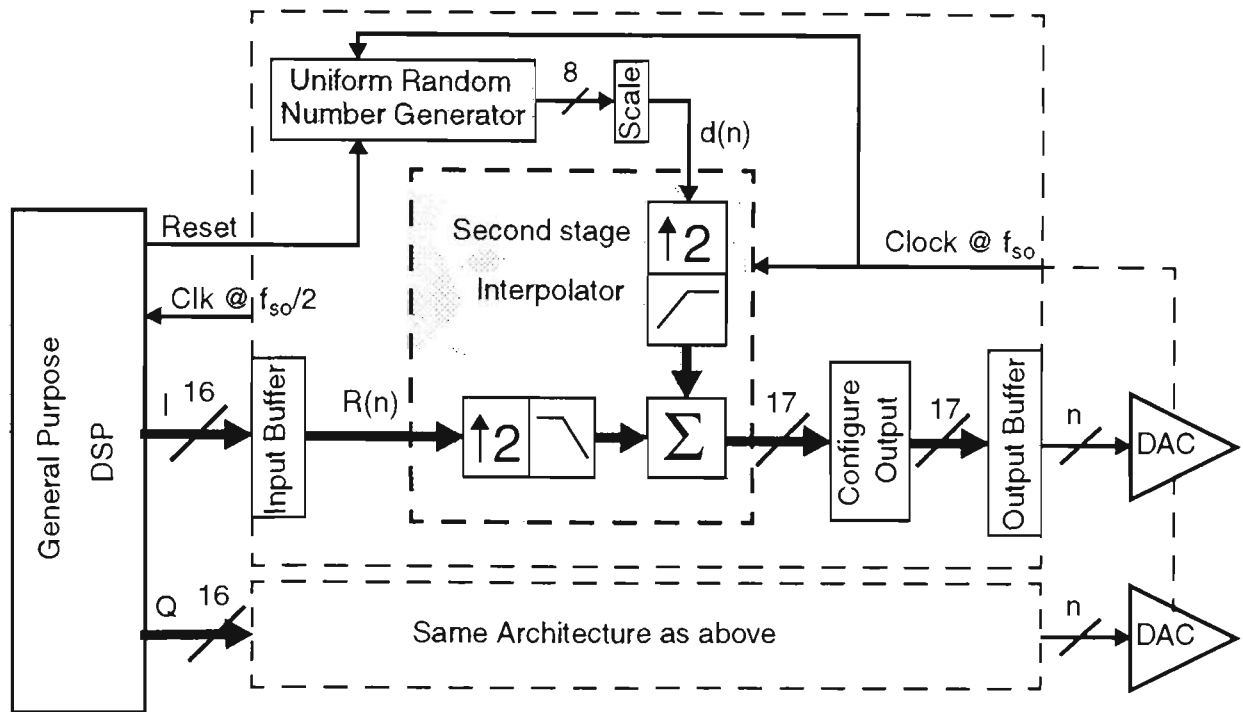


Figure 6.12: Position of the bandlimited dithering ASIC, the main connections and the schematic of the architecture contained within the ASIC

The interface to the preceding DSP is simple and requires no additional circuitry. The ASIC generates a clock signal at the input sampling frequency, $f_{so}/2$. This enables the synchronous transfer of 16 bit two complement data into the input buffer of the ASIC. A reset pulse can be initiated by the DSP to ensure that the uniform random number generators are operating independently on both the In Phase and Quadrature ASIC's.

Two auxiliary functions, dither scaling and configuration of the output data, are also included in the ASIC. The scaling of the 8 bit dither word is required for optimising the performance of the DAC, whilst the output data can be configured as either a two complement or a binary number.

The architecture of the halfband interpolator and dither generator will now be discussed in Sections 6.4.1 and 6.4.2 respectively.

6.4.1 Halfband Interpolator Design

The frequency response for the halfband filter is shown in Fig. 6.13.

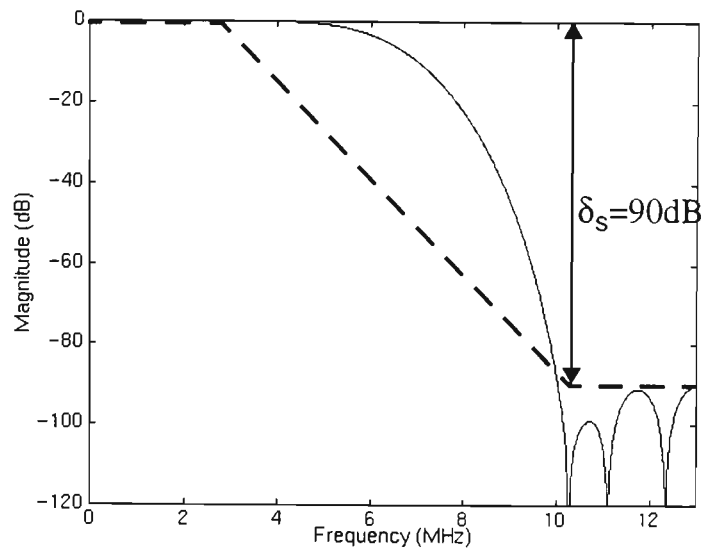


Figure 6.13: *Frequency response for the halfband interpolator*

The second stage halfband interpolator has been designed for a stopband attenuation of 90 dB, so that it can be used for either the GSM or MPT1327 radio systems. The passband and stopband frequencies are set at 2.84 MHz and 10.16 MHz respectively, when the output sampling frequency is 26 MHz. The Parks McClellan equiripple algorithm was used to calculate the 17 bit twos complement filter coefficients from these specifications, Table 6.2. Note that the even coefficients are all zero except for the centre tap, h_{12} .

Table 6.2: *Filter Coefficients for the Halfband Interpolator*

Coefficient	Twos Complement	Equivalent Signed Binary	CSD
h_1	1 1111 1111 1111 0010 (-14)	- 1110	(-1) 0010
h_3	0 0000 0000 0111 1110 (126)	111 1110	1000 00(-1)0
h_5	1 1111 1101 1100 0110 (-570)	- 10 0011 1010	(-1)0 0(-1)00 0110
h_7	0 0000 0111 0011 1110 (1854)	111 0011 1110	100(-1) 0100 00(-1)0
h_9	1 1110 1011 1001 0100 (-5228)	- 1 0100 0110 1100	(-1) 0(-1)00 (-1)001 0100
h_{11}	0 0100 1110 1111 1001 (20217)	101 1110 1111 1001	0101 000(-1) 0000 100(-1)
h_{12}	0 1000 0000 0000 0000 (32768)	1000 0000 0000 0000	Not Used

The hardware efficient shift and add technique was used to implement the multiplication of each coefficient. The coefficients are most efficiently implemented using the Canonical Signed Digit (CSD) representation for signed binary numbers. Each binary digit can take one of three possible values; +1, 0, -1. The result of converting a given coefficient into CSD representation is the reduction in the number of 1's and therefore the number of shift

and adds required to complete the multiplication. This can be verified by examination of Table 6.2. The centre tap, h_{12} , will require only a simple shift right operation (divide by two).

The architecture of the halfband interpolator is shown in Fig. 6.14; this was derived earlier in Fig. 6.2(b). All arithmetic operations occur at the input sampling frequency, whilst only the switch is clocked at the output sampling frequency. To ensure fast operation, pipelining of the data has been used. the result is a latency of 10 clock cycles or 0.385 μ s at an output sampling frequency of 26 MHz.

The halfband filter has been implemented using full precision arithmetic. This means that all filter calculations have been completed at full precision until the last summation stage which truncates the result to 17 bits. This ensures that a build up in quantisation noise will not occur.

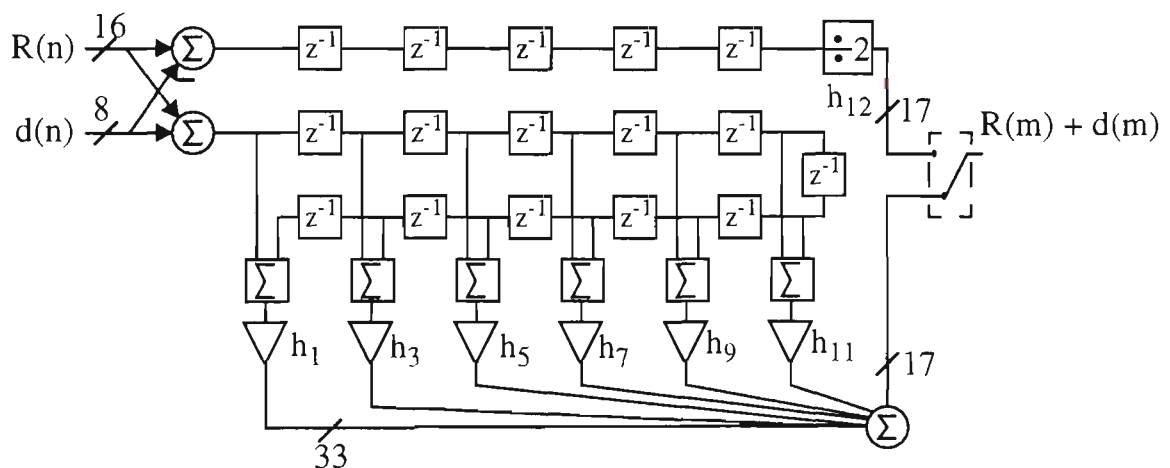


Figure 6.14: *Halfband interpolator architecture with dither shaping incorporated, as implemented in the ASIC.*

The increase in circuitry for the halfband interpolator with dither shaping compared to a standard halfband interpolator, is very small. Only an extra two adders and 5 delay elements are required (shown shaded in Fig. 6.14). In the final layout of the ASIC, the additional circuitry represents only 2.5% of the total die area.

6.4.2 Uniform Dither Generator

The uniform dither generator implementation is based on the Linear Feedback Shift Register (LFSR) technique. However, the LFSR must generate a word rather than the normal serial bit stream. The generation of m-sequences as a series of non-overlapping W bit words is discussed in [58], and the same technique has been applied directly to this application.

The precision of the dither has been selected to equal just the integer quantity required. The reason for this is that the fractional quantity of dither (small scale) did not enhance the performance of a practical DAC. From the measurements of a 9 bit DAC, the optimum scale of the dither occurred at approximately half the 9 bit full scale range, or 8 integer bits. A facility exists to scale the 8 bit dither word.

For the generator to closely approximate white noise, the m-sequence length has been set to $2^{25}-1$. The feedback taps have been derived from the characteristic polynomial for the LFSR as 0 and 3 for $N=25$ [59]. The technique described in [58] is used to ensure that each of the 8 bit streams is shifted from one another by $2^{25}/8 = 4*10^6$ bits. A sufficiently large shift is necessary to ensure that the 8 bit word closely approximates white noise. The schematic of the dither generator is shown in Fig. 6.15.

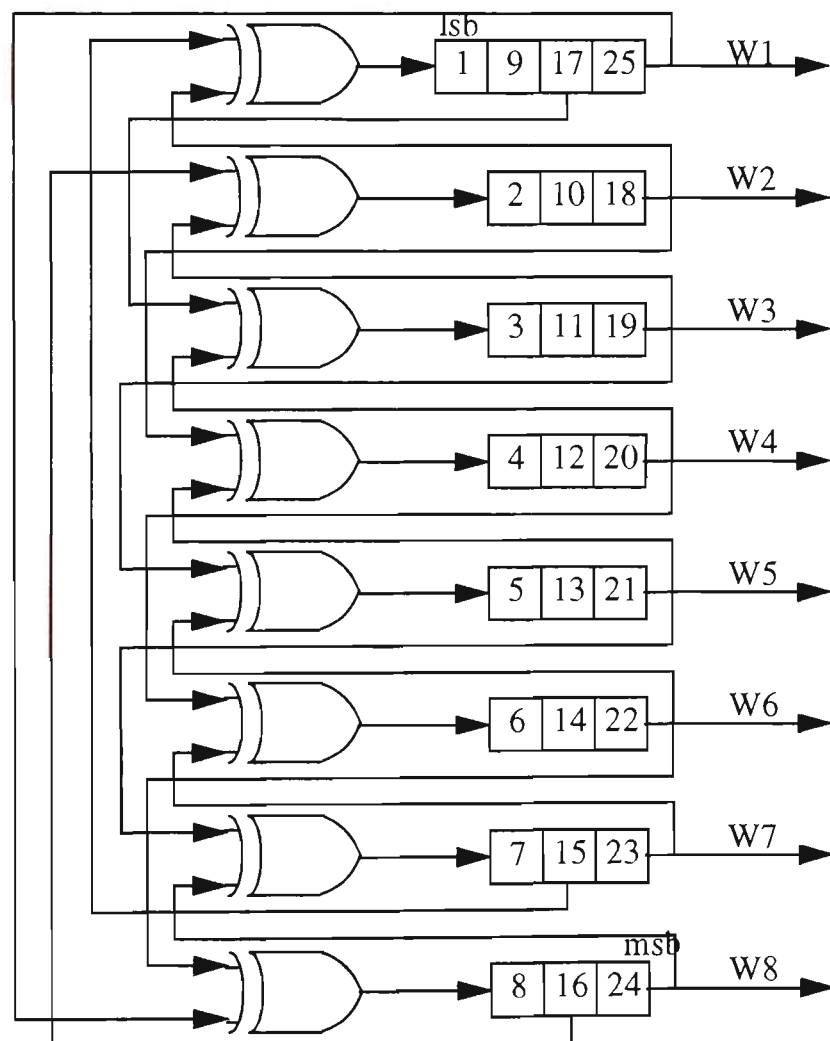


Figure 6.15: 25 stage LFSR 8 bit word generator

6.4.3 The Actual Bandlimited Dithering ASIC

A prototype device has been fabricated using a 1.0 micron CMOS process, demonstrating the suitability of the algorithm for VLSI implementation. The actual die photo of the 68 pin device wire bonded is shown in Fig. 6.16.

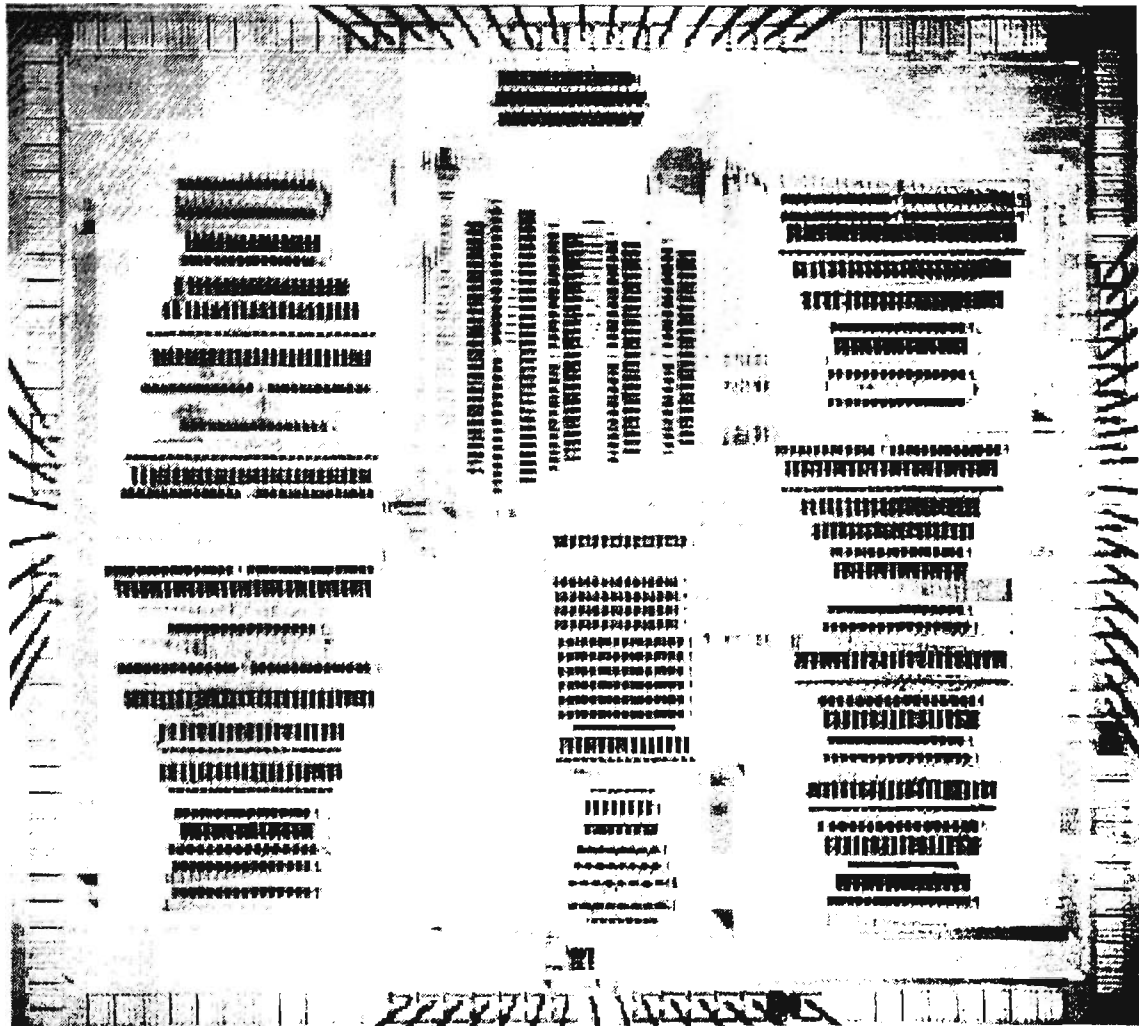


Figure 6.16: Photograph of the actual die of the bandlimited dithering ASIC. Actual size = 7.30mm × 6.74mm; No. of transistors = 45,654.

The device was simulated (although it was fabricated, the ASIC was not tested due to time restrictions) to operate at a speed of 10 MHz, a 100 times faster than the general purpose DSP, but still not fast enough for the required 26 MHz output sampling frequency. The ripple adders that were used to perform the shift and add were the reason for limiting the maximum speed of the device.

6.5 Conclusion

The performance of the bandlimited dithering technique was measured by the carrier to noise and distortion ratio (CaNAD). The distortion was obtained by the spurious free dynamic range (SFDR) and the carrier to noise ratio (CNR), where the noise was measured in a bandwidth of BW_{meas} . The CaNAD of a practical DAC is dominated by the spurious levels, which reduce when bandlimited dither is added. To avoid clipping, the carrier level must be reduced as the dither level is increased, which subsequently reduces the CNR. The CNR then becomes dominant at large dither levels. An optimal CaNAD performance occurs when the SFDR and CNR quantities are approximately equal. For the 9 bit DAC measured in this chapter, a 2 to 4 dB increase in performance was found when the peak to peak dither amplitude covered half the full scale range of the DAC.

The scale of dither required to produce optimal performance will be very dependent on the DAC transfer function. The DAC tested had quite a significant amount of nonlinearity which required the addition of a large scale bandlimited dither to enhance its performance. Wideband dither was shown to provide no benefit because it produced a large increase in the in-band noise floor. In addition, dithering gave no improvement in performance if there was no step nonlinearity in the DAC characteristic (close-to-ideal DAC). Practical DAC's do not usually fall into this category.

The hardware implementation of the bandlimited dithering technique was also described. Central to the technique was found to be the interpolation by a factor 4 required to overcome a 5% mismatch in the reconstruction filters. Two interpolate by 2 stages were used to reduce the processing load. The design of an ASIC for the second and higher sampling frequency stage was implemented. It consisted of a halfband interpolator and a dither generator.

The halfband interpolator increases the sampling rate of the multichannel signal by 2 and also performs the shaping of the wideband dither so that the signal and dither spectrums are mutually exclusive. The architecture requires an extra two adders and 5 delay elements compared to the standard halfband interpolator. The extra circuitry represents only 2.5% of the total die area of the fabricated ASIC.

The dither generator produced a uniformly distributed random number with a DC bias.

This performed better than the other PDF's that were considered and was simply implemented in hardware using the LFSR technique. Only 0.9% of the total die area was used for this function.

A special purpose DSP was built to demonstrate the suitability of the algorithm for integrated circuit implementation and to improve upon the low sampling speed of the general purpose DSP. The ASIC design increased the sampling speed by a factor of 100 (to 10 MHz), still short of the 26 MHz required. The ripple adders restricted the maximum sampling rate, which could be increased by relaxing of the attenuation specification (to account for the roll-off of the reconstruction filters), modifying the halfband canonical transversal filter architecture to the modified transversal filter architecture, reducing the coefficient wordlength, utilising a more advanced silicon technology and cell library (including carry lookahead adders) and introducing more pipelining into the design. The 26 MHz sampling speed required for implementing a system bandwidth of 5 MHz should then become achievable.

Bandlimited dithering technique improves the effective DAC precision by approximately half a bit. This improvement has been achieved for a very small increase in hardware. However, because the dither signal is closer to the desired signal than are the images, higher order and better matched reconstruction filters than those discussed in chapter 4 will be required.

Chapter 7

Conclusion

The thesis has focused on a new multichannel transmitter architecture suitable for current and future radio communication systems. This novel technique has involved combining the channels at low power levels in a digital signal processor before being amplified by a wideband ultra-linear amplifier. This thesis has concentrated on the pre-amplifier stages, that is the low power channel combiner, the digital to analogue converter and the frequency upconverter.

Existing radio base stations use a separate modulator and power amplifier for each channel. The channels are then combined at RF, using expensive, precision made cavity resonators and ferrite isolators, prior to feeding the antenna. Chapter 2 reviewed these main components in detail and showed that the cavity resonators restrict the minimum channel separation and require mechanical adjustment, when retuned to a new transmit frequency. They are responsible for the high cost, large bulk and low flexibility of current base station architectures. Introduction of the low power combining architecture highlighted that the cavity resonator was not needed, and therefore, a reduction in size and cost of the base station could be achieved. In addition, combining the channels in a DSP environment did not limit the frequency agility or the total number of transmitted channels. The DSP architecture is extremely flexible because the entire functionality of the base station, i.e. modulation format, power control, and channel frequency allocation, can be software programmable.

Chapter 2 has also identified four design challenges of the new DSP low power combining architecture:

- multichannel combining,
- frequency conversion to RF,
- DAC interface and
- the wideband ultra-linear power amplifier.

The thesis considered the first three challenges.

The multichannel combining algorithm is made up of an interpolator, multiplier and summer. Chapter 3 investigated three efficient interpolator techniques to minimise the computational load for practical implementation and power consumption reasons. The LUT approach was found to be the most efficient but it is only suitable for digital modulation schemes, where the number of output states (trajectories) is small enough not to require an excessive amount of memory. In contrast, the cascaded halfband approach was shown to be suitable for both analogue and digital modulations at the expense of a larger computational load. A third algorithm, the polyphase FFT technique, was introduced as an efficient algorithm for combining a large number of channels. It was found to be more efficient than the cascaded halfband approach when more than 8 channels were combined.

Chapter 3 also investigated and compared four frequency upconversion techniques which translate the baseband multichannel signal to RF:

- Digital IF upconversion
- Subsampling upconversion
- Analogue direct upconversion - lowpass reconstruction
- Analogue direct upconversion - bandpass reconstruction

These schemes are used or have been proposed for single channel (narrowband) radio transmitters and this work extends their application to the upconversion of a wideband multichannel signal.

Translating the baseband signal to RF via the analogue direct upconverter, utilising lowpass or bandpass reconstruction, was selected as the best solution. The other two

digital techniques are currently limited by the performance of commercially available DAC's and disadvantaged by the large amount of computation required to generate the multichannel signal at a suitably high intermediate frequency.

The linearity of the analogue direct upconverter is compromised by the amplitude and phase mismatch that exists between the In Phase and Quadrature circuits. These imbalances cause sideband responses which exceed radio system specifications. Chapter 4 introduced a novel adaptive compensation technique which cancels the undesired sideband at a number of frequencies across the system bandwidth. All previous techniques have only compensated for a single gain and phase imbalance. The main advantage over previous adaptive compensation techniques is that implementation occurs at the lower channel sampling frequency and frequency dependent imbalances, important in wideband systems, can be corrected. This leads to an improved performance and a lower computational overhead.

Chapter 4 also showed that the lowpass reconstruction filters are the major source of the frequency dependent imbalance between the In Phase and Quadrature channels. The analysis showed that the new compensation technique could meet the GSM and MPT1327 radio system sideband rejection specifications, if the baseband multichannel signal was oversampled by a factor of 3.2 and 5.4 respectively. This assumed that the lowpass reconstruction filters are mismatched by 5%. This analysis represented the major theoretical part of the thesis and it was published in [67] and presented at two conferences [65,66].

The 5% filter mismatch is still a tight specification for an analogue environment. Much of the frequency dependence between the In Phase and Quadrature channels can be removed by replacing the two lowpass reconstruction filters with a bandpass filter at the output of the analogue direct upconverter. Correction of the imbalance is still required and the new correction method is applicable due to its lower computational load.

Chapter 5 introduced a novel implementation of dithering that produces harmonic and intermodulation products caused by unevenly spaced DAC quantisation levels. These spurious responses are particularly troublesome in a multichannel system, because they fall into neighbouring channels. The dither signal was added out of band in the unused

upper part of the spectrum produced by the oversampling requirement of Chapter 4. This is advantageous because large amplitude dither is necessary to overcome the significant step nonlinearities in a practical DAC. Since the dither signal is closer to the desired signal than are the images, a higher order and better matched reconstruction filter than that concluded from Chapter 4 will be required.

The bandlimited dither algorithm was implemented in Chapter 6 and measurements showed that the performance of the DAC was improved by 2 to 4 dB, or approximately half a bit in precision. The algorithm was initially implemented on a single general purpose DSP which limited the maximum sample rate to 100 kHz, well short of the 26 MHz required. Parallel processing or a special purpose DSP is therefore needed. An ASIC was designed to perform the highest speed function: the final interpolate by 2 stage. It was shown that the dither algorithm could be incorporated into the existing interpolator structure with a minimal increase in hardware, equalling 3.4% of the total die area, because the filtering functions required to spectrally shape the dither signal were already in existence. The ASIC was designed for a sample rate of 10 MHz, and further optimisation should enable the 26 MHz specification to be achieved. The bandlimited dithering algorithm developed in this Chapter has recently been accepted for publication [68].

7.1 Future Work and Critique

The effect of reconstruction filter mismatch on analogue direct upconversion and the development of a bandlimited dithering algorithm were the two areas of detailed study completed in this thesis and further work in these areas is detailed below.

The analysis of a 5% mismatch between the lowpass reconstruction filters showed that an oversampling ratio of 4 was sufficient for the compensation technique to suppress the undesired sideband signals to meet radio specifications. A suggested way of improving the situation has been to use analogue direct upconversion with bandpass reconstruction which removes a large proportion of the frequency mismatch and requires a lower oversampling ratio. Analogue direct upconversion utilising either lowpass or bandpass reconstruction will still require correction for the imbalances using the multichannel adaptive compensation technique, which could be improved. Instead of compensating for

one frequency in each channel, an equaliser structure could be used to better frequency match the amplitude and phase errors. Additionally, the feedback error signal could be obtained by a correlator instead of a tuned receiver. Both these techniques have the disadvantage of requiring more computation.

The pre-processing bandlimited dithering algorithm developed in Chapter 6 improved the performance of the DAC but it was only capable of a 10 MHz sampling rate when implemented on an integrated circuit. This fell short of the 26 MHz sampling rate that was required. Given that the ripple adders restrict the speed, the use of a more advanced silicon technology and cell library (including lookahead adders) will enable a higher sampling rate. The speed of the adders can also be increased by reducing the size of the coefficients. Optimisation of the coefficient wordlengths can be achieved if a specific radio system is taken into account. For example, the 17 bit coefficients could be trimmed for the GSM TRX8 specification which requires only a 9 bit DAC interface, and 61.8 dB of stopband attenuation.

The thesis considered only three multichannel combining algorithms. Although the LUT table approach for digital modulation schemes cannot be optimised any further, the more general filtering approach to interpolation can be further improved. Further research should be focused on the algorithms suitability for VLSI fabrication and minimisation of the computational load. Careful choice of the filter coefficients [40] or the use of multiplier less filters [39] are two techniques that could be used to lower the computation requirements.

Another criticism of the thesis could be the selection of analog direct upconversion for translation of the baseband multichannel signal to RF. However, this technique was considered the best choice when the work for the thesis commenced four years ago. Due to the rapid progress in digital signal processing and DAC technology, either digital IF or subsampling upconversion techniques will soon be the best options. Further work into efficient interpolator structures and increasing the precision and speed of the DAC are still required.

Appendix A

Parameters Pertaining to Cavity Resonators

A.1 Cavity Resonator Insertion Loss

Insertion loss is used to describe the effect of inserting a four terminal network between a generator and load, as compared with a direct connection between the two.

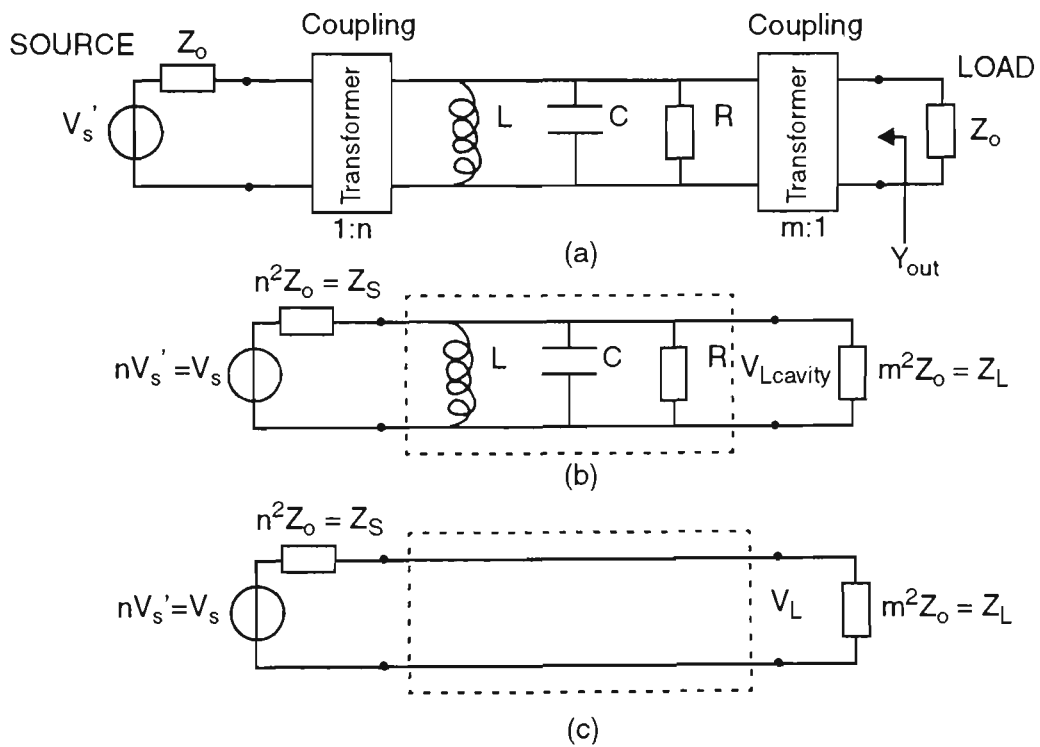


Figure A.1: (a) Model of a cavity resonator near resonance (b) Equivalent circuit model with the cavity resonator (c) Equivalent circuit model with direct connection between load and generator

For simplicity of analysis, assume that the characteristic impedance, Z_0 , is purely resistive. Thus we can write thus Z_L as R_L and Z_S as R_S . Now consider Fig. A.1(c) when there is a direct connection between the generator and the load. The voltage developed across the load is:

$$V_L = \frac{V_S R_L}{R_S + R_L} \quad (\text{A.1})$$

Where V_S is the source voltage, and V_L is the voltage developed across the load. Now when the cavity resonator is inserted, Fig A.1(b), the voltage across the load at resonance becomes:

$$V_{Lcavity} = \frac{V_S R_L R}{R_S R + R_L R + R_L R_S} \quad (\text{A.2})$$

Insertion loss due to the cavity network being inserted can be defined as:

$$IL_{cavity} = 20 \log \frac{V_L}{V_{Lcavity}} \quad dB \quad (\text{A.3})$$

Substituting (A.1) and (A.2) into (A.3) we get:

$$IL_{cavity} = -20 \log \left(\frac{R_S R + R_L R}{R_S R + R_L R + R_L R_S} \right) \quad dB \quad (\text{A.4})$$

Clearly if the resistive element, R , in the cavity model is made large (close to an O/C) then the insertion loss will approach zero, as expected. Insertion loss can also be rewritten in terms of the unloaded and loaded Q of the resonator. The unloaded Q , Q_0 , and loaded Q , Q_L , of the cavity resonator are given by:

$$Q_0 = R / \omega L \quad (\text{A.5})$$

$$Q_L = (R // R_L // R_S) / \omega L \quad (\text{A.6})$$

By substituting (A.5) and (A.6) into (A.4) the insertion loss takes the following form:

$$IL_{cavity} = -20 \log \left(1 - \frac{Q_L}{Q_0} \right) \quad dB \quad (\text{A.7})$$

A.2 Expression for the Output Admittance of a Cavity Resonator

The general expression for the output admittance of the resonator, from Fig. A.1(a), can be written as:

$$Y_{out} = m^2 \left(\left(\frac{1}{R} + \frac{1}{R_s} \right) + j \left(\omega C - \frac{1}{\omega L} \right) \right) \quad (\text{A.8})$$

At resonance the imaginary part of Eqn (A.8) is equal to zero, making $\omega_0^2 = 1/LC$, where ω_0 is the resonant frequency. Also let the output admittance at resonance equal R_{RES} , so that:

$$m^2 \left(\frac{1}{R} + \frac{1}{R_s} \right) = \frac{1}{R_{RES}} \quad (\text{A.9})$$

Now let $\omega = \omega_0(1+\delta)$, which for small δ the following approximation holds, $(1 + \delta)^{-1} \approx 1 - \delta$. The imaginary part of (A.8) can now be rewritten as:

$$m^2 \left(\omega C - \frac{1}{\omega L} \right) \approx m^2 \sqrt{\frac{C}{L}} \cdot 2\delta = m^2 \sqrt{\frac{C}{L}} \cdot 2 \frac{\Delta f}{f_o} \quad (\text{A.10})$$

Further, the bandwidth, BW_{cavity} , of the resonant response is defined when the imaginary and real parts of (1.22) are equal in magnitude and Δf is equal to $BW_{cavity}/2$. By equating (A.10) to $1/R_{RES}$ and through some rearrangement we arrive at the following relationship:

$$m^2 \sqrt{\frac{C}{L}} = \frac{f_o}{R_{RES} \cdot BW_{cavity}} \quad (\text{A.11})$$

Substituting Eqn. (A.11) into Eqn (A.8) gives the output admittance of the cavity resonator approximated in the region near resonance as:

$$Y_{out} = (1 + j2 \cdot \Delta f / BW_{cavity}) / R_{RES} \quad (\text{A.12})$$

A.3 Lossless Quarter Wave Transformer

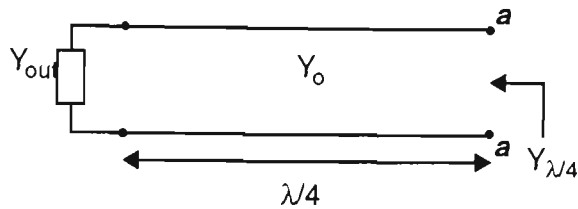


Figure A.2: Lossless Quarter Wave Transformer

The quarter wave transformer consists of a transmission line $\lambda/4$ long as shown in Fig. A.2. Given that the transmission line is lossless the admittance looking from terminals aa is related to the terminated admittance by the following equation:

$$Y_{\lambda/4} = Y_o^2 / Y_{out} \quad (\text{A.13})$$

A.4 Power Transfer at a Parallel Load.

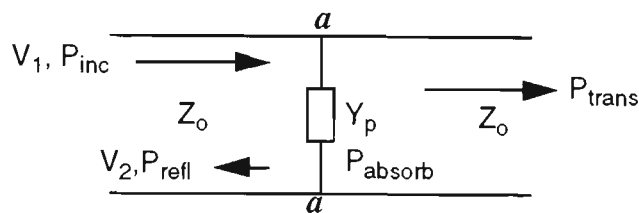


Figure A.3: Power transfer at a parallel connected load. Where P_{absorb} = Power absorbed by the parallel admittance Y_p .

Assuming that the transmission line is lossless the transmission line equations left of terminals aa are:

$$V = V_1 e^{-j\beta z} + V_2 e^{j\beta z} \quad (\text{A.14})$$

$$I = (V_1 e^{-j\beta z} - V_2 e^{j\beta z}) / Z_o \quad (\text{A.15})$$

Where $\beta = 2\pi/\lambda = 2\pi f/v_p$, z is the distance along the transmission line, Z_o is the characteristic impedance of the transmission line and V_1 , V_2 represent the forward and reverse travelling waves respectively.

The forward travelling wave transports an amount of power equivalent to:

$$P_{inc} = V_1 \cdot V_1^* / 2 \cdot Z_o \quad (\text{A.16})$$

Given that the admittance looking right at terminals aa is $(Y_p + Y_o)$, then the reflection coefficient at the terminals aa is given by:

$$\Gamma = -Y_p / (2Y_o + Y_p) \quad (\text{A.17})$$

The reflected power from terminals **aa** is therefore:

$$P_{\text{refl}} = P_{\text{inc}} \Gamma \Gamma^* \quad (\text{A.18})$$

The resultant power travelling forward right of the terminals **aa** is defined as:

$$P_{\text{trans}} = V_a \cdot V_a^* / 2 \cdot Z_o \quad (\text{A.19})$$

where

$$V_a = V_1 + V_2 = V_1(1 + \Gamma) \quad (\text{A.20})$$

Substituting (A.20) into (A.19) we get:

$$P_{\text{trans}} = P_{\text{inc}}(1 + \Gamma)(1 + \Gamma)^* \quad (\text{A.21})$$

The insertion loss due to the parallel load is then:

$$I_{\text{p-load}} = P_{\text{trans}} / P_{\text{inc}} = (1 + \Gamma)(1 + \Gamma)^* \quad (\text{A.22})$$

The power absorbed by the parallel load, Y_p , is found through the conservation of energy principle:

$$P_{\text{absorb}} = P_{\text{inc}} - P_{\text{refl}} - P_{\text{trans}} \quad (\text{A.23})$$

$$= P_{\text{inc}} \cdot -(\Gamma + \Gamma^* + 2\Gamma\Gamma^*) \quad (\text{A.24})$$

Appendix B

Interpolation

Interpolation involves increasing the sampling rate of the signal whilst preserving the signal's integrity. For large changes in the sampling rate, it is more efficient to use cascaded interpolation filters than to use a single interpolation filter. Optimisation of multi-stage interpolators has therefore been the focus of much research.

Optimal designs in terms of minimizing the number of multiplications per second and the amount of storage is presented by Crochiere and Rabiner [28]. One efficient means of implementing any stage in a multi-stage interpolator is through the use of the polyphase architecture. Appendix B.1 will overview this basic design. Crochiere and Rabiner also describe a halfband interpolator, which optimises the hardware requirements under certain restrictions. Appendix B.2 discusses these restrictions and describes the architecture of the halfband filter.

The computation power and hardware complexity of the polyphase and halfband interpolator designs are defined and these values will be used throughout the thesis.

B.1 Polyphase Realization of an Interpolator

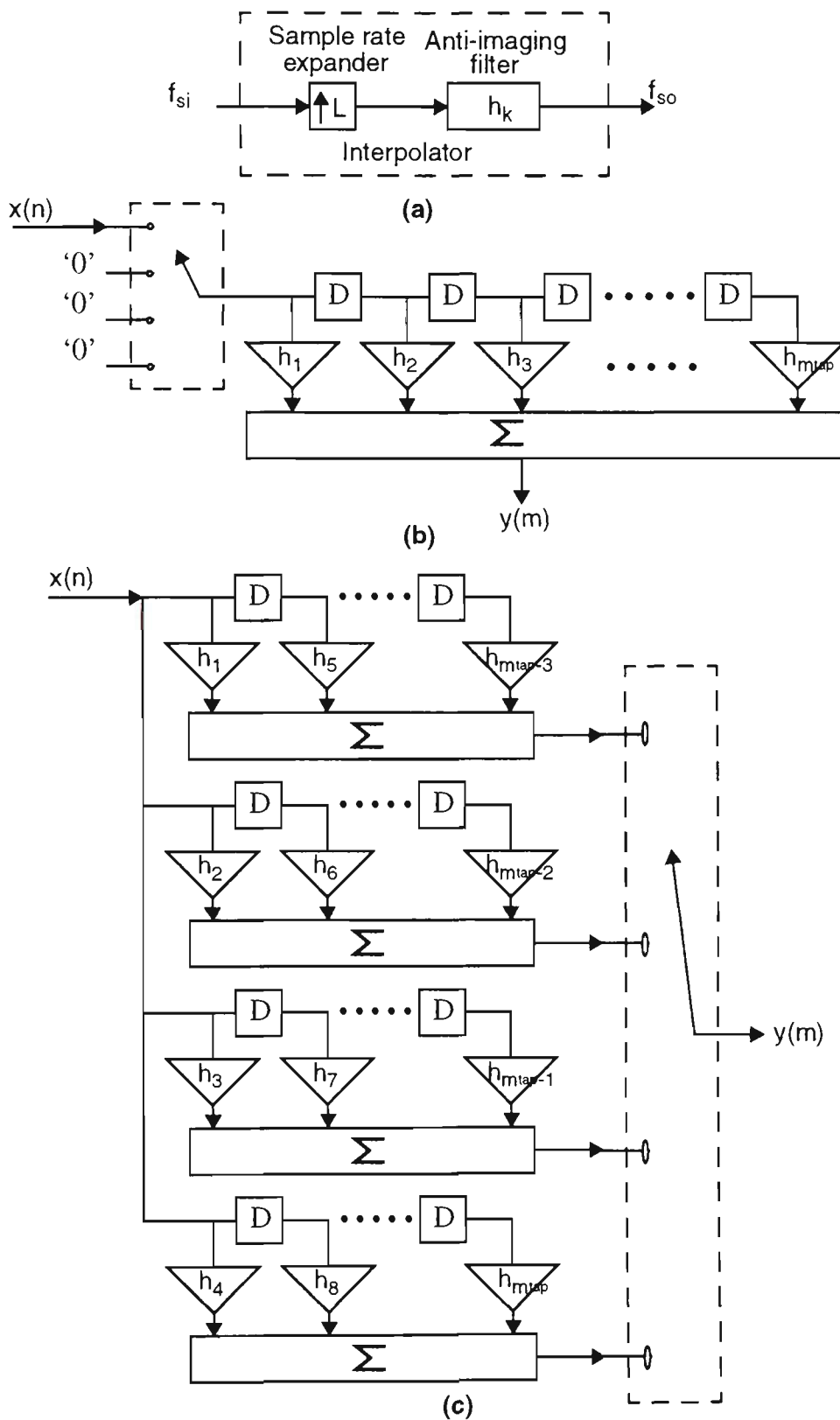


Figure B.1: (a) Block diagram of interpolation (b) Brute force implementation of interpolation, $L=4$ (c) Polyphase approach to interpolation, $L=4$.

Interpolation by a factor of L , Fig. B.1(a), is performed by adding $(L-1)$ zero valued samples for every original sample. This increases the sample rate to $L \times f_{si}$ but has no effect on the original spectrum. Low pass filtering after interpolation is required to remove the unwanted digital alias components caused by zero padding.

Implementation of the interpolator, shown in Fig. B.1(b), is considered brute force as the many zero valued samples do not contribute to the output. A polyphase implementation, Fig. B.1(c), makes use of the zero valued redundancies and is therefore a more efficient architecture. It behaves identically to the brute force technique.

The number of operations required to implement the polyphase architecture is equal to the number of taps, m_{tap} . This assumes that each tap consists of a single Multiply and Accumulate (MAC) instruction that takes one clock cycle.

B.2 A Halfband Interpolator

A halfband interpolator is a special case of the general polyphase interpolator, that is more efficient in computation power and hardware complexity.

As the name suggests the interpolation factor is equal to two. The specification of the filter is restricted to the passband and stopband frequencies of the filter being symmetrical about a quarter of the output sampling frequency, and the stopband and passband ripple being equal, Fig. B.2(a). This results in an odd ordered (m_{tap}) filter and a symmetrical impulse response about the centre tap, $c_{tap} = (m_{tap}+1)/2$, with every even tap being equal to zero. The coefficients are summarised below :

$$h_n = 0 \quad n = 2, 4, \dots, (m_{tap} - 1) \quad (B.1)$$

$$h_n = 0.5 \quad n = \frac{(m_{tap} + 1)}{2} \quad (B.2)$$

$$h_n = h_{m_{tap} + 1 - n} \quad n = 1, 3, \dots, \frac{(m_{tap} - 3)}{2} \quad (B.3)$$

The halfband filter can therefore be implemented a lot more efficiently than the general interpolator design, Fig. B.2(b). The co-efficients are usually scaled such that the centre tap, $h_{(m_{tap}+1)/2}$, is equal to 1. Therefore the number of multipliers and adders are equal to $(m_{tap}+1)/4$ and $(m_{tap}-1)/2$ respectively. Implementation in a general purpose digital signal processor will require $(m_{tap}+1)/4$ MAC and add operations.

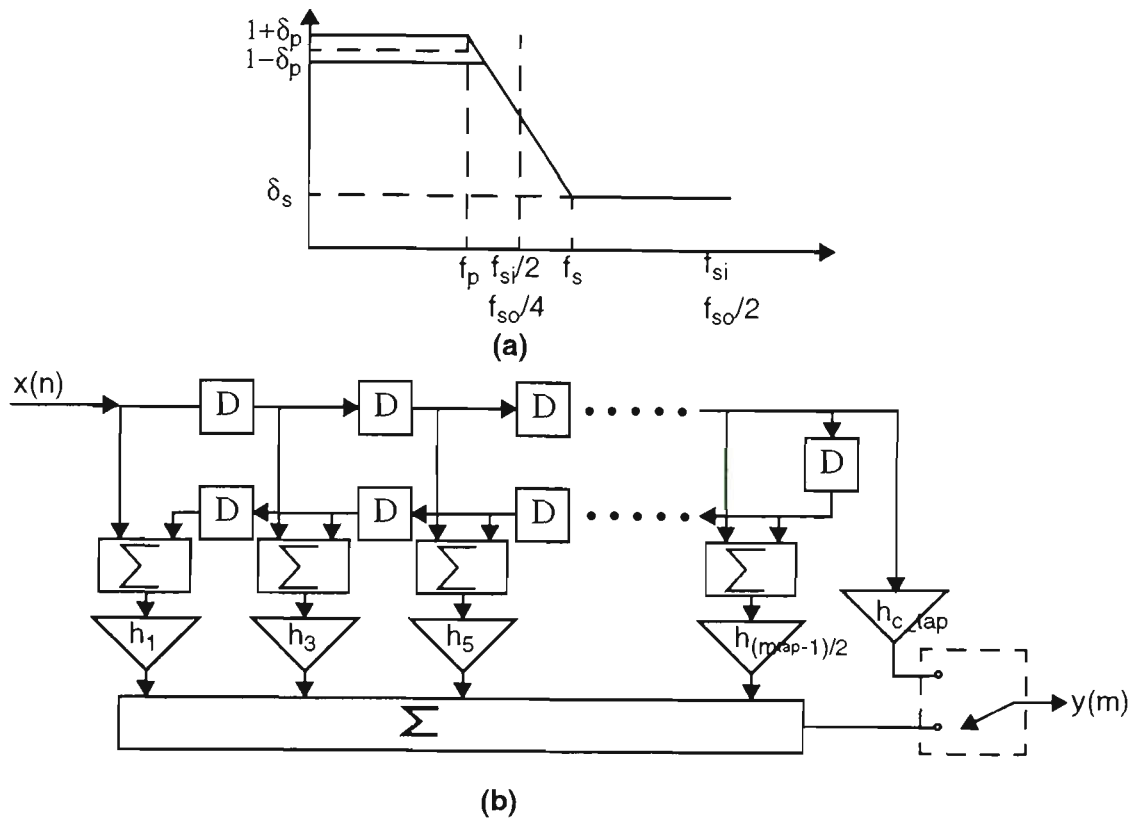


Figure B.2: (a) Halfband filter specification. (b) Efficient implementation of a halfband interpolator

Table B.1 compares the polyphase and halfband interpolator architectures in terms of computation power and hardware complexity. In both cases the half-band filter has significant savings in the amount of computation power and hardware required for implementation. Especially significant in terms of ASIC implementation is the number of multipliers required in each of the designs. The halfband design has approximately 25 % of the multipliers required for an equivalent polyphase design. Multiplier's are area intensive in an ASIC design, so this can be considered to be a real reduction in hardware complexity.

Table B.1: Comparison of the computation power and hardware complexity

Type of Interpolator	Computation Power (Number of Operations)	Hardware Complexity		
		Delays	Adders	Mult's
Polyphase	$m_{tap} @ f_{si}$	$m_{tap}/L - 1$	$m_{tap} - L$	m_{tap}
Halfband	$(m_{tap}+1)/2 @ f_{si}$	$(m_{tap}-1)/2$	$(m_{tap}-1)/2$	$(m_{tap}+1)/4$

Appendix C

DAC Survey

The following table has been compiled to survey the current state of the art in DAC technology.

DAC's are listed in order of their published precision (number of bits) and have been included in the table on the basis of their stated maximum sampling frequency. The actual sampling frequency at which they have been tested is also shown under <Max. f_s >. Commercially available DAC's seem to have a large discrepancy between the stated maximum and tested maximum sampling frequency.

The Effective Number Of Bits (ENOB) refers to the effective precision of an operating DAC. It is approximately related to the measured SFDR by the following formula.

$$\text{SFDR (dB)} = 6 \times \text{ENOB} \quad (\text{C.1})$$

Due to dynamic errors, the SFDR will reduce as the signal frequency increases. Thus when a DAC is tested the SFDR is stated at a specified signal frequency, written as a fraction of the sampling rate. Worse performance is guaranteed beyond the maximum signal frequencies specified.

The glitch energy, rise and settling time parameters are indicators of the dynamic performance of DAC. Low values are required for good high speed performance.

Table C.1 : Current state of the art in DAC technology

Precision	Reference	Stated Max. f_s	Measured Parameters					
			Max. f_s	SFDR (ENOB)	Glitch energy	Rise time ^a	Settling time ^b	
8	Published	[63]	800MHz	800MHz	-	3pV-s	380ps	-
	Comm. Avail	Tri Quint TQ6114	1.5GHz	1GHz	45dBc(7.5)@ $f_s/17$	10pV-s	300ps	2ns
10	Published	[61]	1GHz	1GHz	58dBc(9.6)@ $f_s/100$	<1pV-s	500ps	-
	Comm. Avail	Harris HI5721	125 MHz	125MHz	53dBc(8.8)@ $f_s/5$	1.5pV-s	-	-
12	Published	[64]	1GHz	1GHz	62.4(10.4)@ $f_s/10$	4pV-s	180ps	0.7ns
	Comm. Avail	Burr Brown DAC650	500MHz	100MHz	58dBc(9.6)@ $f_s/4$	20pV-s	500ps	< 5ns
14	Published	[60]	>1GHz	750MHz	50dBc(8.3)@ $f_s/2$ 60dBc(10)@ $f_s/4$	<10pV- s	300ps	1ns
	Comm. Avail	Tri Quint SC-0806-C	1GHz	1GHz	-43dBc(7.2)@ $f_s/4$	-	350ps	-
16	Published	[62]	40MHz	10MHz	82dBc(13.4)@ $f_s/8$	2.5pV-s	2000ps	25ns
	Comm. Avail	Analog Devices AD768	30MHz	10MHz	83dBc(13.5)@ $f_s/10$	35pV-s	-	25ns

a. From 10->90%

b. To settle within +/-0.5 LSB of final value.

Appendix D

The Carrier to Noise Ratio of a Quadrature Upconverter

The purpose of this appendix is to relate the carrier to noise ratio at the output of the quadrature upconverter to the carrier to noise ratio at the output of each DAC.

For simplicity of calculations it has been assumed that a single channel is activated at RF. The In Phase and Quadrature baseband signals, required to generate this RF signal, are equivalent to a rotating phasor, given by:

$$x_i(t) = a_k \cos(\omega t + \theta(t)) = \frac{a_k}{2} \cdot (e^{j(\omega t + \theta(t))} + e^{-j(\omega t + \theta(t))}) \quad (D.1)$$

$$x_q(t) = a_k \sin(\omega t + \theta(t)) = \frac{a_k}{2j} \cdot (e^{j(\omega t + \theta(t))} - e^{-j(\omega t + \theta(t))}) \quad (D.2)$$

For clarity, Eqns. (D.1) & (D.2) have been graphically represented as double sided spectra in Fig. D.1. Each line has a power of magnitude $(a_k^2 / 4)$. The In Phase and Quadrature signals are then mixed with the quadrature phased carrier signals:

$$\cos \omega_c t = \frac{1}{2} \cdot (e^{j\omega_c t} + e^{-j\omega_c t}) \quad (D.3)$$

$$-\sin \omega_c t = -\frac{1}{2j} \cdot (e^{j\omega_c t} - e^{-j\omega_c t}) \quad (D.4)$$

The resulting double sided line spectra can be mathematically described as:

$$x_{mi}(t) = \frac{a_k}{4} \cdot (e^{j((\omega_c + \omega)t + \theta(t))} + e^{-j((\omega_c + \omega)t + \theta(t))} + e^{j((\omega_c - \omega)t - \theta(t))} + e^{-j((\omega_c - \omega)t - \theta(t))}) \quad (D.5)$$

$$x_{mq}(t) = \frac{a_k}{4} \cdot (e^{j((\omega_c + \omega)t + \theta(t))} - e^{-j((\omega_c + \omega)t + \theta(t))} + e^{j((\omega_c - \omega)t - \theta(t))} - e^{-j((\omega_c - \omega)t - \theta(t))}) \quad (D.6)$$

The final stage combines these mixed signals to form the single channel at RF:

$$s(t) = \frac{a_k}{2} \cdot (e^{j((\omega_c + \omega)t + \theta(t))} + e^{-j((\omega_c + \omega)t + \theta(t))}) \quad (D.7)$$

In this example, the carrier power measured at either the DAC or the output of the quadrature upconverter are the same:

$$P_{\text{carrier}} = a_k^2 / 2 \quad (D.8)$$

The DAC quantisation noise is shown with a double sided power spectral density (PSD), of magnitude $N_o/2$. This decreases to $N_o/8$ after mixing with the quadrature phased carrier signals. The In Phase and Quadrature noise power will then add at the combination stage, resulting in a PSD of $N_o/4$.

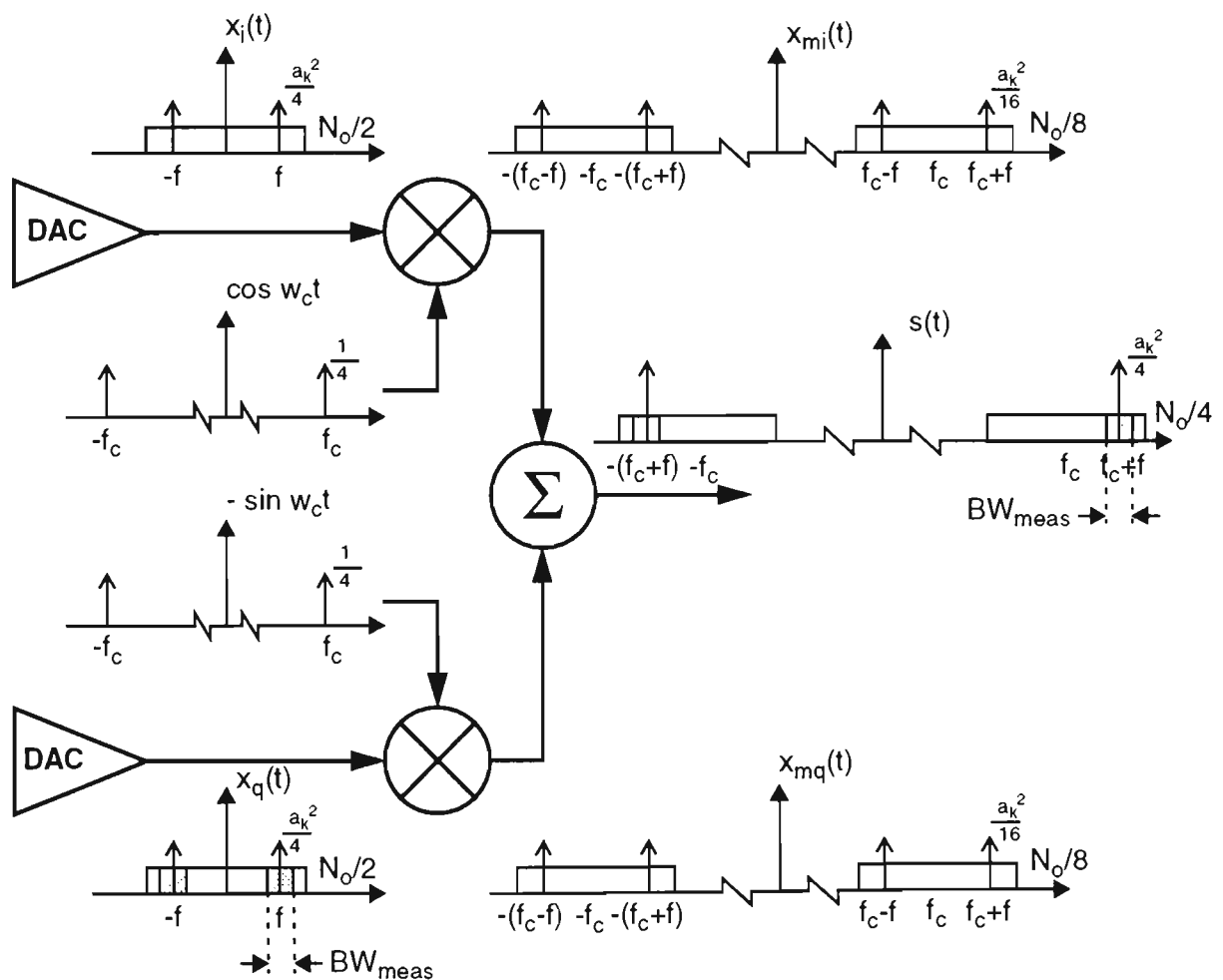


Figure D.1: A quadrature upconverter, showing the line spectra (and corresponding power or power spectral density) at each stage in the process.

The noise power specified in a radio system is measured with a bandpass filter of bandwidth of BW_{meas} . Therefore, the noise power measured at the output of the quadrature upconverter is:

$$P_{\text{N-QU}} = 2 \times BW_{\text{meas}} \times N_o / 4 = BW_{\text{meas}} \times N_o / 2 \quad (\text{D.9})$$

and at the output of the DAC:

$$P_{\text{N-DAC}} = 2 \times BW_{\text{meas}} \times N_o / 2 = BW_{\text{meas}} \times N_o \quad (\text{D.10})$$

The carrier to noise ratio (CNR) at the output of the quadrature converter is therefore twice that of the carrier to noise ratio at the output of each DAC. Although this example only considers a single channel, the same will be true for a multi channel signal. Therefore, the following relationship will hold:

$$\text{CNR}_{\text{multi}}|_{\text{RF}} = 2 \times \text{CNR}_{\text{multi}}|_{\text{DAC output}} \quad (\text{D.11})$$

Appendix E

The Schuchman ‘Sufficiency Condition’

Schuchman [55] first developed a condition for the PDF of the dither signal to cause the quantisation error to become a uniformly distributed white noise which is signal independent. Reference [49] also showed that the Schuchman ‘sufficiency condition’ implied that the sequence of quantisation errors was also independent. The Schuchman condition only applies to ideal quantisers.

The Schuchman condition states that when the characteristic function of the dither signal x_k is equal to zero:

$$M_{q_e}\left(\frac{j2\pi l}{\Delta}\right) = 0 \quad \text{when } l = \text{all integers except } 0 \quad (\text{E.1})$$

then it is sufficient for the following properties to hold:

- The quantisation error, $q_e(X+x_k)$, is independent of the input signal, X .
- The quantisation error, $q_e(X+x_k)$, is a uniformly distributed, $[-\Delta/2 \Delta/2]$, random variable.

The characteristic function is defined as the Fourier transform of the PDF:

$$\begin{aligned} M_W(ju) &= E(e^{juW}) \\ &= \int_{-\infty}^{\infty} p(W)e^{juW} dW \end{aligned} \quad (\text{E.2})$$

where $p(W)$ refers to the PDF of the dither signal. The Schuchman ‘sufficiency condition’

assumes a stationary input process and an ideal quantiser is ideal which does not overload (clip).

Application of Equation (E.1) reveals some interesting properties of the three dither probability density functions, uniform, Gaussian and triangular.

A Uniform PDF

Substitution of dither with a uniform PDF into (E.2) gives:

$$M_U(ju) = \int_{-c/2}^{c/2} \frac{1}{c} e^{juU} dU = \frac{\sin(cu/2)}{cu/2} \quad (\text{E.3})$$

Applying the sufficiency condition, Eqn. (E.1), gives

$$M_U\left(j\frac{2\pi l}{\Delta}\right) = \frac{\sin(\pi lc/\Delta)}{\pi lc/\Delta} = 0 \quad \text{when}(lc/\Delta) \text{ is all integers except } 0 \quad (\text{E.4})$$

as l is defined as an integer [55] then it follows that

$$c = n\Delta \quad \text{where } n \text{ must be any integer except } 0. \quad (\text{E.5})$$

Thus uniform dither with peak to peak amplitude excursions being multiples of the LSB are part of the class of PDF's which satisfy Schuchman 'sufficiency condition'.

A Gaussian PDF

A Gaussian PDF is produced by the sum of N independent identically distributed uniformly random variables:

$$G_N = \sum_{i=1}^N U_i \quad (\text{E.6})$$

where G_N and U_i denote Gaussian and uniform PDF's respectively. The characteristic function is therefore given by:

$$M_G(ju) = \prod_{i=1}^N M_{U_i}(ju) \quad (\text{E.7})$$

where $M_G(ju)$ and $M_{U_i}(ju)$ denote Gaussian and uniform characteristic functions respectively.

For the Gaussian PDF to meet the sufficiency condition all that is required is for one of the

uniformly distributed functions to satisfy the condition specified in Eqn. (E.5). Further, it has been shown [49] that if the standard deviation of the Gaussian PDF, σ , is greater than a LSB, Δ , then $M_G(ju)$ (also referred to as the first order statistics) would be approximately zero. Additionally, second order statistics show that the correlation between the input signal and the quantisation error becomes negligible as σ/Δ , becomes large.

Thus Gaussian dither with a standard deviation greater than 1 LSB can be considered to approximately satisfy the Schuchman 'sufficiency condition'. The approximation gets better as the standard deviation is increased.

A Triangular PDF

Triangular dither is the sum of two uniformly distributed random variables with N set to 2 in Eqns. (E.6) & (E.7). For triangular dither to meet the 'sufficiency condition', the two uniform distributions that make up the triangular distribution must satisfy the condition specified in Eqn. (E.5). The triangular distribution is therefore bounded by:

$$t = n\Delta \text{ where } n \text{ is all integers except } 0 \quad (\text{E.8})$$

the above examples have shown that uniform, Gaussian and triangular distributions are part of a class of PDF's that satisfy the Schuchman 'sufficiency condition'. Given certain restrictions, these PDF's force the quantisation error to be modelled as white noise. However, the Schuchman condition only applies to ideal quantisation functions, where the quantisation levels are equally spaced.

Appendix F

Measurement Testbed

The hardware testbed used during for the measurements in Chapter 6 is based on a single Texas Instrument C40 processor, Fig. F.1. Central to the testbed is an interpolate by two algorithm which can add dither to the main signal with or without bandlimiting.

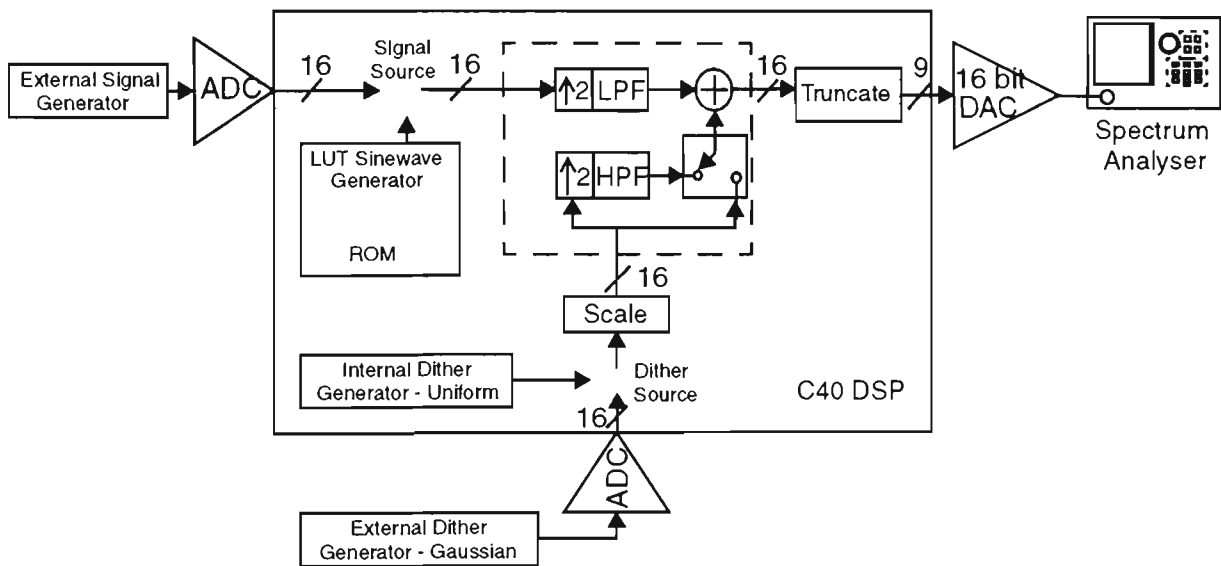


Figure F.1: *Hardware testbed used for dithering measurements in Chapter 6.*

The main signal is either a LUT generated sinewave or an externally generated multichannel signal. The external signal generator (SFDR of 76 dBc) and the 16 bit ADC, will not compromise the accuracy of the measurements because the signals are internally scaled to 9 bits. Only the 9 least significant bits of the 16 bit DAC are used at one time.

The bandlimited dither source can be selected from an internal generator, which is wideband and uniformly distributed, or from an externally generated dither signal, which is also wideband but Gaussian distributed. A Hewlett and Packard 3589A spectrum analyser was used to perform the noise and spurious level measurements. During the measurements the thermal noise floor of the spectrum analyser was at least 10 dB below the quantisation noise floor of the DAC.

Bibliography

Chapter 2

- [1] Reljonen, P., "GSM Base Station Development", Telecommunications, Vol 24, Edition 9, Sept. 1990, pp 85-92.
- [2] Macario, R.C.V, "Personal and Mobile Radio Systems", Peter Peregrinus Ltd, London, UK, 1992, Chapter 12.
- [3] Holbeche, R.J, "Land Mobile Radio Systems", Peter Peregrinus Ltd, UK, 1985, Chapter 4.
- [4] Arnold, P.W & Seymour, K.J, "A New Frequency Agile Transmitter Combining System for North American Cellular", IEEE Vehicular Technology Society, 42nd VTS Conference, 10-13 May, 1992, pp 1024-1033.
- [5] Johnson, A.K & Myer, R, "Linear Amplifier Combiner", IEEE Vehicular Technology Conference, Tampa, Florida, 1987, pp 421-423.
- [6a] Stefanov, J.J, "A Compact Base Station for Small Cells", Proceeding of the 3rd Nordic Seminar on Digital Land Mobile Radio Communications, Copenhagen, 1988, section 14-11.
- [6b] Stefanov, J.J, "Designing Compact Base Stations for Urban Microcells", Digest of IEE Colloquium on "Microcellular Mobile Radio", London, 1989, pp 5/1-9.
- [7] "Winning Team makes Waves", SERC Bulletin, UK, Vol. 5, No 1, Summer 1993, pp 12.
- [8] Manton, R.G, "Hybrid Networks and their uses in Radio Frequency Circuits", The Radio and Electronic Engineer, Vol. 54, Nov/Dec 1984, pp 473-489.
- [9] European Telecommunications, pri-ETS 300 033-2, "Radio Transmission and Reception", Part 2, GSM Rec. 05.05, version 3.15.0.
- [10] MPT 1317, Code of Practice, "Transmission of Digital Information over Land Mobile Radio Systems", Radiocommunications Agency, London, 1984, pp 8-9.
- [11] MPT 1323, Performance Specification, "Angle Modulated Radio Equipment for use at Fixed and Mobile Stations in the Private Mobile Radio Service Operating in the Frequency Band 174-225 MHz", Radiocommunications Agency, London, reprint May 1993.
- [12] "Superconducting Filter Screens Cellular Signals", Microwaves & RF, Dec 1994, pp 226.
- [13] Hagstrom, U & Djuphamar, H, "RBS 884 - A New Generation Radio Stations for the American Standard", Ericsson Review, Sweden, No.1, 1994.

- [14] Kazeminejad, S., Howson, D.P. and Hamer, G., "Base Station multicoupler design for UK Cellular Radio Systems", *Electronic Letters*, Vol 23, No. 15. July 1987, pp 812.
- [15] Zverev, A.I., "Handbook of Filter Synthesis", John Wiley and Sons, Inc. 1967.
- [16] Kazeminejad, S., Howson, D.P., Baghai, A. and Hamer, G., "Cellular Radio Transmitter Combiners for Narrow Co-Channel Spacing", Fifth International Conference on Mobile Radio and Personal Communications, Coventry, UK, 11-14 December, 1989, pp 57-59.
- [17] Kazeminejad, M., Khanifar A. & Howson, S., "Electronically Reconfigurable Cellular Radio Multicouplers", Fifth International Conference on Mobile Radio and Personal Communications, Coventry, UK, 11-14 December, 1989, pp 103-106.
- [18] Gans, M.J., "Some Properties of Multiple Carriers and Intermodulation", *IEEE*, pp 883-886.
- [19] Radio Frequency Systems Product Catalogue (Australia).
- [20] Stewart, R.D. & Tusubira, F.F., "Low Level Combining for Microcell Basestations", Digest of IEE Colloquium on "Microcellular Mobile Radio", London, 1989, pp 4/1-7.

Chapter 3

- [21] Roome, S.J., "Analysis of Quadrature Detectors using Complex Envelope Notation", *IEE proceedings*, Vol 136, Part F, No. 2, April 1989, pp 95-100.
- [22] Bridges, P., "Digital Demodulation Techniques for Radio channels", Masters Thesis, Victoria University of Technology, Australia, March 1993.
- [23] Kaiser, J.F., "Nonrecursive Digital Filter Design using the I_0 -sinh Window Function", *Proc. 1974 IEEE inter. Symp. on Circuits and Systems*, April 1974.
- [24] Bjerede, B., Lipowski, J., Petranovich, J. & Gilbert, S., 'An Intermediate Frequency Modulator using Direct Digital Synthesis Techniques for Japanese Personal Handy Phone (PHP) and Digital European Cordless Telecommunications (DECT)', *IEEE Vehicular Technology Conference*, Vol 1., Stockholm, Sweden, June 1994, pp 467-471.
- [25] J.K.Caver, M.Liao, "Adaptive Compensation for Imbalance and Offset Losses in Direct Conversion Transceivers", *IEEE Vehicular Technology Conference*, St Louis, 1991, pp 578-583.
- [26] M.Faulkner, T. Mattson, W.Yates, "Automatic Adjustment of Quadrature Modulators", *Electronic Letters*, Vol. 27, (3), Jan. 1991, pp 214-216.
- [27] Scheuermann, H. & Gockler, H., "A Comprehensive Survey of Digital Transmultiplexing Methods", *Proceedings of the IEEE*, Vol. 69, No. 11, 1981, pp 1419-1450.

- [28] R.E.Crochiere & L.R.Rabiner, "Multirate Digital Signal Processing". Prentice Hall, 1983.
- [29] A. Bateman & W. Yates, "Digital Signal Processing", Pitman Publishing, 1988.
- [30] Buchanan, D., "Choose DACs for DDS System Applications", *Microwaves and RF*, August 1992, pp 89-98.
- [31] Blanchman, N.M, "Third-Order Intermodulation due to Quantisation". *IEEE Trans. on Communications*, Vol. COM-29, No. 9, Sept. 1991, pp 1386-1389.
- [32] Abuelma'atti, M.T, "The Intermodulation due to Multicarrier Quantisation", *IEEE Transactions on Communications*, Vol. COM-32, No. 11, Nov. 1984, pp 1211-1214.
- [33] Abuelma'atti, M.T, "Spectrum of a Nonlinearly Quantised Sinusoid", *IEEE Proceedings*, Vol. 136, Pt. G, No. 6, Dec. 1989, pp 313-316.
- [34] Abuelma'atti, M.T, "The Effect of Bit-Threshold Errors on the Harmonic and Intermodulation Performance of Successive Approximation A/D Converters", *IEEE Transactions on Communications*, Vol. COM-41, No. 8, Aug. 1993, pp 1155-1160.
- [35] Mitola, J, "The Software Radio Architecture", *IEEE Communications Magazine*, Vol. 33, No. 5, May 1995, pp 26-38.
- [36] Feher, K, "Filtering Inventions Enhance Digitally Modulated RF products", *Microwaves & RF*, April 1995, pp 140-148.
- [37] Papamichalis, P.E., "Digital Signal Processing with the TMS320 Family - Volume 3", Prentice Hall, Englewoods Cliffs, New Jersey, 1990.
- [38] Peled, A. & Bede, L., "A New Hardware Realization of Digital Filters", *IEEE Transactions on ASSP*, Vol. 22, No. 6, Dec. 1974, pp 456-462.
- [39] Hogenauer, E.B, "An Economical Class of Digital Filters for Decimation and Interpolation", *IEEE Transactions on ASSP*, Vol. 29, No. 2, April 1981, pp 155-162.
- [40] Goodman, D.J. & Carey, M.J., "Nine Digital Filters for Decimation and Interpolation", *IEEE transactions on ASSP*, Vol. 25, No. 2, April 1977, pp 121-126.
- [41] Coon, A., "Capabilities and Applications of SAW Coupled-Resonator Filters", Application Note AN-23, RF Monolithics, 4441 Sigma Road, Dallas, Texas, 1990.
- [42] Hill, A. & Surber, J., "Using Aliased-Imaging Techniques in DDS to Generate RF Signals", *RF Design*, Sept. 1993, pp 31-36.
- [43] Sinsky, A.I & Wang, P.C.P, "Error Analysis of a Quadrature Coherent Detector Processor", *IEEE Transactions on Aerospace & Electronic Systems*, Vol AES-10, Nov. 1974, pp 880-883.

Chapter 4

- [44] Churchill, F.E., Ogar, G.W. & Thompson, B.J., "The Correction of I&Q errors in a Coherent Processor", IEEE Transactions on Aerospace & Electronic Systems, Vol AES-17, No 1, Jan 1988, pp131-136.
- [45] Jones, A.E. & Gardiner, J.G, "Phase Error Correcting Vector Modulator for Personal Communications Network (PCN) Transceivers", Electronic letters, Vol 27, (14), July 1991, pp 1231-1232.
- [46] Hilborn, D., Stapleton, S.P. & Cavers, J.K., "An Adaptive Direct Conversion Transmitter", IEEE Transactions on Vehicular Technology, Vol. 43, No. 2, May 1994, pp 223-233.
- [47] Sundstrom, L. & Faulkner, M., "The Effect of Reconstruction Filtering on the Predistortion Linearisation of RF Power Amplifiers", Mobile & Personal Communication Systems, Adelaide, Australia, 12-13 Nov., 1992, pp 357-361.

Chapter 5

- [48] Blesser, B.A & Locanthi, B.N., "The Application of Narrow-Band Dither Operating at the Nyquist Frequency in Digital Systems to Provide Improved Signal-to-Noise Ratio over Conventional Dithering", Journal of Audio Engineering Society, Vol. 35, No 6, June 1987, pp 446-454.
- [49] Sripad, A.B. and Snyder, D.L., "A Necessary and Sufficient Condition for Quantisation Errors to be Uniform and White", IEEE Transactions on Acoustics, Speech and Signal Processing, Vol. ASSP-25, Oct. 1977, pp 442-448.
- [50] Vanderkooy, J. & Lipshitz, S.P., "Dither in Digital Audio", Journal Audio Engineering Society, Vol. 35, No 12, 1987 December, pp 966-975.
- [51] Vanderkooy, J. & Lipshitz, S.P., "Digital Dither", presented at the 81st Convention of the Audio Engineering Society, Journal of Engineering Society (abstracts), Vol. 34., December 1986, preprint 2412, pp 1030.
- [52] Walpole, R.E. & Myers, R.H., "Probability and Statistics for Engineers and Scientists", Macmillan Publishing, 1985, Chapter 3.
- [53] Jayant, N.S & Rabiner, L.R, "The Application of Dither to the Quantisation of Speech Signals", The Bell System Technical Journal, Vol 51, No 6, July-Aug. 1972, pp 1293-1304.
- [54] Bartz, M., "Large Scale Dithering Enhances ADC Dynamic Range", Microwaves and RF, May 1993, pp 192-198.
- [55] Schuhman, L., "Dither signals and their Effect on Quantisation Noise", IRE Transactions in Communication Technology, Vol. COM-12, Dec. 1965, pp. 162-165.
- [56] Bennet, W.R., "Spectra of Quantized Signal", Bell System Technical Journal, Vol. 27, July 1948, pp 446-472.

- [57] Papoulis, A., "Probability, Random Variables and Stochastic Processes". McGraw-Hill Book Company, 1965.

Chapter 6

- [58] O'Rielly, J.J., "Series-Parallel Generation of m-sequences", Radio Electronic Engineering, Vol. 45, No 4, April 1975, pp 171-176.
- [59] Horowitz, P. & Hill, W., The Art of Electronics, Cambridge UK, Cambridge University Press, 1980.

Appendix C

- [60] F.G.Weiss & T.G.Brown, "A 14 bit, 1 Gs/s DAC for Direct Digital Synthesis Applications", GAAs IC Symposium, pp 361-364.
- [61] P. Vorenkamp, J. Verdaasdonk, R. Plassche & D. Scheffer, "A 1Gs/s, 10b Digital to analogue Converter", 1994 IEEE International Solid State Circuits Conference, pp 52-53.
- [62] D. Mercer, "A 16-b D/A Converter with Increased Spurious Free Dynamic Range", IEEE Journal of Solid State Circuits, Vol. 29, No. 10., Oct. 1994, pp 1180-1185.
- [63] K. Nojima & Y. Gendai, "An 8-b 800 MHz DAC", IEEE Journal of Solid State Circuits, Vol. 25, No. 6., Dec. 1990, pp 1353-1359.
- [64] K-C. Hsieh, T.A. Knotts, G.L.Baldwin & T. Hornak, "A 12-bit 1-Gword/s GaAs Digital-to-Analog Converter System", IEEE Journal of Solid State Circuits, Vol. 22, No. 16., Dec. 1987, pp 1048 -1055.

Authors Published Papers

- [65] Leyonhjelm, S.A., Faulkner, M. & Macleod, J., "The Effect of Reconstruction Filter Mismatch in a Digital Signal Processing Multichannel Combiner", IEEE International Conference on Universal Wireless Access, World Congress Centre, Melbourne, Australia, April 18-19, 1994, pp 25-30.
- [66] Leyonhjelm, S.A. & Faulkner, M., "DSP Combining and Direct Conversion for Multichannel Transmitters", 43rd IEEE/VTS Vehicular Technology Conference, Stockholm, Sweden, , Vol. 1 of 3, June 7-10, 1994, pp 494-498.
- [67] Leyonhjelm, S.A. & Faulkner, M., "The Effect of Reconstruction Filters on Direct Upconversion in a Multichannel Environment", IEEE Transactions on Vehicular Technology, Vol. 44, No. 1, Feb. 1995, pp 95-102.
- [68] Leyonhjelm, S.A., Faulkner, M. & Nilsson, P., "An Efficient Implementation of Bandlimited Dithering", Wireless Personal Communications, Accepted for publication on the 27th November, 1996.

The Effect of Reconstruction Filter Mismatch in a Digital Signal Processing Multichannel Combiner

Scott A. Leyonhjelm, Student Member, IEEE, Michael Faulkner, Member, IEEE, and John Macleod, Member, IEEE.

Mobile Communications and Signal Processing Group,

Department of Electrical & Electronic Engineering,

Victoria University of Technology,

PO Box 14428 MMC, Melbourne, VIC 3000, AUSTRALIA.

Email: scott@cabsav.vut.edu.au or mf@cabsav.vut.edu.au

Abstract - Traditionally multicarrier systems are combined in cumbersome and inflexible cavity filters. Future wireless systems will employ versatile and flexible combining techniques. This paper presents a DSP multichannel combiner incorporating a popular upconversion technique, direct conversion. The effect of mismatch in the reconstruction filters driving the direct conversion stage is analysed in a multichannel environment. It is shown that the reconstruction filters cause gain and phase imbalances to be frequency dependant, a significant issue when considering the stringent ACI requirements for radio communication systems. The paper also introduces an adaptive compensation technique as a means of overcoming these frequency dependant imbalances. Analysis reveals the sensitivity of direct upconversion in a multichannel environment to percentage mismatch and differing ACI level.

I. INTRODUCTION

Recent advances in the wideband linearisation of amplifiers suggest that Frequency Division Multiplex (FDM) systems can now be combined at low power levels [1-2]. The low power combination of channels can occur in a DSP environment, before being upconverted and amplified by a linear wideband amplifier, as illustrated below.

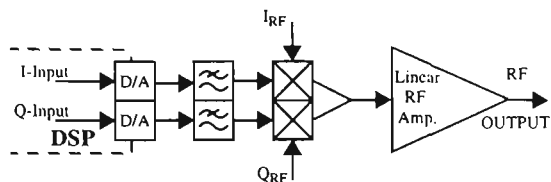


Fig. 1. Analog Quadrature Modulation Upconversion

This paper considers direct upconversion, using an analog quadrature modulator. This technique of upconversion has recently gained a lot of attention due to its suitability as a universal modulator (and demodulator); it is simple, small and has low power consumption. However a mismatch in the In phase and Quadrature (IQ) channels results in an undesired sideband, the magnitude of which is dependant upon the size of the gain and phase errors (imbalances) between the channels [3]. The imbalances are attributed to the non-ideal characteristics of the components, the mixers, summer, splitter and reconstruction filters. It is reasonable to talk of component imbalances (neglecting the reconstruction filters) of 0.3 dB and 3° in a well designed analog quadrature modulator.

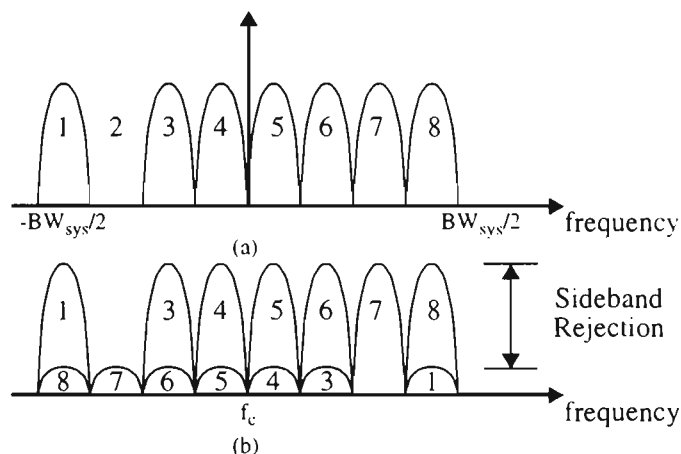


Fig. 2. The effect of phase and gain imbalances in an analog quadrature modulator (a) Original signal displayed in complex baseband format. (b) Desired and sideband (image) signals after passing through an unbalanced quadrature modulator.

Imbalances of this magnitude would result in 30 dB of sideband rejection, sufficient for some single channel applications.

The wideband upconversion application highlights a unique problem. A wideband FDM signal, Fig 2a, when passed through an unbalanced quadrature modulator, will result in both desired and sideband signals, Fig 2b. However different amounts of sideband rejection can be tolerated in a multichannel system. If the sideband signal falls into a channel that is being used then it will distort the desired signal (channel 1 in Fig. 2b), and the required sideband rejection is related to the E_b/N_0 performance of the modulation. The sideband signal could equally fall into a vacant channel position (channel 7 in Fig. 2b). In this situation the system must meet the ACI specifications of the system which are normally specified between -50 dBc and -80 dBc, for Mobile Satellite and Private Mobile Radio (PMR) systems respectively.

The analog quadrature modulator is therefore not usable in a multichannel environment without some form of refinement. A number of correction techniques have subsequently evolved [5-8], all have concentrated on a single channel application. Implementation of one such correction technique, utilising the CRISIS network [8], corrected gain and phase imbalances to 0.02dB and 0.4° respectively. This is equivalent to 49 dB sideband rejection, a definite improvement, but unacceptable in most multichannel applications. Additionally the

effectiveness of current compensation techniques decreases dramatically when the reconstruction filters are mismatched.

Previous analysis has generally neglected the significance of the effect of a mismatch in the reconstruction filters. It has been reported [9] that "in a predistortion linearising system the reconstruction filters are a major source of error", but the analysis was restricted to a single channel (narrowband) system with predistortion.

The next section describes a novel compensation technique that is applicable to a multichannel environment. Whereas previous compensation techniques have only compensated for a single gain and phase imbalance, this novel method cancels at a number of frequencies across the system bandwidth.

Section III shows that the reconstruction filters are the major contributor to frequency dependant imbalances across a wide band and then examines the effect of frequency dependant imbalances on the sideband signal. It is shown that the error vector between the reconstruction filters in the IQ channels is related directly to the amount of sideband rejection.

Section IV uses the relationship found in section III to develop a methodology for analysing the performance of mismatched filters driving an analog quadrature modulator. Two parameters, oversampling ratio and 'channel to system bandwidth' ratio, are introduced to objectively judge the performance of the multichannel adaptive compensation technique.

Finally, analysis reveals the sensitivity of percentage mismatch and differing ACI specification in a multichannel environment.

II. A NOVEL METHOD FOR THE COMPENSATION OF GAIN AND PHASE IMBALANCES

The novelty of the technique revolves around the wideband low-level combiner, which is based on transmultiplexer technology. Transmultiplexers make use of the inherent redundancies of interpolation (N padded zeroes) and the uniform spacing of the channels to form an efficient multirate algorithm [10].

Figure 3 illustrates the proposed technique. N channels are combined through a transmultiplexer to form a wideband signal (as shown in Fig. 2a). The system bandwidth is then directly upconverted via an analog quadrature modulator. The inherent gain and phase imbalances will cause undesired sideband signals (as shown in Fig. 2b). The compensation method deliberately introduces a sideband component (through the complex coefficient C_m) which cancels the undesired sideband. The adaption technique measures the sideband power in a vacant channel using a tuned receiver (error sensing circuitry in Fig. 3) and adjusts the complex coefficient (C_m) to minimise the power of the undesired signal.

The process described above is repeated for every channel in the system but only whilst the channel is vacant. The update rate is slow but this is not considered a problem as the gain and phase imbalances drift slowly with time.

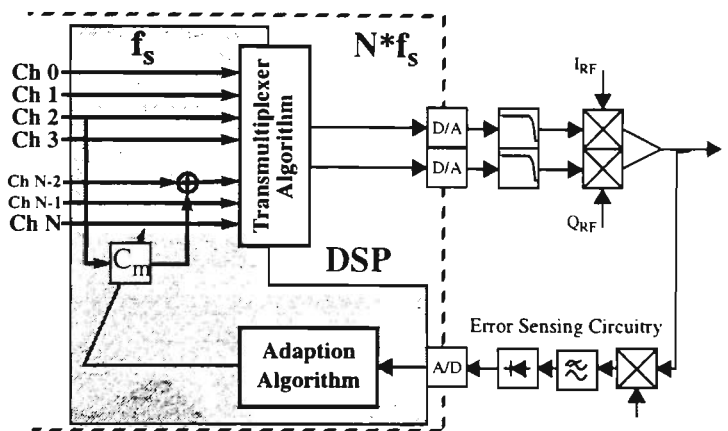


Fig. 3. Multichannel adaptive compensation technique for correcting gain and phase imbalances.

The compensation technique described has a number of advantages over previous adaptive correction techniques.

- *Reduced Computational Load* - The adaption algorithm and the scaling coefficient operate at the channel sampling rate, as opposed to the output sampling rate.
- *Corrects for Frequency Dependant Imbalances across the System Bandwidth* - Previous techniques only compensate for a single bulk gain and phase imbalance across the system band.
- *Increased Sensitivity of Feedback Signal* - This technique detects only the undesired signal, as opposed to both the desired and undesired signal [8], thus increasing the dynamic range of the correction network.

For an uncorrected analog quadrature modulator the power of the sideband will exceed ACI specifications (Fig. 4a). In practice it is necessary to reduce the power in the sideband to comply with a given ACI specification and so there is room for non-ideal cancellation. The multichannel compensation technique exploits this fact by cancelling the phase and gain imbalance at a single frequency (bulk imbalance) and the sideband will be completely removed at this frequency. However the frequency dependant imbalances mean that a differential phase and gain imbalance will remain across the remainder of the channel (differential imbalance), causing a residual sideband response (Fig. 4b).

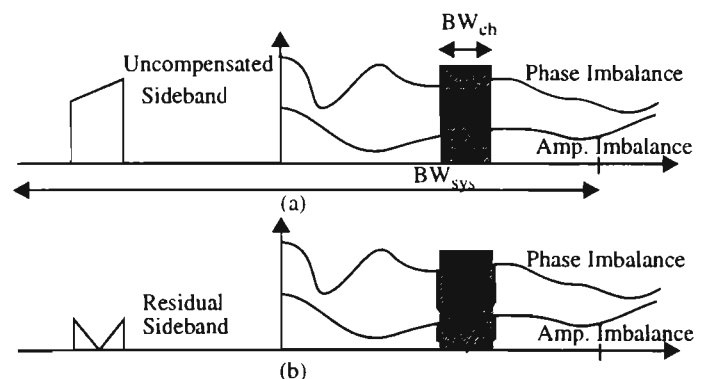


Fig. 4. (a) Sideband response due to frequency dependant imbalances (b) Sideband response after cancellation of the channels bulk imbalance.

To comply with an ACI specification the following condition must hold :

$$ACI = 10 \log \frac{\text{Power in Sideband}}{\text{Power in Signal}} \text{ dBc} \quad (1)$$

The ability to quantify the frequency dependant imbalances is important in analysing the performance of the multichannel adaptive compensation technique.

III. ANALYSIS OF FREQUENCY DEPENDANT IMBALANCES

A. Causes of frequency dependant imbalance in a direct upconverter

Frequency dependant gain and phase imbalances arise from both the quadrature modulator and the mismatch in the reconstruction filters.

The quadrature modulator consists of the mixer, splitter and summer components. The gain and phase through each of these components is dependant on frequency to some extent, although the amount of dependence will depend on the complex design strategies employed. This issue is beyond the scope of the paper.

A typical Mini Circuits IQ Modulator was chosen as an example (Table I generated from data sheet). It can be seen that over a channel bandwidth of 5 MHz around 54 dB of sideband rejection exists if the bulk imbalance is removed (leaving the differential imbalance). Whilst over 70 dB could be achieved if the bandwidth was reduced below 100 kHz.

Table I

Absolute variation of gain and phase imbalance across a specified bandwidth for a Mini Circuits IQ Modulator (MIQD 895)

Bandwidth	Differential gain Variation (dB)	Differential Phase Variation (degree)	Residual Sideband
100 kHz	0.01	0.05	-70 dB
500 kHz	0.02	0.10	-64 dB
5 MHz	0.05	0.30	-54 dB

In most communication systems utilizing the FDM format the channel bandwidth is less than 200 kHz. Therefore to meet system ACI specifications the quadrature modulator would have to produce a slightly better performance than this example. Assuming that this is possible the quadrature modulator can be considered to have constant bulk imbalance across the channel band.

Frequency dependence is then apportioned entirely to the reconstruction filters, which will now be analysed.

B. The effect of filter mismatch on the sideband signal

To analyse the effects of filter mismatch, the reconstruction filters are modelled with relative gain mismatch, $\alpha(f)$, and phase error from quadrature, $\Phi_e(f)$ (radians). The variable $\beta(f)$ is used to account for the absolute attenuation characteristic (or gain transfer function) of the filter and serves to normalise the magnitude at any frequency. Fig. 5 summarises the model :

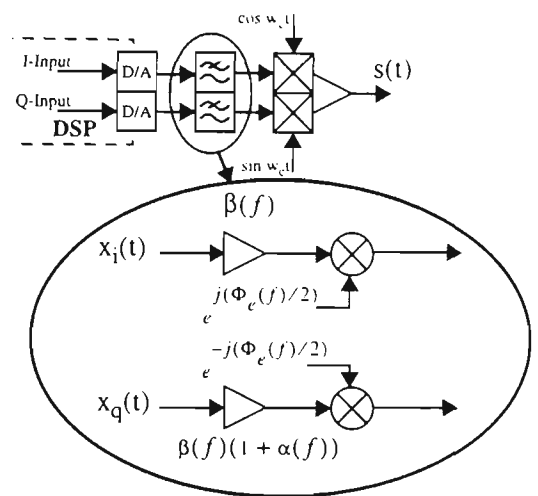


Fig. 5. Modelling the mismatch between reconstruction filters

The amount of sideband rejection is given as the absolute magnitude of the image vector divided by the absolute magnitude of the wanted signal (the form of which is same to the static case analysed in [3]) and is given by :

$$\begin{aligned} \text{Sideband Rejection} &= \frac{|v(t)|}{|u(t)|} \\ &\approx 20 \log \frac{\sqrt{\alpha(f)^2 + \Phi_e(f)^2}}{2} \text{ (dB)} \end{aligned} \quad (2)$$

An alternative way of visualising the previous analysis is to consider the I and Q path filters as vectors. When they are matched they are both equal in magnitude and phase (Fig. 6a), subsequently causing no distortion or sideband response. When the filters are mismatched there exists a phase and gain difference (frequency dependence), this is illustrated in Fig. 6b.

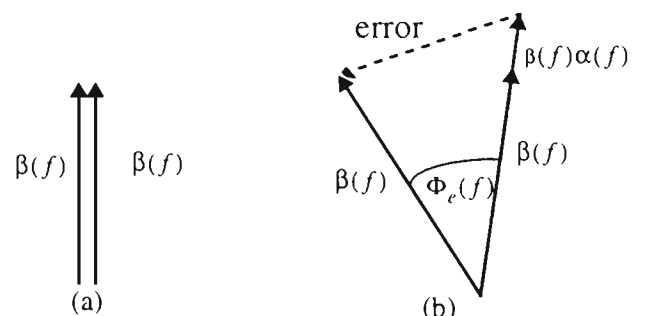


Fig. 6. (a) I and Q path filters matched (b) I and Q path filters mismatched

It can be shown that the error vector is related to the Sideband rejection by :

$$\text{Sideband rejection} = \text{error_vector} / 2 * \beta(f) \quad (3)$$

This can be verified by calculating the magnitude of the error vector in Fig. 6b for small gain and phase imbalances and comparing it to the approximate sideband rejection calculated in Eqn. (2).

For typical values of ACI specified by radio communication systems the sideband has to be of a magnitude that infers very small gain and phase mismatch. The magnitude of sideband rejection can therefore be accurately predicted from Eqn. (2).

A means of comparing the performance of the multichannel compensation technique is now introduced.

IV. METHODOLOGY FOR ANALYSING THE EFFECT OF

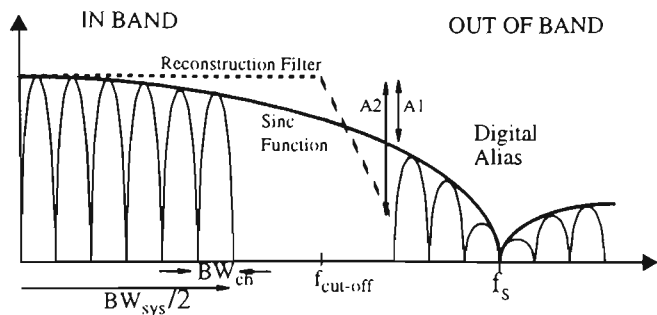


Fig. 7. Overview of Communication System Parameters relevant to Direct Upconversion and a Multichannel Environment.

MISMATCHED RECONSTRUCTION FILTERS.

The methodology calls for a relative comparison of performance when adjusting parameters relevant to filters. It is based on modelling the mismatch between the filters as a percentage increase in the cut-off frequency of one filter. This has limitations, especially when considering the real implementation issues of filters, but for practical analysis purposes it is seen as a realistic yardstick. The relative performance of a particular filter will then be judged by two parameters, the oversampling ratio and 'channel to system bandwidth' (number of channels) ratio. A discussion on how these parameters are calculated is now presented.

For the purpose of analysis the communication system, will be defined in terms of three parameters (Fig. 7) :

- Channel Bandwidth - BW_{ch}
- System Bandwidth - BW_{sys}
- The Adjacent Channel Interference specification.

To meet the ACI specification of a communication system two objectives must be achieved :

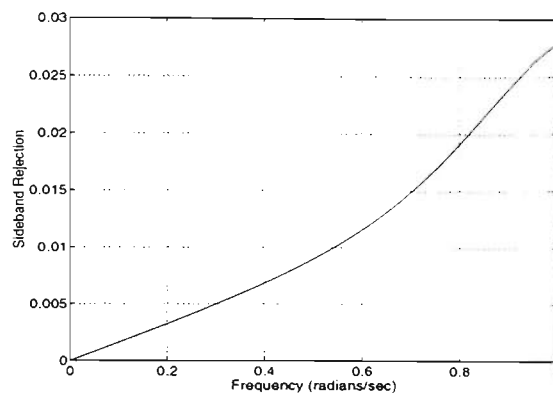
- In System Band : Given a percentage mismatch between the two quadrature filters, the sideband rejection must comply with the ACI specification for the system, as given by the Eqn (1).
- Out of System Band : The digital alias must be attenuated below the same ACI specification for the system. This is achieved by the reconstruction filter (A2) and the sinc response of the D/A converters (A1).

The number of channels is derived solely from the In System Band objective. The mismatch between the filters creates frequency dependant imbalances that require periodic cancellation across the system band to meet a given ACI specification. The worse the mismatch between the filters then the smaller the channel bandwidth must be so that after cancellation the power of the residual sideband complies with ACI specifications. For a fixed system bandwidth this can be equally expressed as more channels, where the number of channels is related to the channel bandwidth by :

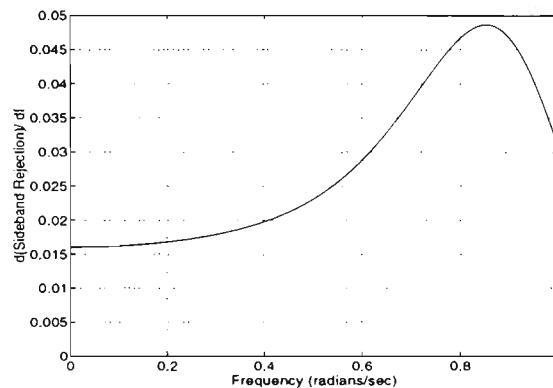
$$N_{ch} = \frac{BW_{sys}}{BW_{ch}} \quad (4)$$

The number of channels is essentially a measure of the frequency dependant mismatch in the system.

To illustrate how the number of channels are calculated a fifth order Butterworth filter is used as a case study. The error vector between the two filters is used to calculate the sideband



(a)



(b)

Fig. 8. Fifth order Butterworth filter with 1% mismatch in the cut-off frequency (a) Sideband rejection (b) Gradient of sideband rejection, Eqn. (3). Fig. 8a illustrates the amount of sideband rejection (amplitude) for a 1% mismatch in the reconstruction filters cut-off frequency. Note that the filters cut-off frequency has been normalised to 1 rads/sec. Here the filters are perfectly matched at DC (no sideband) whilst throughout the passband a sideband magnitude exists, this is due to the frequency dependant imbalance.

To calculate the number of channels needed it is more instructive to view the gradient of the sideband rejection across the passband of the filter, as illustrated in Fig. 8b.

The multichannel adaptive compensation technique will cancel a single frequency in every channel, however total cancellation across the channel band does not occur rather a residual sideband will exist as shown in Fig 4b.

The maximum gradient across the channel band is taken so that a first order approximation can be assumed for calculating the power in the sideband. That is the sideband amplitude resembles a triangular function (power approximates a square law function) given that the desired signal occupies the full channel bandwidth.

It is assumed that the largest gradient to occur across the system bandwidth (which is a fraction of the cut-off frequency) is taken as the absolute constant gradient across any channel, a worst case scenario.

Given the above and using Eqn. (1), the minimum number of channels is related to the system ACI specification :

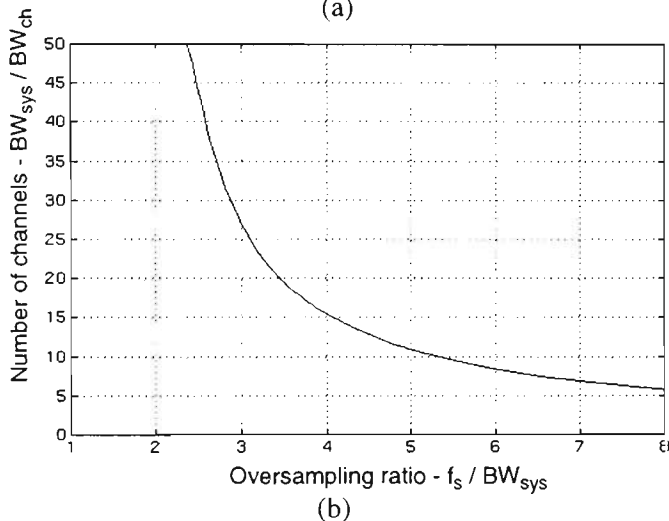
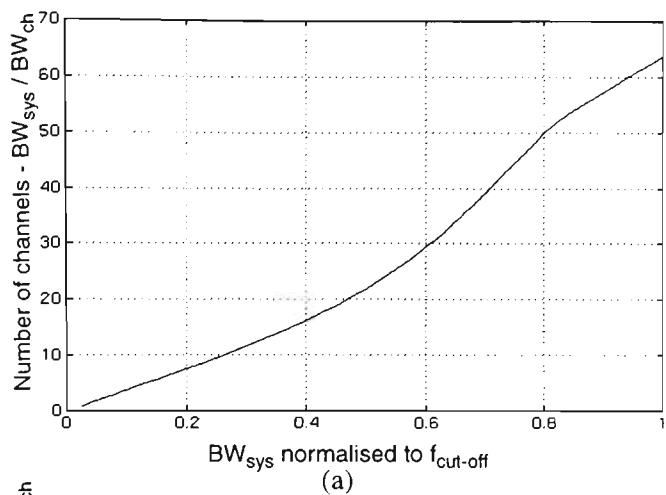


Fig. 9. Fifth order Butterworth filter with 1% mismatch in the cut-off frequency complying with a 60 dB ACI specification (a) In System Band objective (b) Combination of In and Out Of System Band Objectives.

$$N_{ch} = \frac{BW_{sys} \times \sqrt{\frac{d(\text{sideband rejection})}{df}}}{10^{ACI/20} \times \sqrt{12}} \quad (5)$$

By varying the system bandwidth the minimum number of channels needed to comply with the systems ACI specification can be plotted as shown in Fig. 9a. As expected, more channels are needed as the system bandwidth approaches the cut-off frequency of the filter.

The second objective, Out of System Band, is achieved by attenuating the sampling aliases below the ACI specification. The filter attenuation characteristic will dominate the absolute sampling rate required to achieve this condition. The sampling frequency has been normalised to the Nyquist sampling rate of the system, BW_{sys} . This is expressed as the oversampling ratio :

$$\text{Oversampling Ratio} = \frac{f_s}{BW_{sys}} \quad (6)$$

By combining the In and Out of System Band objectives the minimum number of channels can be related to the oversampling ratio for a given mismatch and system ACI specification, Fig. 9b. This methodology is now used to comparatively analyse the performance of the filters by modifying different parameters.

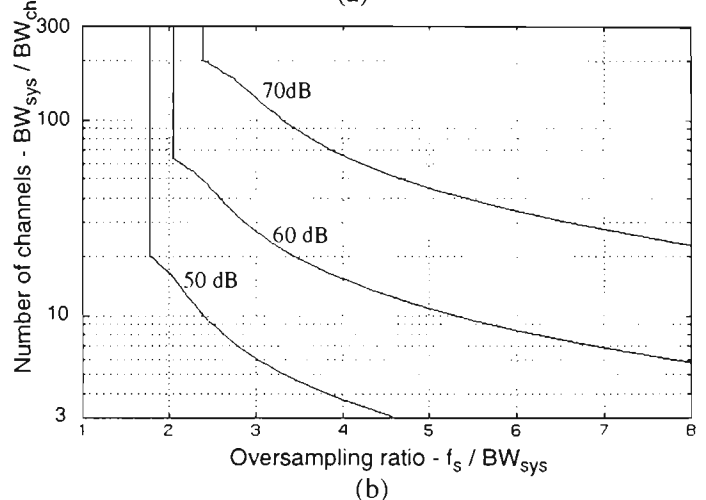
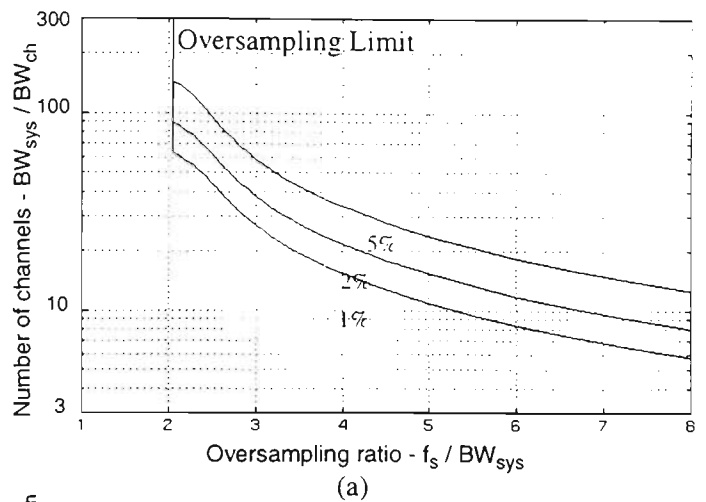


Fig. 10. Fifth order Butterworth filter with a 1% mismatch in the cut-off frequency and complies with a system specification of 60 dB ACI is assumed unless otherwise stated (a) Percentage mismatch in the cut-off frequency varied (b) ACI specification varied.

V. NUMERICAL COMPUTATION AND ANALYSIS

The effect of mismatched reconstruction filters driving an analog quadrature modulator has been shown to introduce frequency dependant imbalances. These imbalances can be corrected by the adaptive compensation technique introduced in Section II. However the amount of mismatch in the reconstruction filters will put certain restrictions on the design, that is the number of channels and the oversampling ratio needed to comply with the systems ACI specification.

A. Filter Mismatch

Increasing the mismatch between the filters is the same as increasing the tolerance of the components used in implementing the filter. This effect has been modelled as a percentage shift in the cut-off frequency.

For a small number of channels the oversampling ratio increases with an increase in percentage mismatch (Fig. 10a). However in a system with a large number of channels (140 and upwards) the amount of mismatch (as long as it is less than 5 %) becomes irrelevant as the oversampling limit (vertical asymptote in Fig. 10a) is reached.

The oversampling limit occurs when the system bandwidth

equals the cutoff frequency, it is possible to go beyond this point by pre-emphasising the outer channels but this will not be considered here. The In System Band condition therefore determines the minimum number of channels, any further increase in the number of channels will improve the undesired sideband further below the ACI specification (In System Band condition) but will have no effect on the oversampling ratio. This is because the system bandwidth cannot be extended further and therefore the Out of System Band objective, which is not dependant on percentage mismatch, will govern the lowest oversampling ratio.

It can be concluded that the filters must be able to be designed to meet tight specifications and also be reliably reproduced in the manufacturing process.

B. ACI Specification

Increasing the ACI specification has a similar effect to increasing the percentage mismatch. Fig. 10b illustrates that the larger the ACI specification the higher the oversampling ratio required for a fixed number of channels. This is especially important for a small number of channels, say around 20, which for 70 dB ACI would require an oversampling ratio greater than 8. Depending on the bandwidth of the channel, such a large oversampling ratio will place severe limitations on the bandwidth of the system, primarily due to the sampling frequency that would be required for the digital processing.

Notice also that the oversampling limit decreases with a lowering of the systems ACI specification. To further lower this limit the filter order would have to be increased.

V. CONCLUSION

Mismatch between the reconstruction filters produce frequency dependant imbalances that cause undesired sideband responses in a multichannel environment. A novel adaptive compensation technique has been introduced to reduce these sideband signals to comply with radio communication system ACI specifications, nominally 50 to 80 dBc. The ability to correct for frequency dependant imbalances and the fact that the correction occurs at the channel sampling frequency are the two distinct advantages this technique possesses over previous adaptive compensation techniques.

Analysis of the frequency dependant imbalances yielded a relationship between the error vector of two mismatched filters and the amount of sideband rejection (ACI). This relationship was used to develop a methodology that related the number of channels to the oversampling ratio required to comply with a communication system ACI specification when the new adaptive compensation technique was employed.

The methodology objectively compared the performance of the system when mismatch in the reconstruction filters is considered. The main objective was to keep the oversampling ratio as low as possible, both for technology and power consumption reasons.

It was found that tightly matched reconstruction filter are required to minimise the oversampling ratio for a given ACI requirement.

REFERENCES

- [1] A.K.Johnson & R.Myer. "Linear amplifier combiner". *IEEE Vehicular Technology Conference*. Tampa, Florida, pp 422-423, 1987.
- [2] J.Stefanov. "A compact base station for small cells". Department of Electronics and Computer Science. *Third Nordic Seminar on Digital Land Mobile Radio Communications*, Copenhagen, 1988.
- [3] A.I.Sinsky & P.C.P.Wang. "Error Analysis of a quadrature coherent detector processor". *IEEE Transactions on Aerospace and Electronic Systems*, vol. AES-10, pp 880-883, Nov. 1974.
- [4] S. Haykin, *Digital Communications*. John Wiley & Sons, Inc., 1988.
- [5] F.E.Churchill,G.W.Ogar,B.J.Thompson. "The correction of I&Q errors in a coherent processor". *IEEE transactions on aerospace & electronic systems*, Vol AES-17, No 1, pp131-136, Jan 1988.
- [6] A.E.Jones and J.G.Gardiner. "Phase Error Correcting Vector Modulator for Personal Communications Network (PCN) Transceivers". *Electronic letters*, Vol 27, (14), pp 1231-1232, July 1991.
- [7] J.K.Cavers,M.Liao. "Adaptive compensation for imbalance and offset losses in direct conversion transceivers". *IEEE transactions on Vehicular Technology*, pp 581-588, 1991.
- [8] M.Faulkner,T.Mattsson,W.Yates. "Automatic adjustment of quadrature modulators". *Electronic letters*, Vol 27, (3), pp 214-216, Jan. 1991.
- [9] L.Sundstrom, M Faulkner. "The effect of reconstruction filtering on the predistortion linearisation of RF power amplifiers". *Mobile & Personal Communication Systems*, Adelaide, Australia, pp 357-361, 12-13 Nov. 1992.
- [10] R.E. Crochiere & L.R. Rabiner, *Multirate Digital Signal Processing*. New Jersey : Prentice-Hall, Inc. 1983.

Digital Signal Processing and Direct Conversion for Multichannel Transmitters

Scott A. Leyonhjelm and Dr Michael Faulkner
Mobile Communications and Signal Processing Group,

Department of Electrical & Electronic Engineering,

Victoria University of Technology,

PO Box 14428 MMC, Melbourne, VIC 3000, AUSTRALIA.

Email: scott@cabsav.vut.edu.au or mf@cabsav.vut.edu.au

Abstract - A multichannel transmitter architecture is presented, combining an efficient transmultiplexer algorithm with direct conversion. Direct conversion is chosen for its simplicity and low cost, but it is necessary to compensate for the inherent amplitude and phase imbalances. These imbalances are shown to be frequency dependant in a multichannel environment, generating unacceptable levels of spurious sidebands and rendering current adaption techniques inappropriate. The paper proposes a compensation technique based on the multichannel transmitter architecture. It is computationally more efficient than the previous adaptive compensation techniques and simulations show that the undesired sideband can be controlled to meet ACI specifications.

I. INTRODUCTION

Recent advances in the wideband linearisation of amplifiers suggest that future Frequency Division Multiplex (FDM) systems can now be combined at low power levels. The low power combination can occur in a DSP environment, before being upconverted and amplified by a linear wideband amplifier.

A wideband low level combiner has numerous advantages over the conventional high power combining technique [1-2]. The flexibility of low level combining is further enhanced through the use of a DSP environment. The DSP algorithm performs the task of modulating and multiplexing the channels together into a FDM format. The broad class of algorithm that has been isolated for this specific task is called a transmultiplexer.

Extensive research during the 1970's (and early 1980's) revealed efficient transmultiplexer algorithms [3] that could interconnect two types of signals, Time Division Multiplex and Frequency Division Multiplex signals (SSB). More recently, satellite architectures [4] have incorporated these algorithms as a means to improve performance through increased flexibility, minimisation of weight and lower power consumption. Additionally these algorithms can be equally applied to the low-level power combining of digitally modulated signals.

Following the combination of channels, the band (centred at baseband) needs to be upconverted to radio frequency (RF). Direct conversion is one technique that has received a lot of attention due to its suitability as a universal

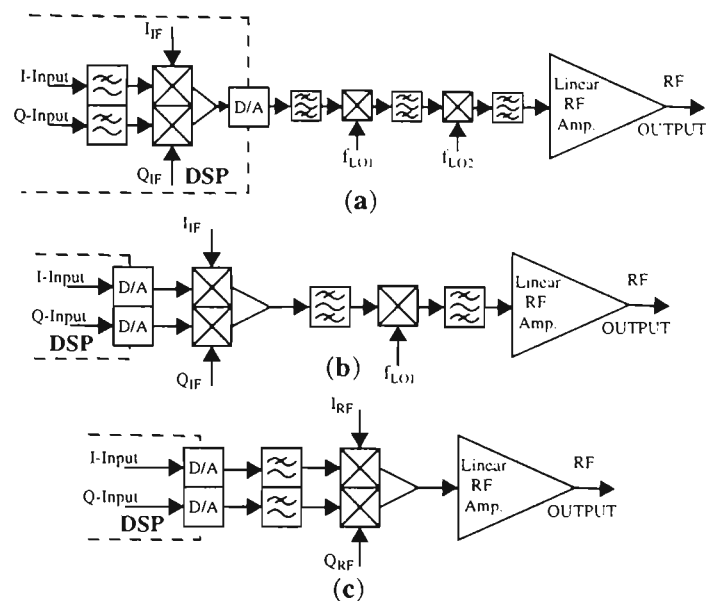


Fig. 1. (a) Combined Digital Quadrature Modulation and Analog Heterodyne Upconversion. (b) Combined Analog Quadrature Modulation and Heterodyne Upconversion. (c) Analog Quadrature Modulation Upconversion

modulator (and demodulator); it is simple, small, has low power consumption, and can be applied to any modulation scheme. Unfortunately for a wideband system the specifications for Adjacent Channel Interference¹ are stringent, specifications range between -50 dBc to -80 dBc for Mobile Satellite and Land Mobile Radio (LMR) systems respectively. This paper will show that ACI is very sensitive to any mismatch in the I & Q paths, especially the reconstruction filters, of the direct converter.

Different versions of upconversion have been isolated for their suitability in a wideband application. They are illustrated in Fig. 1.

Digital quadrature modulation, Fig. 1(a), is limited by current DSP technology. The maximum sampling rate dictates the selection of the intermediate frequency (I_{IF} & Q_{IF}), which ultimately limits the upconversion to a low intermediate frequency band. Consequently a double

1. Adjacent Channel Interference (ACI) "is a broad term. It includes next-channel (the channel next to the operating channel) interference and neighbouring-channel (more than one channel away from the operating frequency) interference" [5]. In the context of this paper it is used to infer any spurious signals produced by the combining and/or upconversion process

conversion heterodyne approach is usually needed to complete the upconversion to the required RF band. The precision of a digital quadrature modulator overcomes the problems of gain and phase imbalance, DC offset and performance drift (all characteristics of the analog quadrature modulator) but there still exists some potential problems. These problems include :

- Replacing Analog with Digital processing increases the DC power consumption.
- Reduced spectral purity due to settling times and quantisation error of the DAC.
- The system in Fig. 1(a) requires approximately 3 dB more dynamic range than that of Fig. 1(b) and 1(c).
- The need for a heterodyne upconverter increases the cost and complexity.

The second method generates a higher intermediate frequency, allowing a simpler single upconversion heterodyne approach, as illustrated in Fig 1(b). The first bandpass filter reconstructs the signal and attenuates the digital aliases that are created by the D/A process. The intermediate frequency is chosen as a trade-off between the oversampling rate and bandpass filter rolloff. The gain and phase imbalances of the mixers and summer cause an undesired sideband signal that requires compensation if the system is to meet ACI specifications. The correction of these imbalances, assumed constant across the band of interest, has been previously addressed [6-9] and the novel technique presented in this paper is also applicable.

Analog quadrature modulation upconversion (Fig. 1(c)), or Direct Conversion, has recently gained a lot of attention through advances in RF device fabrication and also due to its suitability as a universal modulator. However, phase and gain imbalances force the need for compensation if it is to be used in modern day wideband wireless communication systems.

It can be shown that if a wideband channelised signal, Fig. 2(a), is passed through an unbalanced quadrature modulator, the result will consist of both wanted and sideband signals (Fig. 2(b)). The amount of sideband rejection is related to the amount of imbalance [10]:

$$\text{Sideband Rejection} = \frac{|\text{Wanted Signal}|}{|\text{Sideband Signal}|} \quad (1)$$

$$\approx 20 \log \frac{\sqrt{\alpha^2 + \Phi_e^2}}{2} \quad (\text{dB})$$

Where α = Differential gain between the I & Q paths.
 Φ_e = Phase mismatch from an ideal of 1.57 radians.

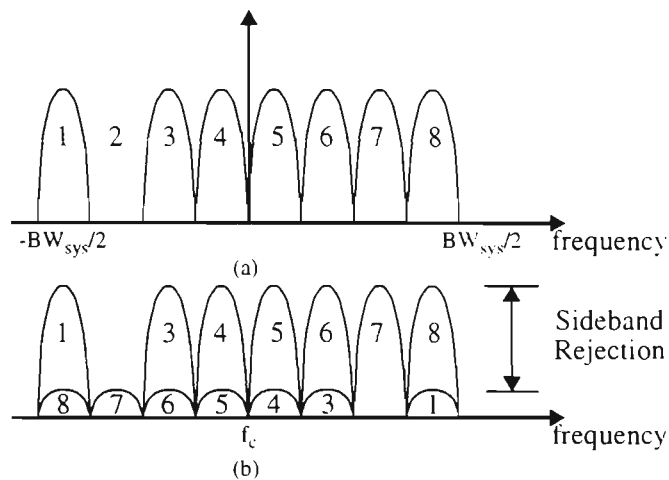


Fig. 2. The effect of phase and gain imbalances in a quadrature modulator (a) Original signal displayed in complex baseband format. (b) Wanted and sideband (image) signals after passing through an unbalanced quadrature modulator.

Different amounts of sideband rejection can be tolerated in a multichannel system. If the sideband signal falls into a channel that is being used then it will distort the desired signal (channel 1 in Fig. 2(b)). The required sideband rejection is then related to the E_b/N_0 performance of the modulation scheme. The sideband signal could equally fall into a vacant channel position (channel 7 in Fig. 2(b)). In this situation the system must meet the 50 dBc to 80 dBc system ACI specifications.

It is reasonable to talk of component imbalances (mixer and summer) of 0.3 dB and 3° in a well designed analog quadrature modulator. Imbalances of this magnitude would result in 30 dB of sideband rejection, sufficient for some single channel applications. The analog quadrature modulator is therefore not usable in a multichannel environment without some form of refinement. A number of correction techniques have evolved [6-9], all have concentrated on a single channel application. However the performance of these techniques is such that it is unacceptable in most multichannel applications. Furthermore the effectiveness of this type of compensation decreases dramatically when the reconstruction filters driving the analog quadrature modulator are mismatched.

The next section briefly reviews present compensation techniques and discusses their deficiencies. The novel method for the compensation of frequency dependant phase and gain imbalances in a multichannel environment is then introduced.

Section III proceeds to fully describe the novel method for compensation in a multichannel system. The technique utilises the most desirable features of the existing compensation techniques.

The adaption algorithm used in the simulations is briefly discussed in Section IV, whilst the simulations in Section V, verify the novel architecture, and also highlight the subtleties of its operation.

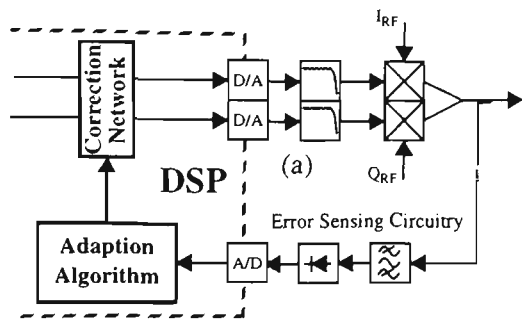


Fig. 3. Generic Adaptive Cancellation Architecture

II. TECHNIQUES FOR THE COMPENSATION OF GAIN AND PHASE IMBALANCES

Two recent methods of adaptive compensation have proved to be successful in narrow band applications. Although they have similar architectures (Fig. 3), there is a subtle difference to how the feedback (error) signal is obtained. The error signal is either detected from both the wanted and undesired signal [8] or in certain applications only the undesired signal is isolated [9].

The correction method, called CRISIS (CRoss-coupled Intra-Symbol Interference Suppression), that utilizes both the wanted and undesired signals [8], diode detects the RF power corresponding to a set of test vectors. The correction network coefficients are subsequently modified to minimise the measured error and therefore compensate for the quadrature modulator imbalance. This technique is limited in performance by :

- The wideband nature of the diode detector and the harmonic outputs of the mixer, which cause erroneous outputs. Pre-filtering improves but does not completely solve the problem.
- Drifting between measurements due to noise and 50 Hz pick-up.
- Quantisation error in the A/D limits the accuracy of the feedback signal.

Implementation of this technique corrected the gain and phase imbalances to 0.02 dB and 0.4° respectively. This is equivalent to 49 dB sideband rejection, barely meeting mobile satellite specifications. Theoretically the amount of compensation can be increased by detecting the unwanted signal alone, because without the larger wanted signal the dynamic range of the adaptive system is increased.

The correction network that utilizes this method (detecting only the unwanted signal) requires a non-linear amplifier to spread the spectrum. It filters out the wanted signal and uses the remaining adjacent channel interference to provide the necessary feedback information. The performance is still limited by the same problems experienced by the first technique, but to a lesser extent because the system is more sensitive to the error signal. The selectivity of the filter is critical to the ultimate performance of this correction technique.

Both systems suffer from the disadvantage that the actual

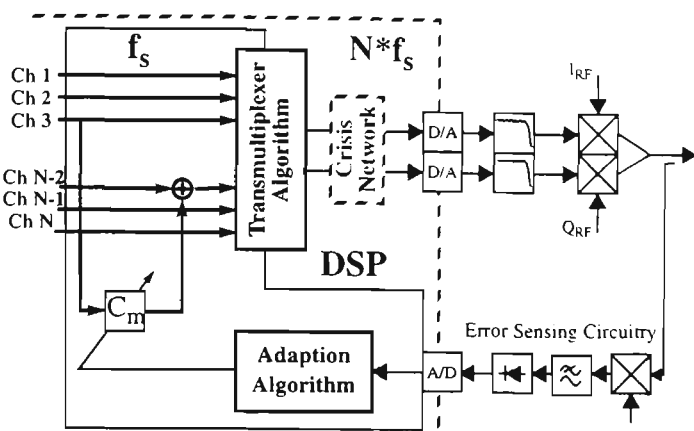


Fig. 4. Novel technique for compensation of gain and phase imbalances in a wideband multichannel system

compensation network requires additional processing at the output sampling frequency. The additional multiplications and additions are applied to each sample that is output. The high sampling rate required for the output of a wideband system makes the additional processing load of these adaptive corrective networks an unfavourable option.

The compensation systems discussed also imply that the gain and phase imbalances are constant across the system bandwidth. This may be valid when considering a single channel, but for many channels across the system bandwidth this assumption is not valid. Especially when the mismatch between the reconstruction filters is taken into account.

A novel method of compensation is now presented overcoming the two disadvantages mentioned above. That is, it reduces the computational load of and it can correct for variations in phase and gain imbalance across the system bandwidth.

III. A NOVEL METHOD FOR THE COMPENSATION OF PHASE AND GAIN IMBALANCES

The novelty of the technique revolves around combining the best features of techniques that have been discussed in previous sections. These techniques include a wideband low-level combiner, analog quadrature modulation upconversion and adaptive compensation of quadrature modulators.

A wideband low-level combiner is based on transmultiplexer technology [3], which makes use of the inherent redundancies of interpolation (N padded zeroes) and the uniform spacing of the channels to form an efficient multirate algorithm.

The quadrature modulator upconverter is chosen for its simplicity and low cost, although it is necessary to compensate for the imbalances so that ACI specifications are met.

The chosen adaption technique is based on a form of pre-distortion, that is the original signal is distorted in a predetermined manner such that the added distortion is cancelled by the following quadrature modulator network.

Figure 4 illustrates the proposed technique. Here N channels are combined through a transmultiplexer to form a

wideband signal (as shown in Fig. 2(a)). The system band is then directly upconverted via an analog quadrature modulator. The inherent gain and phase imbalances will cause the sideband signals. The adaption technique then selects a vacant channel position and the undesired sideband (error) signal is isolated by the filter, increasing the dynamic range. This error signal is then sensed, by a diode detector, and used in the adaption algorithm to suitably modify the scaling coefficient (C_m) so that the feedback signal is minimised.

The process described above is repeated for every channel in the system but only whilst the channel is vacant. This infers slow adaption, and is not considered a problem as the gain and phase imbalances drift slowly with time.

Additionally as illustrated in Fig. 4, the scaling coefficient operates at the channel sampling rate, as opposed to the output sampling rate, thus substantially lowering the computational load on the system.

IV. ADAPTION ALGORITHM

The adaption algorithm is based on utilizing an error signal proportional to the magnitude of the sideband signal. The real and imaginary parts of the pre-distort coefficient are then adjusted accordingly using a simple one dimensional search technique [8].

The one dimensional search technique adjusts one part of the coefficient in incremental steps until the error begins to increase, the other coefficient is then selected for incremental adjustment. The process is repeated with reducing step sizes until the minimum is reached. Convergence is assured whilst the amount of sideband suppression achieved will depend on the final step size.

A faster algorithm could be implemented at the cost of more computational complexity.

V. SIMULATIONS

The compensation technique introduced in this paper and illustrated in Fig. 4 has been simulated to verify its operation.

Fig. 5(a) shows the output of an ideal quadrature modulator with three channels being activated by a single tone. Note that no sidebands are generated and adaption would not be necessary.

Introducing a bulk 10% gain and phase imbalance (constant across system bandwidth) into the quadrature modulator generates significant image signals, Fig 5(b). Obviously 20 dB sideband rejection is not a favourable result and will not achieve ACI specifications. Previous methods (see Section II) would actually be able to cancel this type of constant imbalance across the system bandwidth. But as Fig. 4 highlights, the compensation takes place at the higher sampling rate (CRISIS Network).

In a real wideband system gain and phase imbalances will vary across the system bandwidth, making them frequency dependant. Reasons for the variance include the frequency response of the mixers and summer and the mismatch in the reconstruction filters. This will result in

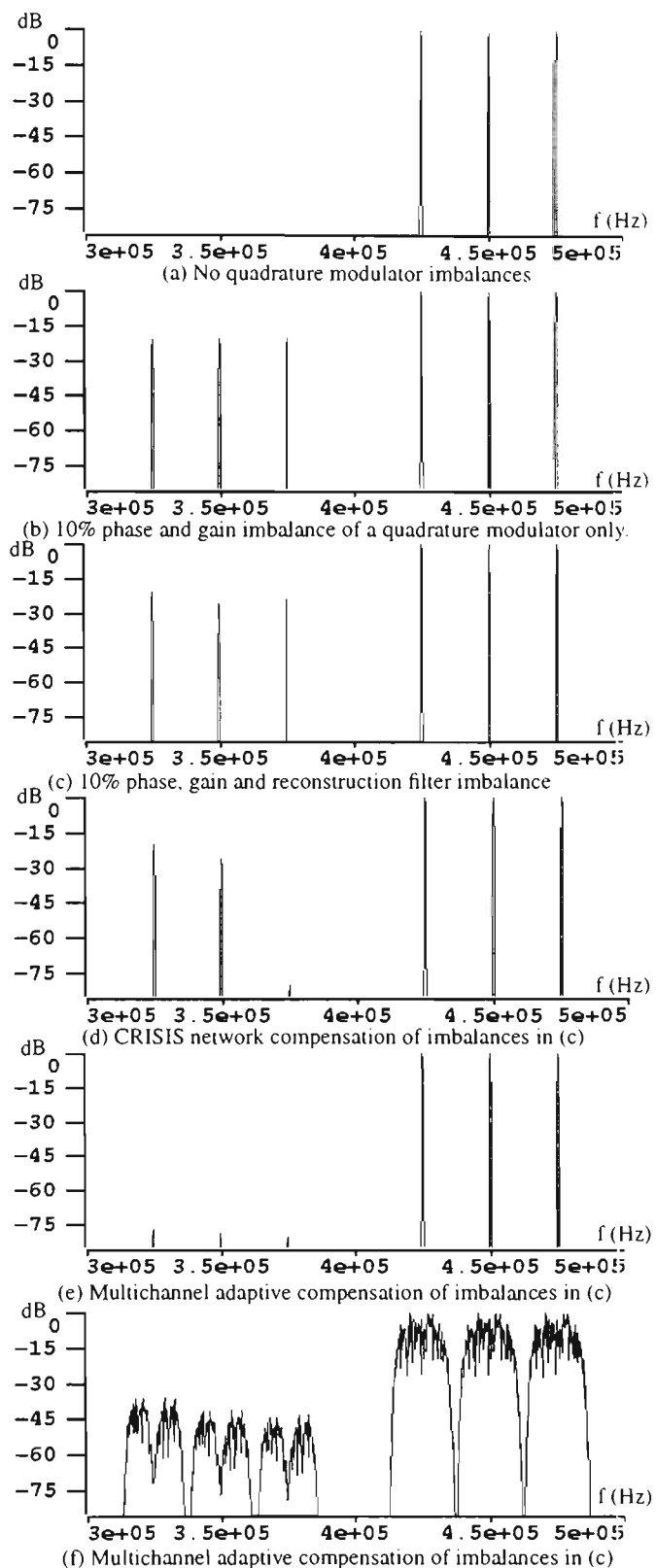


Fig. 5. Simulation of the Novel Architecture presented in Fig. 4.

image signals that differ in level across the band, Fig. 5(c).

The compensation networks based on the CRISIS network can only cancel bulk gain and phase imbalance, and therefore if applied to a multichannel system only one of the image signals could be completely cancelled, as illustrated in Fig. 5(d). The other channels remain uncompensated.

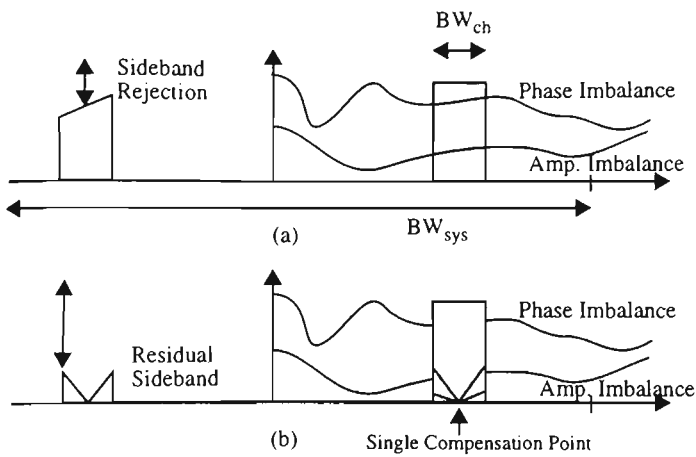


Fig. 6. (a) Sideband response due to frequency dependant imbalances (b) Sideband response after cancellation of one channels bulk imbalance.

The new approach cancels all the image signals (Fig. 5(e)). Notice however that we are only representing the activation of a channel as a single tone at the centre of the channel, inferring that cancellation would also occur across the channel band, Unfortunately this is not the case, as Fig. 5(f) highlights. Here the channels are fully activated, and only one frequency in each image channel is completely cancelled. The rest of the channel still exhibits an unacceptable amount of sideband rejection.

Frequency dependence of these imbalances in wideband systems is far more critical than in single channel (narrowband) systems. This is because if the sideband falls into a vacant channel it must meet with ACI specifications of the system (50 to 80 dBc). To quantify the amount of mismatch that can be tolerated requires consideration of gain and phase variance across a single channel, not the whole system bandwidth. To explain this in more detail we need to consider the new adaptive technique together with the frequency dependant imbalances.

Fig. 6(a) illustrates how the magnitude of the sideband will vary across the channel bandwidth, a direct consequence of frequency dependant imbalances. The novel compensation technique can cancel out the phase and gain imbalance (bulk imbalance) at a single frequency, but not across the whole channel band. The differential phase and gain imbalance across the channel (differential imbalance) causes a residual sideband response that must be kept within ACI specifications (Fig. 6(b)). For every channel within the system bandwidth a similar scenario exists, therefore the technique cancels out a number of bulk imbalances across the system bandwidth.

An improvement to the single coefficient cancellation technique would be to replace it with an N tap equaliser (FIR filter) circuit. This would better match the phase and gain imbalances across the channel band at the expense of increased computational complexity.

A novel compensation technique has been presented in conjunction with a low power Digital Signal Processing based multichannel combiner.

The technique was shown to be less sensitive than that described in [8] to frequency dependant imbalances, which are significant in the wideband multichannel situation. The computational requirements are lower than previous adaptation techniques, especially when not all the channels across the system are activated (normal situation).

The technique could equally be applied to the method of upconversion shown in Fig. 1b, where a bandpass filter performs the reconstruction requirements. The major advantage is again in the lower computational requirements.

REFERENCES

- [1] A.K.Johnson & R.Myer, "Linear amplifier combiner". *IEEE Vehicular Technology Conference*, Tampa, Florida, pp 422-423, 1987.
- [2] J.Stefanov, "A compact base station for small cells". *Third Nordic Seminar on Digital Land Mobile Radio Communications*, Copenhagen, 1988.
- [3] H.Scheuermann, H.Gockler, "A comprehensive survey of digital transmultiplexing methods". *Proceedings of the IEEE*, Vol 69, No. 11, pp 1419-1450, 1981.
- [4] A.D.Craig, C.K.Leong & A. Wishart, "Digital Signal Processing in Communications Satellite Payloads", *Electronics and Communication Engineering Journal*, pp 107-114, June 1992.
- [5] W.C.Y.Lee, *Mobile Cellular Telecommunications Systems*, McGraw Hill, pp 215, 1990.
- [6] F.E.Churchill, G.W.Ogar, B.J.Thompson, "The correction of I&Q errors in a coherent processor", *IEEE transactions on Aerospace & Electronic systems*, Vol AES-17, No 1, pp131-137, Jan 1988.
- [7] J.K.Cavers & M.Liao, "Adaptive compensation for imbalance and offset losses in direct conversion transceivers", *IEEE transactions on Vehicular Technology*, pp 581-588, Nov. 1993.
- [8] M.Faulkner, T.Mattsson, W.Yates, "Automatic adjustment of quadrature modulators", *Electronic letters*, Vol 27, (3), pp 214-216, 1991.
- [9] D.Hilborn, S.P.Stapleton and J.K.Cavers, "An adaptive direct conversion transmitter", *42nd Vehicular Technology Conference*, pp 764-767, May 1992.
- [10] A.I.Sinsky & P.C.P.Wang, "Error Analysis of a quadrature coherent detector processor", *IEEE Transactions on Aerospace & Electronic Systems*, vol AES-17, No 1, pp 880-883, Nov. 1974.

The Effect of Reconstruction Filters on Direct Upconversion in a Multichannel Environment

Scott A. Leyonhjelm, Student Member, IEEE, and Michael Faulkner, Member, IEEE.

Mobile Communications and Signal Processing Group,

Department of Electrical & Electronic Engineering,

Victoria University of Technology,

PO Box 14428 MMC, Melbourne, VIC 3000, AUSTRALIA.

Email: scott@cabsav.vut.edu.au or mf@cabsav.vut.edu.au

Abstract - The effect of reconstruction filters on direct upconversion is analysed in a multichannel environment. It is shown that the reconstruction filters cause gain and phase imbalances to be frequency dependant, a significant issue when considering the stringent ACI requirements for radio communication systems. The paper introduces an adaptive compensation technique as a means of overcoming these frequency dependant imbalances. Additionally the error vector between the mismatched filters is shown to be directly related to the amount of sideband rejection. This analysis is then used to develop a methodology for analysing the performance of the novel compensation technique with respect to the mismatched filters. Analysis of the classical all-pole filter algorithms reveal the sensitivity of direct upconversion in a multichannel environment to filter order, type, percentage mismatch and differing ACI level.

I. INTRODUCTION

Recent advances in the wideband linearisation of amplifiers suggest that Frequency Division Multiplex (FDM) systems can now be combined at low power levels [1-2]. The low power combination of channels can occur in a DSP environment, before being upconverted and amplified by a linear wideband amplifier, as illustrated below.

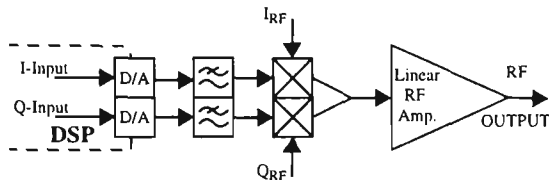


Fig. 1. Analog Quadrature Modulation Upconversion

This paper considers direct upconversion, using an analog quadrature modulator. This technique of upconversion has recently gained a lot of attention due to its suitability as a universal modulator (and demodulator); it is simple, small and has low power consumption. However a mismatch in the In phase and Quadrature (IQ) channels results in an undesired sideband, the magnitude of which is dependant upon the size of the gain and phase errors (imbalances) between the channels [3]. The imbalances are attributed to the non-ideal characteristics of the components, the mixers, summer, splitter and reconstruction filters. It is reasonable to talk of component imbalances (neglecting the reconstruction filters) of 0.3 dB and 3° in a well designed analog quadrature modulator.

Imbalances of this magnitude would result in 30 dB of sideband rejection, sufficient for some single channel applications.

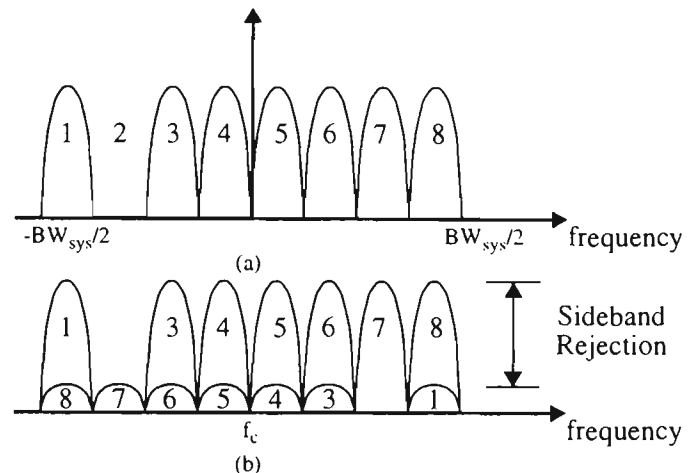


Fig. 2. The effect of phase and gain imbalances in an analog quadrature modulator (a) Original signal displayed in complex baseband format. (b) Desired and sideband (image) signals after passing through an unbalanced quadrature modulator.

The wideband upconversion application highlights a unique problem. A wideband FDM signal, Fig 2a, when passed through an unbalanced quadrature modulator, will result in both desired and sideband signals, Fig 2b. However different amounts of sideband rejection can be tolerated in a multichannel system.

If the sideband signal falls into a channel that is being used then it will distort the desired signal (channel 1 in Fig. 2b), as is the situation for a single channel quadrature modulator. The required sideband rejection is related to the E_b/N_o performance of the modulation. For example to achieve a bit error rate of 10^{-3} using the QPSK modulation technique the required E_b/N_o is 7.5 dB [4] (Note : $S/N \sim 2 * E_b/N_o$ for QPSK). For the NADC system which uses QPSK, the distortion introduced by the imbalances would want to be 10 dB below this level so that there is no noticeable effect. Additionally if power control is employed (35 dB from NADC specifications) then sideband rejection should be in the order of 50 to 60 dB so not to affect the error rate performance of the system.

The sideband signal could equally fall into a vacant channel position (channel 7 in Fig. 2b). In this situation the system

must meet the ACI specifications of the system which are normally specified between -50 dBc and -70 dBc, for Mobile Satellite and Private Mobile Radio (PMR) systems respectively.

The analog quadrature modulator is therefore not usable in a multichannel environment without some form of refinement. A number of correction techniques have subsequently evolved [5-9], all have concentrated on a single channel application. Implementation of one such correction technique, utilising the CRISIS network [8], corrected gain and phase imbalances to 0.02dB and 0.4° respectively. This is equivalent to 49 dB sideband rejection, a definite improvement, but unacceptable in most multichannel applications. Additionally the effectiveness of current compensation techniques decreases dramatically when the reconstruction filters are mismatched.

Previous analysis has generally neglected the significance of the effect of a mismatch in the reconstruction filters. It has been reported [10] that "in a predistortion linearising system the reconstruction filters are a major source of error", but the analysis was restricted to a single channel (narrowband) system with predistortion.

The next section describes a novel compensation technique that is applicable to a multichannel environment. Whereas previous compensation techniques have only compensated for a single gain and phase imbalance, this novel method cancels at a number of frequencies across the system bandwidth.

Section III shows that the reconstruction filters are the major contributor to frequency dependant imbalances across a wide band and then mathematically analyses the effect of frequency dependant imbalances on the sideband signal. It is shown that the error vector between the reconstruction filters in the IQ channels is related directly to the amount of sideband rejection.

Section IV uses the relationship found in section III to develop a methodology for analysing the performance of mismatched filters driving an analog quadrature modulator. Two parameters, oversampling ratio and 'channel to system bandwidth' ratio, are introduced to objectively judge the performance of the multichannel adaptive compensation technique.

Analysis of the classical all-pole filter algorithms reveal the sensitivity of filter order, filter type, percentage mismatch and differing ACI specification in the novel compensation technique.

II. A NOVEL METHOD FOR THE COMPENSATION OF GAIN AND PHASE IMBALANCES

The novelty of the technique revolves around the wideband low-level combiner, which is based on transmultiplexer technology. Transmultiplexers make use of the inherent redundancies of interpolation (N padded zeroes) and the uniform spacing of the channels to form an efficient multirate algorithm [11].

Figure 3 illustrates the proposed technique. N channels are combined through a transmultiplexer to form a wideband signal (as shown in Fig. 2a). The system bandwidth is then directly upconverted via an analog quadrature modulator. The inherent gain and phase imbalances will cause undesired

sideband signals (as shown in Fig. 2b). The compensation method deliberately introduces a sideband component (through the complex coefficient C_m) which cancels the undesired sideband. The adaption technique measures the sideband power in a vacant channel using a tuned receiver (error sensing circuitry in Fig. 3) and adjusts the complex coefficient (C_m) to minimise the power of the undesired signal.

The process described above is repeated for every channel in the system but only whilst the channel is vacant. The update rate is slow but this is not considered a problem as the gain and phase imbalances drift slowly with time.

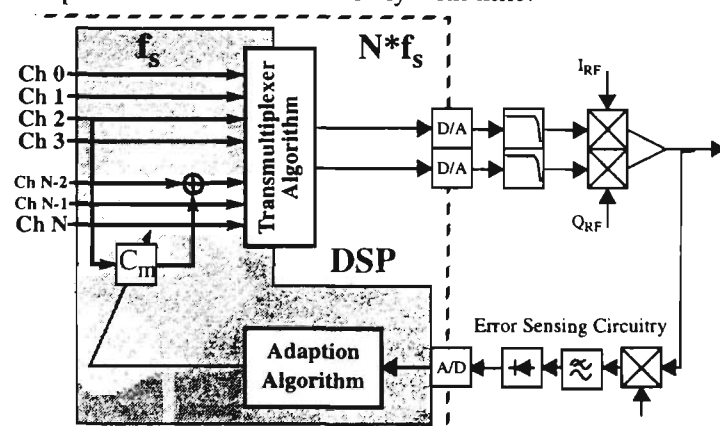


Fig. 3. Multichannel adaptive compensation technique for correcting gain and phase imbalances.

The compensation technique described has a number of advantages over previous adaptive correction techniques.

- *Reduced Computational Load* - The adaption algorithm and the scaling coefficient operate at the channel sampling rate, as opposed to the output sampling rate.
- *Corrects for Frequency Dependant Imbalances across the System Bandwidth* - Previous techniques only compensate for a single bulk gain and phase imbalance across the system band.
- *Increased Sensitivity of Feedback Signal* - This technique detects only the undesired signal, as opposed to both the desired and undesired signal [8], thus increasing the dynamic range of the correction network.

For an uncorrected analog quadrature modulator the power of the sideband will exceed ACI specifications (Fig. 4a). In practice it is necessary to reduce the power in the sideband to comply with a given ACI specification and so there is room for non-ideal cancellation. The multichannel compensation technique exploits this fact by cancelling the phase and gain imbalance at a single frequency (bulk imbalance) and the sideband will be completely removed at this frequency. However the frequency dependant imbalances mean that a differential phase and gain imbalance will remain across the remainder of the channel (differential imbalance), causing a residual sideband response (Fig. 4b).

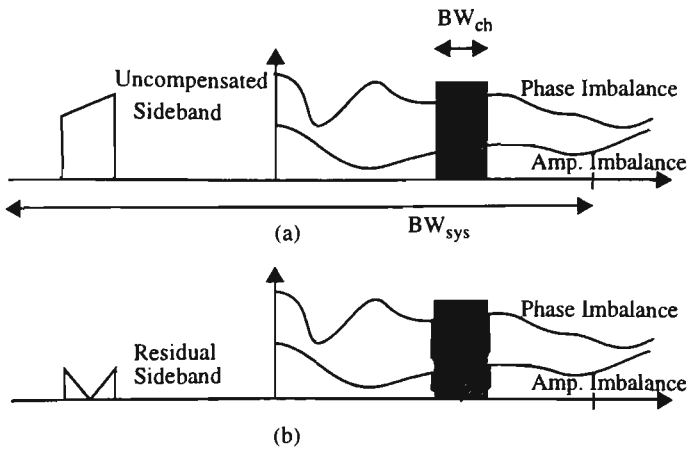


Fig. 4. (a) Sideband response due to frequency dependant imbalances (b) Sideband response after cancellation of the channels bulk imbalance.

To comply with an ACI specification the following condition must hold :

$$ACI = 10 \log \frac{\text{Power in Sideband}}{\text{Power in Signal}} \text{ dB} \quad (1)$$

The ability to quantify the frequency dependant imbalances is important in analysing the performance of the multichannel adaptive compensation technique.

III. ANALYSIS OF FREQUENCY DEPENDANT IMBALANCES

A. Causes of frequency dependant imbalance in a direct upconverter

Frequency dependant gain and phase imbalances arise from both the quadrature modulator and the mismatch in the reconstruction filters.

The quadrature modulator consists of the mixer, splitter and summer components. The gain and phase through each of these components is dependant on frequency to some extent, although the amount of dependence will depend on the complex design strategies employed. This issue is beyond the scope of the paper.

A typical Mini Circuits IQ Modulator was chosen as an example (Table I generated from data sheet). It can be seen that over a channel bandwidth of 5 MHz around 54 dB of sideband rejection exists if the bulk imbalance is removed (leaving the differential imbalance). Whilst over 70 dB could be achieved if the bandwidth was reduced below 100 kHz.

Table I

Absolute variation of gain and phase imbalance across a specified bandwidth for a Mini Circuits IQ Modulator (MIQD 895)

Bandwidth	Differential gain Variation (dB)	Differential Phase Variation (degree)	Residual Sideband
100 kHz	0.01	0.05	-70 dB
500 kHz	0.02	0.10	-64 dB
5 MHz	0.05	0.30	-54 dB

In most communication systems utilizing the FDM format the channel bandwidth is less than 200 kHz. Therefore to meet ACI specifications of 70dB, the quadrature modulator would have to produce a slightly better performance than this example. Assuming that this is possible the quadrature modulator can be considered to have constant bulk imbalance across the channel band.

Frequency dependence is then apportioned entirely to the reconstruction filters, which will now be analysed.

B. Mathematical Analysis - The effect of filter mismatch on the sideband signal

To analyse the effects of filter mismatch, the reconstruction filters are modelled with relative gain mismatch, $\alpha(f)$, and phase error from quadrature, $\Phi_e(f)$ (radians). The variable $\beta(f)$ is used to account for the absolute attenuation characteristic (or gain transfer function) of the filter and serves to normalise the magnitude at any frequency.

Let the gain of the I path be given by transfer function, $\beta(f)$, of the ideal filter in question :

$$\beta(f) = \beta(f)(1 + (\alpha(f)/2)) - \beta(f) \cdot \alpha(f)/2 \quad (2)$$

and the gain of the Q path be given by a percentage change, $\beta(f) \cdot \alpha(f)$, in the transfer function of the ideal filter :

$$\beta(f)(1 + \alpha(f)) = \beta(f)(1 + (\alpha(f)/2)) + \beta(f) \cdot \alpha(f)/2 \quad (3)$$

Similarly the phase mismatch between the filters is split equally between the two paths, $\Phi_e(f)/2$. The quadrature modulator and DAC's are assumed to be ideal. These assumptions isolate the reconstruction filters as the source of error, Fig. 5 summarises the model :

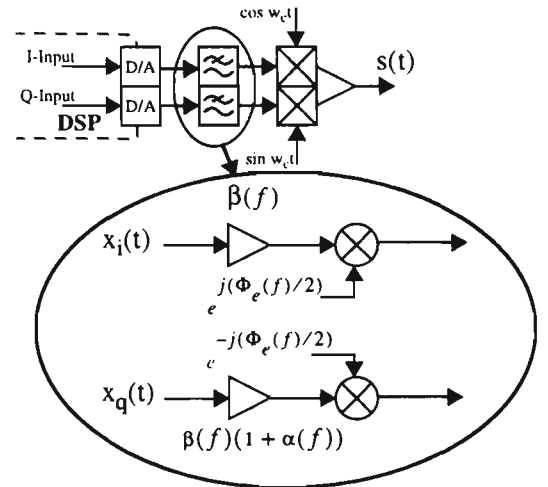


Fig. 5. Modelling the mismatch between reconstruction filters

The quadrature signal that is driven from the DSP, can be represented as a complex signal with a real (I channel) and an imaginary (Q channel) component. The same signal can be represented as a vector with an instantaneous magnitude and phase :

$$\begin{aligned} r(t) &= x_i(t) + jx_q(t) \\ &= |r(t)|e^{j\phi(t)} \end{aligned} \quad (4)$$

If there is no mismatch between the filters then the

upconverted signal is given by :

$$s(t) = \text{Re} \left\{ r(t) \cdot e^{j\omega_c t} \right\} \quad (5)$$

The mismatch in the reconstruction filter design causes the original signal to be distorted (additional sideband component) when it is translated to the carrier frequency. The output, $s(t)$, from the direct converter shown in Fig. 3 is given by the following equation :

$$s(t) = \text{Re} \left\{ \beta(f) \left(1 + \frac{\alpha(f)}{2} \right) \cdot \begin{pmatrix} |r(t)| e^{j\phi(t)} \cos\left(\frac{\Phi_e(f)}{2}\right) + \\ j|r(t)| e^{-j\phi(t)} \sin\left(\frac{\Phi_e(f)}{2}\right) \end{pmatrix} e^{j\omega_c t} \right. \\ \left. + \beta(f) \left(\frac{\alpha(f)}{2} \right) \cdot \begin{pmatrix} |r(t)| e^{j\phi(t)} \cos\left(\frac{\Phi_e(f)}{2}\right) + \\ j|r(t)| e^{-j\phi(t)} \sin\left(\frac{\Phi_e(f)}{2}\right) \end{pmatrix} e^{-j\omega_c t} \right\} \quad (6)$$

After mathematical analysis Eqn. (6) can be shown to be equivalent to :

$$s(t) = \beta(f) \left(1 + \frac{\alpha(f)}{2} \right) \cos\left(\frac{\Phi_e(f)}{2}\right) |r(t)| \cos(\omega_c t + \phi(t)) - \\ \beta(f) \left(1 + \frac{\alpha(f)}{2} \right) \sin\left(\frac{\Phi_e(f)}{2}\right) |r(t)| \sin(\omega_c t - \phi(t)) + \\ \beta(f) \left(\frac{\alpha(f)}{2} \right) \cos\left(\frac{\Phi_e(f)}{2}\right) |r(t)| \cos(\omega_c t - \phi(t)) + \\ \beta(f) \left(\frac{\alpha(f)}{2} \right) \sin\left(\frac{\Phi_e(f)}{2}\right) |r(t)| \sin(\omega_c t + \phi(t)) \quad (7)$$

Equation (7) mathematically describes four signals that are generated by the mismatch between the reconstruction filters. By selecting a complex plane that is referenced to the carrier frequency of the quadrature modulator, the four signals can be represented as baseband complex vectors :

$$u_1(t) = \beta(f) \left(1 + \frac{\alpha(f)}{2} \right) \cos\left(\frac{\Phi_e(f)}{2}\right) \cdot r(t) \quad (8)$$

$$u_2(t) = \beta(f) \left(\frac{\alpha(f)}{2} \right) \sin\left(\frac{\Phi_e(f)}{2}\right) e^{j\frac{\pi}{2}} \cdot r(t) \quad (9)$$

$$v_1(t) = \beta(f) \left(\frac{\alpha(f)}{2} \right) \cos\left(\frac{\Phi_e(f)}{2}\right) \cdot r^*(t) \quad (10)$$

$$v_2(t) = \beta(f) \left(1 + \frac{\alpha(f)}{2} \right) \sin\left(\frac{\Phi_e(f)}{2}\right) e^{j\frac{\pi}{2}} \cdot r^*(t) \quad (11)$$

They have been classified as a desired ($u(t)$) signal or a sideband ($v(t)$) signal. The desired signals are determined from the fact that they rotate in the same direction as the original signal, $r(t)$. Whereas the sideband signals rotate in the reverse direction, thus appearing in the mirror image position illustrated in Fig. 2b. The four vectors are illustrated

below :

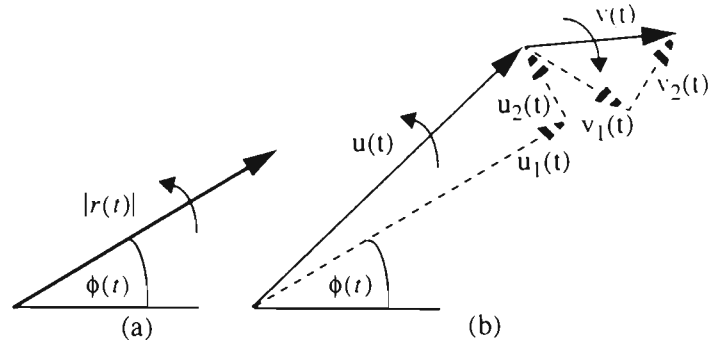


Fig. 6. Vector representation of (a) Undistorted signal - $r(t)$ (b) Distorted signals due to direct conversion imbalances.

Fig. 6a represents the original signal upconverted to the carrier frequency by an ideal quadrature modulator. If the quadrature modulator was non-ideal, as modelled in Fig. 5, the original signal would be distorted to form four vectors as shown in Fig. 6b, and described by Eqn. (8) to (11). The sideband signal is therefore the vector sum of Eqn. (10) and (11):

$$v(t) = r^*(t) \cdot \beta(f) \left(\left(\frac{\alpha(f)}{2} \right) \cos\left(\frac{\Phi_e(f)}{2}\right) + j \left(1 + \frac{\alpha(f)}{2} \right) \sin\left(\frac{\Phi_e(f)}{2}\right) \right) \\ \approx r^*(t) \cdot \beta(f) \left(\frac{\alpha(f)}{2} + j \left(1 + \frac{\alpha(f)}{2} \right) \frac{\Phi_e(f)}{2} \right) \quad (12)$$

Eqn. (12) shows that the sideband signal can be represented as the complex conjugate of the original signal multiplied by a complex coefficient, which is a function of both gain and phase imbalance. From Eqn. (12) the approximate absolute magnitude of the sideband signal is :

$$|v(t)| \approx \frac{\beta(f) \sqrt{\alpha(f)^2 + \Phi_e(f)^2}}{2} \quad (13)$$

From the vector addition of Eqn. (8) and (9), the approximate magnitude of the wanted signal can be shown to be approximately $\beta(f)$. Therefore the amount of sideband rejection is given as the absolute magnitude of the image vector divided by the absolute magnitude of the wanted signal (the form of which is same to the static case analysed in [3]):

$$\text{Sideband Rejection} = \frac{|v(t)|}{|u(t)|} \\ \approx \frac{\sqrt{\alpha(f)^2 + \Phi_e(f)^2}}{2} \quad (14)$$

An alternative way of visualising the previous analysis is to consider the I and Q path filters as vectors. When they are matched they are both equal in magnitude and phase (Fig. 7a), subsequently causing no distortion or sideband response. When the filters are mismatched there exists a phase and gain difference (frequency dependance), this is illustrated in Fig. 7b.

It can be shown that the error vector is related to the Sideband rejection by :

$$\text{Sideband rejection} = \frac{|\text{error_vector}|}{2 \cdot \beta(f)} \quad (15)$$

This can be verified by calculating the magnitude of the

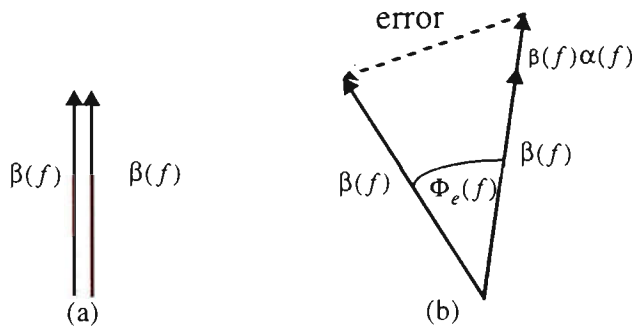


Fig. 7. (a) I and Q path filters matched (b) I and Q path filters mismatched error vector in Fig. 7b for small gain and phase imbalances and comparing it to the approximate sideband rejection calculated in Eqn. (14).

For typical values of ACI specified by radio communication systems the sideband has to be of a magnitude that infers very small gain and phase mismatch. The magnitude of sideband rejection can therefore be accurately predicted from Eqn. (14).

A means of comparing the performance of the multichannel compensation technique is now introduced.

IV. METHODOLOGY FOR ANALYSING THE EFFECT OF MISMATCHED RECONSTRUCTION FILTERS.

The methodology calls for a relative comparison of performance when adjusting parameters relevant to filters. It is based on modelling the mismatch between the filters as a percentage increase in the cut-off frequency of one filter. This has limitations, especially when considering the real implementation issues of filters, but for practical analysis purposes it is seen as a realistic yardstick. The relative performance of a particular filter will then be judged by two parameters, the oversampling ratio and 'channel to system bandwidth' (number of channels) ratio. A discussion on how these parameters are calculated is now presented.

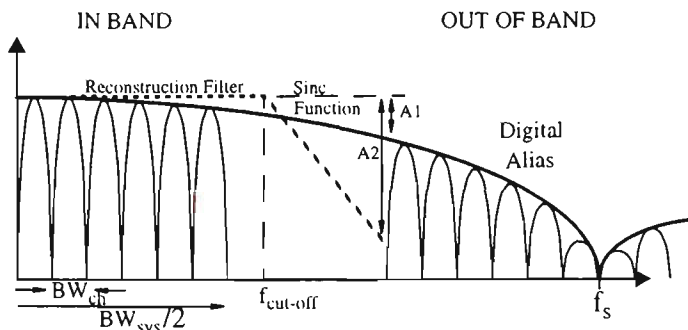


Fig. 8. Overview of Communication System Parameters relevant to Direct Upconversion and a Multichannel Environment.

For the purpose of analysis the communication system, will be defined in terms of three parameters :

- Channel Bandwidth - BW_{ch}
- System Bandwidth - BW_{sys}
- and the Adjacent Channel Interference specification - ACI.

To meet the ACI specification of a communication system two objectives must be achieved :

- In System Band : Given a percentage mismatch

between the two quadrature filters, the sideband rejection must comply with the ACI specification for the system, as given by the Eqn (1).

- Out of System Band : The digital alias must be attenuated below the same ACI specification for the system. This is achieved by the reconstruction filter (A2) and the sinc response of the D/A converters (A1).

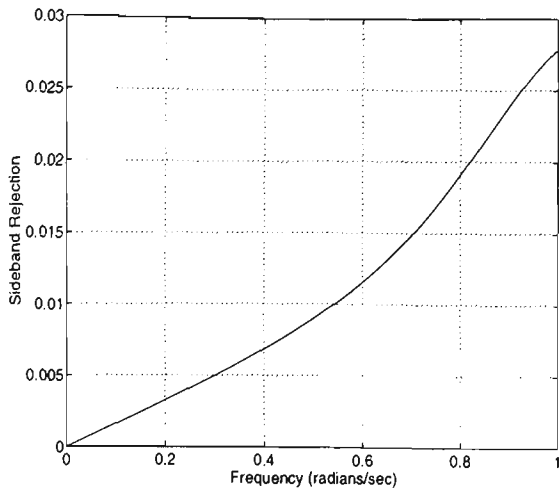
The number of channels is derived solely from the In System Band objective. The mismatch between the filters creates frequency dependant imbalances that require periodic cancellation across the system band to meet a given ACI specification. The worse the mismatch between the filters then the smaller the channel bandwidth must be so that after cancellation the power of the residual sideband complies with ACI specifications. For a fixed system bandwidth this can be equally expressed as more channels, where the number of channels is related to the channel bandwidth by :

$$N_{ch} = \frac{BW_{sys}}{BW_{ch}} \quad (16)$$

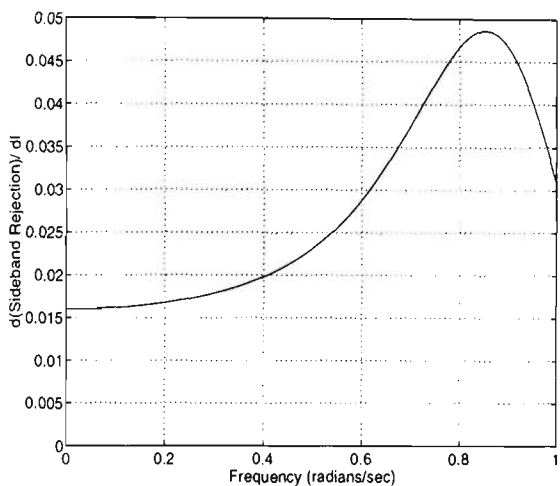
The number of channels is essentially a measure of the frequency dependant mismatch in the system.

To illustrate how the number of channels are calculated a fifth order Butterworth filter is used as a case study. The error vector between the two filters is used to calculate the sideband rejection, Eqn. (15). Fig. 9a illustrates the amount of sideband rejection (amplitude) for a 1% mismatch in the reconstruction filters cut-off frequency. Note that the filters cut-off frequency has been normalised to 1 rads/sec. Here the filters are perfectly matched at DC (no sideband) whilst throughout the passband a sideband magnitude exists, this is due to the frequency dependant imbalance.

To calculate the number of channels needed it is more instructive to view the gradient of the sideband rejection across the passband of the filter , as illustrated in Fig. 9b.



(a)



(b)

Fig. 9. Fifth order Butterworth filter with 1% mismatch in the cut-off frequency (a) Sideband rejection (b) Gradient of sideband rejection.

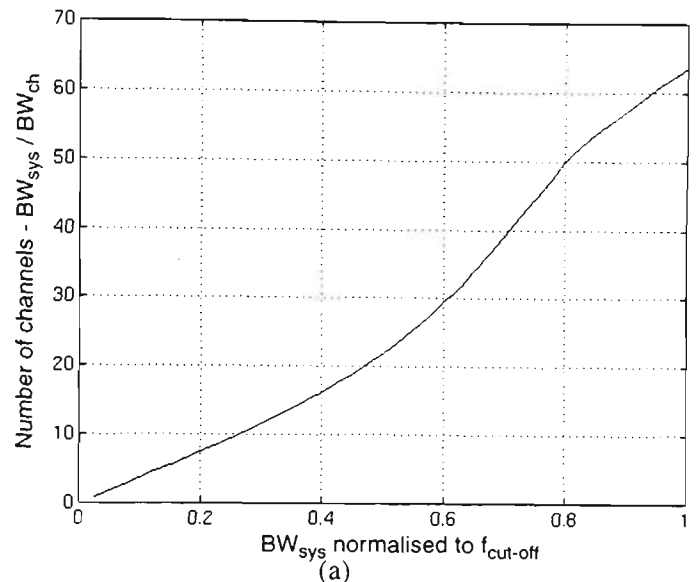
The multichannel adaptive compensation technique will cancel a single frequency in every channel, however total cancellation across the channel band does not occur rather a residual sideband will exist as shown in Fig 4b.

If the gradient is assumed constant across the channel band then a first order approximation can be assumed for calculating the power in the sideband. That is the sideband amplitude resembles a triangular function (power approximates a square law function) given that the desired signal occupies the full channel bandwidth.

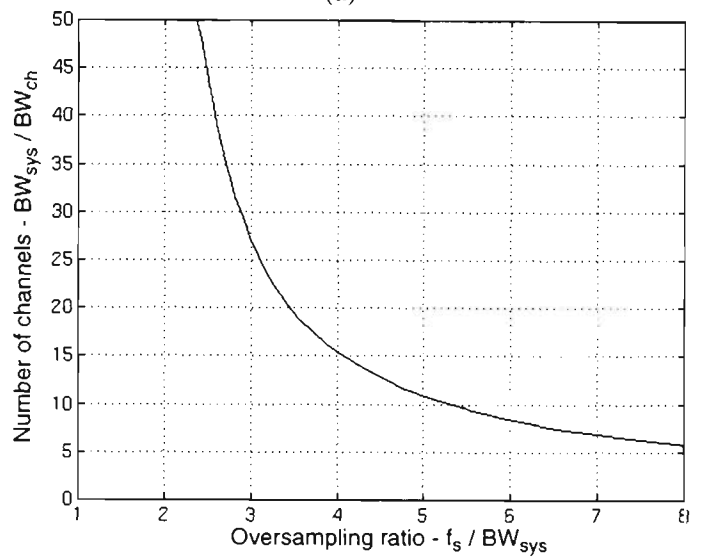
It is assumed that the largest gradient to occur across the system bandwidth (which is a fraction of the cut-off frequency) is taken as the absolute constant gradient across any channel, a worst case scenario.

Given the above and using Eqn. (1), the minimum number of channels is related to the system ACI specification :

$$N_{ch} = \frac{BW_{sys} \times \sqrt{\frac{d(\text{sideband rejection})}{df}}}{10^{ACI/20} \times \sqrt{12}} \quad (17)$$



(a)



(b)

Fig. 10. Fifth order Butterworth filter with 1% mismatch in the cut-off frequency complying with a 60 dB ACI specification (a) In System Band objective (b) Combination of In and Out Of System Band Objectives.

By varying the system bandwidth the minimum number of channels needed to comply with the systems ACI specification can be plotted as shown in Fig. 10a. As expected, more channels are needed as the system bandwidth approaches the cut-off frequency of the filter.

The second objective, Out of System Band, is achieved by attenuating the sampling aliases below the ACI specification. The filter attenuation characteristic will dominate the absolute sampling rate required to achieve this condition. The sampling frequency has been normalised to the Nyquist sampling rate of the system, BW_{sys} . This is expressed as the oversampling ratio :

$$\text{Oversampling Ratio} = \frac{f_s}{BW_{sys}} \quad (18)$$

By combining the In and Out of System Band objectives the minimum number of channels can be related to the oversampling ratio for a given mismatch and system ACI specification, Fig. 10b. This methodology is now used to

comparatively analyse the performance of the filters by modifying different parameters.

V. NUMERICAL COMPUTATION AND ANALYSIS

The effect of mismatched reconstruction filters driving an analog quadrature modulator has been shown to introduce frequency dependant imbalances. These imbalances can be corrected by the adaptive compensation technique introduced in Section II. However the amount of mismatch in the reconstruction filters will put certain restrictions on the design, that is the number of channels and the oversampling ratio needed to comply with the systems ACI specification.

By varying different parameters the methodology, which relates the number of channels in a communication system to the oversampling ratio, can be used to analyse the effect on performance.

Four parameters are considered :

A. Filter Mismatch

Increasing the mismatch between the filters is the same as increasing the tolerance of the components used in implementing the filter. This effect has been modelled as a percentage shift in the cut-off frequency.

For a small number of channels the oversampling ratio increases with an increase in percentage mismatch (Fig. 11a). However in a system with a large number of channels (140 and upwards) the amount of mismatch (as long as it is less than 5 %) becomes irrelevant as the oversampling limit (vertical asymptote in Fig. 11a) is reached.

The oversampling limit occurs when the system bandwidth equals the cutoff frequency, it is possible to go beyond this point by pre-emphasising the outer channels but this will not be considered here. The In System Band condition therefore determines the minimum number of channels, any further increase in the number of channels will improve the undesired sideband to further below the ACI specification (In System Band condition) but will have no effect on the oversampling ratio. This is because the system bandwidth cannot be extended further and therefore the Out of System Band objective, which is not dependant on percentage mismatch, will govern the lowest oversampling ratio.

It can be concluded that the filters must be able to be designed to meet tight specifications and also be reliably reproduced in the manufacturing process.

B. ACI Specification

Increasing the ACI specification has a similar effect to increasing the percentage mismatch. Fig. 11b illustrates that the larger the ACI specification the higher the oversampling ratio required for a fixed number of channels. This is especially important for a small number of channels, say around 20, which for 70 dB ACI would require an oversampling ratio greater than 8. Depending on the bandwidth of the channel, such a large oversampling ratio will place severe limitations on the bandwidth of the system, primarily due to the sampling frequency that would be required for the digital processing.

Notice also that the oversampling limit decreases with a lowering of the systems ACI specification. To further lower this limit the filter order would have to be increased.

C. Filter Type

The filters chosen contribute one desirable characteristic each; Maximum flat amplitude response, maximal flat group delay and the steepest roll-off obtained by the Butterworth, Bessel and Chebychev filters respectively. The cut-off frequency is defined as the frequency for which the filter attenuation has reached 3 dB.

The Chebychev filter is shown in Fig. 11c to have the best overall performance. The lowest oversampling limit is achieved by a higher ripple in the Chebychev filter, this is due to the inherently steeper roll-off. It is difficult to discern from Fig. 11c whether varying the ripple of the Chebychev filter increases performance below the oversampling limit. However as the ripple approaches zero the Chebychev response will approach the Butterworth response.

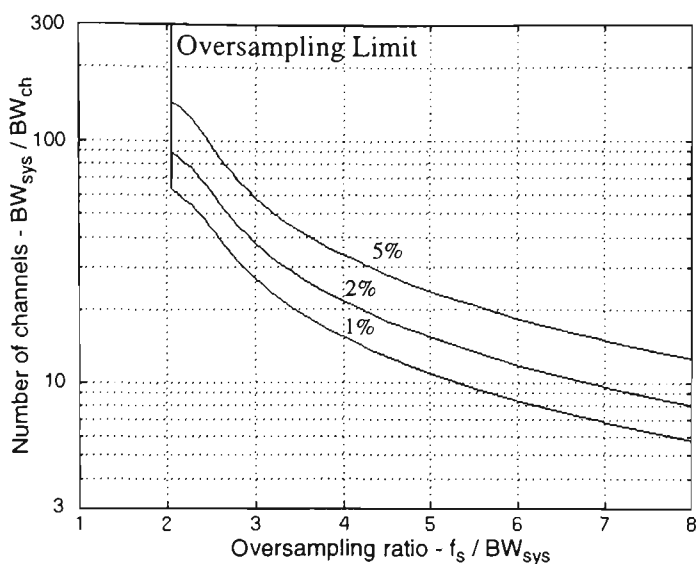
The Butterworth filter is comparable to the Chebychev filter, although it consistently has worse performance (albeit slightly).

The Bessel filter has difficulties achieving a low oversampling ratio, for a fifth order Bessel its oversampling limit is 2.8. This is mainly due to its relatively slow roll-off and could be lowered by using a higher order filter.

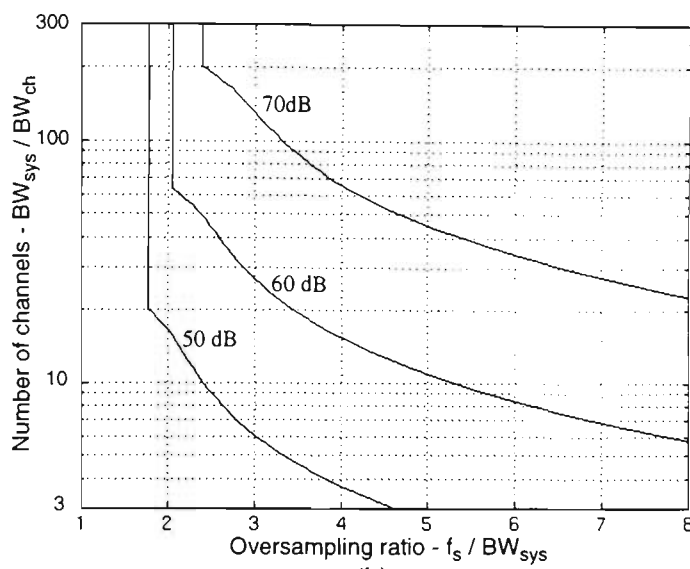
D. Filter Order

Increasing the filter order lowers the oversampling limit because of the steeper roll-off. However for an increase in order there is not an equivalent improvement in performance, because a steeper roll-off is accompanied by a larger In System Band gradient. For example a system with 10 channels a fourth and sixth order filter requires an oversampling ratio of 6 and 5 respectively. Whereas increasing the order of the filter to ten has small gain in performance, the oversampling ratio is 4.7.

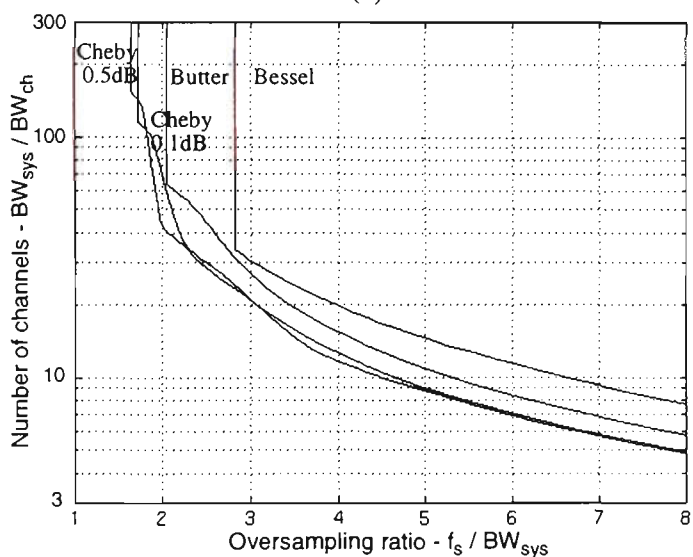
In a system that has many channels it would be better to use a higher order filter as long as the percentage mismatch could be guaranteed. The higher the filter order the more sensitive it is to component tolerances and its overall percentage mismatch will rise. However for a system with a small number of channels a lower order filter should be employed because of its reduced complexity and comparative performance to higher order filters.



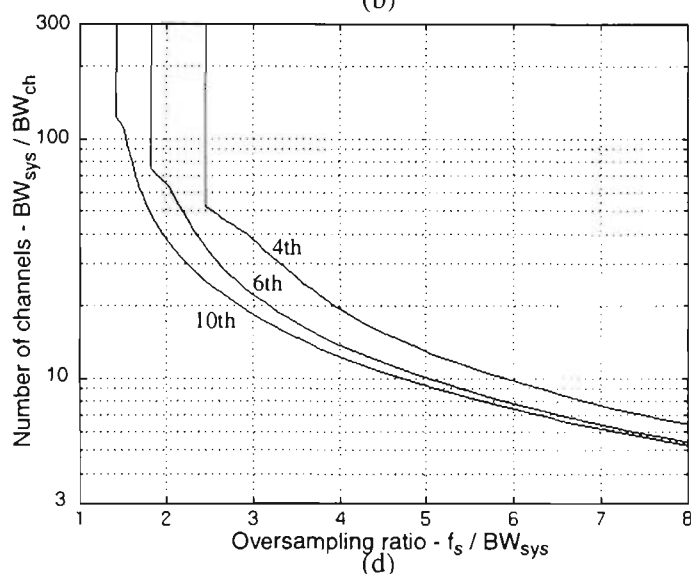
(a)



(b)



(c)



(d)

Fig. 11. Fifth order Butterworth filter with a 1% mismatch in the cut-off frequency and complies with a system specification of 60 dB ACI is assumed unless otherwise stated (a) Percentage mismatch in the cut-off frequency varied (b) ACI specification varied. (c) Fifth order Chebychev (0.1 dB & 0.5 dB ripple), Bessel & Butterworth Filter types (d) Butterworth 4th, 6th & 10th order filters

V. CONCLUSION

Mismatch between the reconstruction filters produce frequency dependant imbalances that cause undesired sideband responses in a multichannel environment. A novel adaptive compensation technique has been introduced to reduce these sideband signals to comply with radio communication system ACI specifications, nominally 50 to 70 dB. The ability to correct for frequency dependant imbalances and the fact that the correction occurs at the channel sampling frequency are the two distinct advantages this technique possesses over previous adaptive compensation techniques.

Analysis of the frequency dependant imbalances yielded a relationship between the error vector of two mismatched filters and the amount of sideband rejection (ACI). This relationship was used to develop a methodology that related

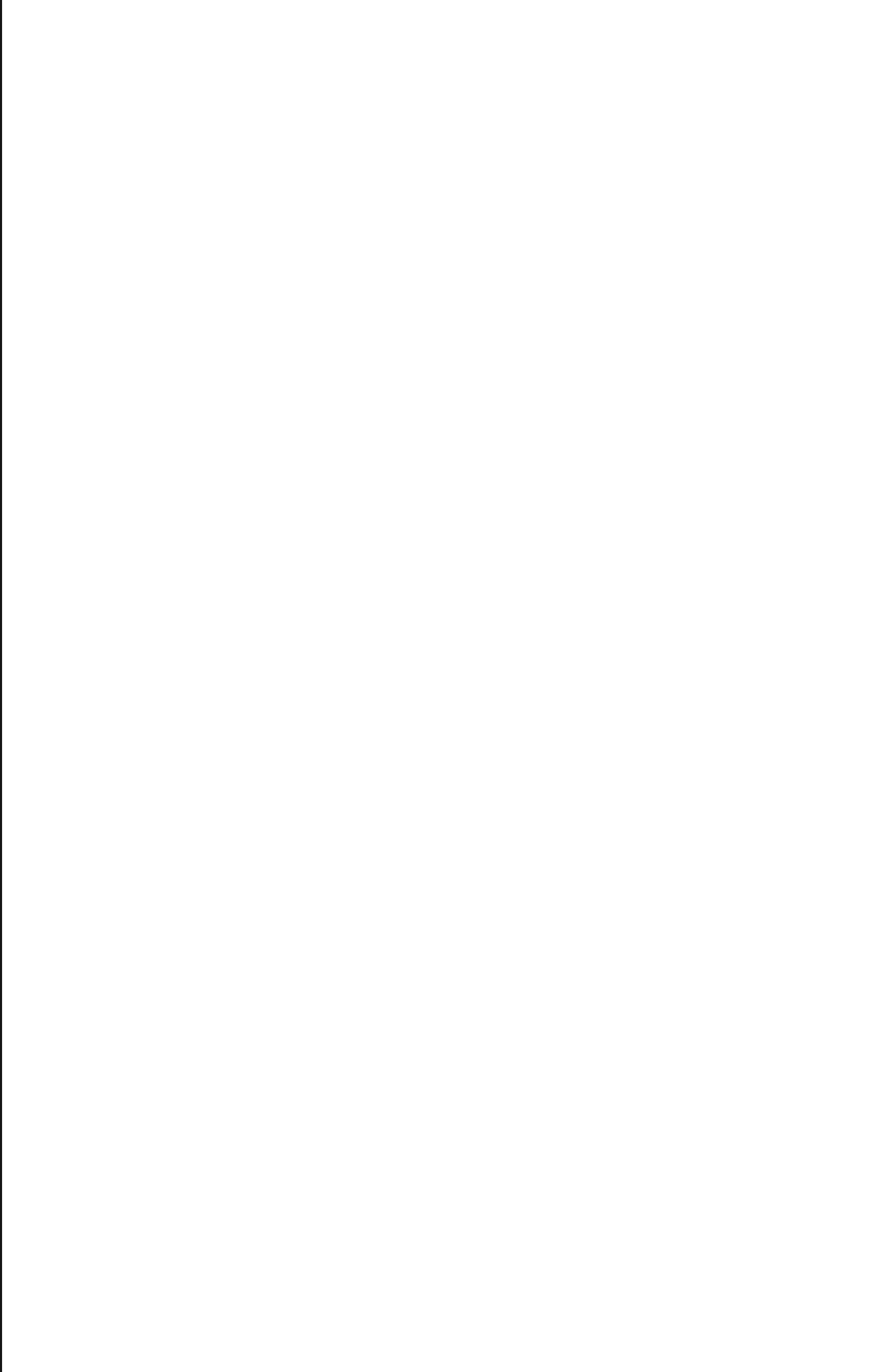
the number of channels to the oversampling ratio required to comply with a communication system ACI specification when the new adaptive compensation technique was employed.

The methodology objectively compared the performance of the system when four parameters were varied. The main objective was to keep the oversampling ratio as low as possible, both for technology and power consumption reasons.

It was found that the Chebychev filter offered the best overall performance no matter how many channels existed in the system. The order of the filter should be then chosen on the size of the system. For small systems (less than 10 channels) a low order filter offered lower complexity with comparable performance, however for larger systems a higher order filter offers increased performance. However for higher order filters an anomaly exists; due to their higher complexity they will be more sensitive to component tolerances, and therefore their ultimate performance will be degraded. Ultimately the achievable tolerance of the filter is the highest priority design issue.

REFERENCES

- [1] A.K.Johnson & R.Myer, "Linear amplifier combiner", *IEEE Vehicular Technology Conference*, Tampa, Florida, pp 422-423,1987.
- [2] J.Stefanov, "A compact base station for small cells", Department of Electronics and Computer Science, The University of Southampton England.
- [3] A.I.Sinsky & P.C.P.Wang, "Error Analysis of a quadrature coherent detector processor", *IEEE Transactions on Aerospace and Electronic Systems*, vol. AES-10, pp 880-883, Nov. 1974.
- [4] S. Haykin, *Digital Communications*, John Wiley & Sons, Inc., 1988.
- [5] F.E.Churchill,G.W.Ogar,B.J.Thompson, "The correction of I&Q errors in a coherent processor", *IEEE transactions on aerospace & electronic systems*, Vol AES-17, No 1, pp131-136, Jan 1988.
- [6] A.E.Jones and J.G.Gardiner, "Phase Error Correcting Vector Modulator for Personal Communications Network (PCN) Transceivers", *Electronic letters*, Vol 27, (14), pp 1231-1232, July 1991.
- [7] J.K.Cavers,M.Liao, "Adaptive compensation for imbalance and offset losses in direct conversion transceivers", *IEEE Vehicular Technology Conference*, St Louis, pp 578-583, 1991.
- [8] M.Faulkner,T.Mattson,W.Yates, "Automatic adjustment of quadrature modulators", *Electronic letters*, Vol 27, (3), pp 214-216, Jan. 1991.
- [9] D.Hilborn,S.P.Stapleton and J.K.Cavers,"An adaptive direct conversion transmitter", *IEEE Transactions on Vehicular Technology*
- [10] L.Sundstrom, M Faulkner, "The effect of reconstruction filtering on the predistortion linearisation of RF power amplifiers", *Mobile & Personal Communication Systems*, Adelaide, Australia, pp 357-361, 12-13 Nov. 1992.
- [11] R.E. Crochiere & L.R. Rabiner, *Multirate Digital Signal Processing*, New Jersey : Prentice-Hall, Inc. 1983.



An Efficient Implementation of Bandlimited Dithering

Abstract: A simple implementation of bandlimited dithering using halfband interpolation filters is described. Measurements show that the performance of a 9 bit DAC is improved by 4 dB at the expense of a small increase, 3.4%, in total die area of a halfband interpolator ASIC.

Scott A. Leyonhjelm, Michael Faulkner and Peter Nilsson

Introduction:

The quantisation error of a practical Digital to Analogue Converter (DAC) with non-evenly spaced quantisation levels will introduce signal dependant harmonic and intermodulation products which cannot be accurately modelled by the additive white noise model [1]. These spurious responses cause problems. For example in the application of multichannel radio base station transmitters the problem arises because the spuri fall into neighbouring channels.

The addition of a wideband noise signal (dithering) before quantisation can lower the spurious level. Practical DAC's with significant quantisation non-linearity require a large amplitude dither signal [2] to reduce the spurious levels. The added dither signal increases the noise power which can end up dominating the spurious levels. To rectify this problem the dither signal could be subtracted after the DAC, this dramatically increases the complexity of the implementation. A simpler solution is to add out-of-band (bandlimited) dither which will minimise the increase of in-band noise power, whilst at the same time reducing the spurious level [3].

In the application of multichannel radio base station transmitters oversampling is used to reduce the complexity and the effect of frequency dependant mismatch of the reconstruction filters [4], Figure I. This allows the dither signal to be inserted in the unused spectrum, centred around the Nyquist frequency. It will then be removed by the reconstruction filters following the DAC. This paper describes

a bandlimited dithering algorithm that adds the dither signal to the baseband signal during the interpolation process with very little increase in hardware. It has been implemented on a CMOS Application Specific Integrated Circuit (ASIC) which is capable of an output sampling rate of 10 MHz.

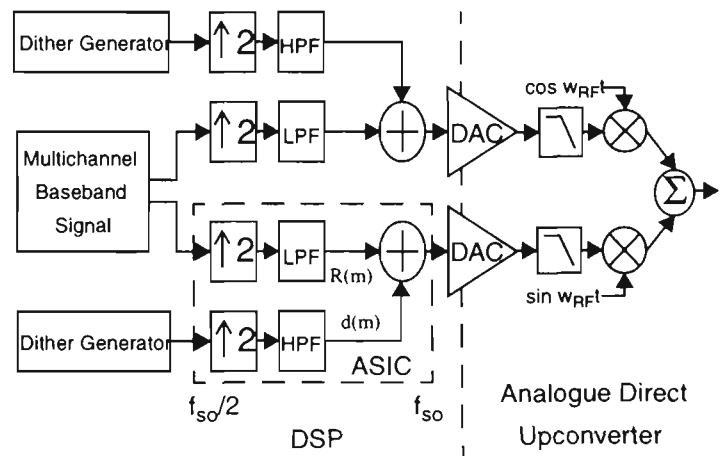


Figure I. Adding bandlimited dither during the interpolation process in a DSP multichannel base station transmitter

Bandlimited Dithering Architecture:

Given that the lowpass and highpass halfband interpolating filters, Figure I, have opposite frequency specifications, then the coefficients of the High Pass Filter (HPF) required to shape the dither signal can be obtained directly from the Low Pass Filter (LPF) by changing the sign of every other coefficient. Efficiencies in the interpolator design are then made by using a halfband filter design. This results in an odd ordered filter with a symmetrical impulse response and the even taps being equal to zero. This makes the

lowpass to highpass transformation trivial, with only the centre tap requiring a change in sign. The two halfband interpolating filters can now be easily merged to form a highly efficient architecture as shown in Figure II.

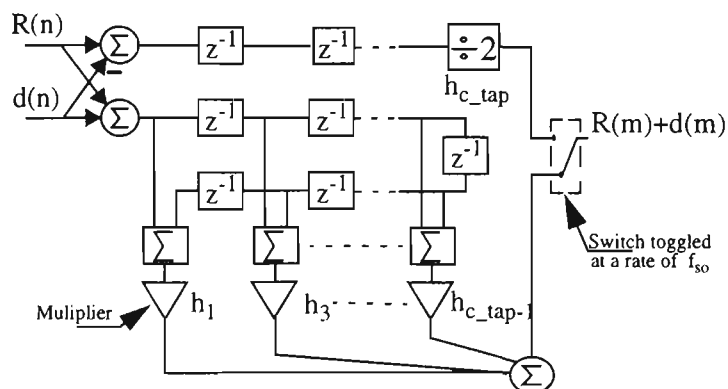


Figure II. Halfband interpolator architecture with highpass dither shaping incorporated. Note that all components except for the switch operate at the input sampling rate, $f_{so}/2$. $R(n)$: Multichannel signal, $d(n)$: dither signal, Σ : adder, z^{-1} : sample delay, h_n : filter coefficient.

Compared to the lowpass interpolator, only two more adders and a delay line (shown shaded in Figure II) are needed to carry out the shaping and addition of dither. Thus the benefits of bandlimited dithering using halfband interpolators can be achieved for very little increase in circuitry. In the final layout of the ASIC, the additional circuitry represented only 2.5% of the total die area. The wideband dither generator is based on the Linear Feedback Shift Register Technique (LFSR). The dither generator was designed using the generation of m-sequences as a series of non-overlapping W bit words [5]. The dither signal had only a positive magnitude i.e. a DC offset of the half the dither amplitude. For the generator to closely approximate white noise the m-sequence length was set to $2^{25}-1$. Only 0.9% of the total die area was used for this function.

Measurements:

The effect of the non-ideal 9 bit DAC is demonstrated in Figure III(a), where four channels are activated. Only the spurious responses that fall in-band or close to the edges of

the system bandwidth are considered in the calculation of the Spurious Free Dynamic Range (SFDR), as the others will be eliminated by the reconstruction filters. When no dither is added the SFDR is 47 dBc and by adding bandlimited dither the SFDR has increased to 53 dBc, Figure III(b). The out-of-band dither has little effect on the in-band noise floor. The DC offset of the dither Probability Density Function (PDF) has also generated a sinusoid at $f_{so}/2$, Figure III(b), and this combined with the random dither signal can produce additional benefits [6].

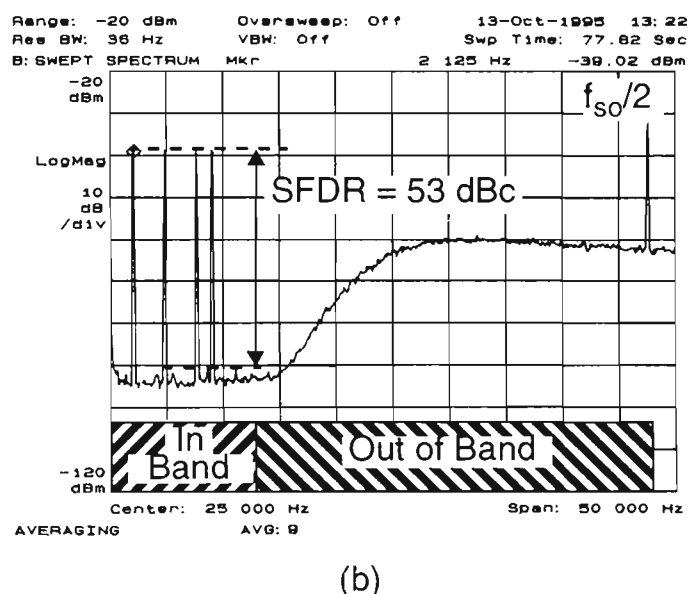
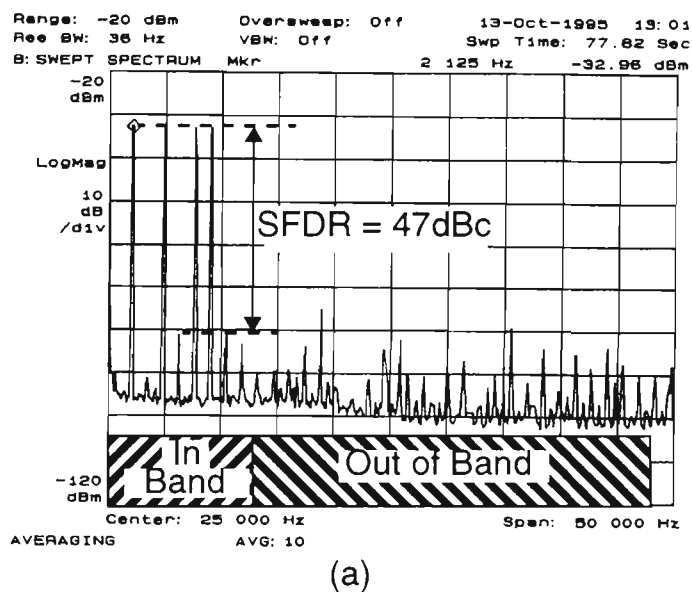


Figure III. (a) Four channels activated with no dither added. $f_{so} = 95\text{kHz}$ (b) Four channels activated with bandlimited dither added.

Figure IV shows that the SFDR only improves when there is greater than $1000\Delta^2$ (where Δ is the average amplitude of the Least Significant Bit in the measured 9 bit DAC) of dither power. Note that when the dither level was increased, the signal level was reduced so that the sum of the two signals did not exceed the 9 bit full scale range of the DAC. In other words, no clipping was allowed to occur.

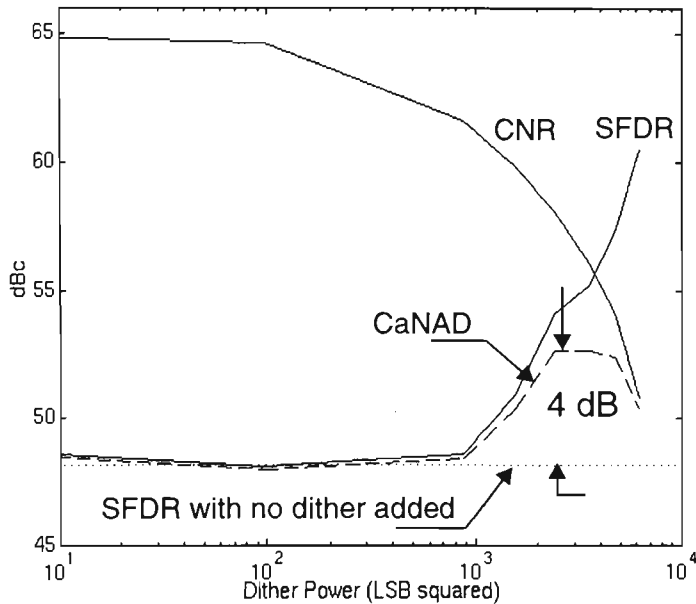


Figure IV. The effect of adding bandlimited dither.

The Carrier to Noise Ratio (CNR) is calculated using a noise measurement bandwidth of BW_{meas} . This bandwidth can be obtained from radio system specifications e.g. 30 kHz for GSM. As the bandlimited dither level increases, the in-band noise floor remains approximately constant, but the carrier power decreases, reducing the CNR. The SFDR and CNR can now be combined into a quantity called the Carrier to Noise and Distortion ratio (CaNAD), where the distortion power is the sum of the noise and spurious power measured within a bandwidth of BW_{meas} . The CaNAD for the worst channel is defined as:

$$\text{CaNAD} = (\text{SFDR}^{-1} + \text{CNR}^{-1})^{-1} \quad (1)$$

For bandlimited dithering the SFDR dominates the CNR for small values of dither power, whilst the reverse is true for larger values of dither power. The CaNAD improves by 4 dB

when the SFDR and CNR are approximately equal. Observe that small scale dither (amplitude variation in the order of 1 LSB) produces minimal improvement ($<0.5\text{dB}$), implying that wideband dither would show no improvement unless the dither can be subtracted after the DAC.

Conclusion:

Bandlimited dither has been added to the interpolated baseband signal with a very small increase in hardware, 3.4% of the total ASIC die area. The technique achieved a 4 dB increase in performance for the 9 bit practical DAC measured. Dither amplitude equal to half the full scale range of the DAC was required to achieve this improvement.

Acknowledgements:

The Department of Applied Electronics, Lund University, for providing the resources needed to design and fabricate the ASIC's. The Australian Telecommunications and Electronic Research Board and the DITAC Bilateral Science and Technology Co-operation Program for providing financial support.

Authors:

Scott A. Leyonhjelm received the B. S. degree from the University of Melbourne, Australia, in 1988, and in 1996 on the topic of wideband radio, he received the PhD degree from the Victoria University of Technology, Australia.

During 1989 he worked as an electrical engineer for Janssen Pharmaceutica, Belgium, and Colstons Ltd., UK. During 1990 and 1991 he was employed at Philips Radio Communications Systems, Australia, engaging in Private Mobile Radio (PMR) products and research and development into a GMSK modem. After completing his PhD studies in 1995 he joined Ericsson Radio Systems, Sweden, as a design and development engineer. His current interests are in the area of wireless communication systems, including adaptive algorithms for feedforward linearisation and digital signal processing techniques for wideband radio.

Michael Faulkner received the B.Sc.(Eng) from Queen Mary College, London University, UK, in 1970, the M.E. degree from the University of New South Wales, Australia in 1978, and the PhD from University of Technology, Sydney in 1993.

From 1975 to 1977 he was with the University of New South Wales, and since then as a lecturer and then Associate Professor at Victoria University of Technology, Melbourne, Australia. During 1983 he spent 6 months with Siemens Plessey working in military communications and between 1988 and 1996 he spent three periods at Lund University, Sweden, where he is currently visiting professor. His current interests are, signal processing, radio, circuit design and spread spectrum.

Department of Electrical and Electronic Engineering, Victoria University of Technology, Melbourne, Australia.

Peter Nilsson was born in Borlänge, Sweden on December 9, 1958 and has grown up in Skåne in the south of Sweden. He received the M.S.E.E. at Lund University, Lund, Sweden in 1988. In February 1988 he joined the Department of Applied Electronics, Lund University, where he had made his diploma work and where he, in May 1992, received his Licentiate degree. In May 1996 he received the Ph.D. degree and is currently working as an Assistant Professor in the ASIC/DSP group at the same department. He's main interests are in the field of silicon implementation of custom DSP's related to the communication area, especially with parallel-serial architectures.

References:

- [1] Bennet, W.R., "Spectra of quantized signal", Bell System Technical Journal, Vol. 27, pp 446-472, July 1948.
- [2] Bartz, M., "Large scale dithering enhances ADC dynamic range", Microwaves and RF, pp 192-198, May 1993.
- [3] Blesser, B & Locanthi, B., "The application of narrow-band dither operating at the Nyquist frequency in digital systems to provide improved signal-to-noise ratio over conventional dithering", J. Audio Eng. Soc., Vol. 35, No 6, pp 446-454, June 1987.
- [4] Leyonhjelm, S. & Faulkner, M., "The effect of reconstruction filters on direct upconversion in a multichannel environment", IEEE Trans. on Veh. Tech., Vol. 44, No. 1, pp 95-102, Feb. 1995.
- [5] O'Rielly, J.J.: 'Series-parallel generation of m-sequences', Radio Electronic Engineering, Vol. 45, No. 4, pp 171-175, 1975.
- [6] Vanderkooy, J. & Lipshitz, S.P., "Dither in digital audio", J. Audio Eng. Soc., Vol. 35, No 12, pp 966-975, Dec. 1987.

